**National River Conservation Directorate**
Ministry of Jal Shakti,
Department of Water Resources,
River Development & Ganga Rejuvenation
Government of India

# Climatologic Profile of Narmada River Basin

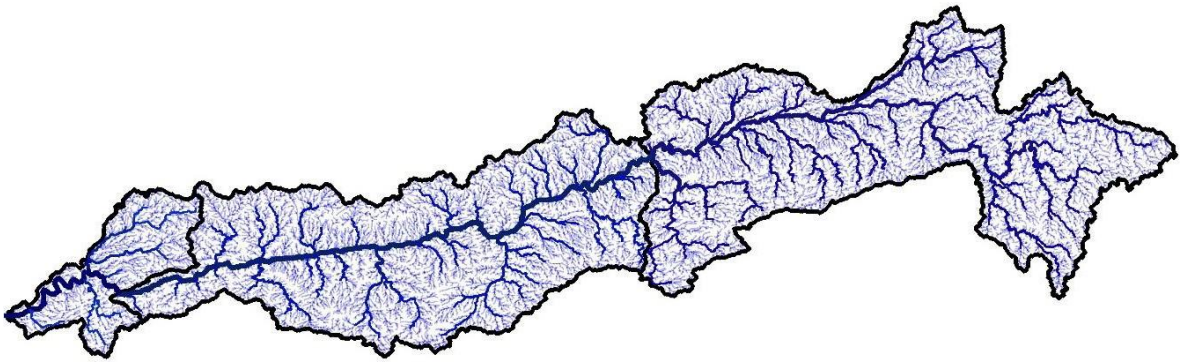

**March 2025**

# Climatologic Profile of Narmada River Basin


## National River Conservation Directorate (NRCD)

The National River Conservation Directorate, functioning under the Department of Water Resources, River Development & Ganga Rejuvenation, and Ministry of Jal Shakti providing financial assistance to the State Government for conservation of rivers under the Centrally Sponsored Schemes of 'National River Conservation Plan (NRCP)'. National River Conservation Plan to the State Governments/ local bodies to set up infrastructure for pollution abatement of rivers in identified polluted river stretches based on proposals received from the State Governments/ local bodies.

**www.nrcd.nic.in**

## Centres for Narmada River Basin Management and Studies (cNarmada)

The Center for Narmada River Basin Management and Studies (cNarmada) is a Brain Trust dedicated to River Science and River Basin Management. Established in 2024 by IIT Gandhinagar and IIT Indore, under the supervision of cGanga at IIT Kanpur, the center serves as a knowledge wing of the National River Conservation Directorate (NRCD). cNarmada is committed to restoring and conserving the Narmada River and its resources through the collation of information and knowledge, research and development, planning, monitoring, education, advocacy, and stakeholder engagement.

**www.cnarmada.org**

## Centres for Ganga River Basin Management and Studies (cGanga)

cGanga is a think tank formed under the aegis of NMCG, and one of its stated objectives is to make India a world leader in river and water science. The Centre is headquartered at IIT Kanpur and has representation from most leading science and technological institutes of the country. cGanga's mandate is to serve as think-tank in implementation and dynamic evolution of Ganga River Basin Management Plan (GRBMP) prepared by the Consortium of 7 IITs. In addition to this, it is also responsible for introducing new technologies, innovations, and solutions into India.

**www.cganga.org**

## Acknowledgment

This report is a comprehensive outcome of the project jointly executed by IIT Gandhinagar (Lead Institute) and IIT Indore (Fellow Institute) under the supervision of cGanga at IIT Kanpur. It was submitted to the National River Conservation Directorate (NRCD) in 2024. We gratefully acknowledge the individuals who provided information and photographs for this report.

## Team Members

Pranab Kumar Mohapatra, cNarmada, IIT Gandhinagar
Manish Kumar Goyal, cNarmada, IIT Indore
Srija Roy, cNarmada, IIT Indore
Bhanu Parmar, cNarmada, IIT Gandhinagar
Sunil Kumar, cNarmada, IIT Gandhinagar

## PREFACE

The Narmada River Basin, with its complex climatic regime and diverse physiographic characteristics, plays a pivotal role in sustaining ecosystems, agriculture, and livelihoods across central and western India. As climate variability intensifies and extreme weather events become more frequent, understanding the basin's climatological behaviour has become more critical than ever for effective water resource planning and sustainable development.

This report is a comprehensive effort to analyze and document the meteorological and climatological dynamics of the Narmada River Basin. Drawing upon long-term observational data, high-resolution reanalysis datasets, and climate model projections, the study offers detailed insights into key parameters such as rainfall, temperature, wind patterns, humidity, solar radiation, and drought characteristics. Special attention has been given to temporal trends, spatial variability, and the implications of future climate scenarios to better inform basin-level planning and risk management.

Our objective has been to present a scientifically robust yet accessible reference that can support evidence-based decision-making for climate adaptation, agricultural planning, and water resource governance in the basin. The findings and analyses provided herein are intended to assist researchers, policymakers, planners, and stakeholders in addressing both present challenges and long-term climatic shifts.

We are deeply grateful to the institutions, agencies, and individuals whose data, insights, and support have made this study possible. Their contributions have significantly enriched the quality and relevance of this work. It is our hope that this report will contribute meaningfully to ongoing and future efforts aimed at enhancing the climate resilience of the Narmada River Basin and securing the well-being of its people and ecosystems.

Centre for Narmada River Basin
Management and Studies (cNarmada)
IIT Gandhinagar, IIT Indore

# TABLE OF CONTENTS

# LIST OF FIGURES

# LIST OF TABLES

# ABBREVIATIONS AND ACRONYMS

| | |
|---|---|
| **cGanga** | Centres for Ganga River Basin Management and Studies |
| **cNarmada** | Centres for Narmada River Basin Management and Studies |
| **CWC** | Central Water Commission |
| **NRCD** | National River Conservation Directorate |
| **IPCC** | Intergovernmental Panel on Climate Change |
| **ECMWF** | European Centre for Medium-Range Weather Forecasts |
| **ERA5** | ECMWF Reanalysis v5 |
| **IMD** | Indian Meteorological Department |
| **CAMELS** | Catchment Attributes and Meteorology for Large-Sample Studies |
| **MCM** | Million Cubic Meters |
| **RH** | Relative Humidity |
| **CMIP6** | Coupled Model Intercomparison Project Phase 6 |
| **SSP** | Shared Socioeconomic Pathway |
| **GCM** | General Circulation Model |
| **RCM** | Regional Climate Model |
| **SPEI** | Standardized Precipitation Evapotranspiration Index |
| **WRIS** | Water Resources Information System |

# Chapter 1: Introduction

## 1.1 BACKGROUND AND SIGNIFICANCE OF THE NARMADA RIVER

The Narmada River, originating from the Amarkantak Plateau in Madhya Pradesh, is one of India's most significant west-flowing rivers, spanning approximately 1,312 kilometers before draining into the Arabian Sea. Its basin, covering 95,959.7 square kilometers, exhibits diverse geomorphological features, including steep gradients in the upper reaches, basaltic formations in the middle basin, and expansive alluvial plains downstream.

The river's hydraulic profile is shaped by its unique physiography and tectonic settings, particularly the Narmada Rift Valley flanked by the Vindhya and Satpura ranges. This geological framework influences the flow regime, sediment dynamics, and discharge patterns, making the river a vital case study for hydraulic research and water resource management. Geographic location of basin is shown in Figure 1.

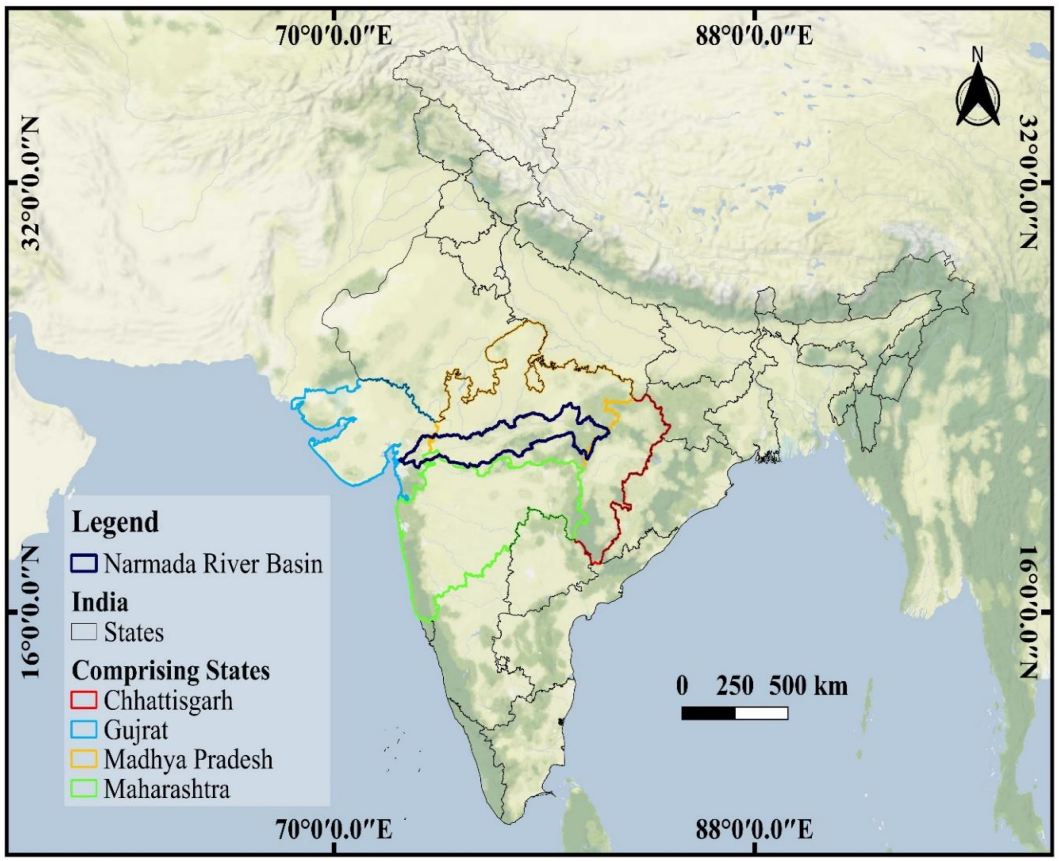


Figure 1: Geographical location map

### 1.1.1 Geographic Profile of the Narmada River

Originating from the Amarkantak Plateau in Madhya Pradesh, the Narmada River flows westward for 1,312 km before emptying into the Arabian Sea through the Gulf of Khambhat. Its basin extends from 21° 40' 12" to 23° 41' 24" N latitudes and 72° 48' 36" to 81° 45' 36" E longitudes, covering 95,959.70 sq. km—approximately 3% of India's total geographical area as shown in Figure 2. The basin's elongated shape spans 915.65 km from east to west and 236 km from north to south.

The river's physiography is defined by three distinct zones: the upper, middle, and lower reaches. The upper Narmada flows through rugged and forested terrain, characterized by steep slopes and narrow valleys. Notable topographical features include the Kapildhara Falls near the river's origin and the Marble Rocks gorge at Bhedaghat near Jabalpur. The middle Narmada is marked by wider valleys and fertile plains, with prominent basaltic formations from ancient volcanic activity. This region is ideal for agriculture and supports several large irrigation projects. The lower Narmada basin transitions into the Gujarat plains, featuring alluvial deposits and a gentler gradient as it approaches the Arabian Sea.

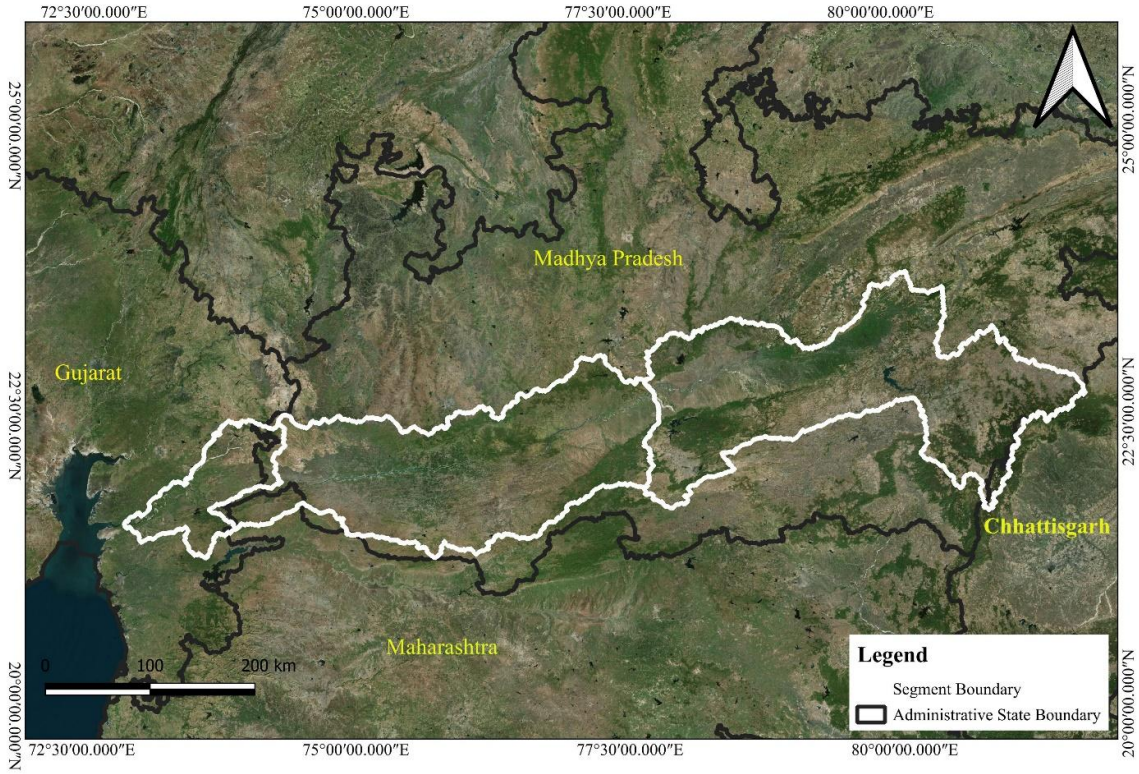


Figure 2: Drainage area of the Narmada River with its three segments

The Narmada Rift Valley, a tectonic feature, significantly influences the river's course. Flanked by the Vindhya Range to the north and the Satpura Range to the south, this valley provides a unique geological setting. The river's flow is further augmented by its 41 tributaries, including the Tawa, Hiran, and Shakkar Rivers, which contribute to the hydraulics, hydrological and ecological diversity of the basin.

### 1.1.2 Sub-Divisions of the Basin

The Narmada River basin is divided into three sub-basins based on geomorphology, hydrology, and hydraulics, each with unique characteristics and challenges:

**Upper Narmada Sub-Basin**: Extending from Amarkantak to Hoshangabad (~720 km), this region encompasses the river's origin at the Amarkantak Plateau and its flow through rugged, forested terrain. The area is characterized by steep gradients and narrow valleys, making it ideal for hydropower projects such as the Bargi Dam. However, these steep slopes and high rainfall levels also make the sub-basin prone to soil erosion and sedimentation issues, affecting downstream water quality and reservoir capacity.

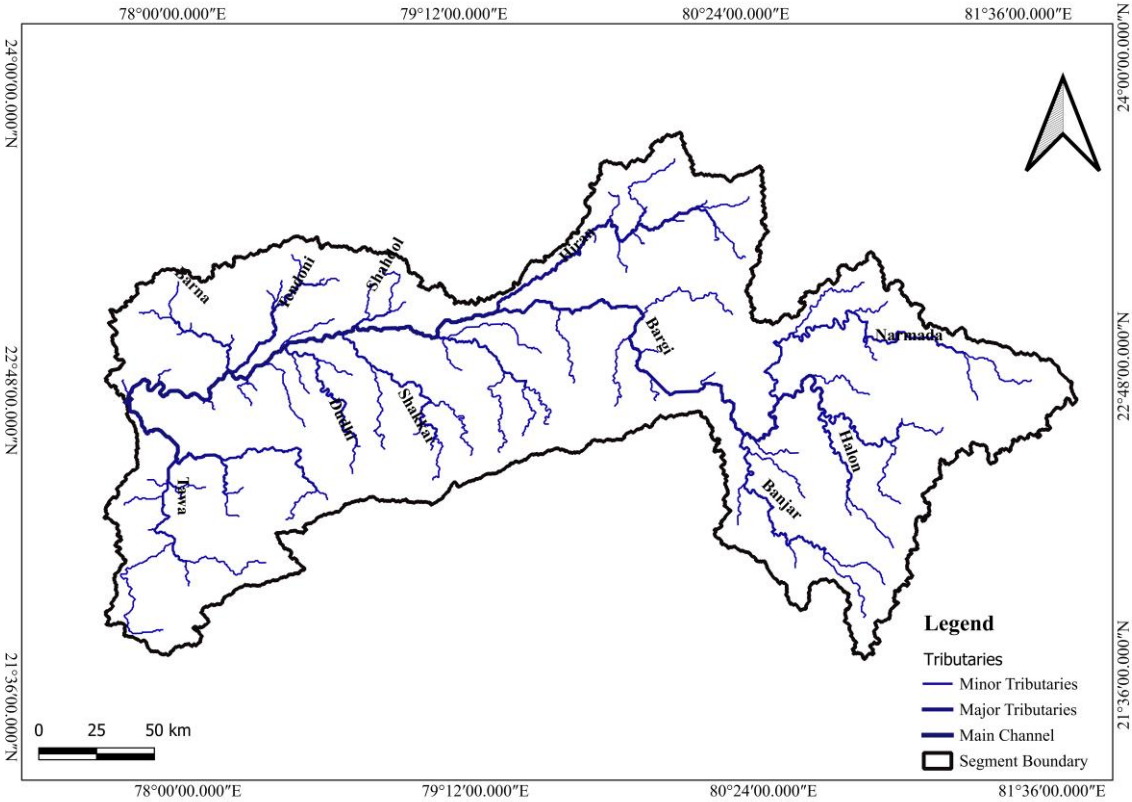


Figure 3: Tributaries of Upper Narmada River segment

**Middle Narmada Sub-Basin**: Spanning Hoshangabad to Navagam (~485 km), the middle sub-basin is marked by wider valleys, fertile plains, and basaltic rock formations. This region supports extensive agricultural activity, thanks to irrigation systems fed by major projects like the Indira Sagar and Omkareshwar Dams. Despite its agricultural productivity, the middle Narmada faces challenges such as deforestation in the surrounding uplands, leading to increased siltation, and pollution from untreated urban and industrial effluents.

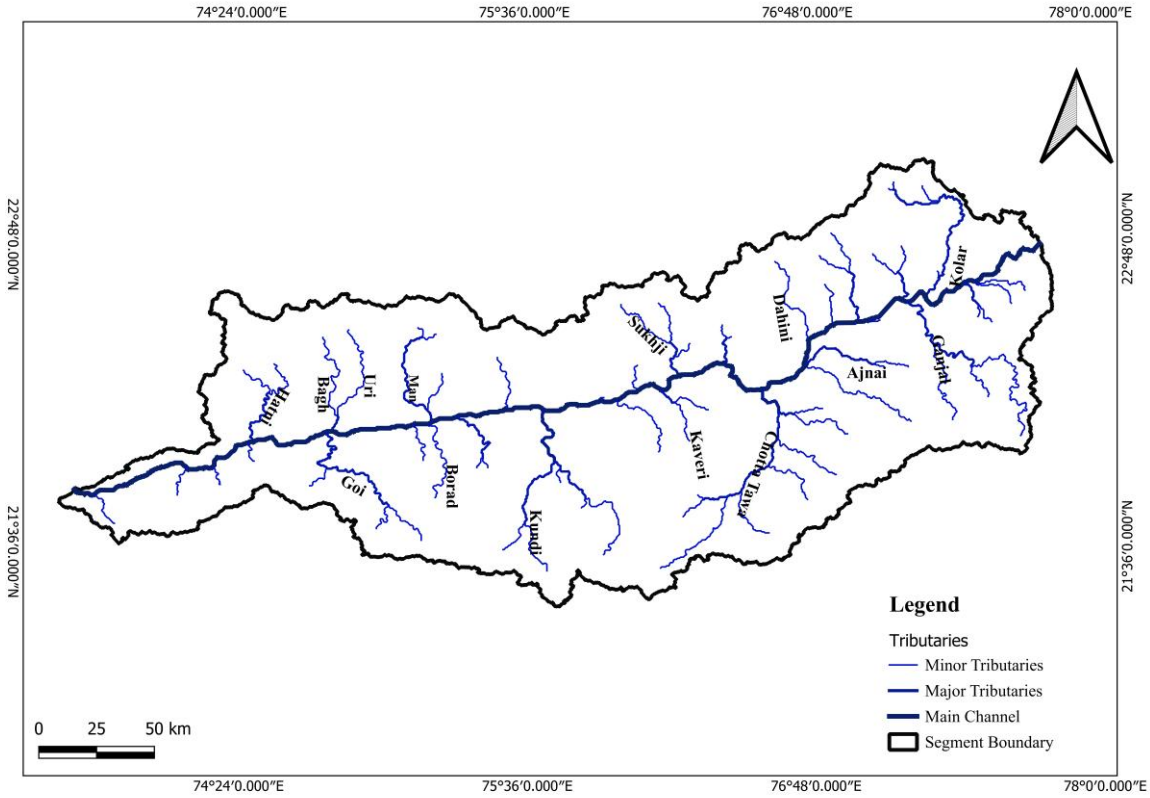


Figure 4: Tributaries of the Middle Narmada River segment

**Lower Narmada Sub-Basin**: Covering the area from Navagam to the Gulf of Khambhat (~145 km), the lower sub-basin transitions into the flat alluvial plains of Gujarat. Here, the river slows down, creating rich floodplains that support diverse ecosystems and fertile agricultural lands. This region includes the Sardar Sarovar Dam, a critical infrastructure for irrigation, water supply, and power generation. However, the lower Narmada is heavily impacted by industrial discharges, sand mining, and changes in sediment flow due to upstream damming, leading to coastal erosion near the river's mouth.

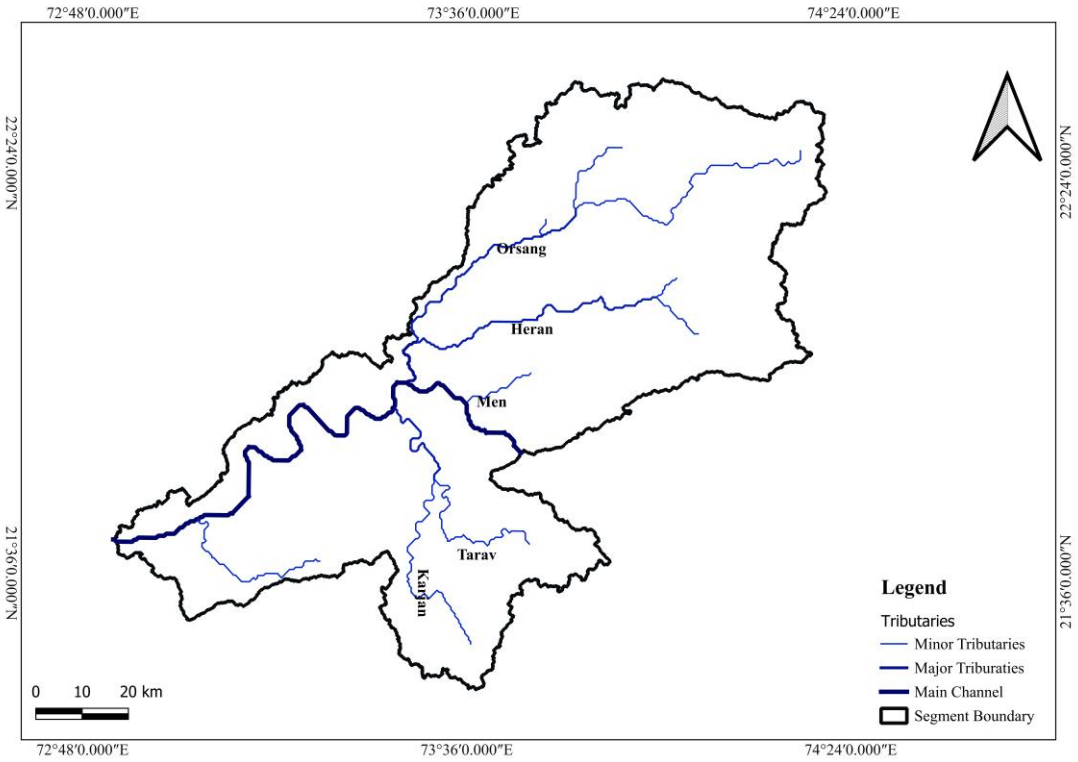


Figure 5: Tributaries of Lower Narmada River segment

## 1.2 OVERVIEW OF CLIMATE IN THE NARMADA RIVER BASIN

The Narmada River Basin lies predominantly in a humid tropical climate zone, with the Tropic of Cancer passing through its upper plains. While the climate is generally tropical, significant variations in temperature and precipitation occur across the basin. Seasonal changes bring distinct weather patterns, ranging from dry and cool winters to hot summers and intense monsoon rains.

The basin experiences four well-defined seasons. The cold weather season extends from November to February, characterized by clear skies, cool temperatures, and dry conditions. Minimal precipitation occurs during this period, and nights are often accompanied by cold winds. The hot weather season, from March to mid-June, is typically dry, with May being the hottest month. This period sees a significant rise in daytime temperatures, particularly in the central plains. The southwest monsoon season begins in mid-June and lasts until early October, bringing the majority (85–95%) of the annual precipitation. The weather remains humid and sometimes oppressive, especially in areas

close to the river. The post-monsoon season, spanning October and November, marks a transition from the wet monsoon months, contributing around 9% of the total annual rainfall.

Rainfall distribution varies significantly across the basin. The upper hilly regions receive the highest precipitation, exceeding 1400 mm annually, with localized peaks up to 1800 mm around Pachmarhi. Moving downstream, rainfall gradually decreases. In the upper plains (stretching from Jabalpur to Punasa Dam), annual rainfall reduces from 1400 mm to below 1000 mm. The lower plains, particularly around Barwani, represent the driest part of the basin, with annual rainfall falling below 650 mm. Interestingly, in the lower hilly areas, precipitation increases slightly again, exceeding 750 mm annually.

The intensity of 24-hour rainfall events also shows spatial variation. The southern section of the upper Narmada basin experiences the most intense rainfall events, with 24-hour totals reaching 360 mm. In contrast, the lower middle basin records less than 260 mm of rainfall in a 24-hour period. Overall, nearly 90% of the total rainfall occurs during the monsoon months from June to October, with July and August alone contributing around 60% of the total precipitation.

Temperature patterns in the basin resemble those of Central India, with high seasonal variability. The hottest month is May, while January records the lowest temperatures. The upper basin generally experiences cooler temperatures compared to the middle and lower reaches. In contrast, the lower basin, due to its proximity to the Arabian Sea, maintains relatively moderate temperatures. Historical temperature data indicates that in the coldest month (January), the minimum temperature can drop to 10.87°C, while in the hottest month (May), maximum temperatures can reach 40.58°C.

## 1.3 REPORT OBJECTIVES

This report aims to provide a comprehensive understanding of the climatology and meteorology of the Narmada River Basin by analyzing historical climate trends, rainfall patterns, temperature variations, and drought characteristics. The study utilizes diverse datasets and methodologies to assess the basin's climatic conditions and their implications. The key objectives of each chapter are outlined below:

Chapter 1: Introduction – This chapter introduces the geographic and climatic significance of the Narmada River Basin, along with its sub-divisions and climate profile. It

sets the foundation for understanding the basin's meteorological conditions and the need for this study.

Chapter 2: Data Acquisition and Methodology – This chapter describes the sources of climate data, including rainfall and temperature records, and outlines the methodological framework used for analyzing historical trends and climate variability across the basin.

Chapter 3: Climatic Characteristics – This section presents an in-depth analysis of key climatic elements, including rainfall, temperature, wind, humidity, cloud cover, and solar radiation, which influence the hydrology and ecology of the basin.

Chapter 4: GCM / RCM Data – This chapter explores Global Climate Models (GCMs) and Regional Climate Models (RCMs) to assess future climate projections for the Narmada Basin, providing insights into potential climate change impacts.

Chapter 5: Drought Characteristics – This section examines the historical occurrence and spatial variability of droughts, using SPEI (Standardized Precipitation and Evapotranspiration Index) to assess long-term drought trends in the basin.

Chapter 6: Conclusions and Recommendations – The final chapter summarizes the key findings of the report and discusses their implications for water resource management and climate adaptation strategies. It also data applications.

These objectives collectively contribute to a holistic understanding of the Narmada River Basin's climate, helping in sustainable water management and climate resilience planning.

# Chapter 2: Data Acquisition and Methodology

## 2.1 DATA SOURCES

The study on the climatologic and meteorologic characteristics of the Narmada River Basin relies on a diverse set of data sources that provide hydrological, meteorological, and climatic datasets. The key sources utilized in this research are outlined below:

**1. India Water Resources Information System (India-WRIS)**: The India-WRIS platform, developed by the Ministry of Jal Shakti, serves as a comprehensive repository of hydrological data. It provides detailed information, including river basin shape files, dam and canal details, and tributary characteristics. This platform forms the backbone of the spatial and hydrological datasets used in this study. **Source:** India-WRIS

**2. CAMELS-India Dataset**: The CAMELS-India dataset, as described by (Nikunj K. Mangukiya, 2025), offers hydrometeorological time series and catchment attributes for 472 catchments across Peninsular India. This dataset was instrumental in analysing climatic variability, hydrological patterns, and water resource trends within the Narmada River Basin.

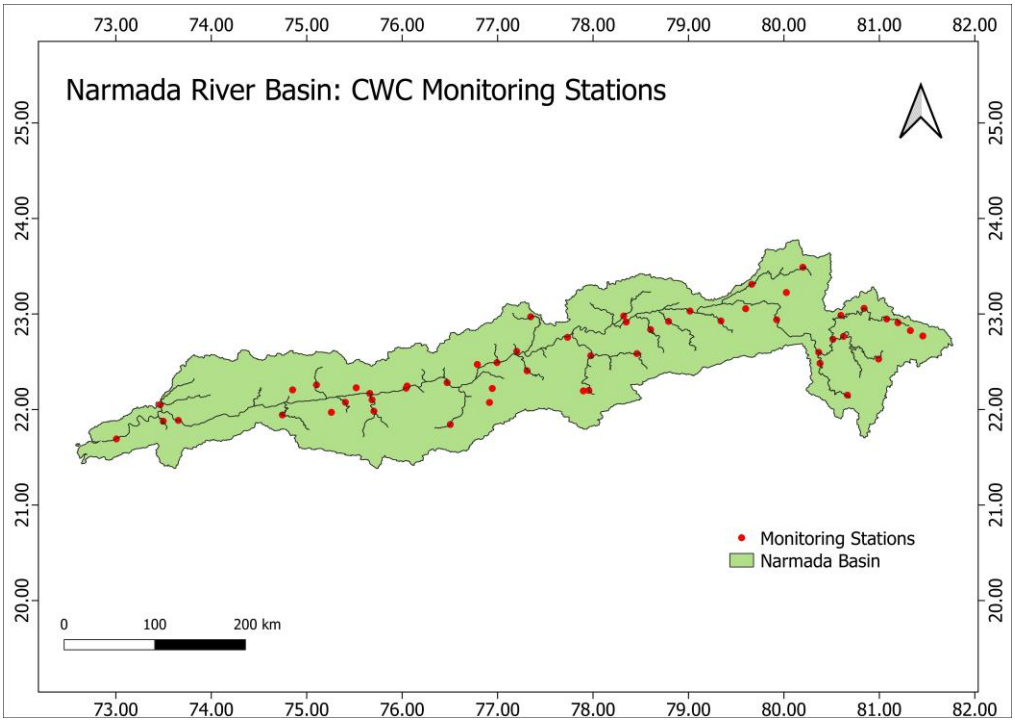


Figure 6 Narmada River Basin : CWC Monitoring Stations

**3. Central Water Commission (CWC) Data:** The Central Water Commission (CWC) provided essential discharge and water level data for multiple monitoring stations across the Narmada River Basin as shown in Figure 6. These datasets were crucial for assessing flow dynamics, seasonal variations, and hydrological trends. The location and characteristics of the CWC monitoring stations were also integrated into the analysis to ensure comprehensive coverage of the river basin's hydrology.

**4. ERA5 Climate Reanalysis Data**: The ERA5 dataset, produced by the European Centre for Medium-Range Weather Forecasts (ECMWF), offers high-resolution climate reanalysis data. This dataset provides critical atmospheric variables such as temperature, wind speed, relative humidity, and solar radiation at monthly means. ERA5 data were extensively utilized to analyze historical climatic trends and variability within the Narmada River Basin.
**Source:** ERA5 Climate Data

**5. GCM / RCM Data:** This study employs a high-resolution, bias-corrected climate dataset specifically developed for South Asia using outputs from 13 General Circulation Models (GCMs) participating in the Coupled Model Intercomparison Project Phase 6 (CMIP6). The dataset was generated by Mishra et al., (2020) using Empirical Quantile Mapping (EQM) as a statistical bias correction method. It provides daily precipitation, maximum temperature, and minimum temperature data at a 0.25° spatial resolution, covering both historical (1951–2014) and future (2015–2100) periods under four Shared Socioeconomic Pathways (SSPs): SSP126, SSP245, SSP370, and SSP585.

**6. Drought Atlas of India**: The Drought Atlas of India provides valuable insights into historical drought occurrences and their spatial distributions across India. This dataset was essential for assessing drought characteristics within the Narmada River Basin and understanding long-term trends in water scarcity and climatic variability.
**Source:** Drought Atlas of India

These datasets collectively form the foundation for the climatological and meteorological analysis conducted in this study. By integrating multiple data sources, the study ensures a robust assessment of hydrological trends and climatic variability across the Narmada River Basin.

## 2.2 METHODOLOGICAL FRAMEWORK

The methodological framework adopted in this study involves a combination of data acquisition, spatial extraction and temporal aggregation. The overall objective is to analyze the climatological and meteorological characteristics of the Narmada River Basin using reliable datasets and systematic techniques.

The steps followed in the methodology are outlined below:

- **Data Compilation and Preprocessing**: Relevant datasets were compiled from various national and international sources including India-WRIS, CAMELS-India, CWC, ERA5, and the Drought Atlas of India. These datasets were assessed for quality, completeness, and suitability for climatological analysis. Basin-level spatial layers such as shapefiles were used to extract relevant data corresponding to the Narmada River Basin boundary.
- **Climatological Parameter Extraction**: Key climate variables such as rainfall, temperature, wind speed, relative humidity, cloud cover, and solar radiation were extracted. For ERA5 data, monthly means at appropriate spatial resolution were considered. For observed datasets, station-wise data points within or adjacent to the basin boundary were compiled.
- **Temporal and Spatial Analysis**: Monthly and annual statistics were computed to assess the variability and trends in climatic parameters. The temporal analysis focused on identifying patterns such as seasonal distribution, inter-annual variability, and long-term trends. Spatial analysis involved the mapping of basin-wide patterns using GIS tools.
- **GCM / RCM Data**: The 13 GCMs included were selected based on the availability of daily data for all three variables across all required periods. The raw CMIP6 output initially provided at spatial resolutions ranging from 0.7° to over 2°—were regridded to 1° resolution using bilinear interpolation and then bias-corrected to 0.25° using observational gridded datasets. For India, gridded precipitation and temperature observations from the India Meteorological Department (IMD) were used, while for regions outside India, the dataset by Sheffield et al. (2006) was employed. The EQM-based bias correction method adjusts model outputs by aligning their cumulative distribution functions (CDFs) with those of observations for a reference period. This

approach has demonstrated strong performance in correcting biases not only in the mean values but also in the extremes of temperature and precipitation, which is crucial for impact assessments involving climate extremes. Thus, in this study, climate projections are derived from 13 GCMs that participated in the Coupled Model Intercomparison Project Phase 6 (CMIP6). These models were selected based on the availability of daily data for three key climate variables: precipitation, maximum temperature, and minimum temperature. Each of the 13 GCMs provides climate data over a long period, covering:

- Historical period: 1850–2014
- Future projections: 2015–2100

Future scenarios in CMIP6 are represented by four Shared Socioeconomic Pathways (SSPs), which reflect different levels of greenhouse gas emissions and radiative forcing by the end of the 21st century:

- SSP1-2.6: A low-emission, sustainability-focused scenario
- SSP2-4.5: A moderate, middle-of-the-road scenario
- SSP3-7.0: A high-emission, regional rivalry scenario
- SSP5-8.5: A high-emission, fossil fuel-intensive scenario

- **Drought Assessment Methodology**: The assessment of drought conditions in the Narmada River Basin was carried out using the Standardized Precipitation and Evapotranspiration Index (SPEI) data provided in the Drought Atlas of India developed by Chuphal et al. (2024). This dataset includes pre-computed SPEI values at various timescales for the entire country, derived from high-resolution precipitation and temperature data. For this study, relevant SPEI data corresponding to the Narmada River Basin were extracted and analyzed to evaluate both temporal trends and spatial variations in drought severity and frequency. The analysis focused on identifying major historical drought events and regional disparities in drought impact across different sub-basins.
- **Visualization**: Various statistical and spatial outputs were visualized through graphs, charts, and maps. These visual representations aid in interpreting the basin's climatic

conditions and provide an intuitive understanding of temporal changes and spatial heterogeneity.

This framework ensures a consistent, replicable, and scientifically robust approach for analyzing the climatological dynamics of the Narmada River Basin.

# Chapter 3: Climatic Characteristics

## 3.1 GENERAL

This chapter provides an overview of the key climatic characteristics of the Narmada River Basin, focusing on critical meteorological parameters such as rainfall, temperature, wind speed, relative humidity, cloud cover, and solar radiation. These variables are fundamental to understanding the hydrological behaviour and environmental dynamics of the basin. The analysis is based on long-term datasets, primarily covering the period from 1980 to 2020, obtained from both ground-based stations and climate reanalysis products. The findings presented through spatial maps and time-series plots aim to support informed water resource planning, climate impact assessments, and adaptation strategies at the basin scale.

## 3.2 RAINFALL

This section analyses the spatial distribution of rainfall across the Narmada River Basin. Understanding the spatial patterns of rainfall is crucial for identifying areas with high and low precipitation, which can inform water resource management decisions.

### 3.2.1 Spatial Variation of Rainfall

The spatial variation of rainfall is illustrated in Figure 7 and Figure 8. Figure 7 depicts the annual average rainfall distribution, while Figure 8 shows the monsoon annual average rainfall distribution. These figures highlight the areas with high and low precipitation, providing valuable insights into the spatial variability of rainfall across the basin.

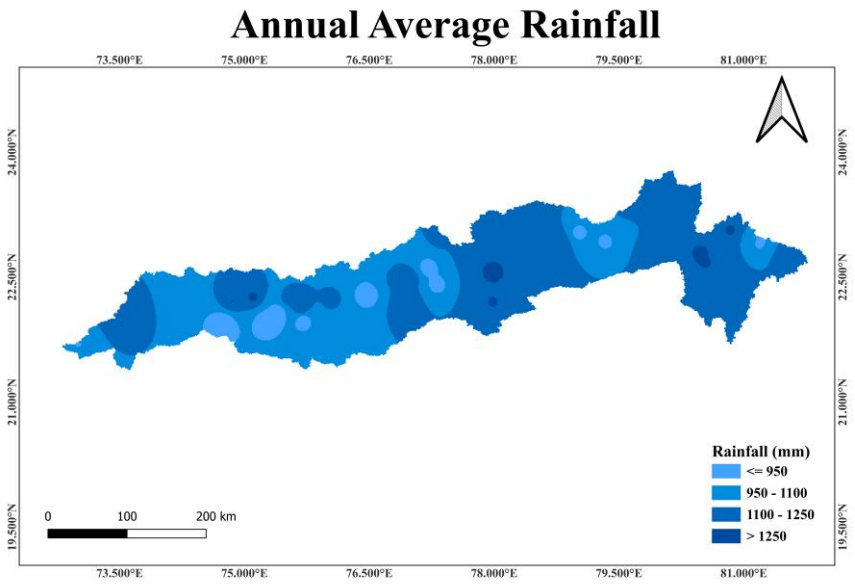


Figure 7: Annual Average Rainfall in the Narmada River Basin.

As depicted in Figure 7, the annual average rainfall distribution in the Narmada River Basin exhibits significant spatial variability.

The spatial distribution of monsoon annual average rainfall in the Narmada River Basin is shown in Figure 8.

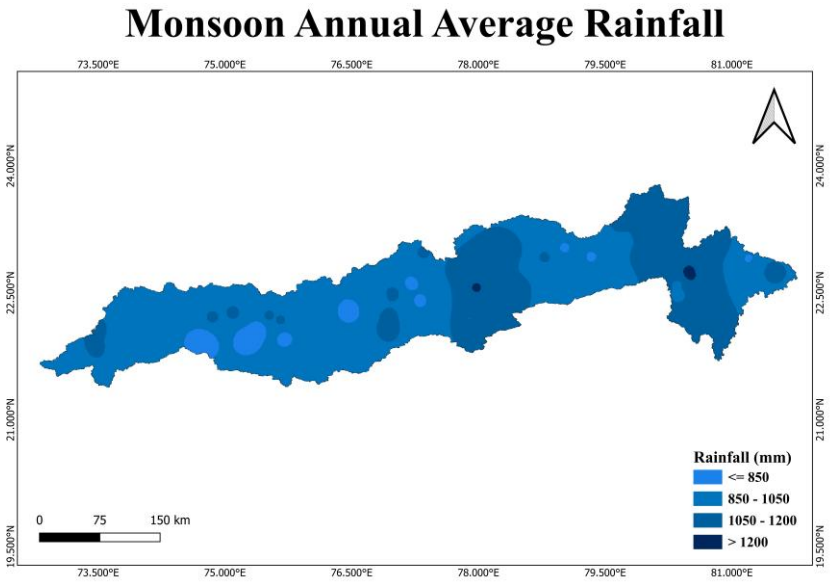


Figure 8: Monsoon Annual Average Rainfall in the Narmada River Basin

Figure 8 illustrates the spatial variability of monsoon rainfall in the Narmada River Basin, highlighting the areas that receive significant rainfall during the monsoon season.

### 3.2.2 Temporal Variation of Rainfall

This section examines the temporal variation of rainfall at ten selected sites within the Narmada River Basin. For each site, two figures are presented, showing:

1. Yearly Precipitation
2. Yearly Monsoon Precipitation

#### 1. Yearly Precipitation

The analysis of yearly precipitation patterns at various stations across the Narmada River Basin over the period from 1980 to 2020 provides significant insights into temporal rainfall variability. Figure 9 to Figure 21 illustrate annual precipitation trends at key stations, including Patan, Belkheri, Bharuch, Garudeshwar, and others.

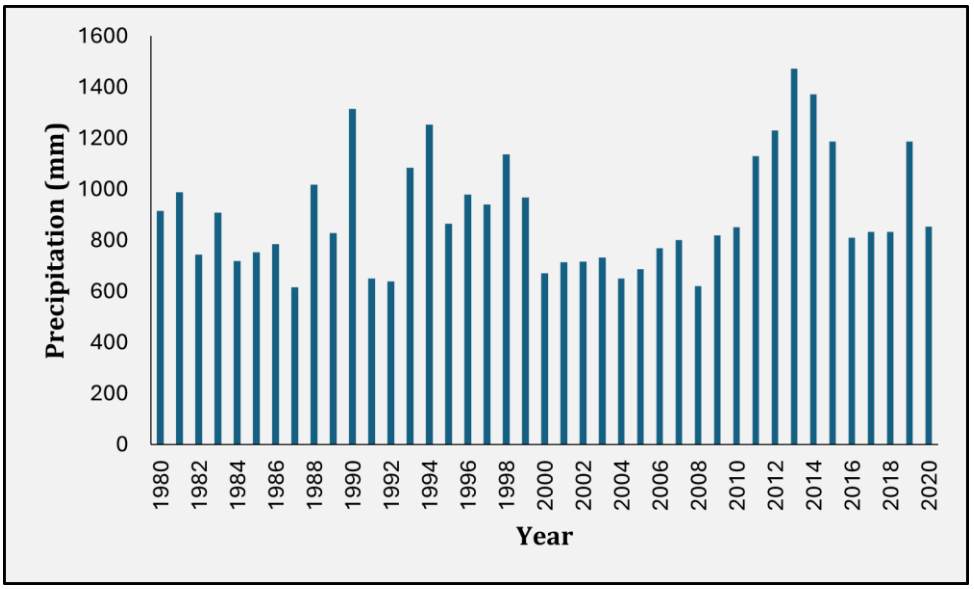


Figure 9: Annual Precipitation (mm) at Belkheri Station (1980-2020)

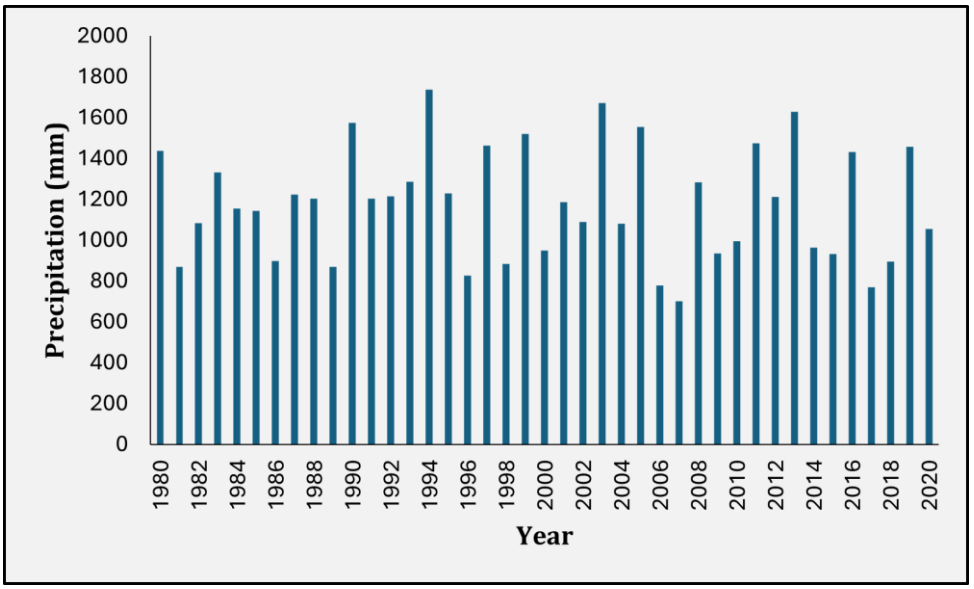


Figure 10: Annual Precipitation (mm) at Patan Station (1980-2020)

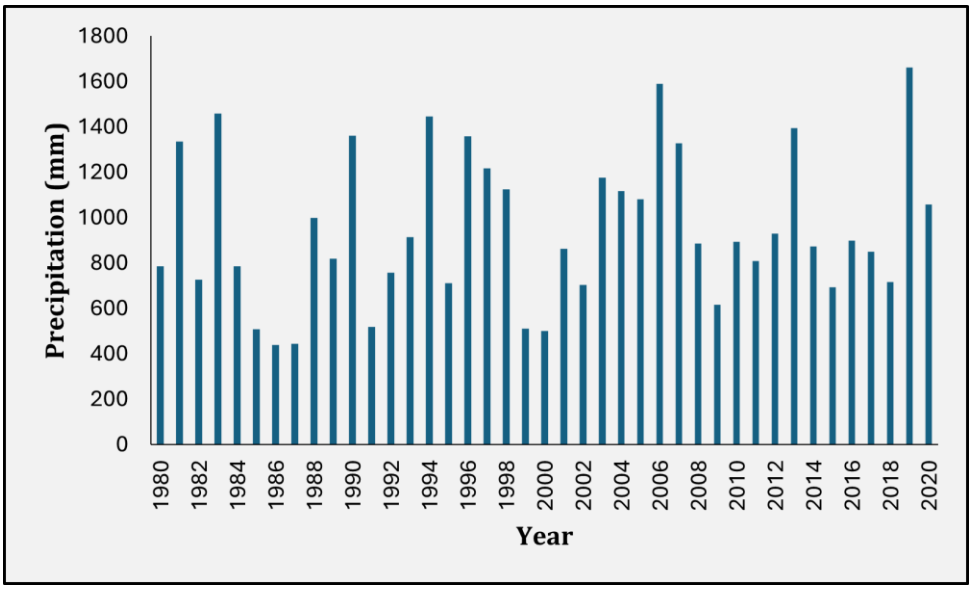


Figure 11: Annual Precipitation (mm) at Bharuch Station (1980-2020)

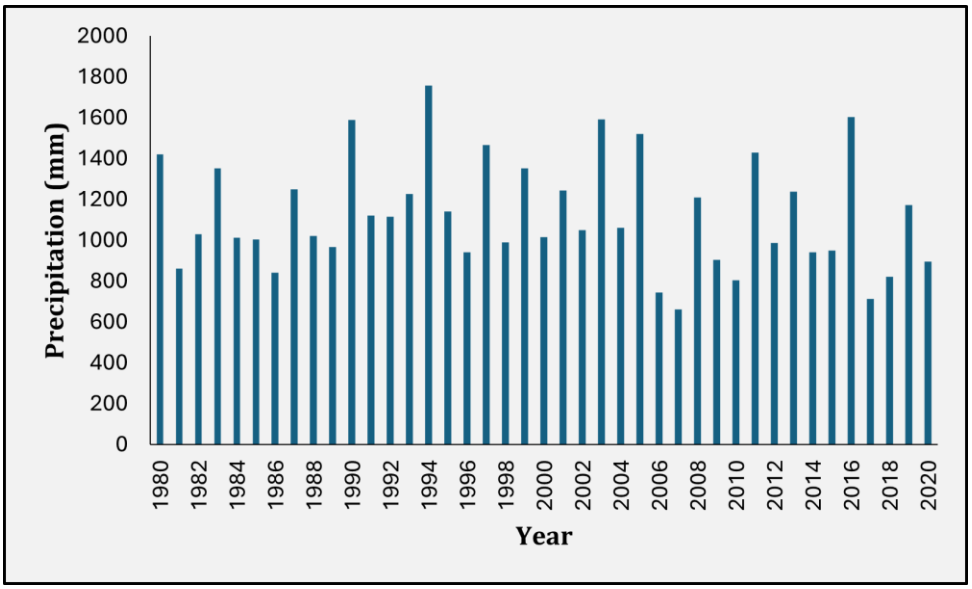


Figure 12: Annual Precipitation (mm) at Garudeshwar Station (1980-2020)

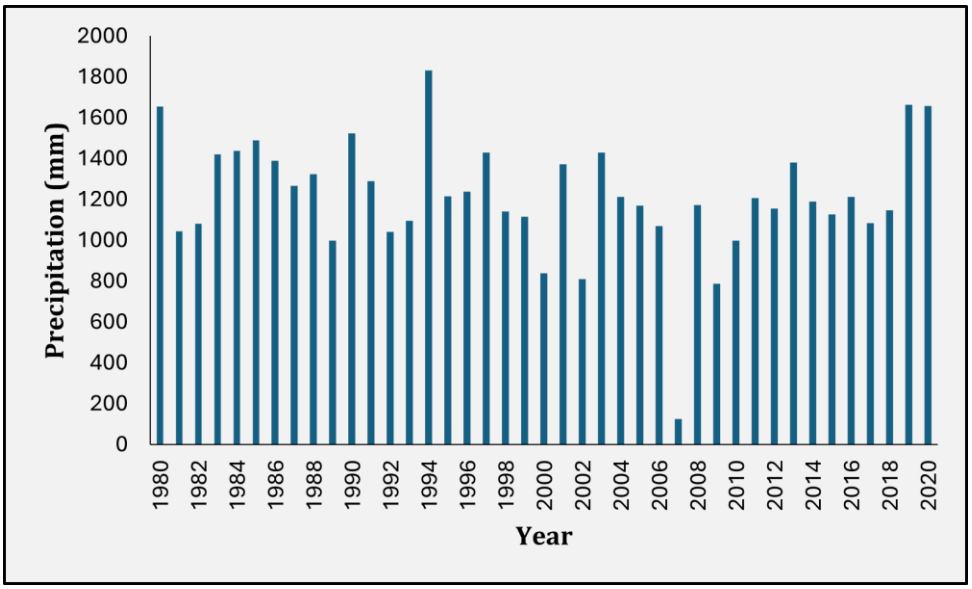


Figure 13: Annual Precipitation (mm) at Ghunghara Station (1980-2020)

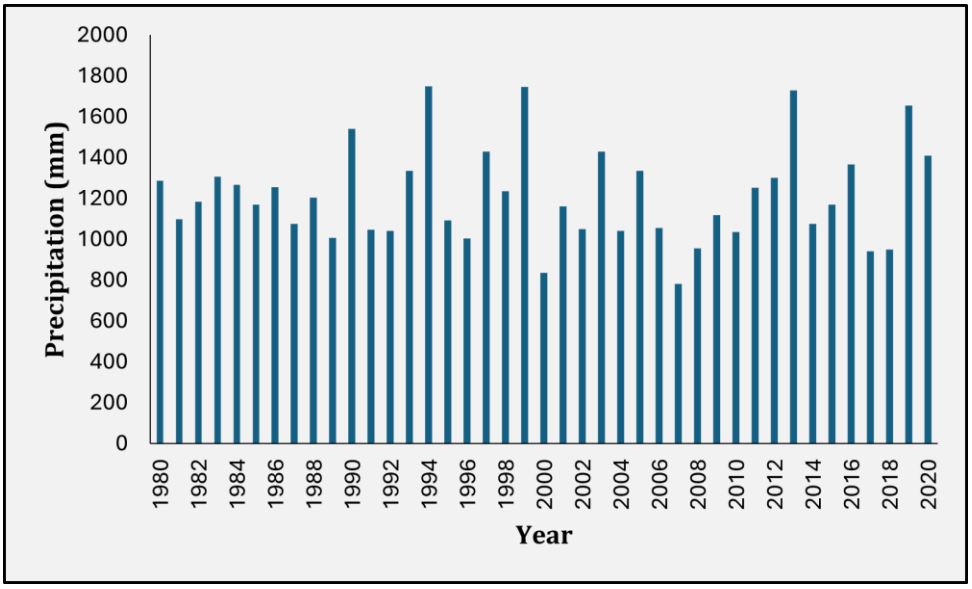


Figure 14: Annual Precipitation (mm) at Gorakhpur Station (1980-2020)

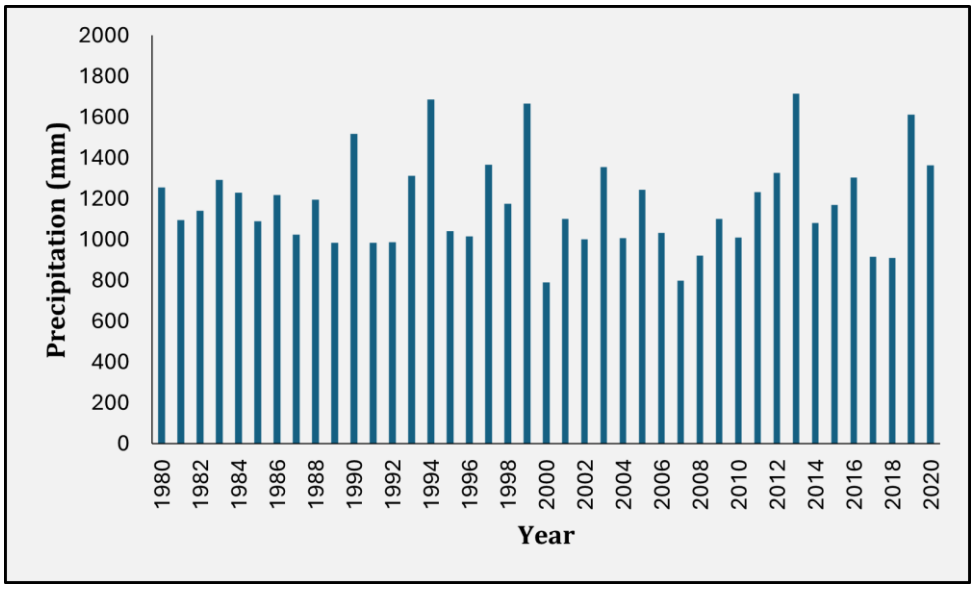


Figure 15: Annual Precipitation (mm) at Hoshangabad Station (1980-2020)

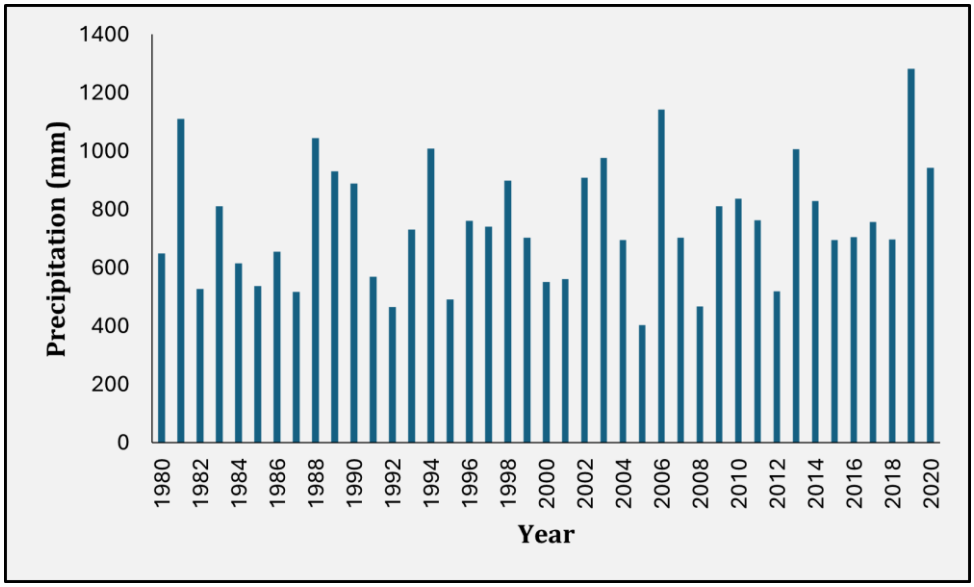


Figure 16: Annual Precipitation (mm) at Indirasagar Dam Station (1980-2020)

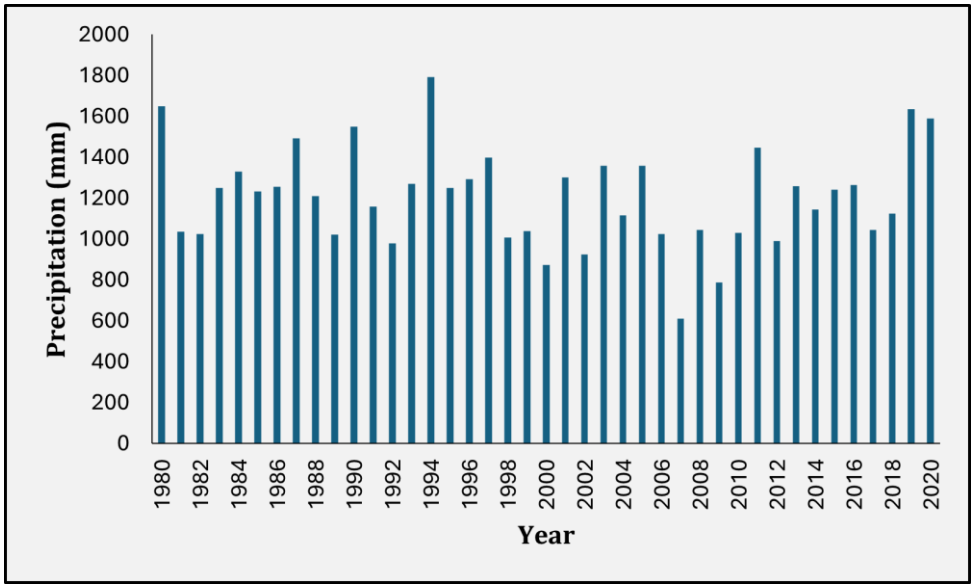


Figure 17: Annual Precipitation (mm) at Kotrai Station (1980-2020)

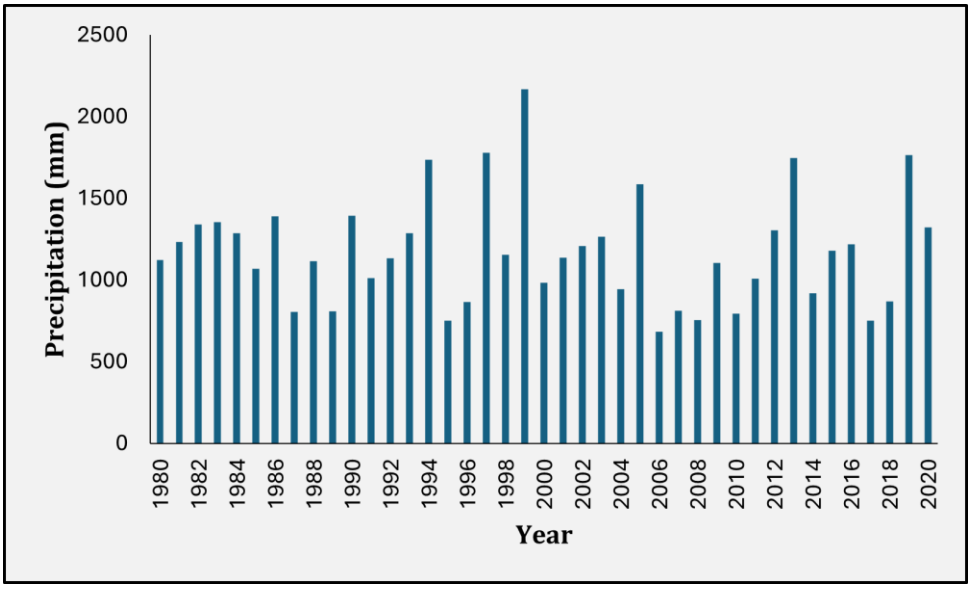


Figure 18: Annual Precipitation (mm) at Mukki Station (1980-2020)

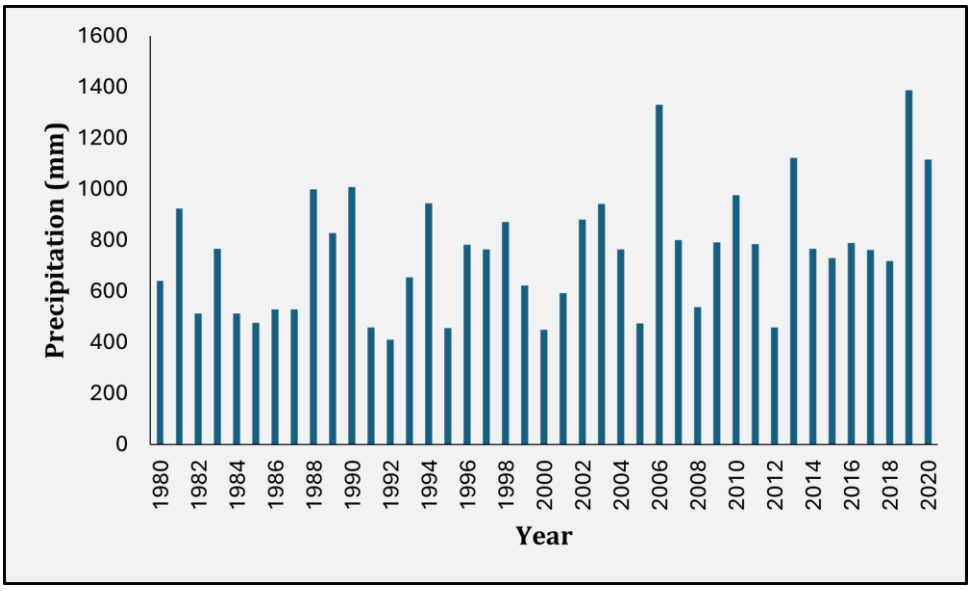


Figure 19: Annual Precipitation (mm) at Pati Station (1980-2020)

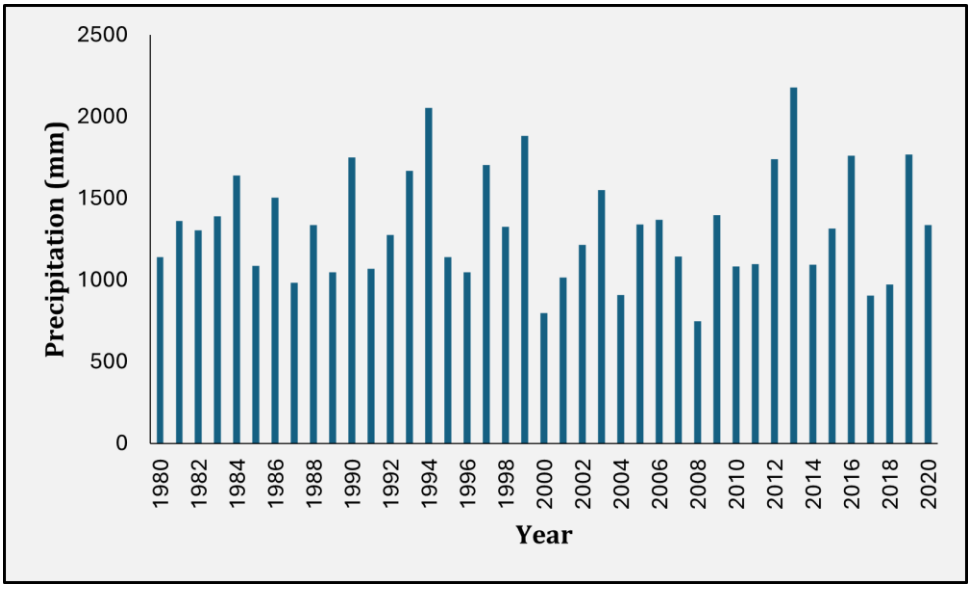


Figure 20: Annual Precipitation (mm) at Tawanagar Station (1980-2020)

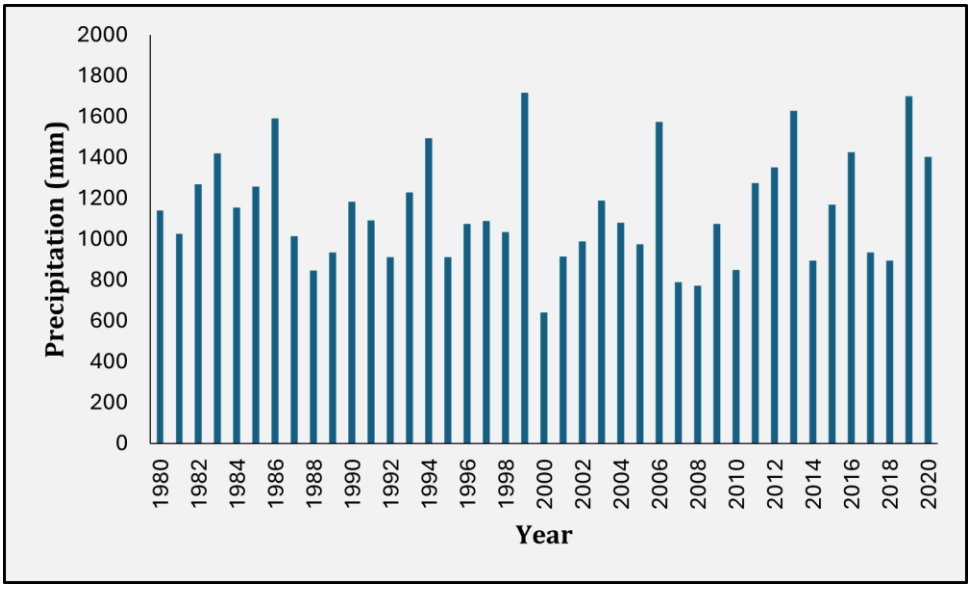


Figure 21: Annual Precipitation (mm) at Veerpur Station (1980-2020)

The observed trends indicate significant fluctuations in annual rainfall, highlighting the influence of regional climatic variability and changing weather patterns. Stations like Patan demonstrate considerable year-to-year variation, with precipitation ranging from around 600 mm to nearly 1800 mm. Such variability underscores the need for detailed temporal analysis to better understand evolving hydrological patterns, which are crucial for effective water resource planning and management within the basin. Supplementary graphs

for additional stations are provided in Annexure I, offering a more comprehensive perspective on rainfall trends across the entire basin. All underlying data used in these analyses are included in the supplementary material.

## 2. Monsoon Precipitation

The monsoon season, contributing a significant portion of the annual rainfall, is pivotal to the hydrological regime of the Narmada River Basin. Figure 22 to Figure 34 showcase monsoon precipitation trends at the same stations, emphasizing the temporal distribution of rainfall during this critical period.

The data underscore the reliance on monsoonal rainfall, with variations indicative of both inter-annual and intra-seasonal shifts. Such insights are vital for anticipating water availability and addressing potential challenges associated with extreme monsoon events, including flooding or drought conditions.

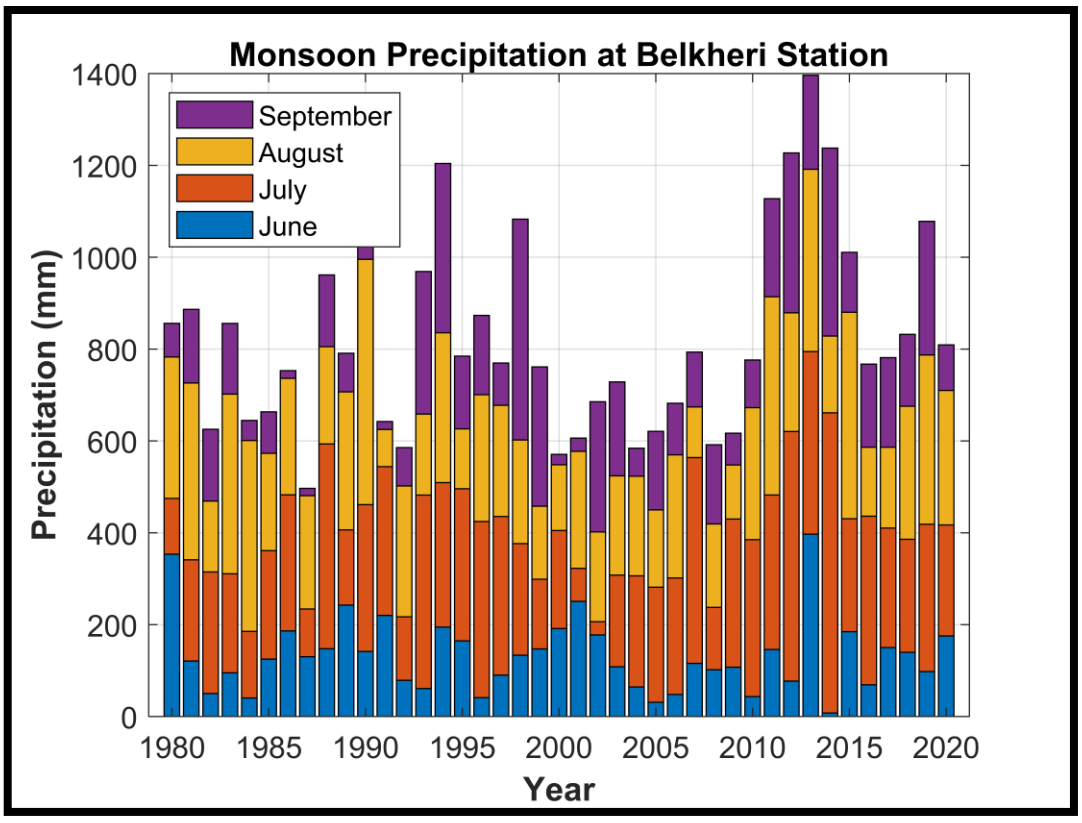


Figure 22: Monsoon Precipitation(mm) at Belkheri Station (1980-2020)

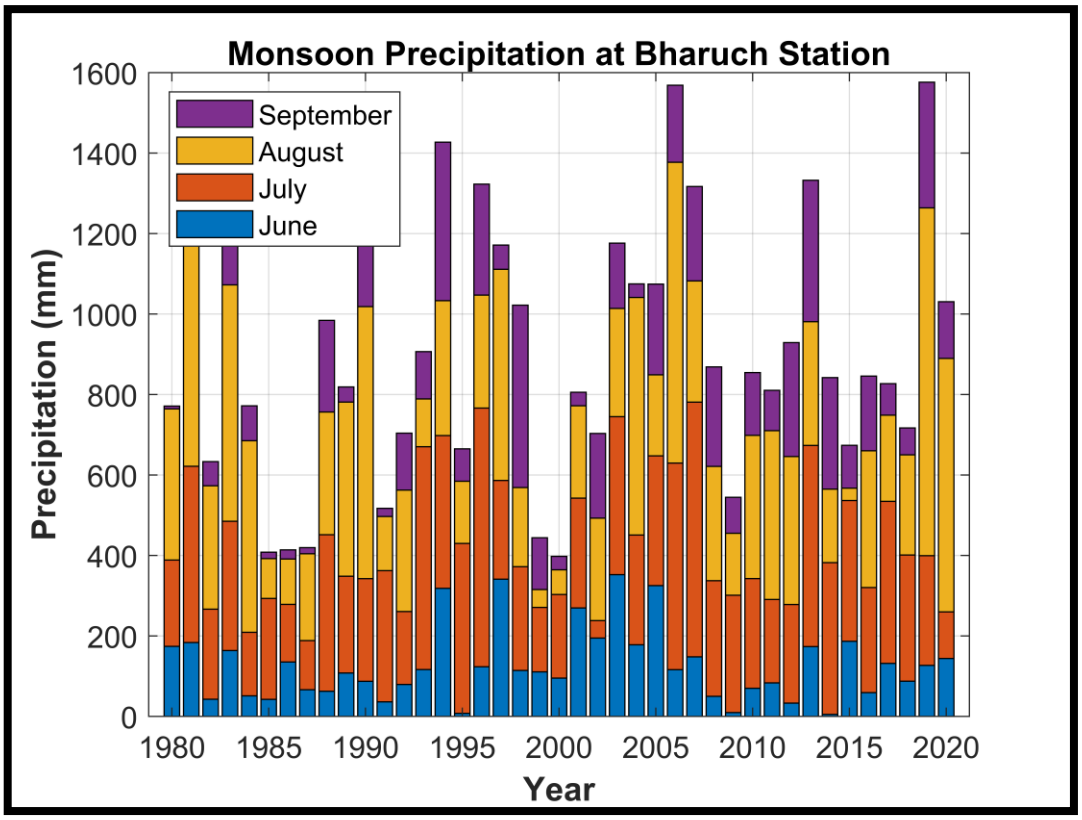


Figure 23: Monsoon Precipitation(mm) at Bharuch Station (1980-2020)

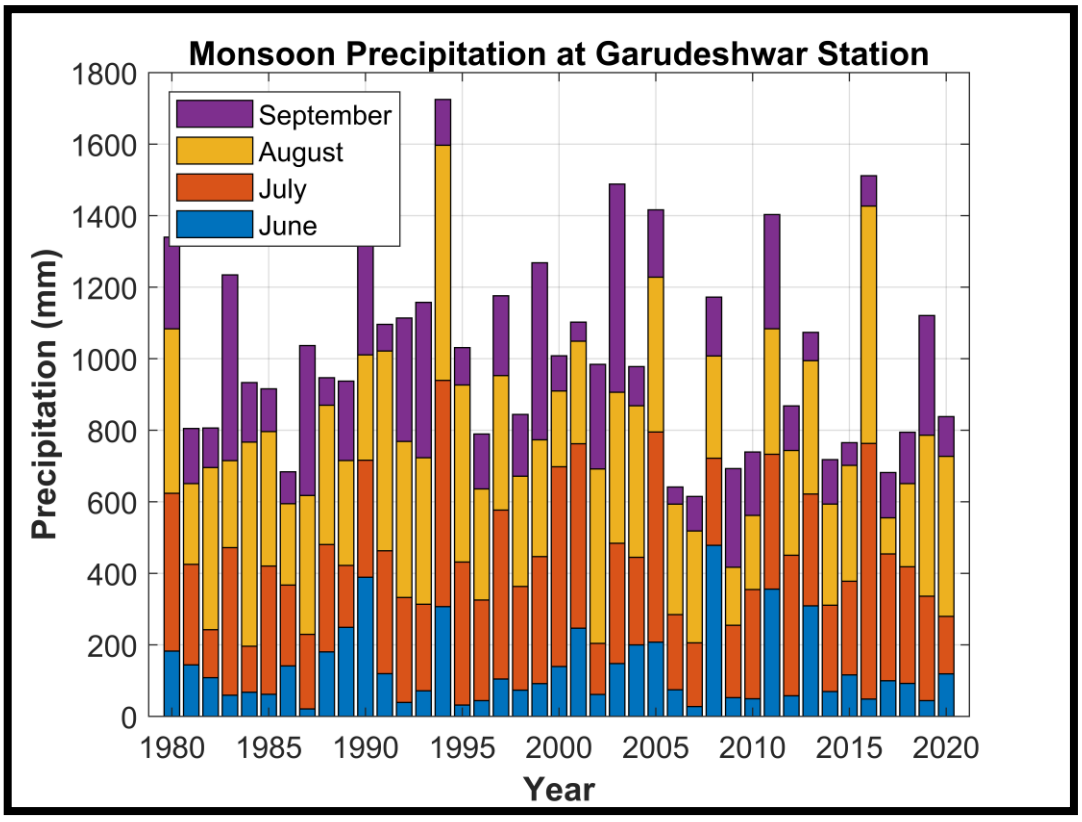


Figure 24: Monsoon Precipitation(mm) at Garudeshwar Station (1980-2020)

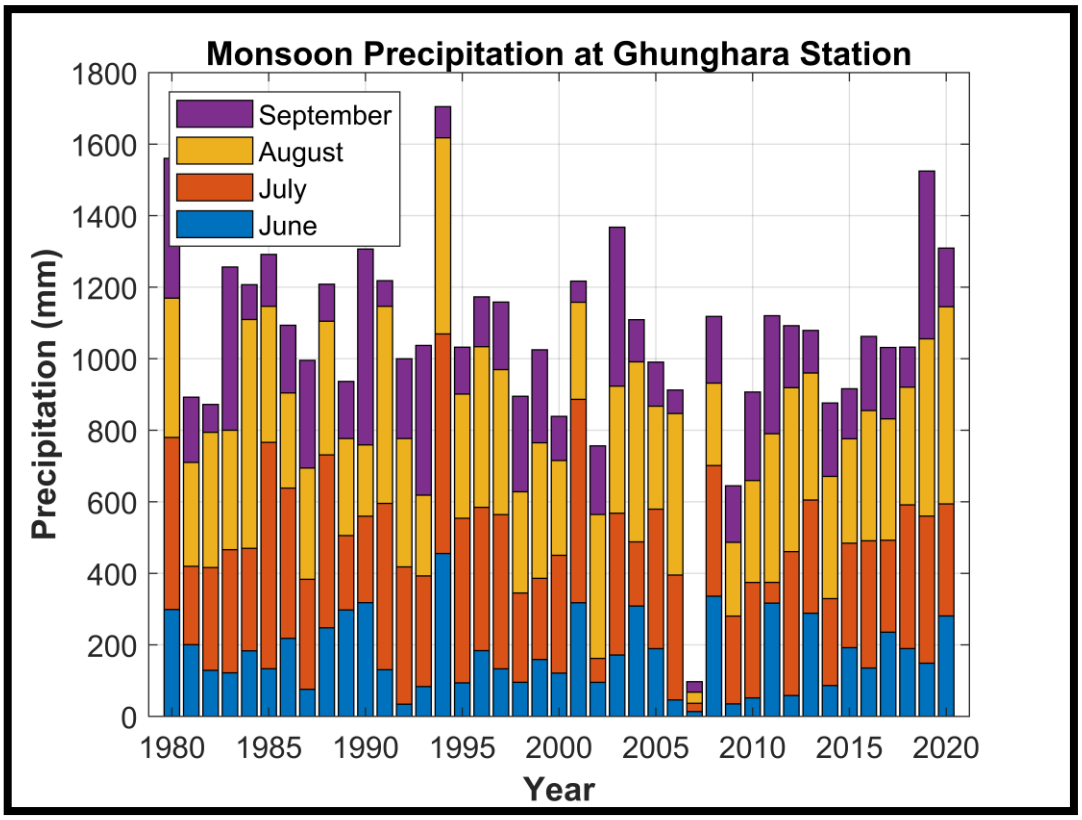


Figure 25: Monsoon Precipitation(mm) at Ghunghara Station (1980-2020)

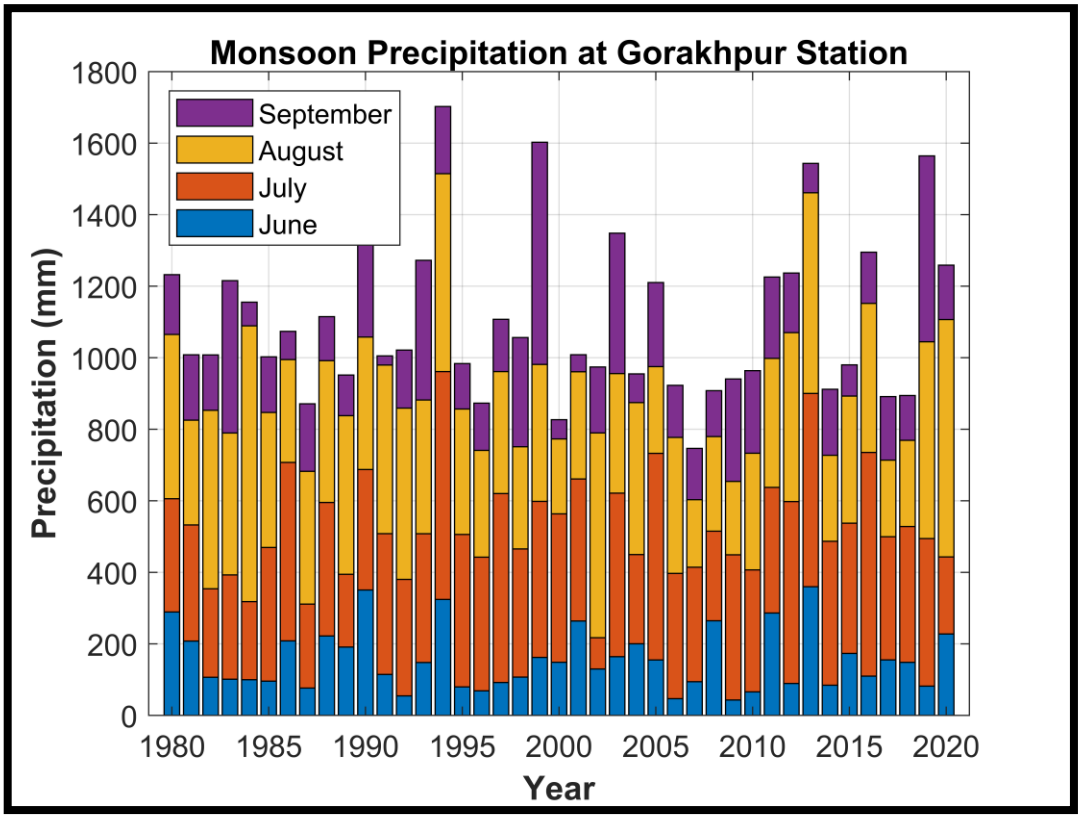


Figure 26: Monsoon Precipitation(mm) at Gorakhpur Station (1980-2020)

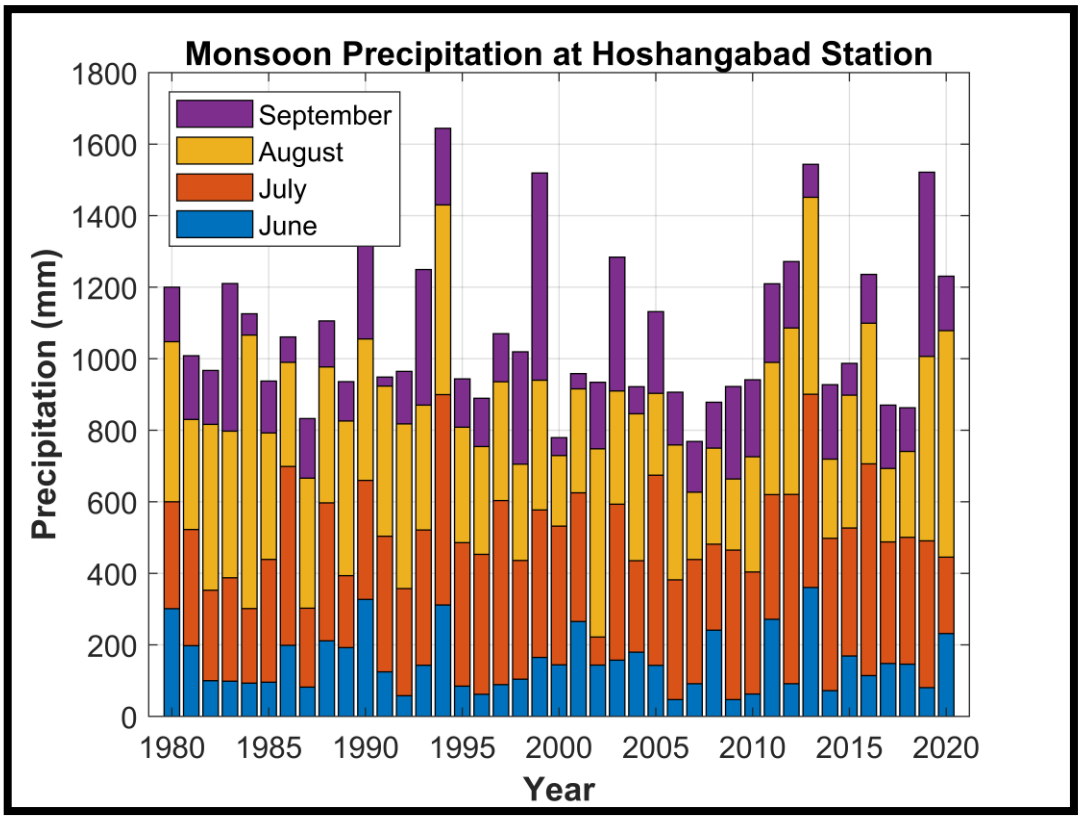


Figure 27: Monsoon Precipitation(mm) at Hoshangabad Station (1980-2020)

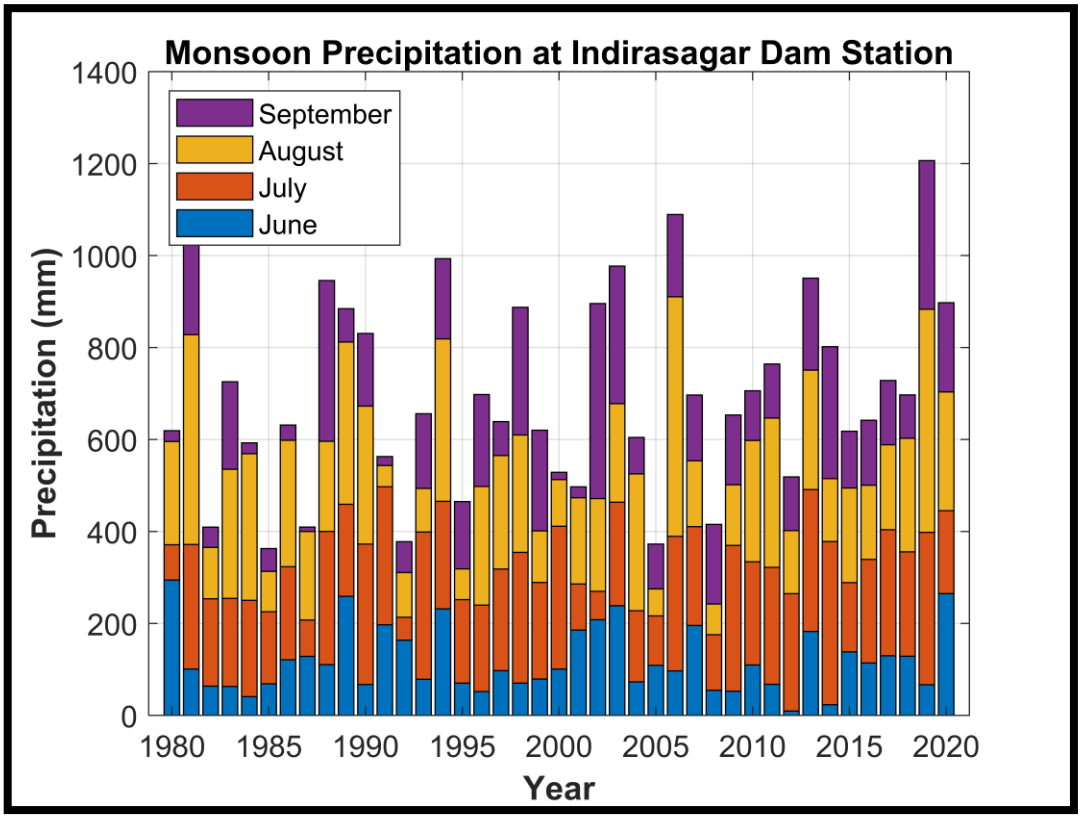


Figure 28: Monsoon Precipitation(mm) at Indirasagar Dam Station (1980-2020)

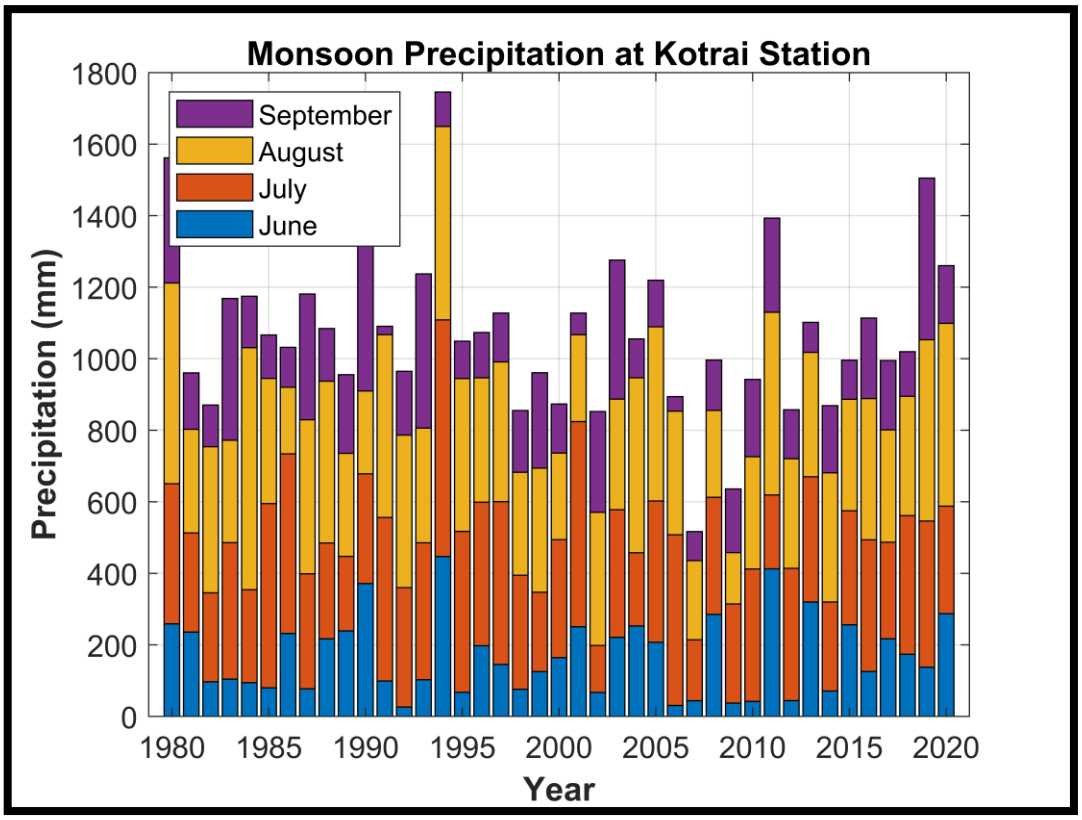


Figure 29: Monsoon Precipitation(mm) at Kotrai Station (1980-2020)

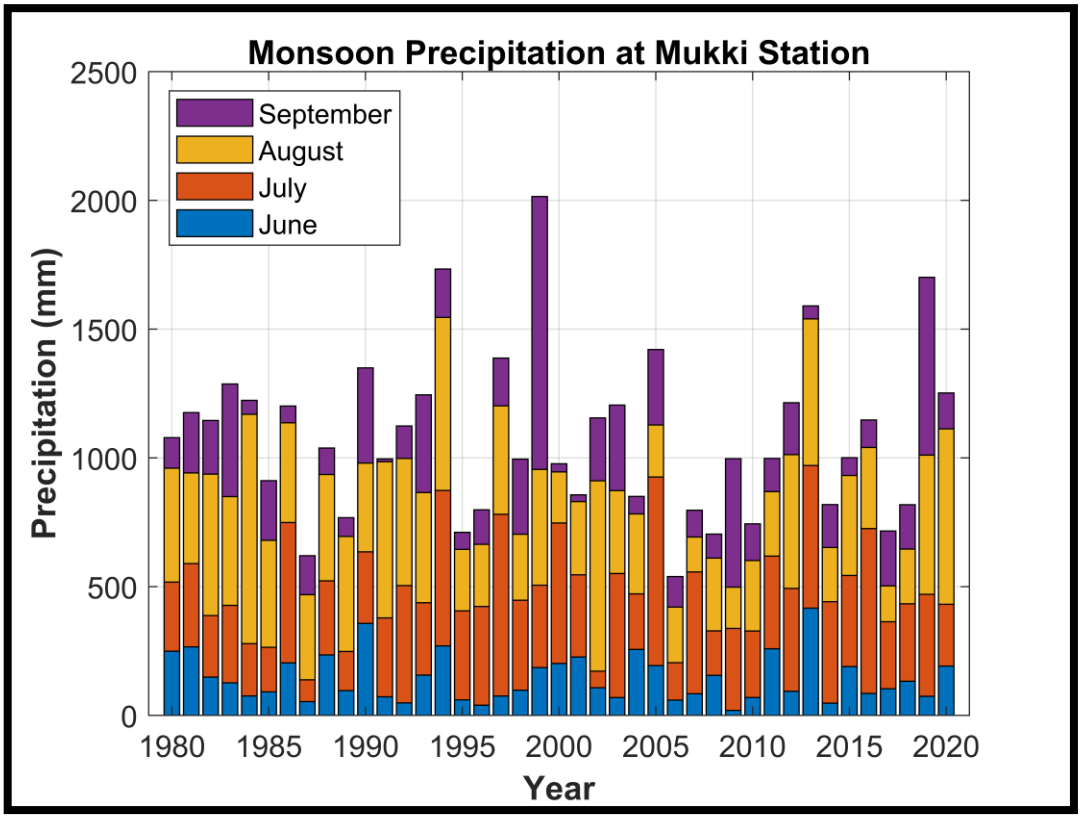


Figure 30: Monsoon Precipitation(mm) at Mukki Station (1980-2020)

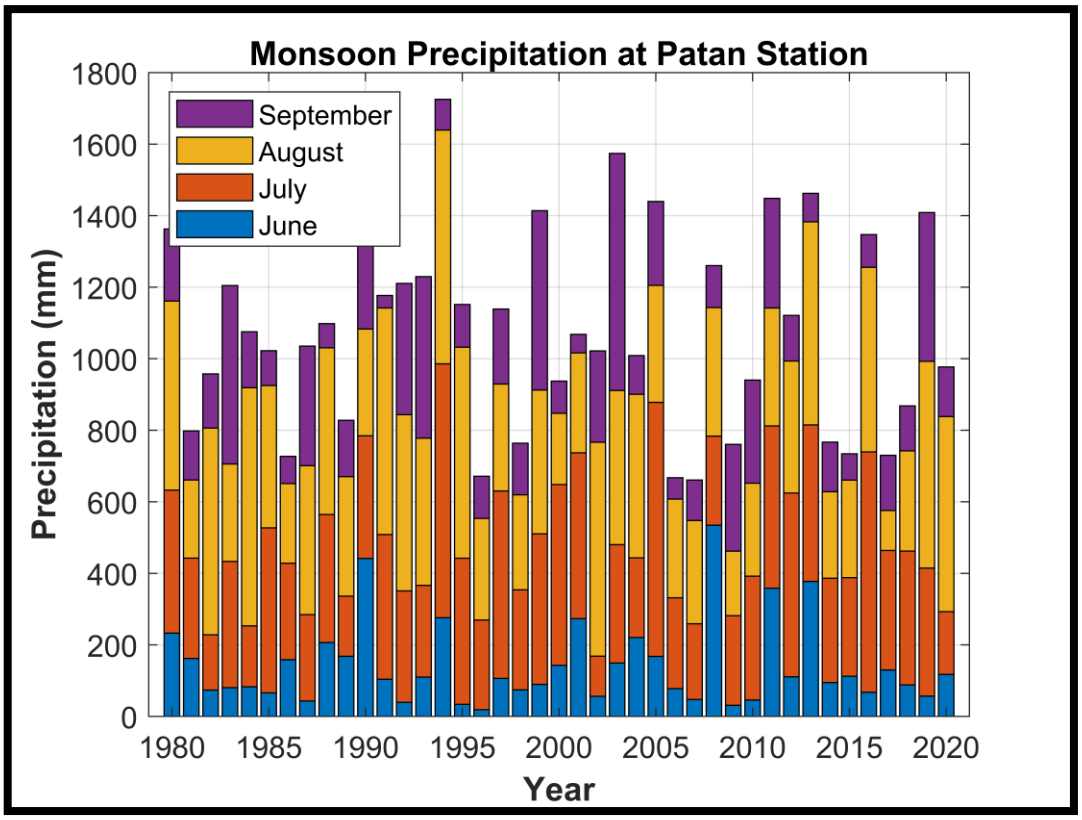


Figure 31: Monsoon Precipitation(mm) at Patan Station (1980-2020)

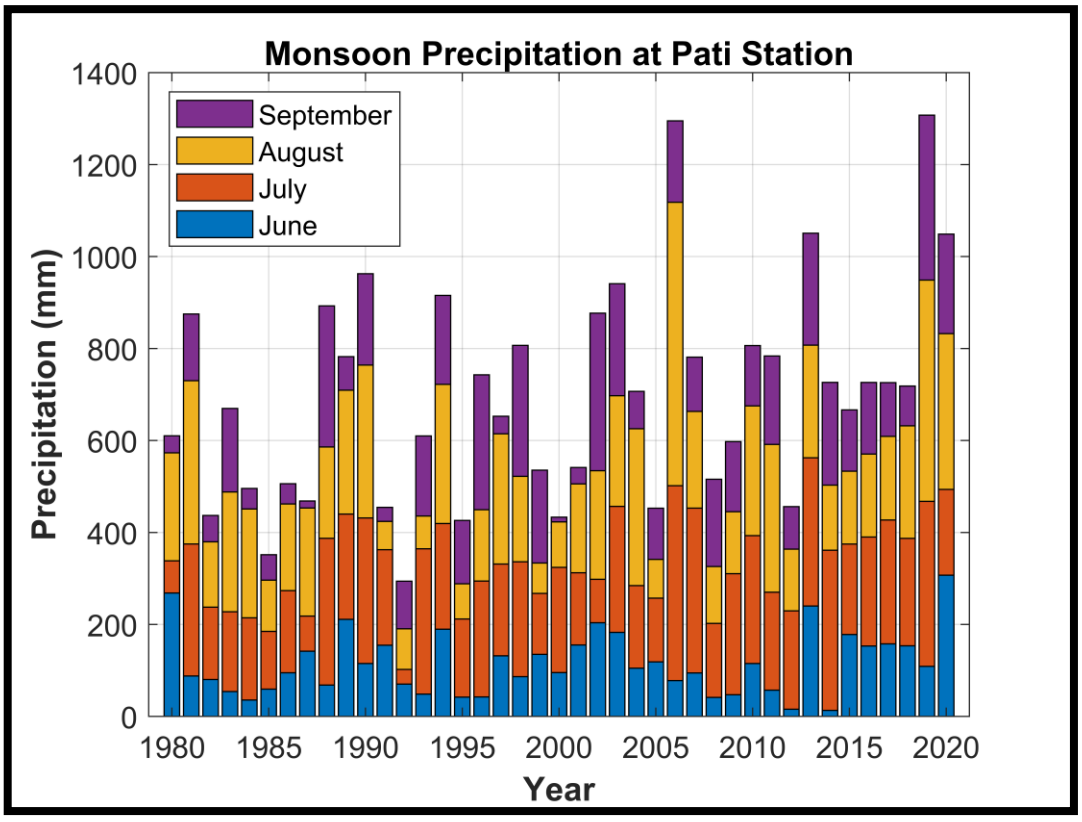


Figure 32: Monsoon Precipitation(mm) at Pati Station (1980-2020)

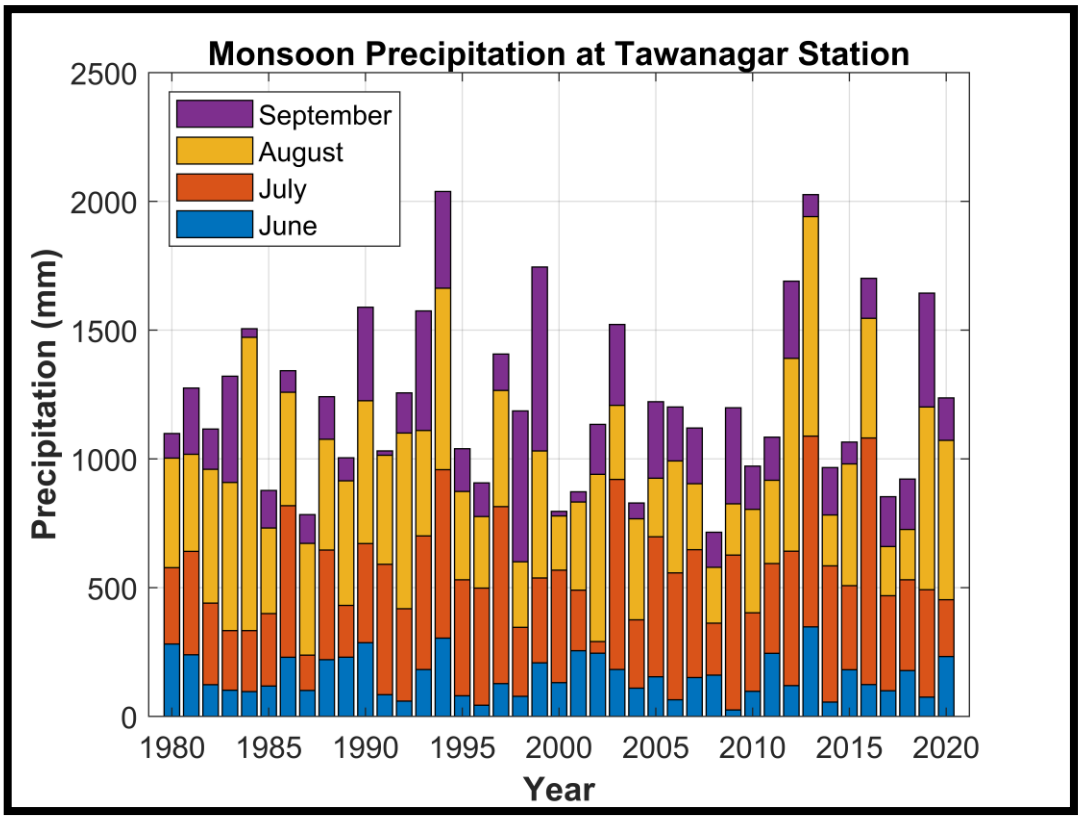


Figure 33: Monsoon Precipitation(mm) at Tawanagar Station (1980-2020)

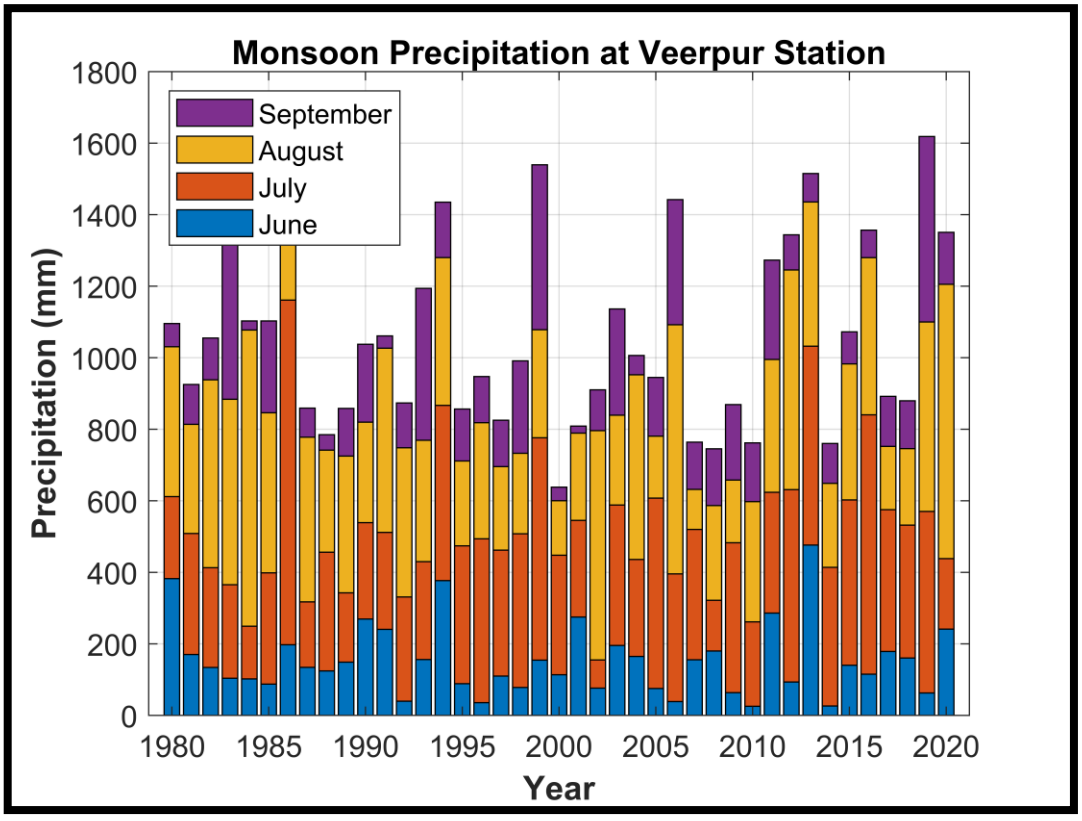


Figure 34: Monsoon Precipitation(mm) at Veerpur Station (1980-2020)

Additional graphs for other stations are included in the annexure I, providing a comprehensive view of basin-wide trends. All data used for these plots and additional analyses are provided in the supplementary material.

## 3.3 TEMPERATURE

The temporal variation of temperature in the Narmada River Basin from 1980 to 2020 highlights critical insights into the region's changing climatic dynamics. Monthly temperature trends across several key stations, including Belkheri, Bharuch, Garudeshwar, Ghunghara, and others, reveal significant patterns of seasonal and annual variability. Figure 35 to Figure 47 provide a visual representation of these trends.

Seasonal peaks in temperature are observed during the summer months, with notable fluctuations between stations. For instance, Bharuch station, located in the lower basin near the coast, consistently records higher temperatures than upper-basin stations such as Belkheri, influenced by altitude and proximity to water bodies.

The increasing temperature trend observed in most stations has important implications for hydrological and ecological systems. It points to rising evapotranspiration rates, which can impact water balance and agricultural productivity across the basin.

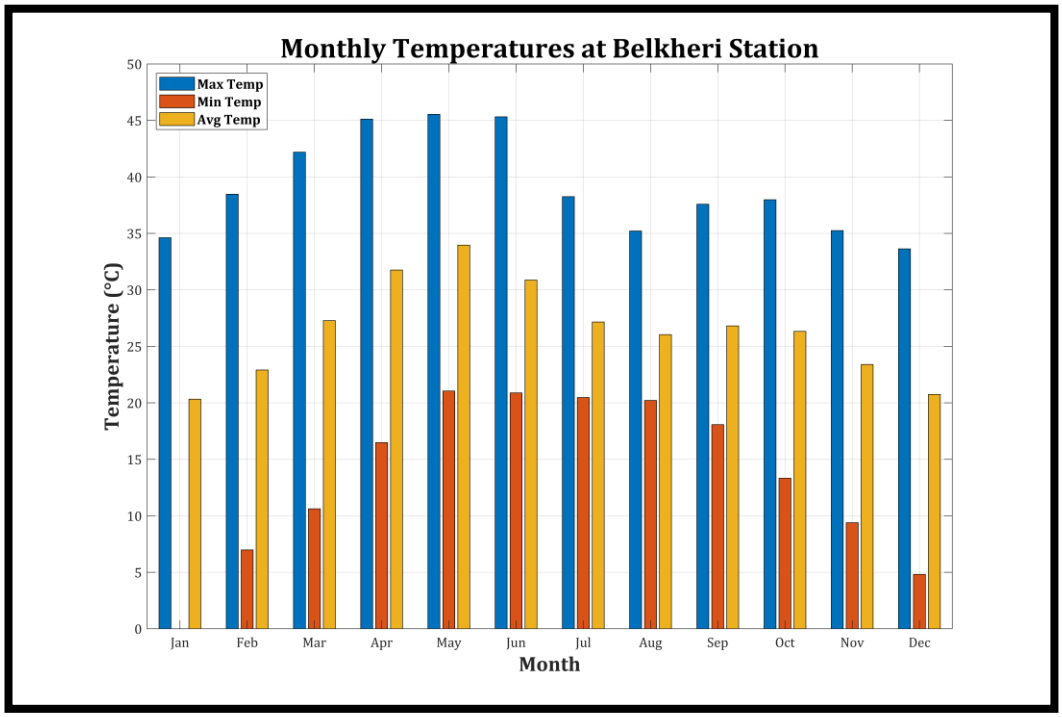


Figure 35: Monthly Temperature (°C) trends at Belkheri Station (1980–2020)

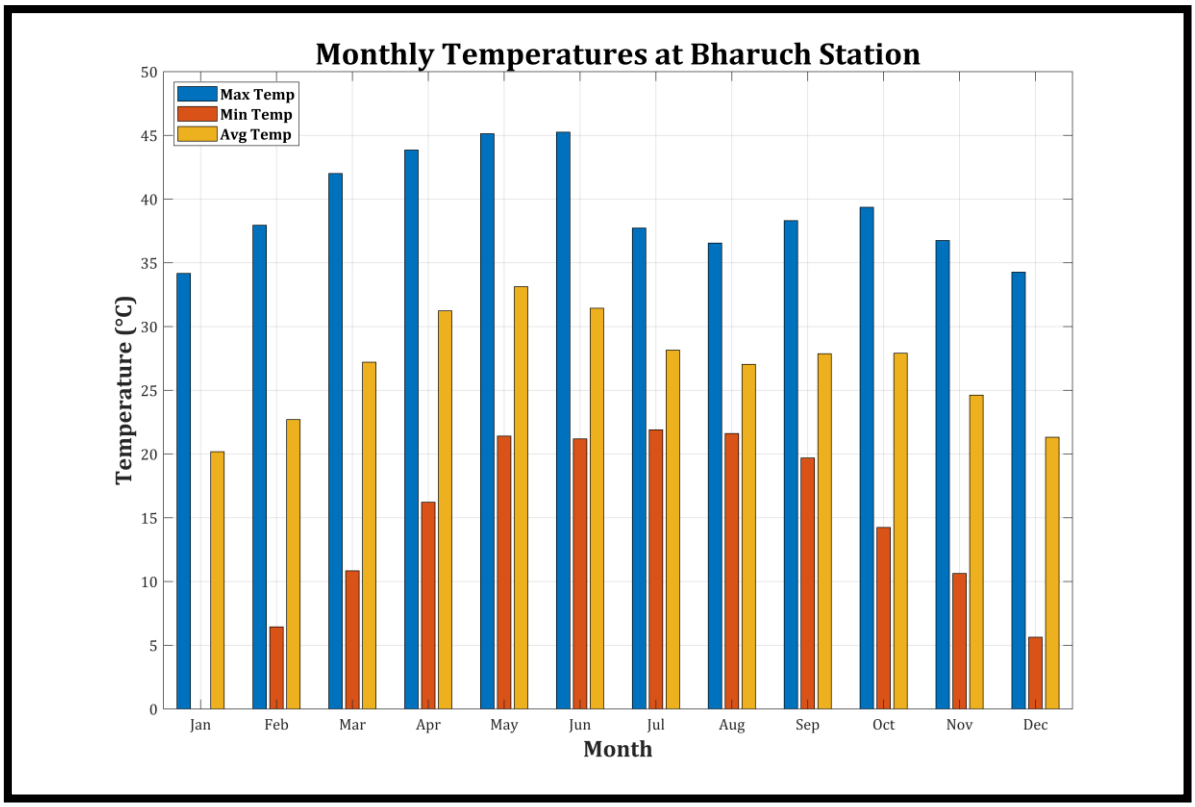


Figure 36: Monthly Temperature (°C) trends at Bharuch Station (1980–2020)

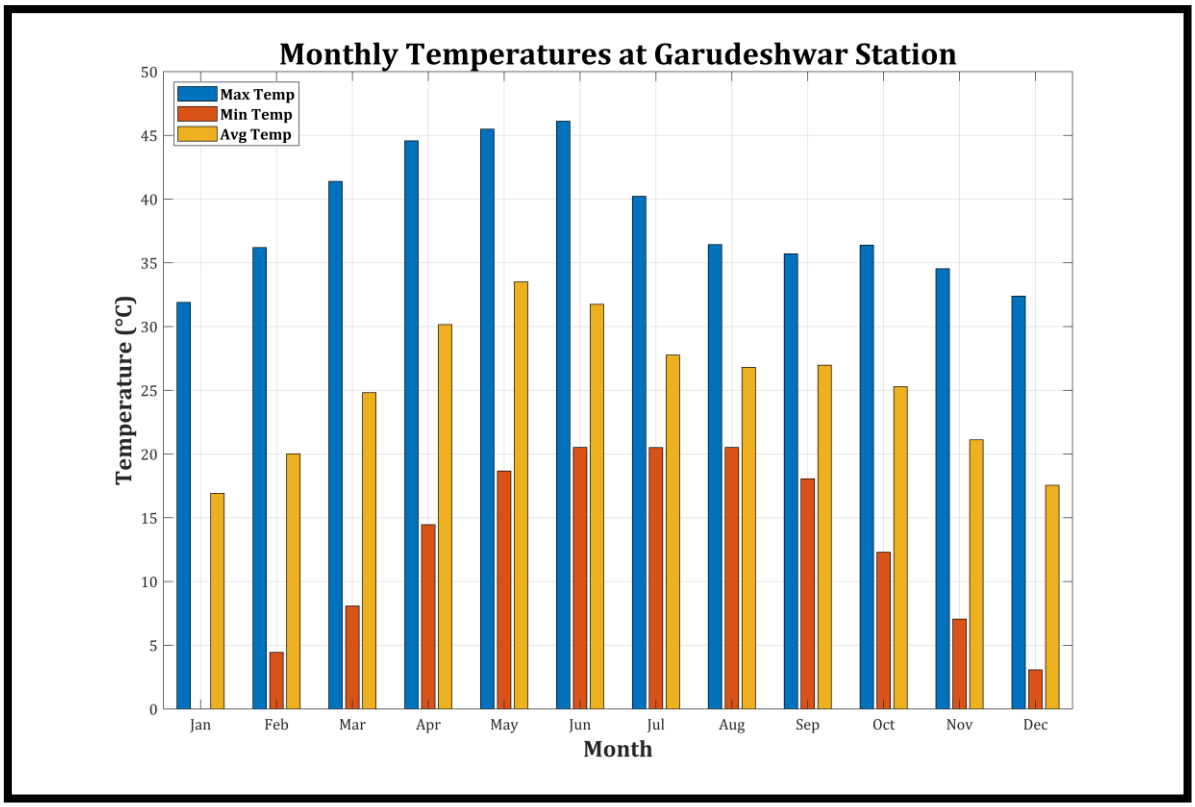


Figure 37: Monthly Temperature (°C) trends at Garudeshwar Station (1980–2020)

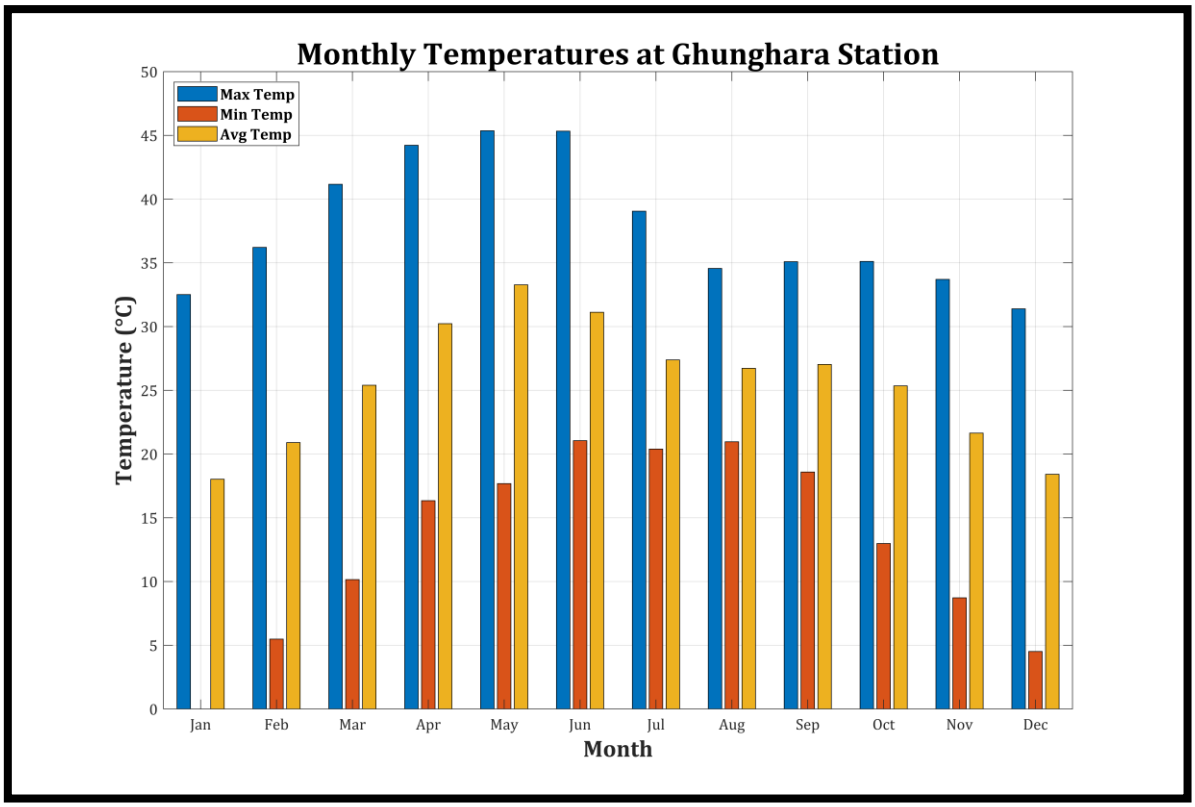


Figure 38: Monthly Temperature (°C) trends at Ghunghara Station (1980–2020)

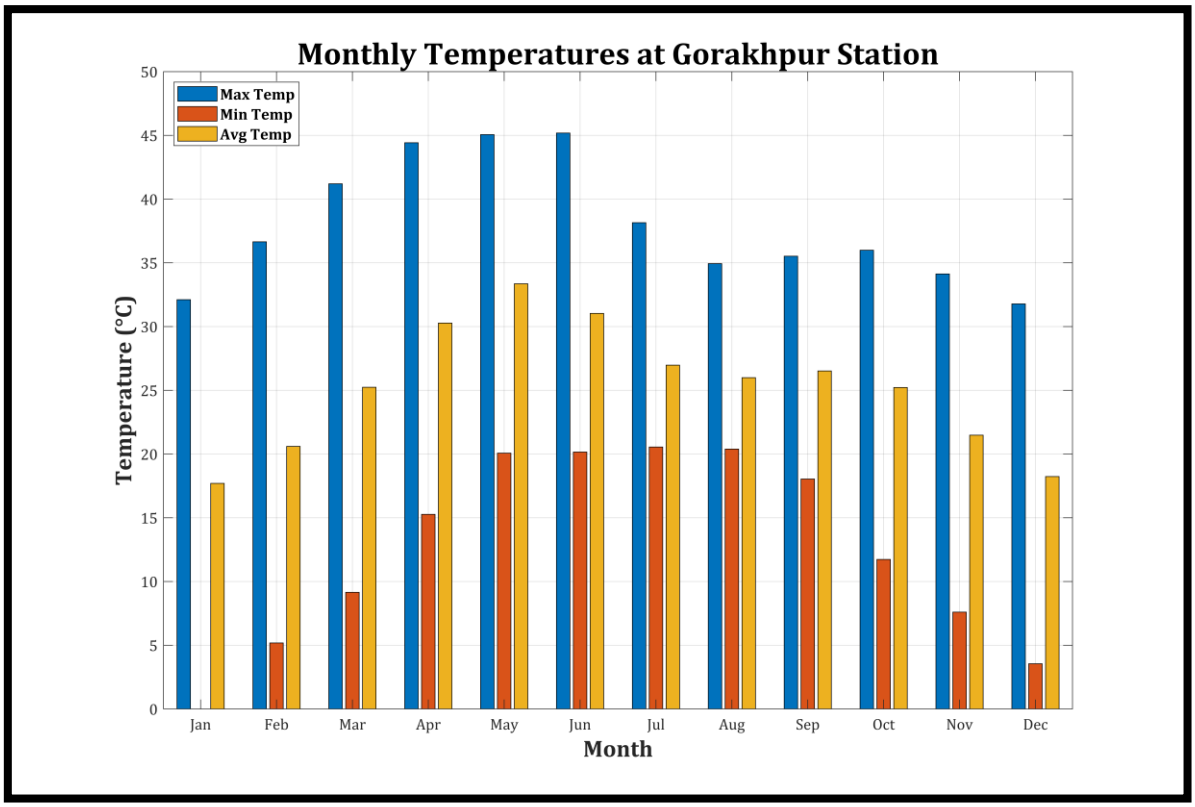


Figure 39: Monthly Temperature (°C) trends at Gorakhpur Station (1980–2020)

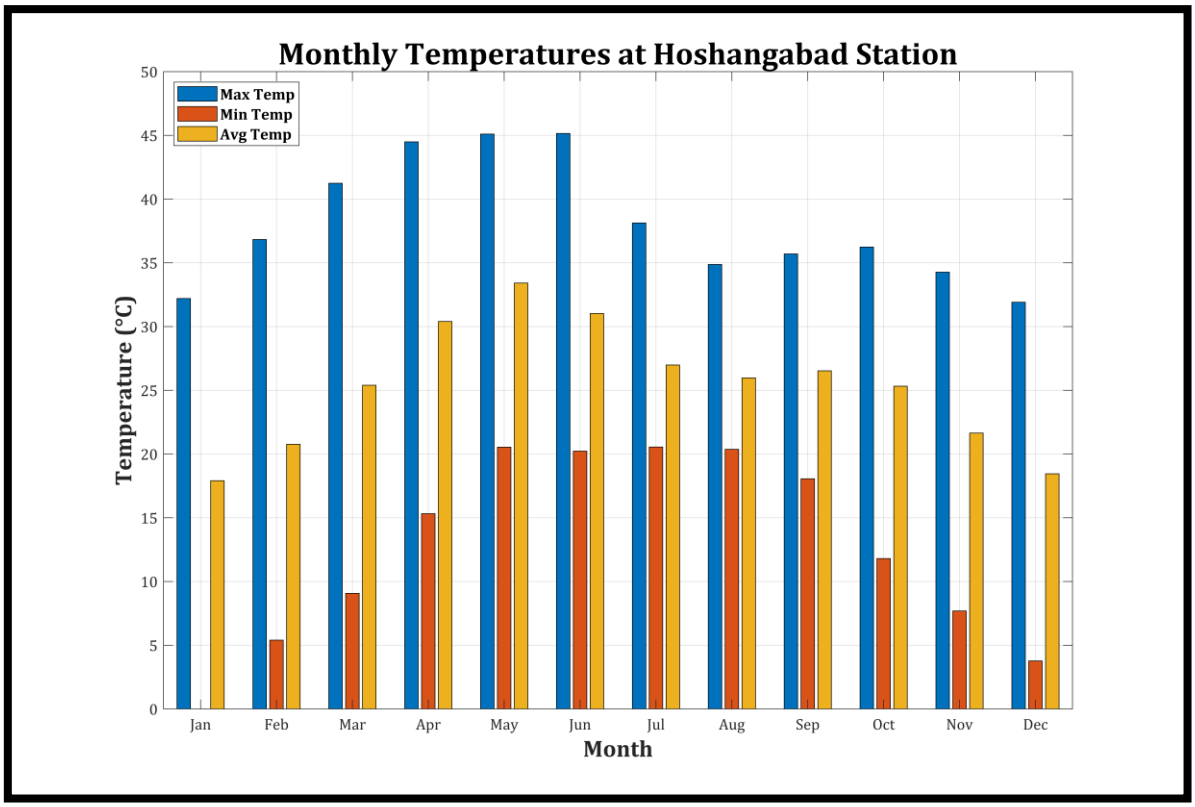


Figure 40: Monthly Temperature (°C) trends at Hoshangabad Station (1980–2020)

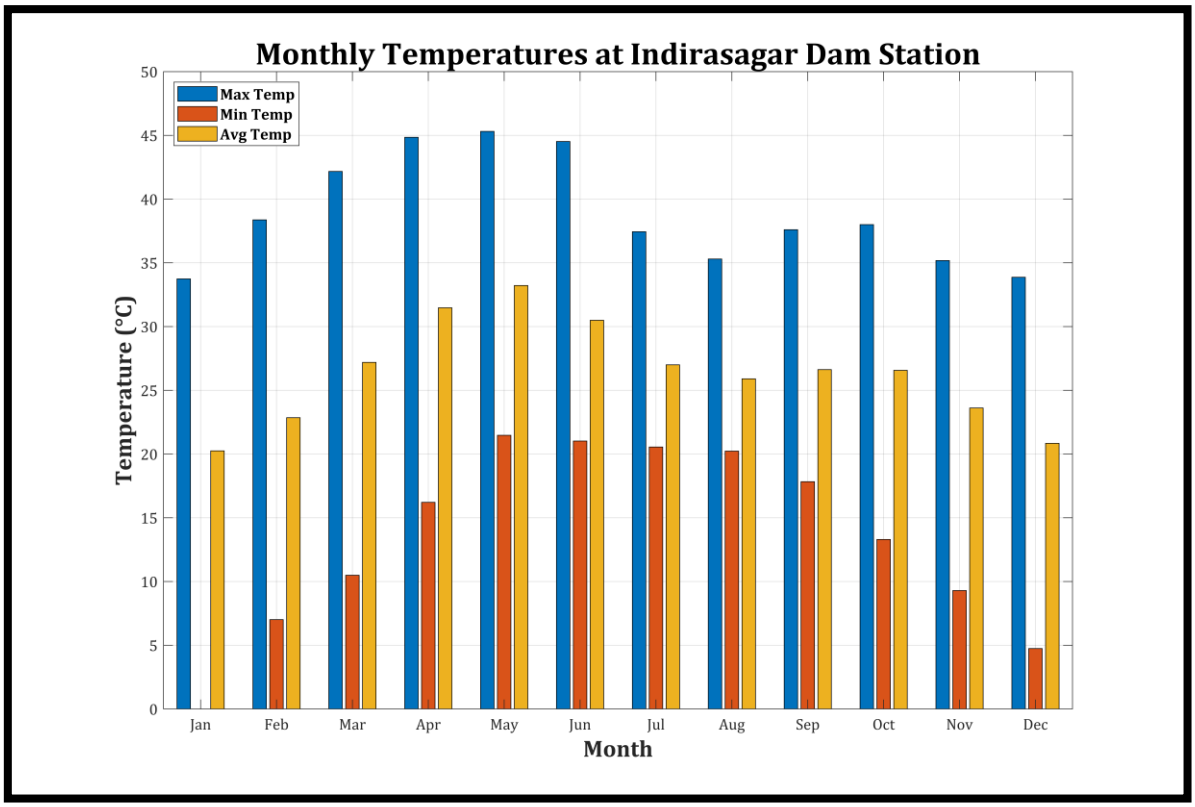


Figure 41: Monthly Temperature (°C) trends at Indirasagar Dam Station (1980–2020)

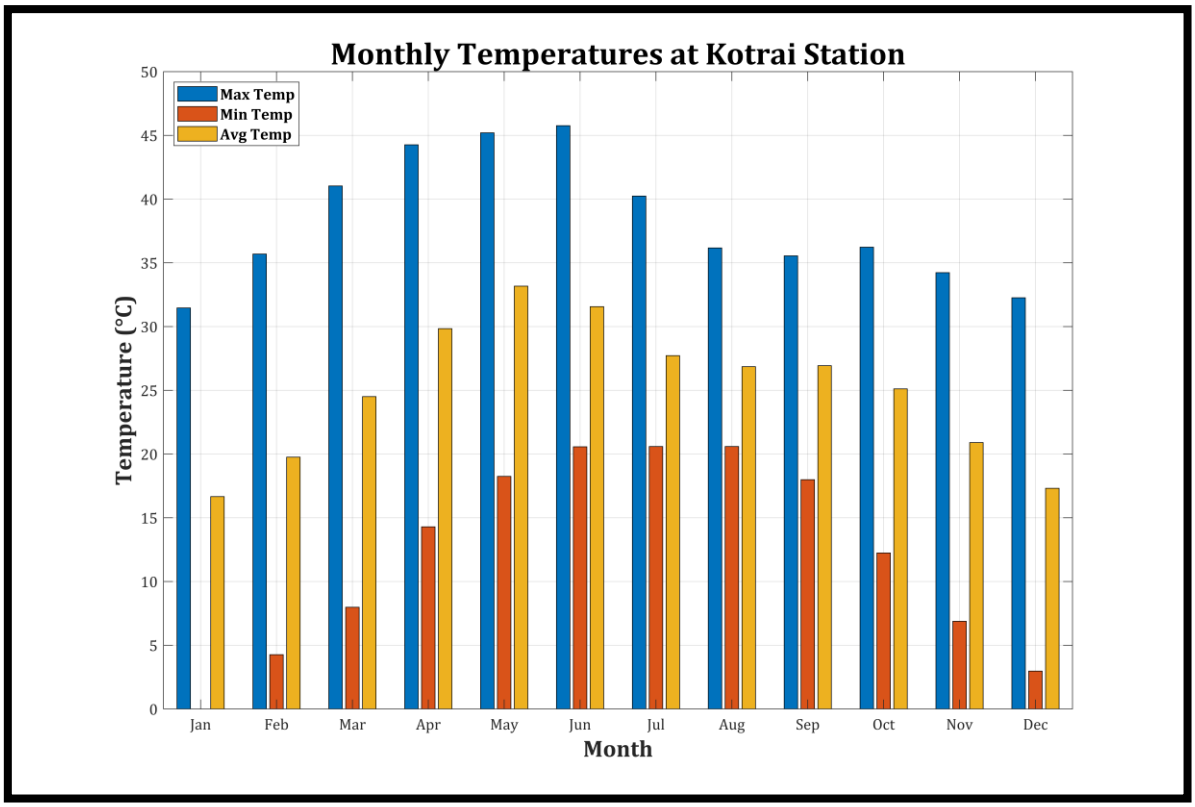


Figure 42: Monthly Temperature (°C) trends at Kotrai Station (1980–2020)

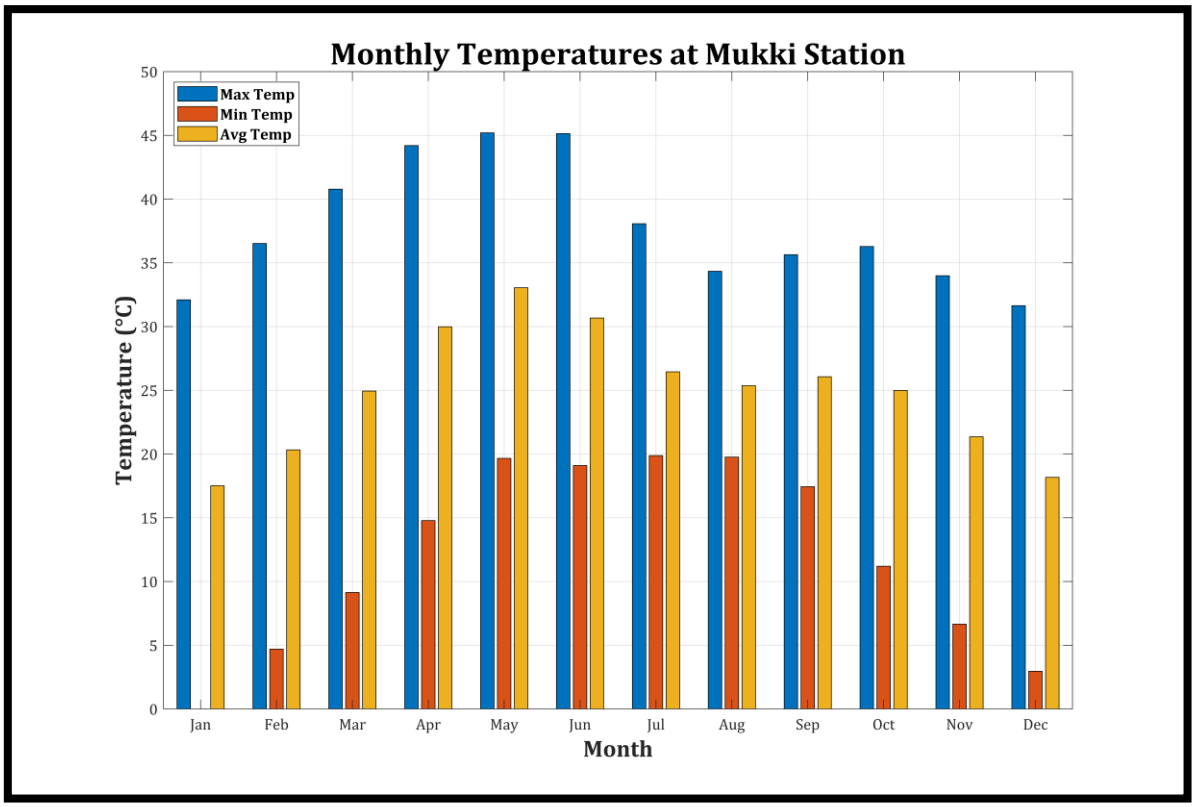


Figure 43: Monthly Temperature (°C) trends at Mukki Station (1980–2020)

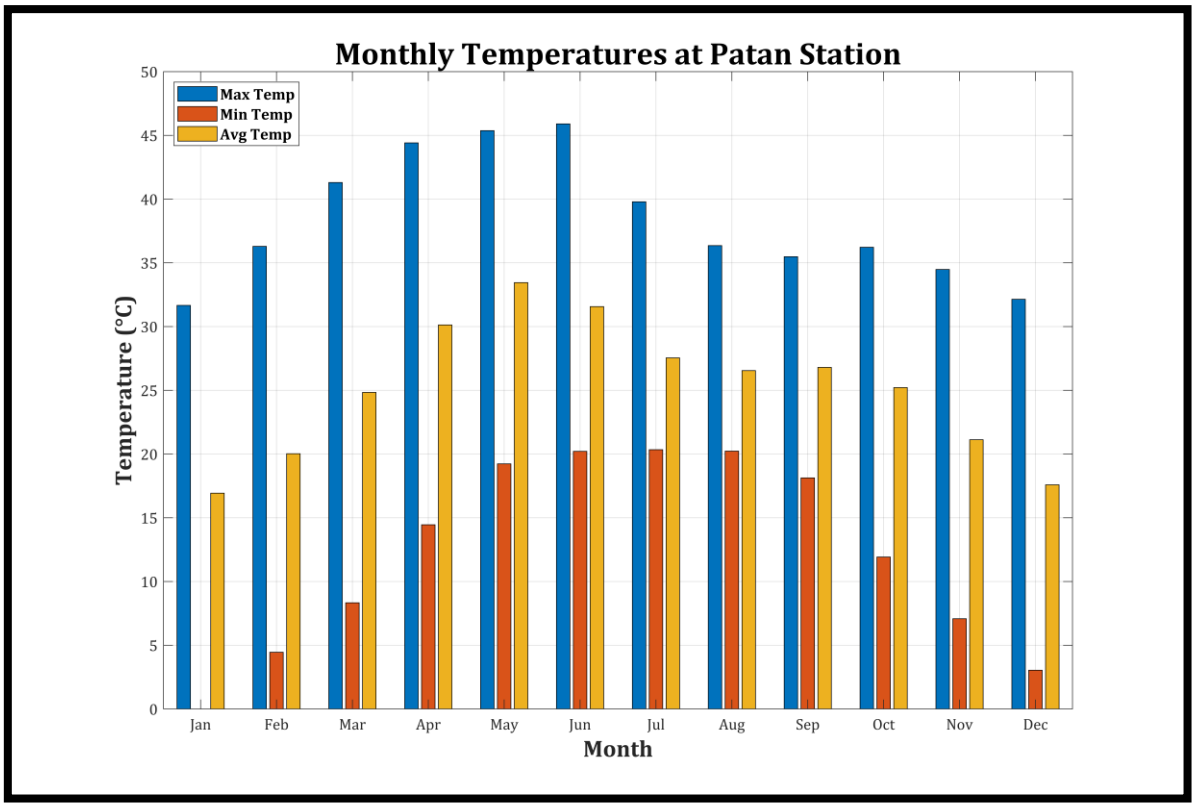


Figure 44: Monthly Temperature (°C) trends at Patan Station (1980–2020)

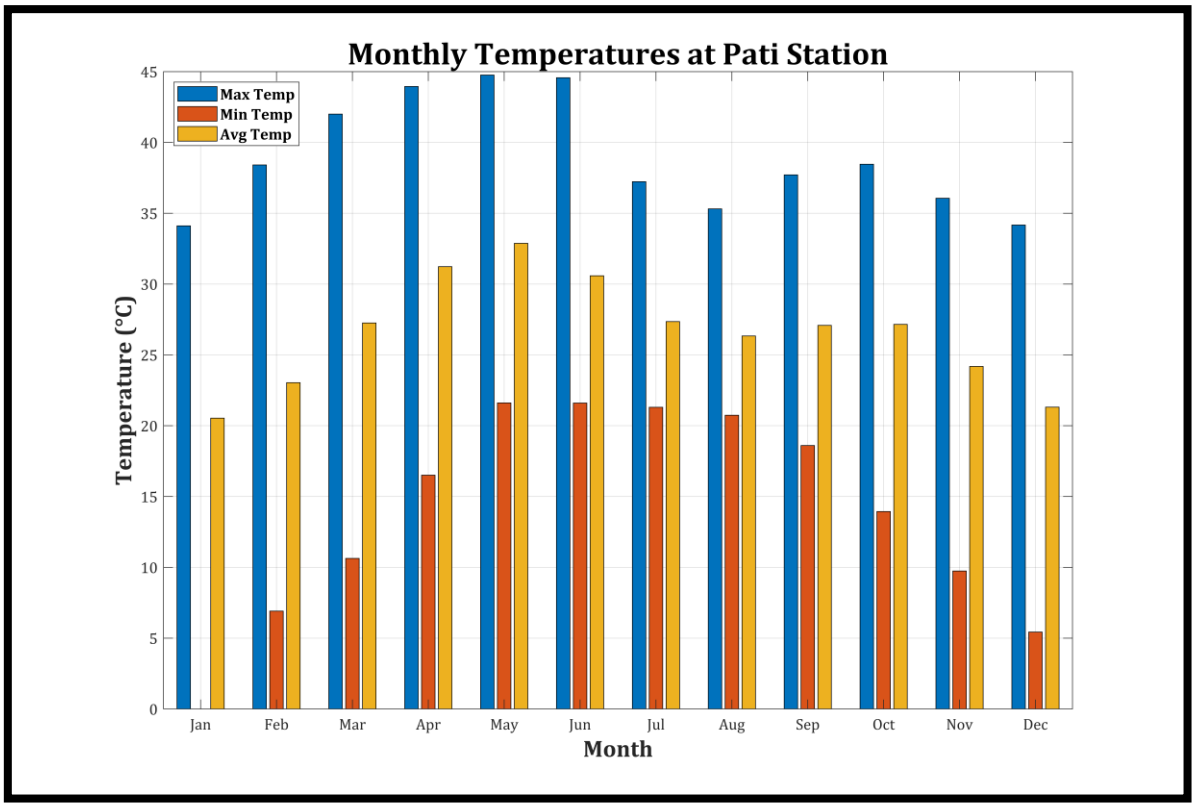


Figure 45: Monthly Temperature (°C) trends at Pati Station (1980–2020)

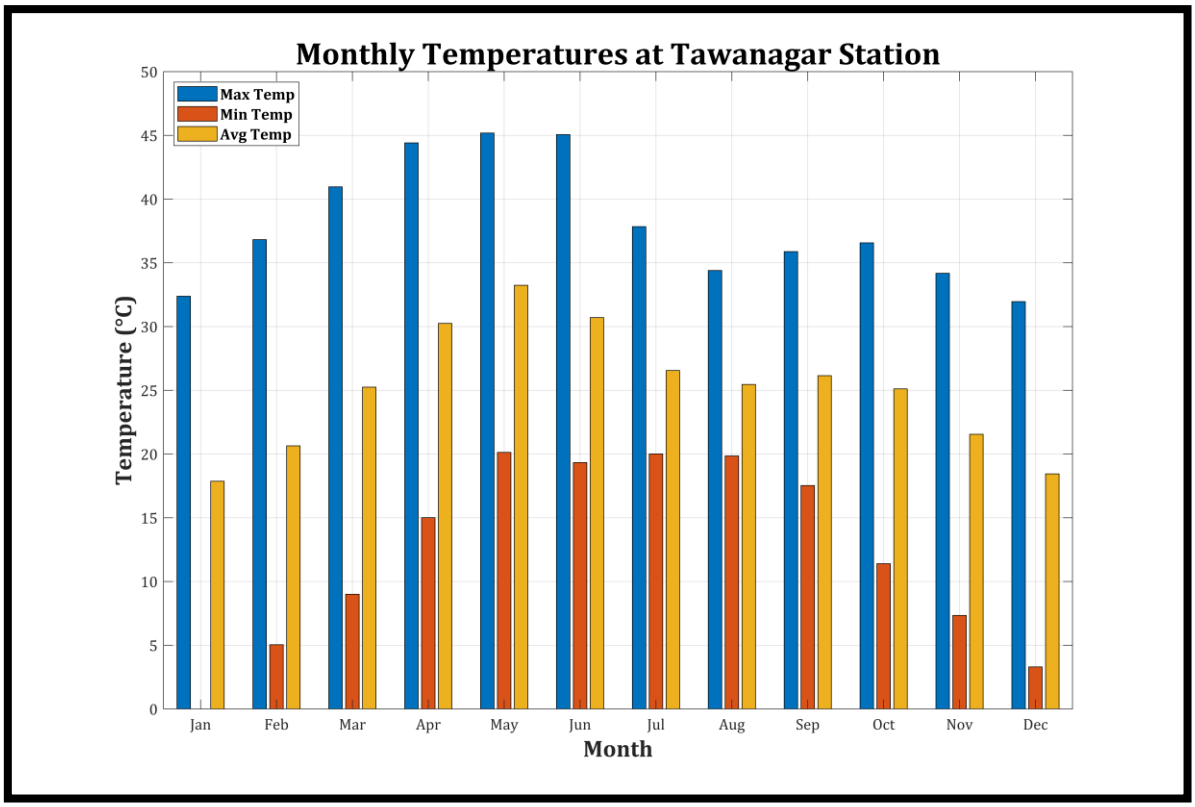


Figure 46: Monthly Temperature (°C) trends at Tawanagar Station (1980–2020)

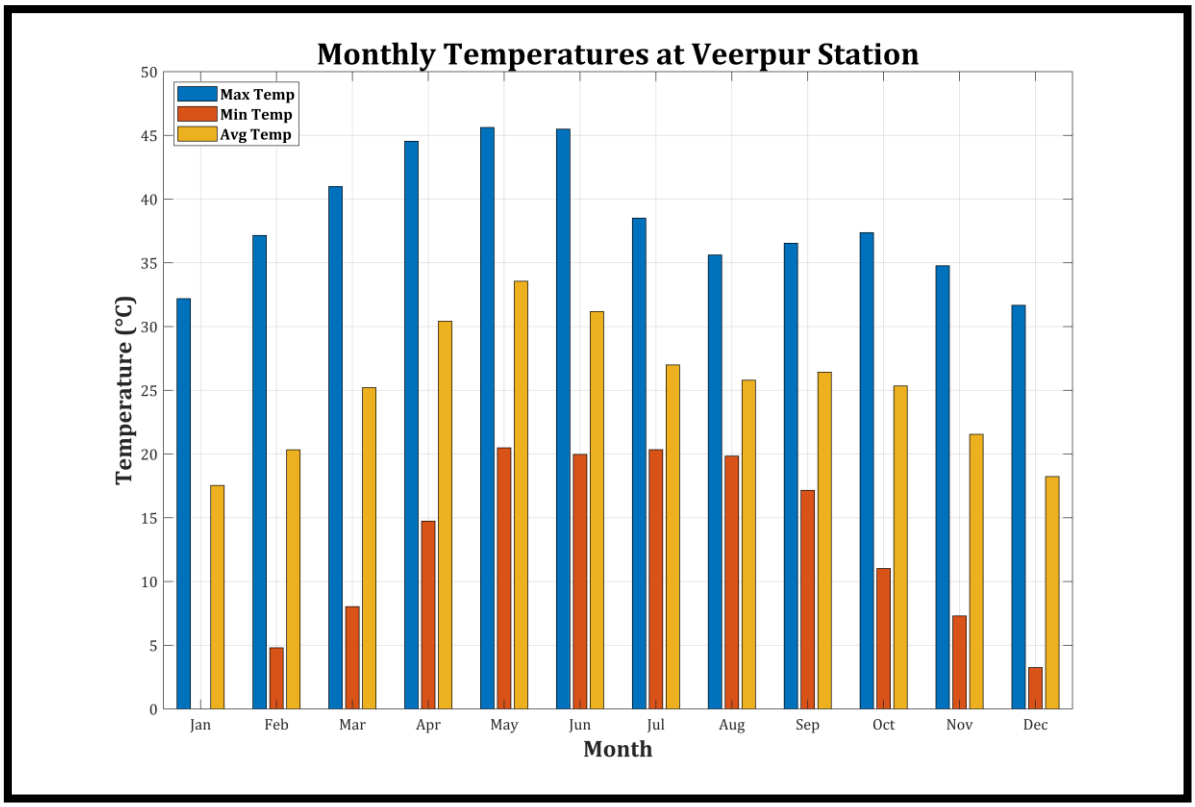


Figure 47: Monthly Temperature (°C) trends at Veerpur Station (1980–2020)

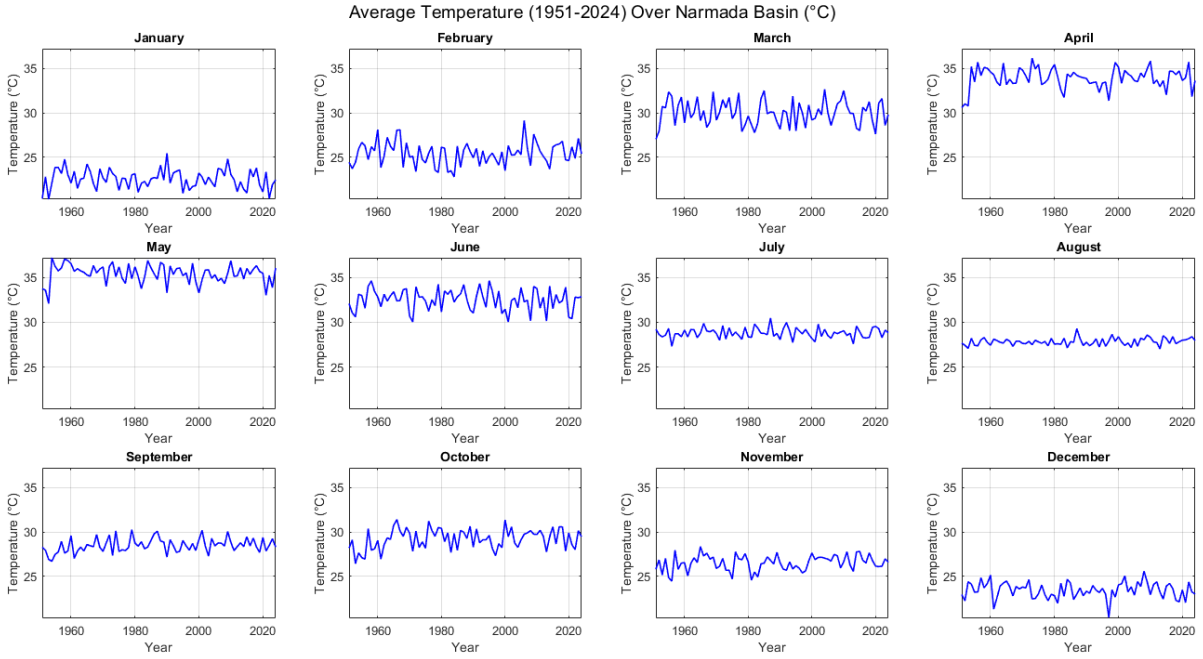


Figure 48:Temporal Variation of Average Temperature (1951-2024) Over Narmada Basin (ERA5)

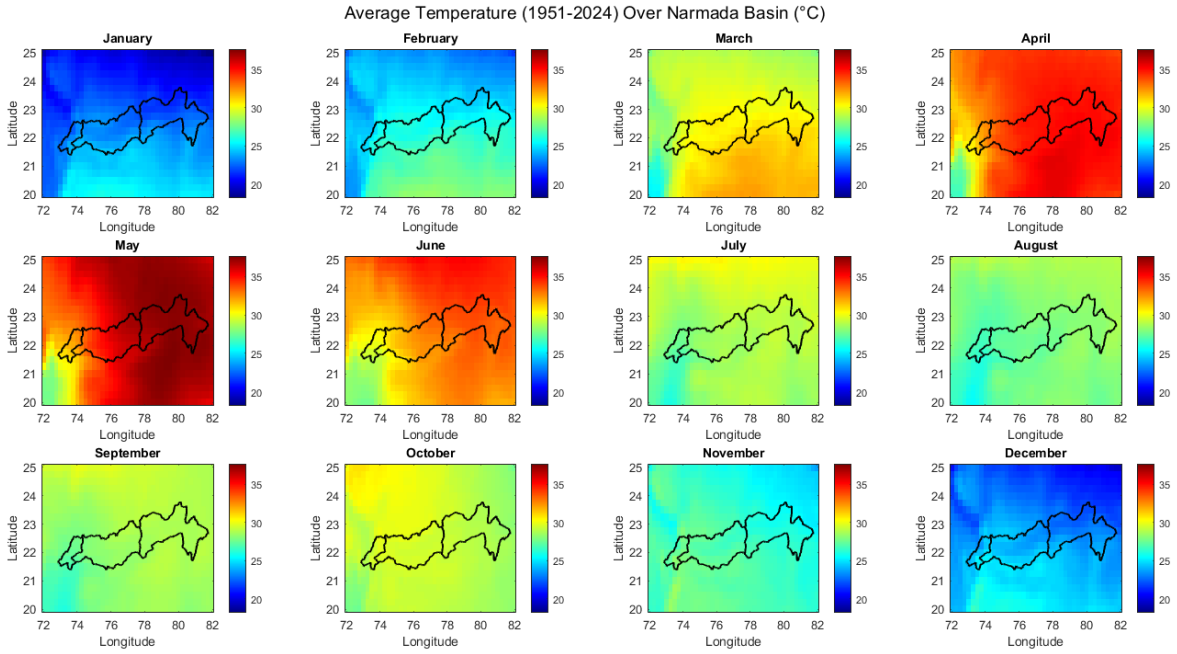


Figure 49: Spatial Variation of Average Temperature (1951-2024) Over Narmada Basin (ERA5)

The spatial variability in temperature trends across the basin underscores the influence of local geographical and climatic factors. Coastal regions like Bharuch not only exhibit higher average temperatures but also experience smaller seasonal variations compared to inland and higher-altitude stations. Such spatial differences emphasize the need for region-

specific strategies to manage the impacts of rising temperatures on water resources and agriculture. Additional graphs for other stations are included in the annexure II, providing a comprehensive view of basin-wide trends. All data used for these plots and additional analyses are provided in the supplementary material.

## 3.4 WIND

Wind speed plays a critical role in various hydrological and environmental processes, affecting evaporation, surface water dynamics, and overall climatic behaviour. This section presents a comprehensive analysis of wind speed trends at multiple stations across the study region over the past four decades. The analysis utilizes both monthly average wind speed and annual average wind speed data to highlight temporal variations and long-term changes.

### 3.4.1 Annual Wind Speed Trends

Annual average wind speed are depicted for 6 stations (e.g.,Figure 50: Annual Average Wind Speed at Belkheri Station). The results indicate a noticeable decline in average wind speeds over the 40-year study period. At Belkheri Station, for example, the average wind speed decreased from approximately 2.95 m/s in the early 1980s to around 2.3 m/s by 2020. This reduction in wind speed may be attributed to changing climatic conditions, urbanization, or large-scale environmental shifts affecting wind dynamics. Such long-term trends are significant for assessing potential impacts on regional hydrology, including changes in evaporation rates and their implications for water resource management.

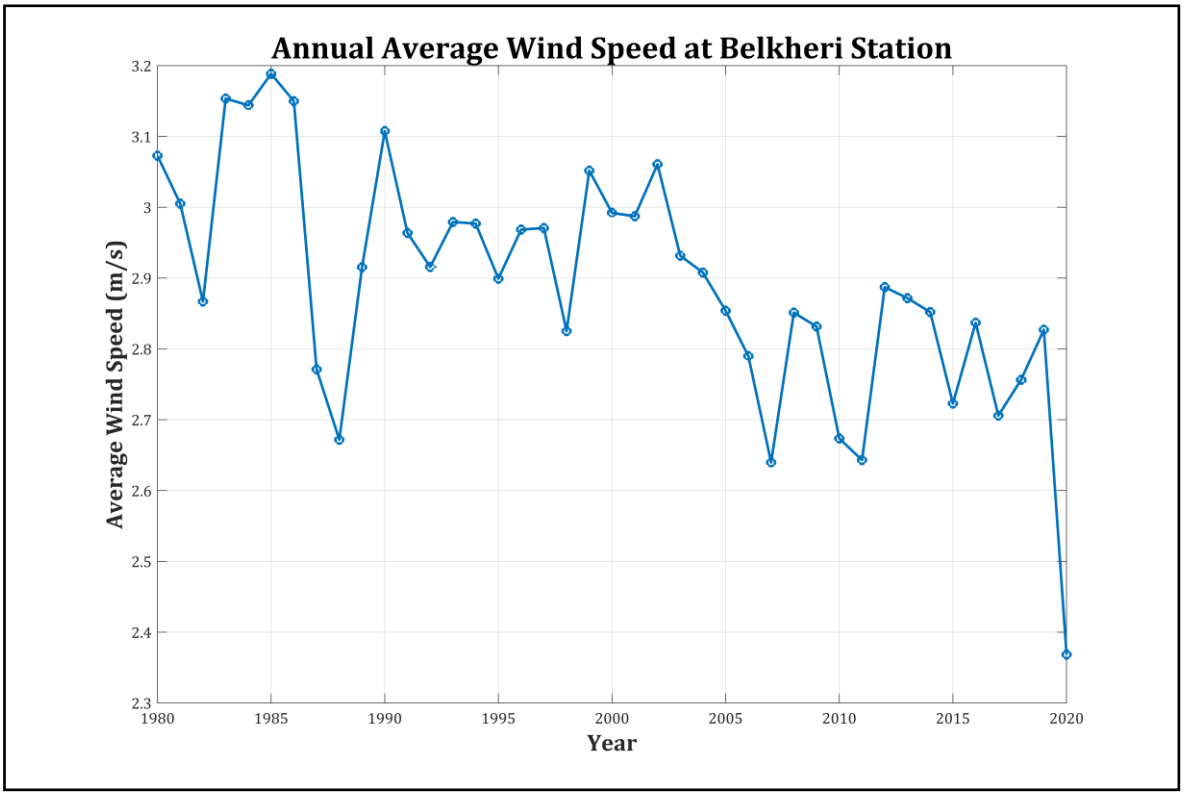


Figure 50: Daily Annual Average Wind Speed at Belkheri Station (1980–2020)

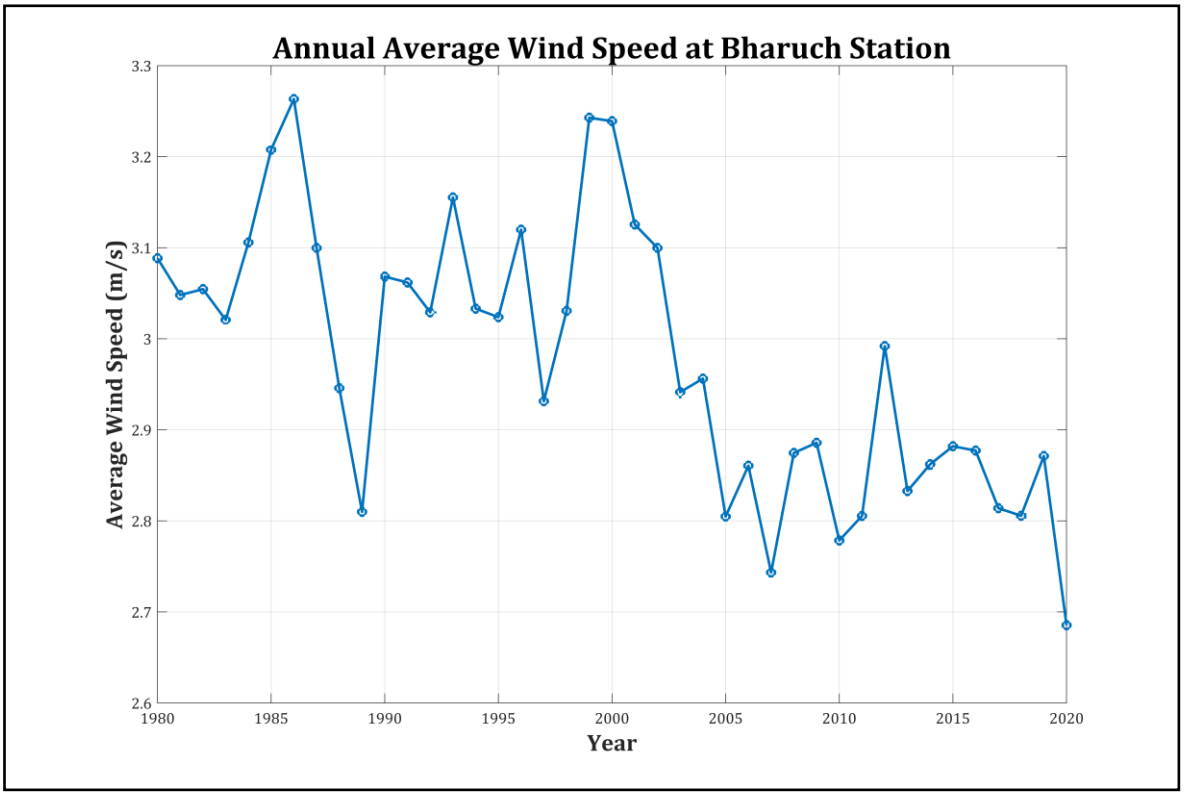


Figure 51: Daily Annual Average Wind Speed at Bharuch Station (1980–2020)

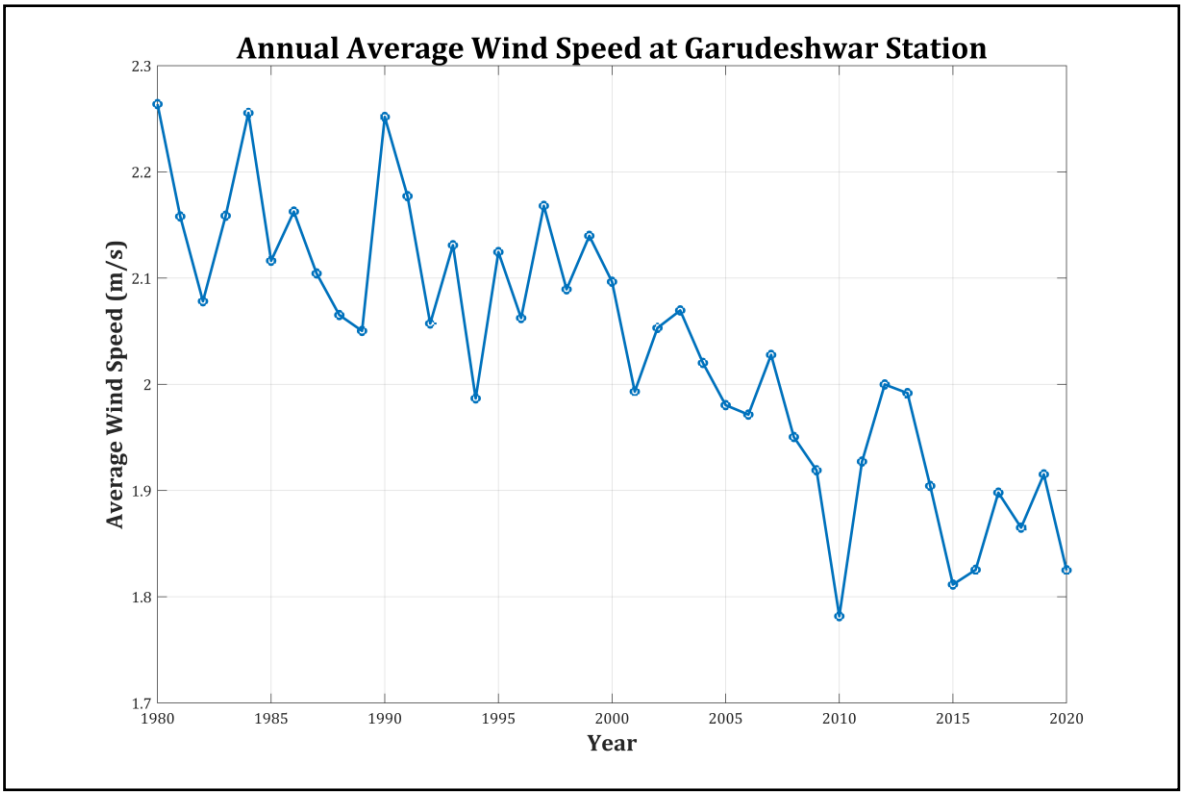


Figure 52: Daily Annual Average Wind Speed at Garudeshwar Station (1980–2020)

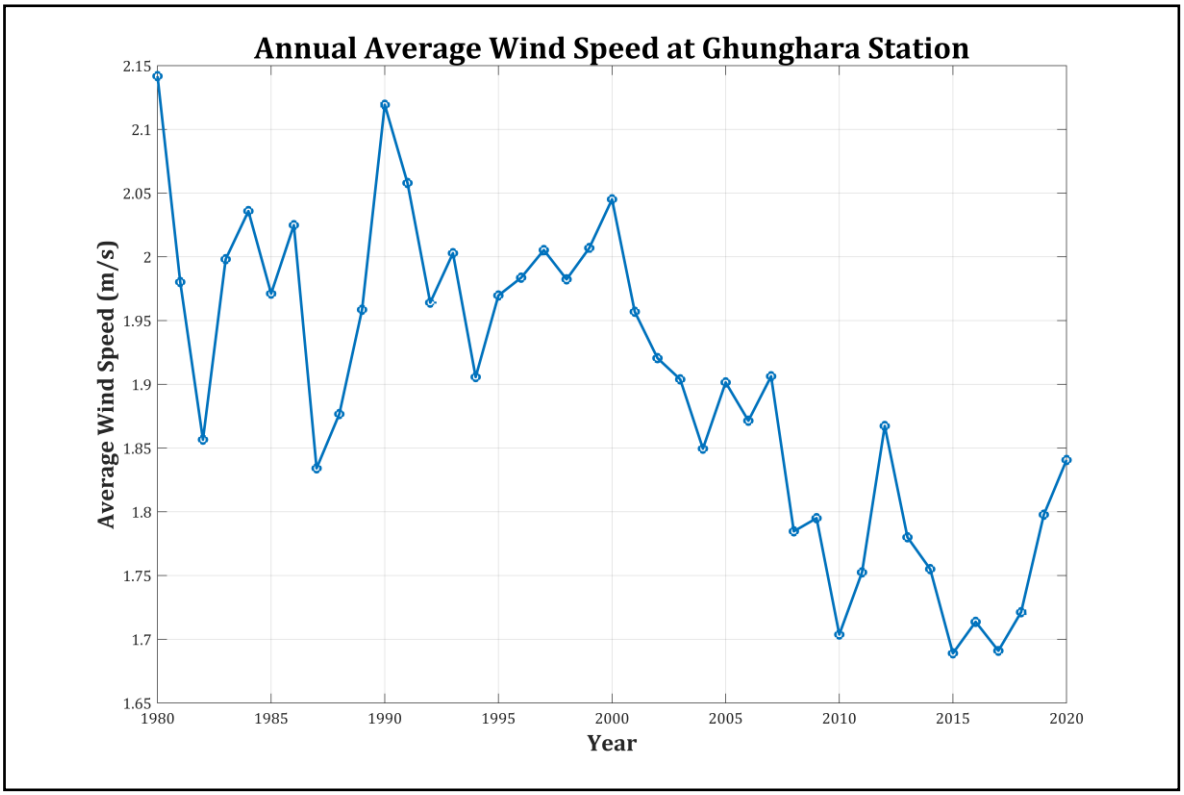


Figure 53: Daily Annual Average Wind Speed at Ghunghara Station (1980–2020)

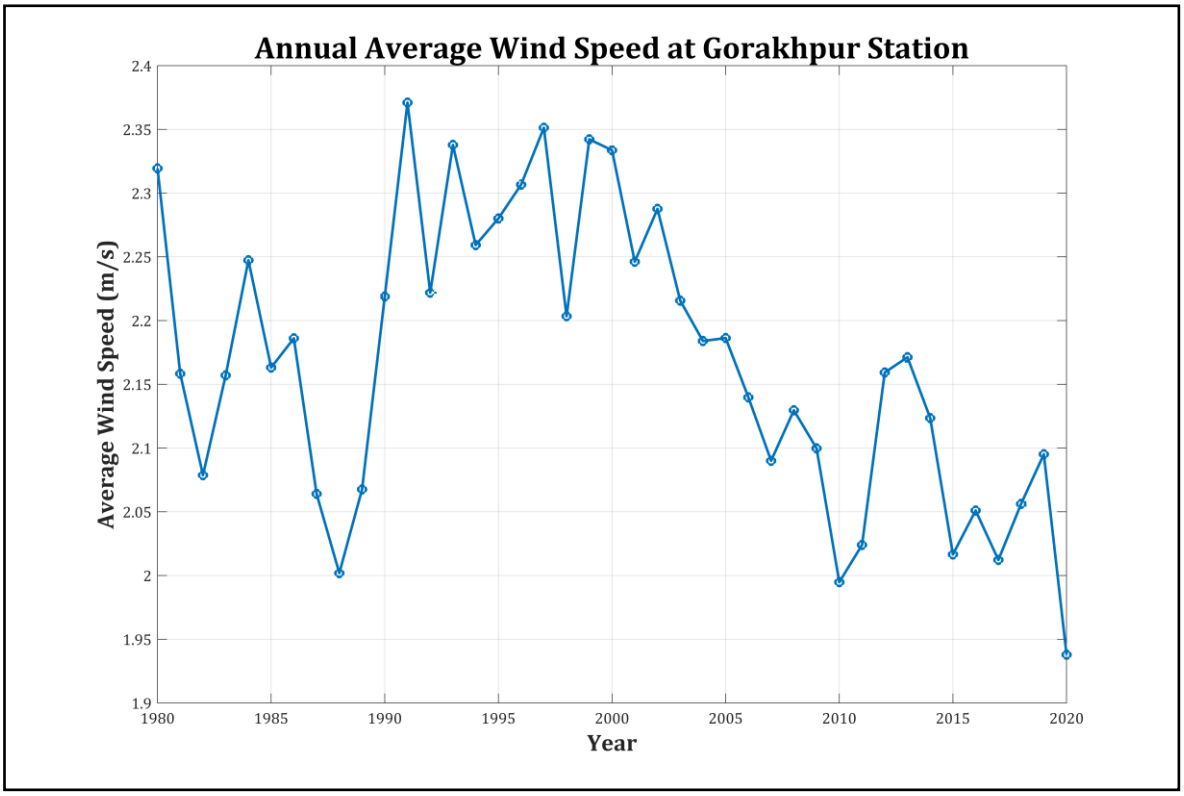


Figure 54: Daily Annual Average Wind Speed at Gorakhpur Station (1980–2020)

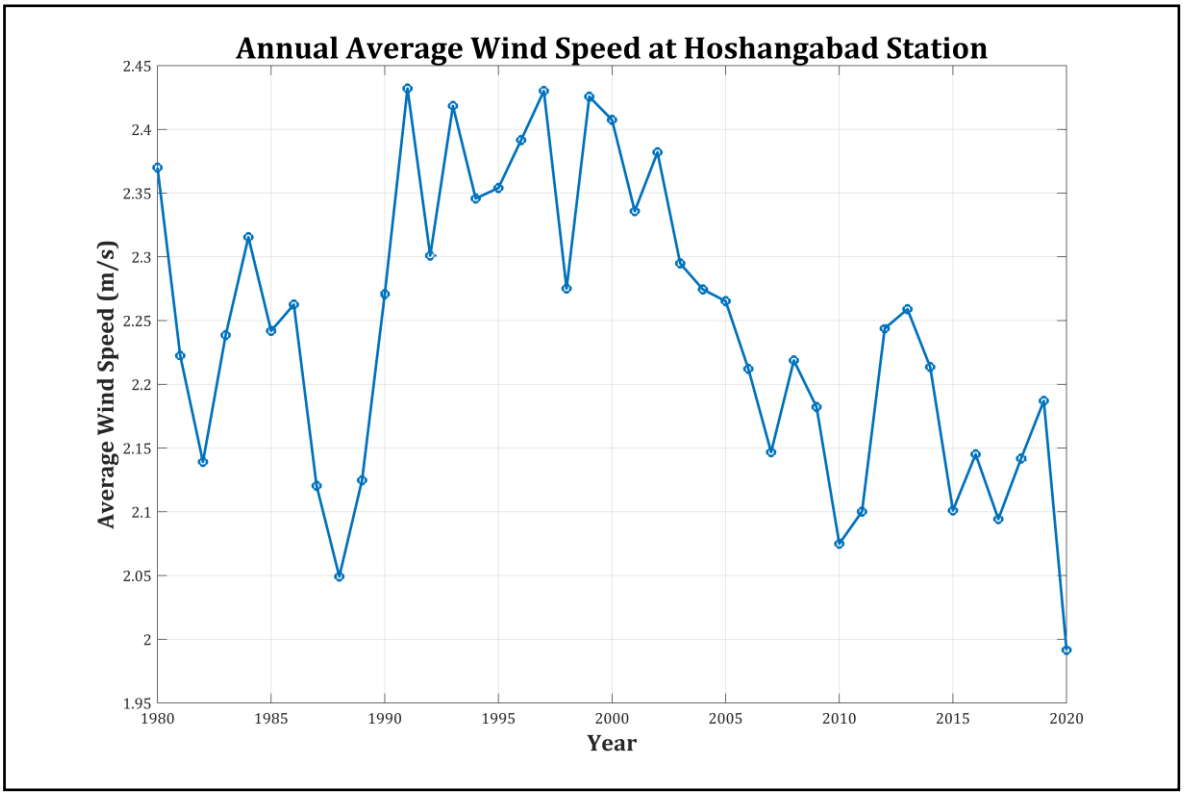


Figure 55: Daily Annual Average Wind Speed at Hoshangabad Station (1980–2020)

### 3.4.2 Monthly Wind Speed Trends

Figures representing the monthly average wind speeds (e.g., Figure 56: Daily Average Wind Speed at Indirasagar Dam Station (1980–2020)) show significant seasonal fluctuations. The wind tends to peak during Monsoon months. Conversely, wind speed reductions are observed in October, November, December, reflecting calmer atmospheric conditions typical of that period. Such seasonal variations are crucial for understanding the interplay between wind-driven evaporation and surface water availability.

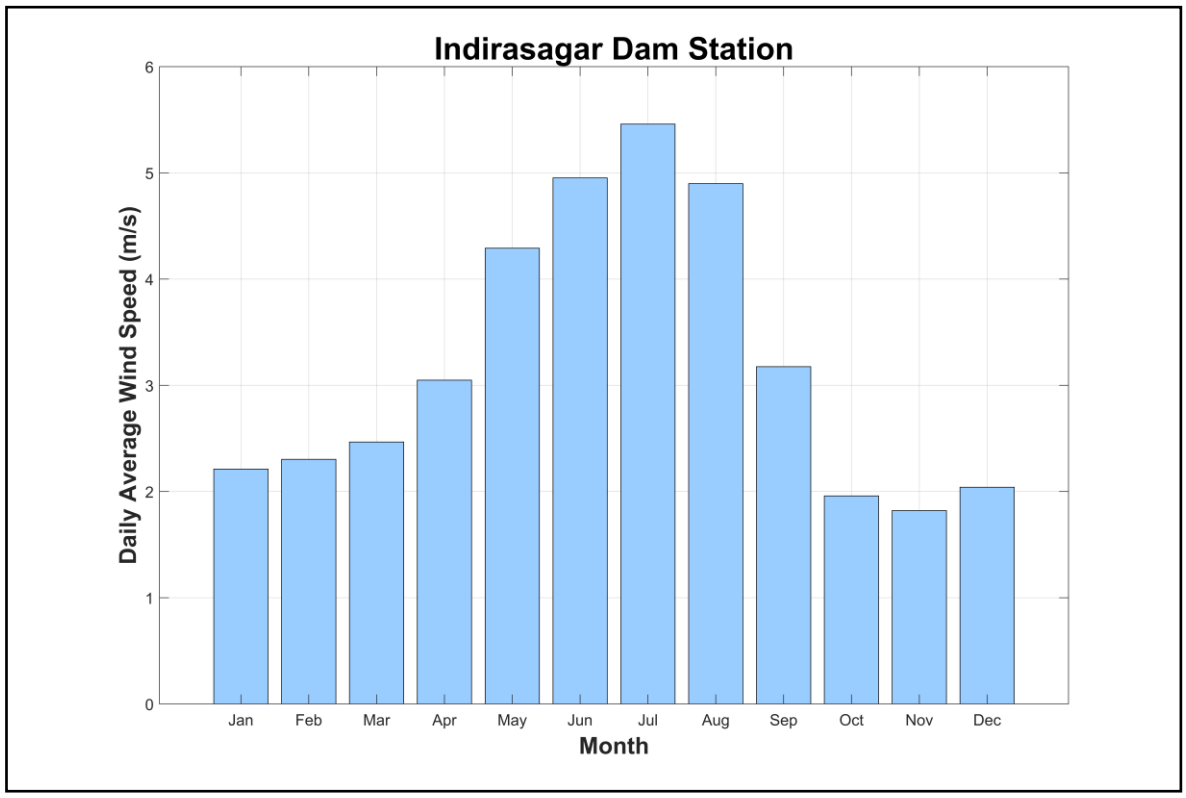


Figure 56: Daily Average Wind Speed at Indirasagar Dam Station (1980–2020)

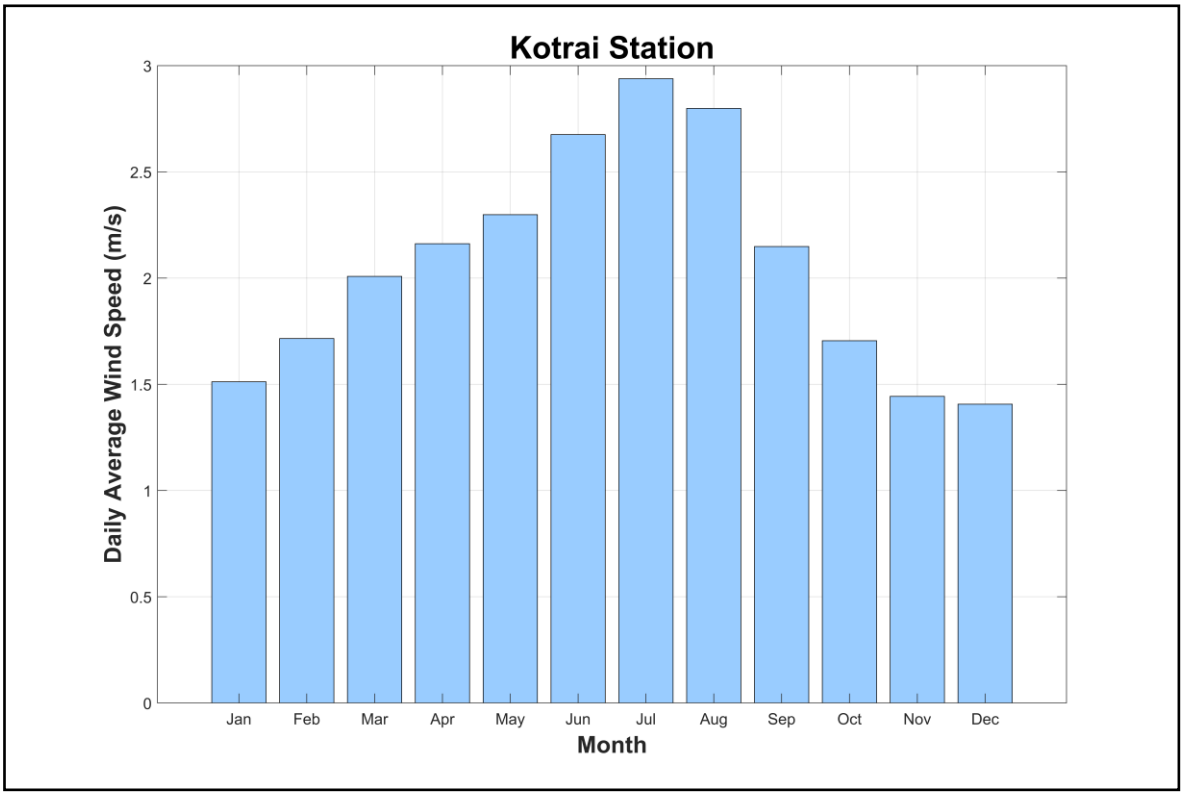


Figure 57: Daily Average Wind Speed at Kotrai Station (1980–2020)

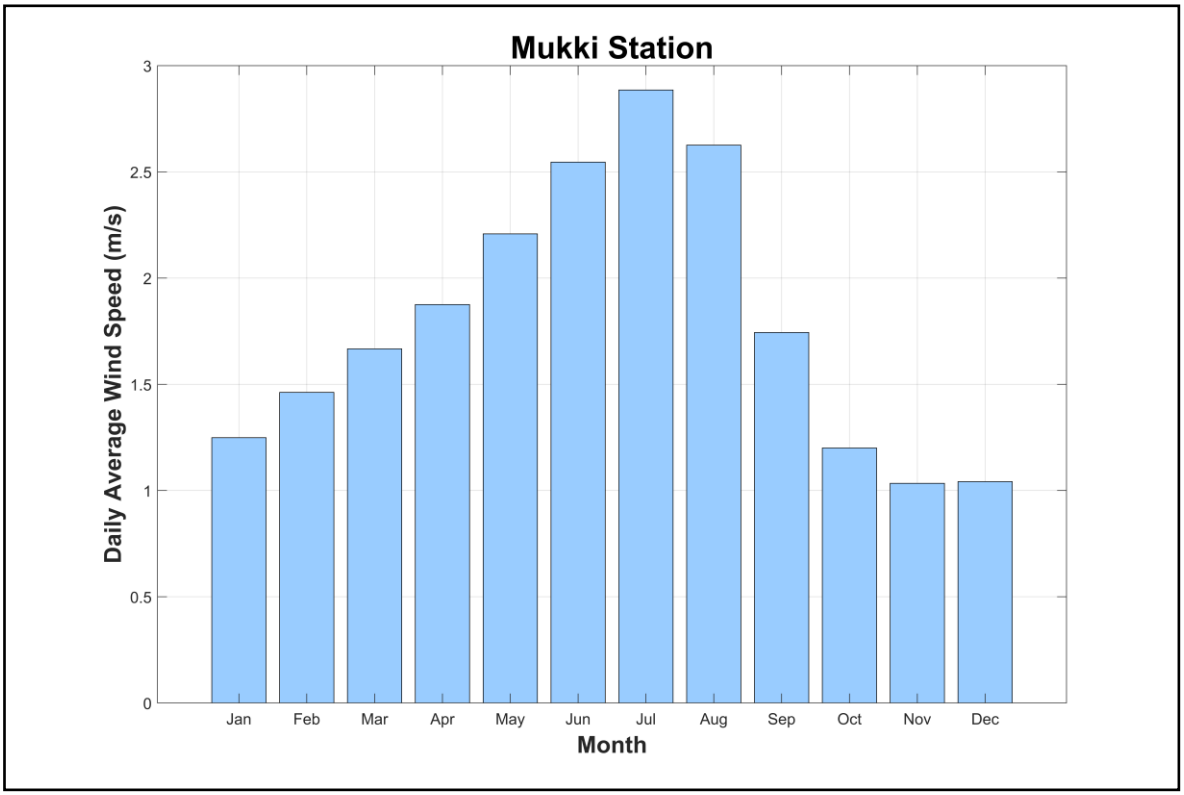


Figure 58: Daily Average Wind Speed at Mukki Station (1980–2020)

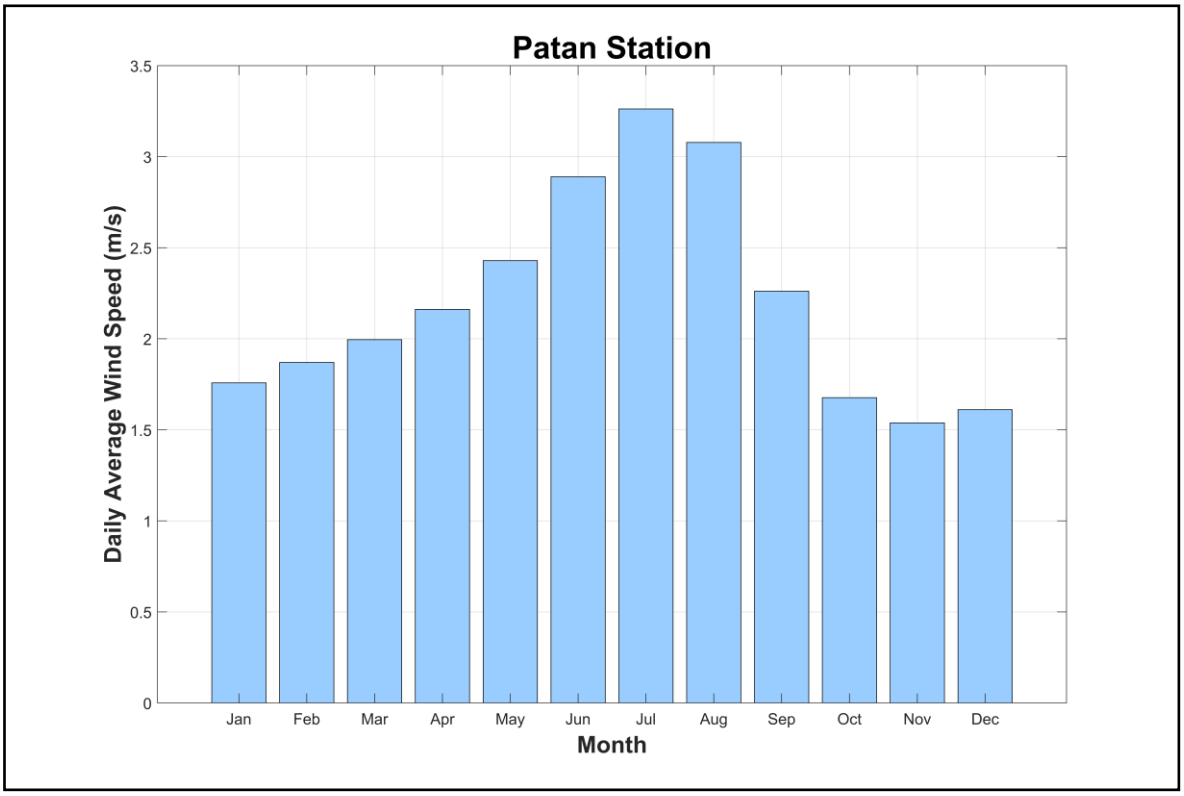


Figure 59: Daily Average Wind Speed at Patan Station (1980–2020)

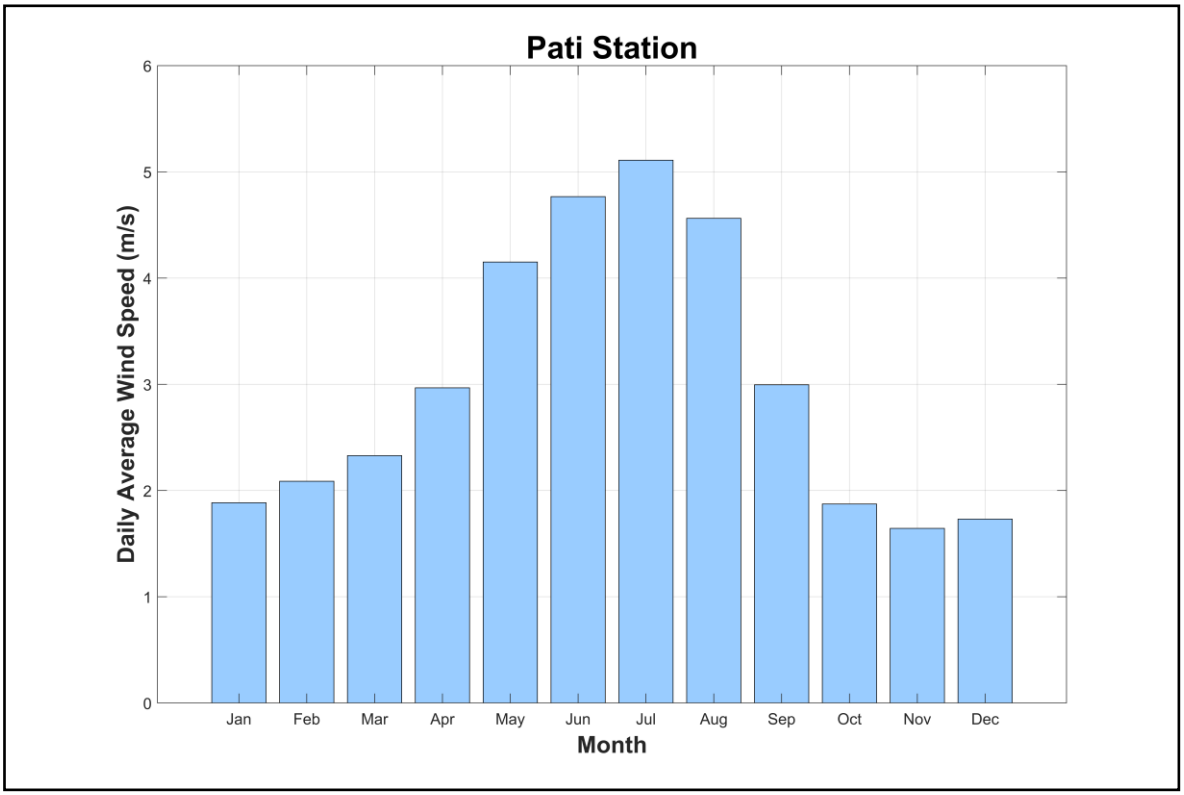


Figure 60: Daily Average Wind Speed at Pati Station (1980–2020)

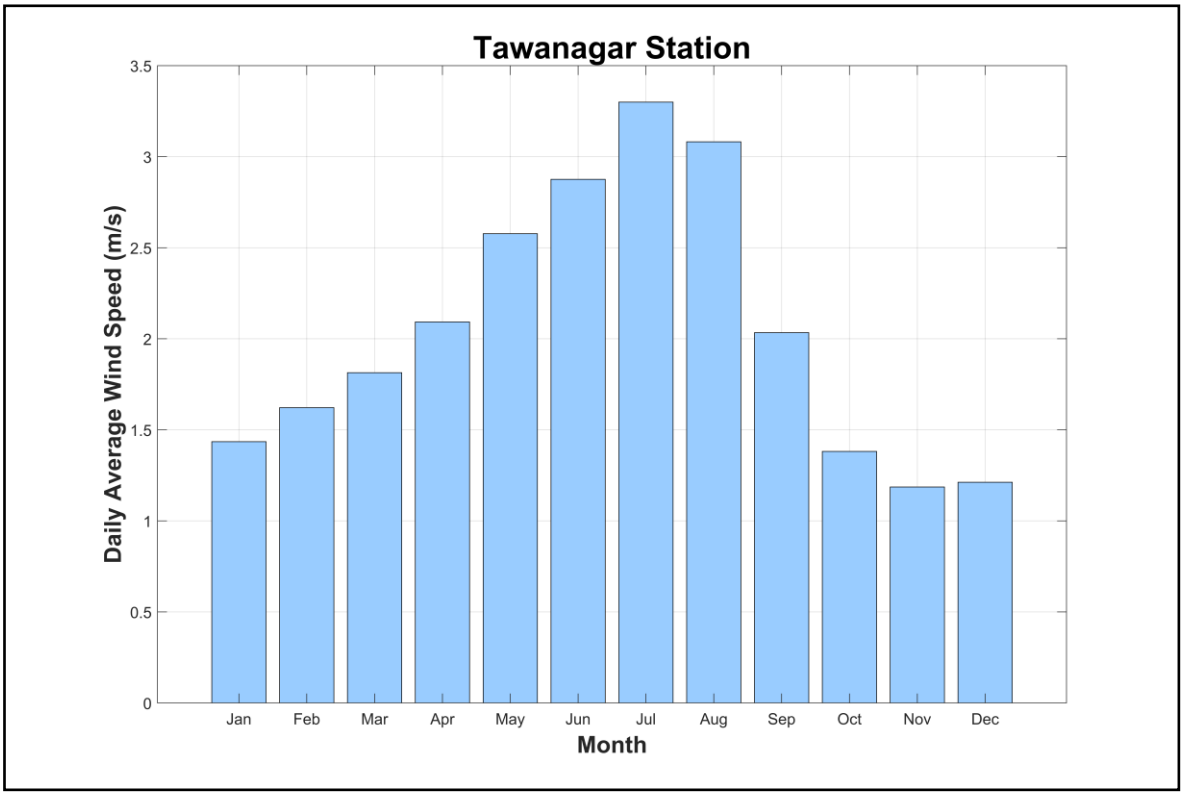


Figure 61: Daily Average Wind Speed at Tawanagar Station (1980–2020)

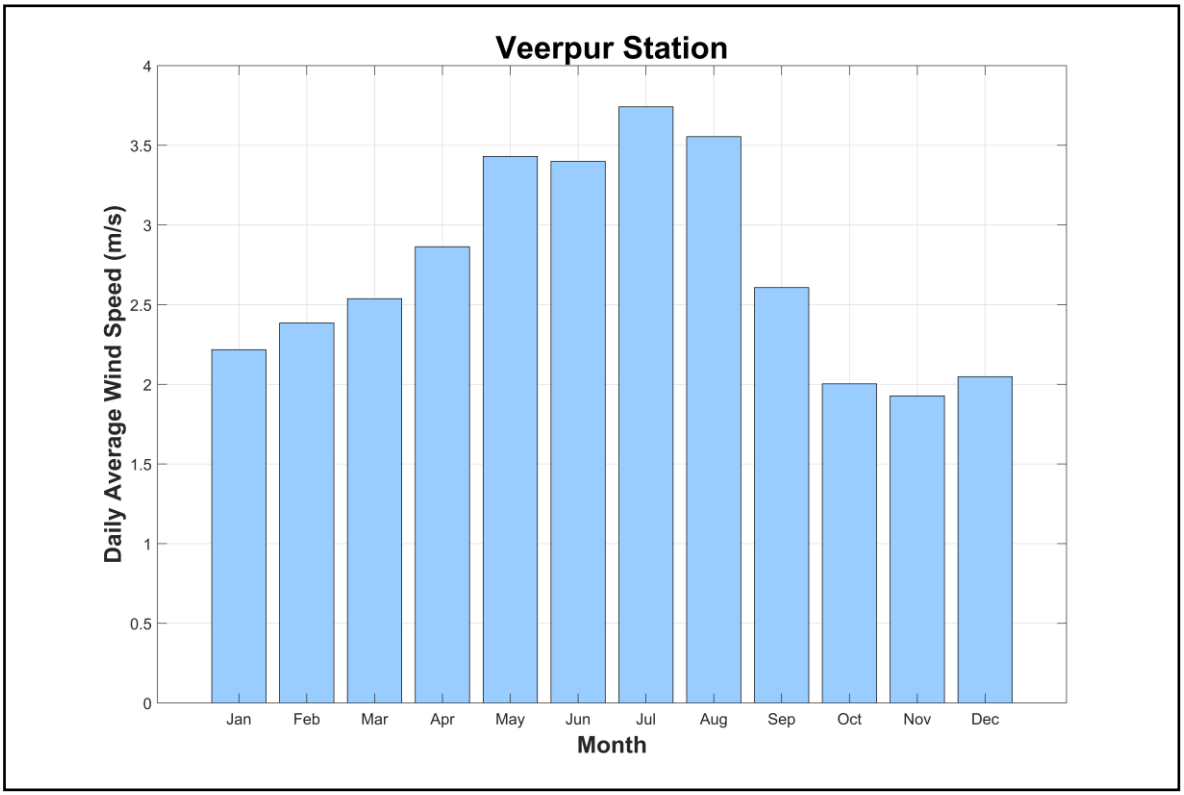


Figure 62: Daily Average Wind Speed at Veerpur Station (1980–2020)

While the complete wind speed dataset is available in the supplementary material, Annexure III contains figures visualizing wind speed.

Figure 63 presents the temporal variation of wind speed over the Narmada River Basin based on ERA5 data. The plot indicates noticeable seasonal fluctuations, with higher wind speeds observed during the pre-monsoon and early monsoon periods. A slight declining trend in wind speeds is evident in recent decades, which may be associated with increasing vegetation cover, urban expansion, or larger-scale climatic shifts.

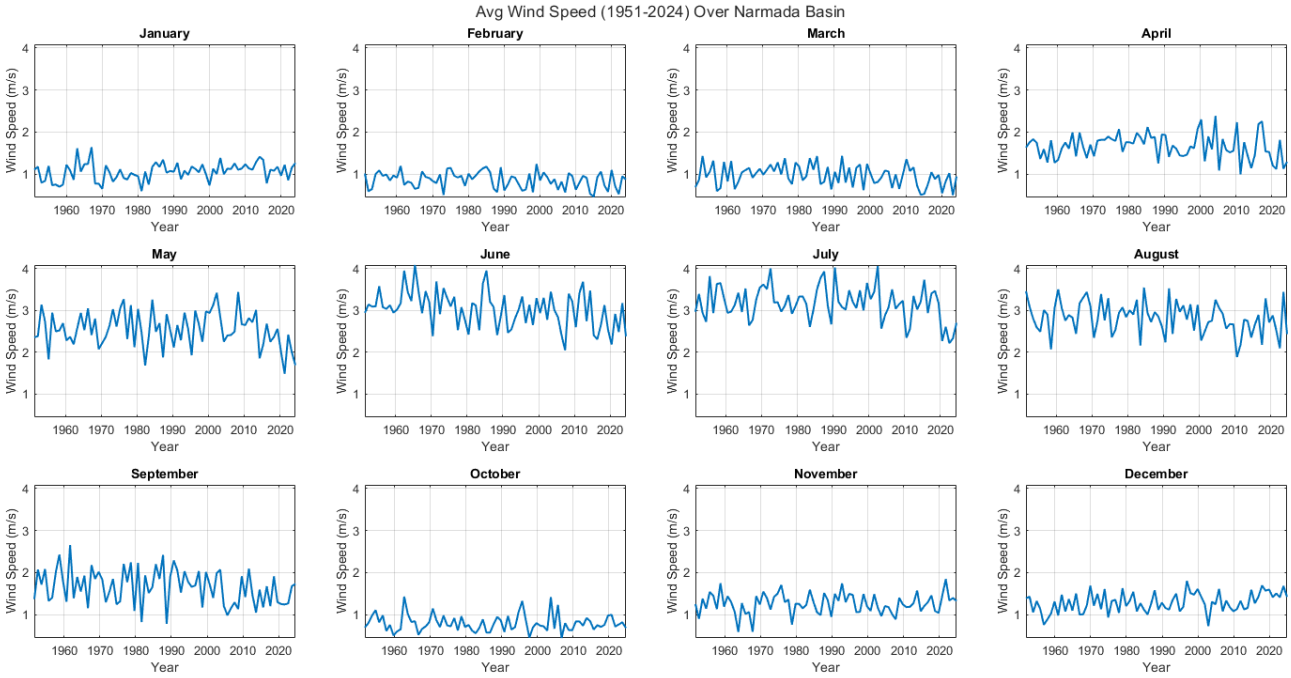


Figure 63: Temporal Variation of Wind Speed over Narmada Basin (ERA5)

Figure 64 shows the spatial variation in average wind speed across the basin. It highlights that the lower and western parts of the basin, particularly areas closer to Gujarat and the Arabian Sea, experience relatively stronger winds, possibly influenced by regional topography and coastal proximity. Conversely, the central and upper sub-basins exhibit relatively calmer conditions due to forest cover and terrain shielding. These spatial differences in wind regime have implications for localized evaporation rates and microclimate conditions.

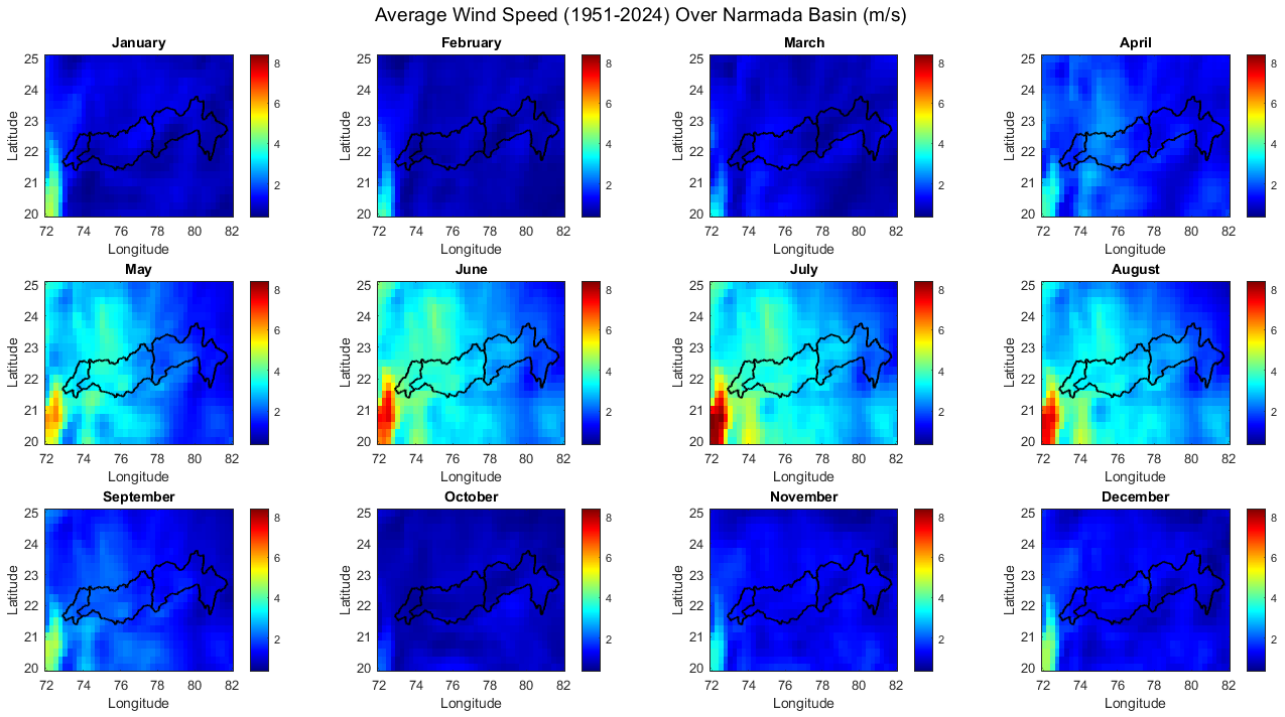


Figure 64: Spatial Variation of Wind Speed over Narmada Basin (ERA5)

## 3.5 RELATIVE HUMIDITY

Relative humidity (RH) is a measure of atmospheric moisture and a key indicator of atmospheric saturation. It influences plant transpiration, human thermal comfort, and cloud formation. High RH typically corresponds with increased cloudiness and potential precipitation, while low RH intensifies evaporation and can increase the risk of drought and wildfire.

Figure 65 illustrates the temporal variation of RH across the Narmada Basin. The seasonal cycle is pronounced, with peak RH during the monsoon season (June to September) due to sustained moisture influx from the southwest monsoon. Drier conditions are recorded in the pre-monsoon months (March–May), coinciding with rising temperatures and increased solar radiation. The interannual pattern remains relatively stable with no significant long-term trend, suggesting that large-scale atmospheric moisture input has not undergone major shifts.

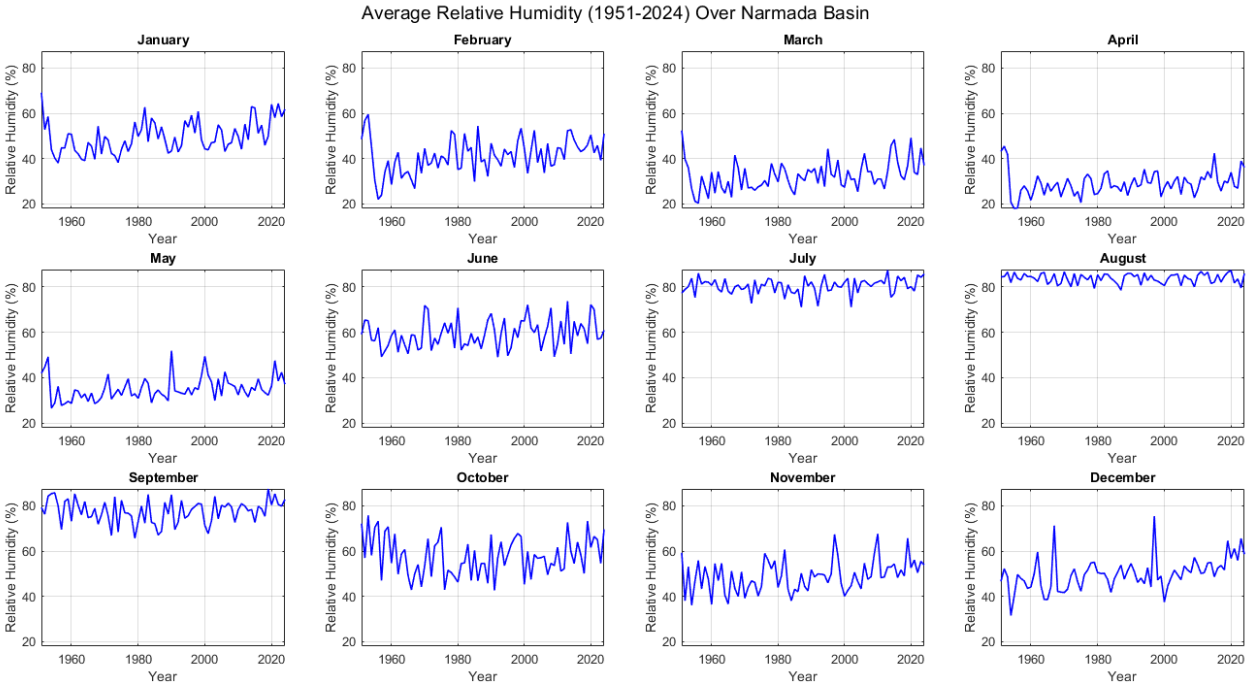


Figure 65: Temporal Variation of Relative Humidity over Narmada Basin (ERA5)

Figure 66 provides the spatial distribution of mean RH. The coastal and downstream regions of the basin show persistently higher humidity levels, owing to their proximity to the sea and dense vegetation. In contrast, the central and eastern portions of the basin, especially those with less forest cover and higher elevation, exhibit comparatively lower RH values. This spatial heterogeneity in RH plays a vital role in influencing evapotranspiration rates and vegetation dynamics across different sub-basins.

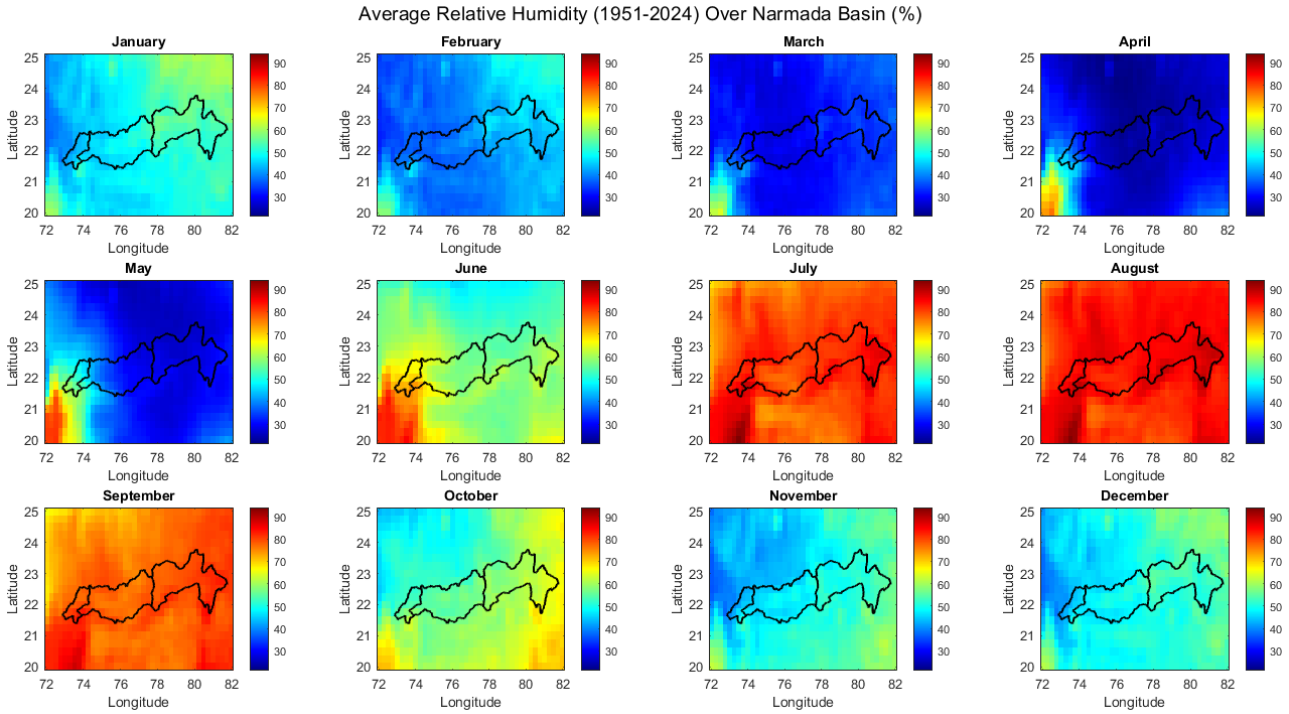


Figure 66: Spatial Variation of Relative Humidity over Narmada Basin (ERA5)

## 3.6 CLOUD COVER

Cloud cover modulates Earth's radiation balance by reflecting incoming solar radiation and trapping outgoing longwave radiation. It directly impacts surface temperatures, photosynthesis, and the hydrologic cycle by influencing precipitation formation. Persistent cloud cover can reduce solar radiation, suppress surface evaporation, and regulate diurnal temperature range.

Figure 67 shows the temporal trend of cloud cover over the basin, with a clear monsoonal pattern marked by increased cloudiness from June to September. These months correspond to the period of highest rainfall and lowest solar radiation, confirming the strong link between cloud dynamics and monsoon activity. Post-monsoon and winter periods record much lower cloud cover, leading to increased radiation receipt and cooling during nights.

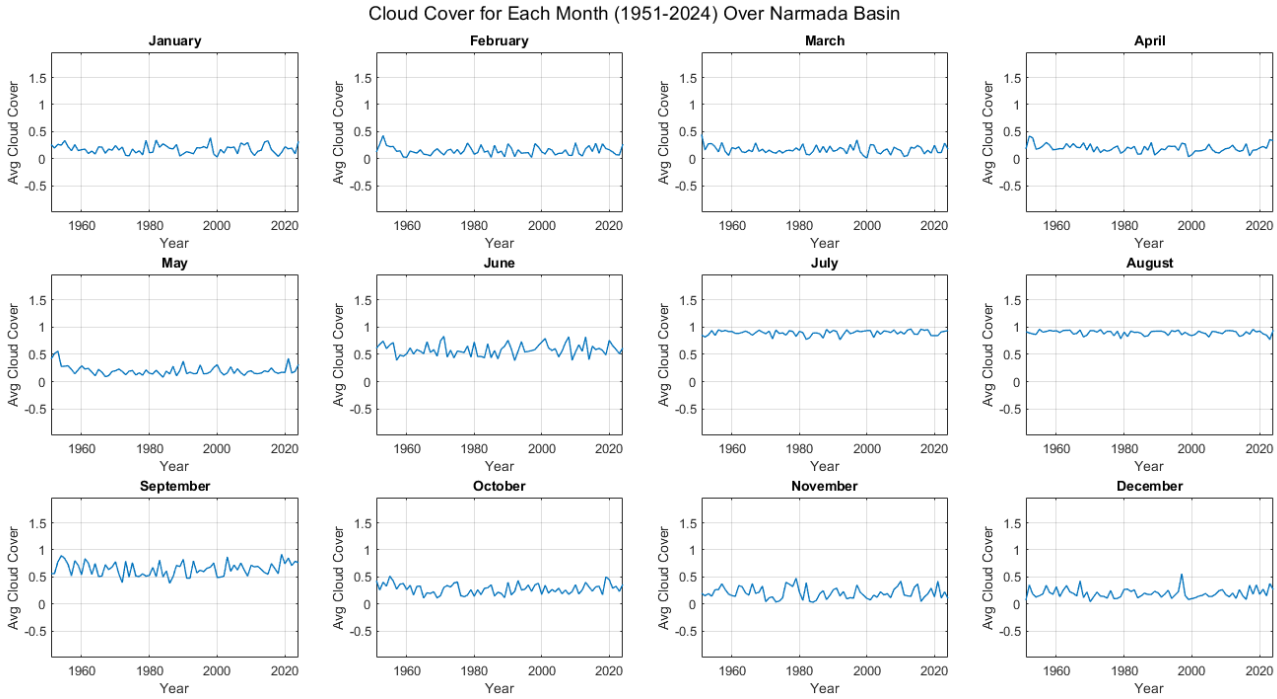


Figure 67: Temporal Variation of Cloud Cover over Narmada Basin (ERA5)

Figure 68 displays the spatial distribution of cloud cover, indicating heavier cloud presence in the upper and middle reaches of the basin—areas dominated by forest and undulating terrain that foster convective activity. The lower basin near the coast shows relatively reduced cloud cover, likely influenced by local circulation dynamics. This variation in cloudiness directly influences the spatial distribution of rainfall, solar energy input, and even drought severity.

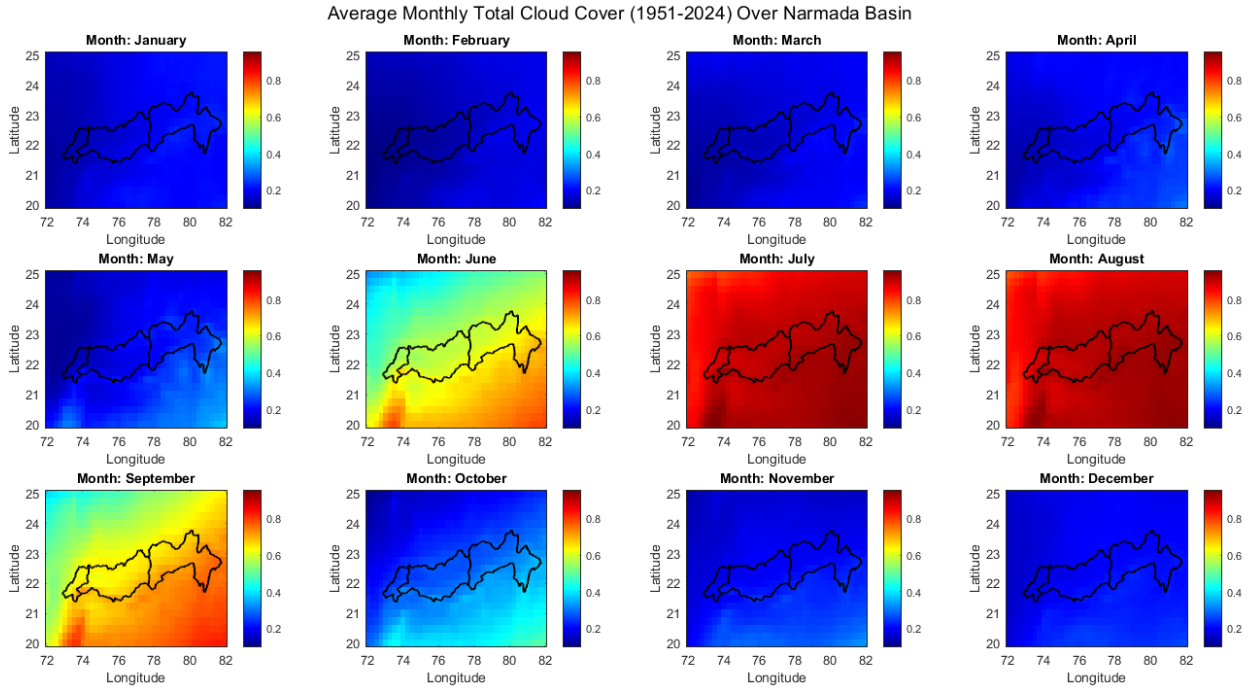


Figure 68: Spatial Variation of Cloud Cover over Narmada Basin (ERA5)

## 3.7 SOLAR RADIATION

Solar radiation is the primary source of energy driving atmospheric processes, hydrological cycling, and ecosystem productivity. It governs surface temperature, evapotranspiration, and is crucial for agricultural output and energy applications such as solar power generation.

Figure 69 presents the temporal variation in solar radiation over the basin. The trend shows strong seasonality, with the highest radiation levels during the pre-monsoon months (March to May), coinciding with clear skies and high temperatures. A pronounced dip is observed during the monsoon season due to cloud cover and increased atmospheric moisture. Minor interannual variations are observed, but the long-term average remains stable.

Figure 70 reveals the spatial variation of incoming solar radiation across the basin. The central and western regions exhibit higher solar energy levels, attributed to flatter terrain and fewer cloud days. In contrast, the upper reaches—characterized by forested hills and frequent cloud formation—receive comparatively lower solar input. These differences impact not only hydrological responses such as evapotranspiration but also agricultural productivity and the potential for solar energy development.

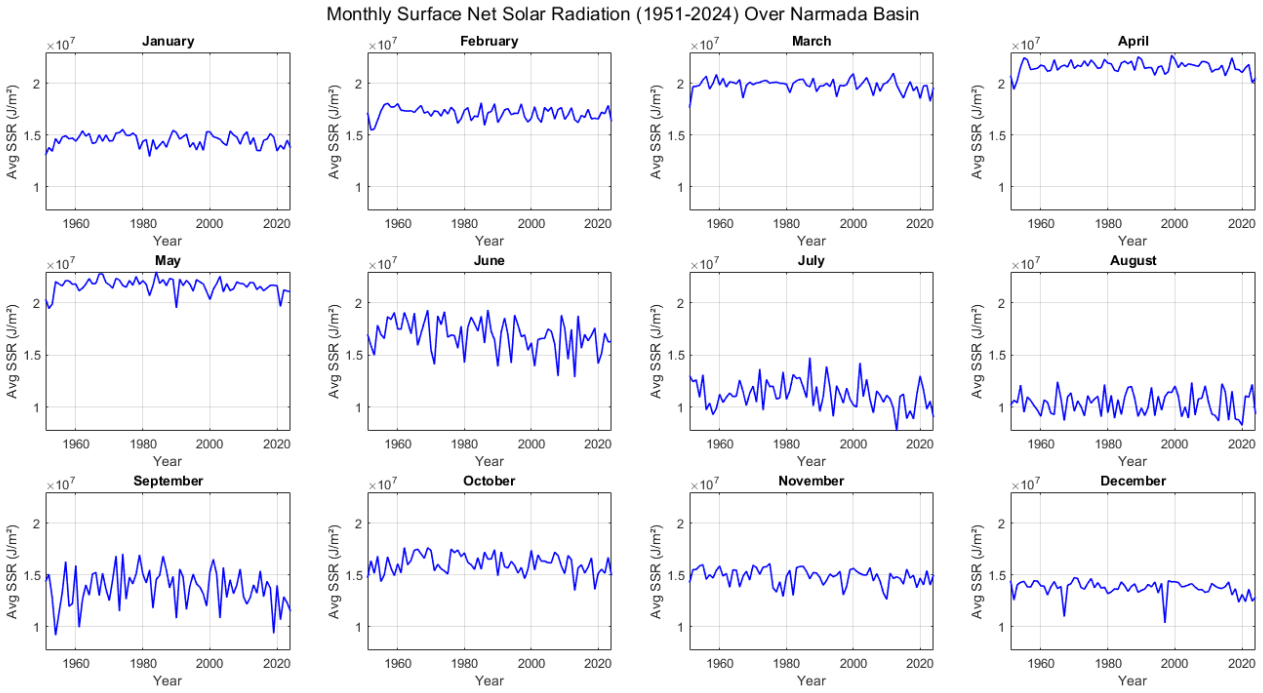


Figure 69: Temporal Variation of Solar Radiation over Narmada Basin (ERA5)

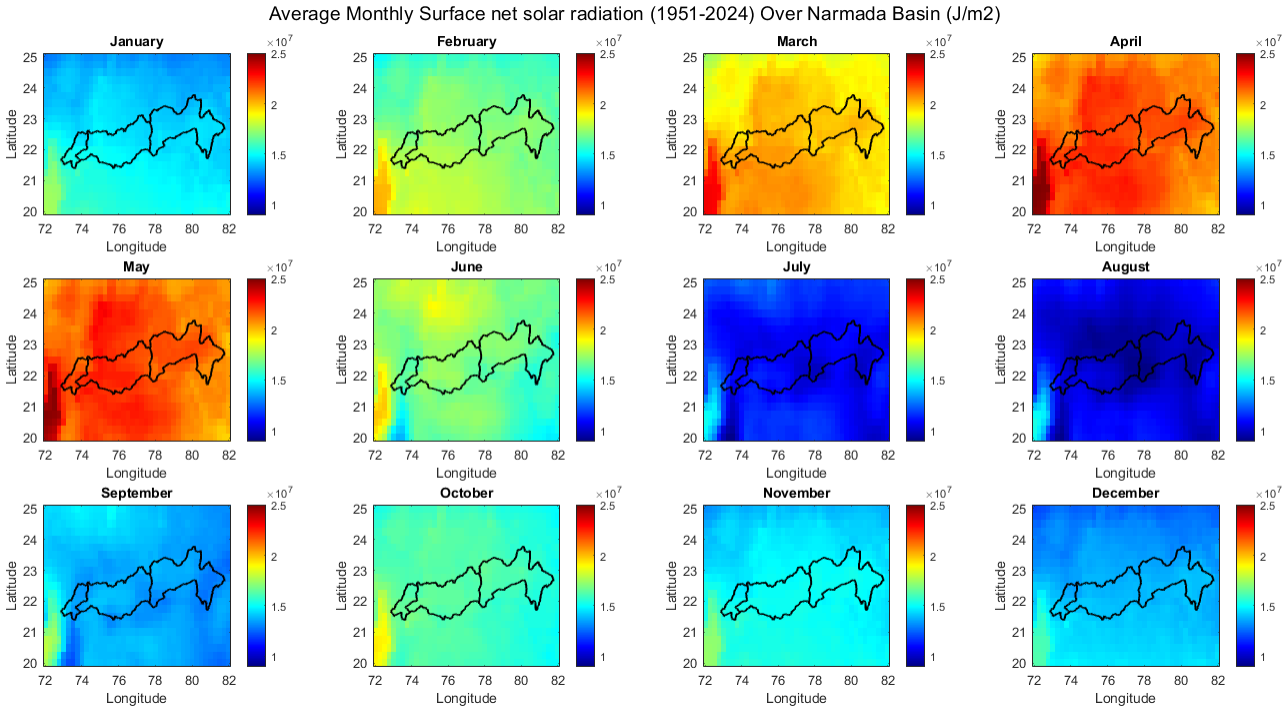


Figure 70: Spatial Variation of Solar Radiation over Narmada Basin (ERA5)

# Chapter 4: GCM / RCM Data

## 4.1 GENERAL

Global Climate Models (GCMs) and Regional Climate Models (RCMs) are sophisticated numerical tools developed to simulate the Earth's climate system over extended temporal and spatial scales. GCMs operate at coarse spatial resolutions (typically 100–250 km), encompassing the entire globe, and account for fundamental physical processes across the atmosphere, ocean, cryosphere, and land surface. These models form the backbone of climate projections by simulating large-scale responses of the climate system to various greenhouse gas (GHG) emission scenarios (IPCC, 2021). However, due to their coarse resolution, GCMs often fail to capture regional-scale climate processes, especially in areas with complex topography or land–atmosphere interactions. To address this limitation, Regional Climate Models (RCMs) are employed through a process called dynamical downscaling. RCMs nest within GCMs and provide high-resolution simulations (typically 10–50 km) for specific regions of interest, allowing for more accurate representation of localized climate phenomena such as monsoons, extreme precipitation events, and orographic rainfall (Giorgi & Gutowski, 2015).

The Coupled Model Intercomparison Project Phase 6 (CMIP6) offers a comprehensive archive of GCM simulations under different Shared Socioeconomic Pathways (SSPs), which represent plausible future emission trajectories (Eyring et al., 2016). Similarly, regional projections are facilitated through the Coordinated Regional Climate Downscaling Experiment (CORDEX), which provides RCM outputs that are spatially refined and bias-corrected to support impact assessments at regional and basin scales (Jacob et al., 2014).

## 4.2 REGIONAL CLIMATE MODELS (RCMS)

While General Circulation Models (GCMs) are excellent for simulating large-scale climate processes, their coarse spatial resolution limits their usefulness for local- or basin-scale studies. This is where Regional Climate Models (RCMs) become important.

RCMs are high-resolution climate models that simulate regional weather and climate patterns by using boundary conditions from GCMs. In simple terms, GCMs provide the "big

picture" of global climate, and RCMs zoom in to simulate finer-scale processes—often at resolutions of **10–50 km**. These characteristics make RCMs particularly valuable for impact studies involving agriculture, water resources, infrastructure planning, and disaster risk management.

However, RCMs also have limitations:

- They are computationally expensive to run.
- They inherit biases from the GCMs that drive them.
- Despite higher resolution, biases in temperature and precipitation often remain.

Therefore, in many studies—including this one—statistical bias correction methods are still applied to RCM outputs to improve their accuracy. In fact, the bias correction method used in this dataset (Empirical Quantile Mapping or EQM) is suitable for both GCM and RCM outputs.

In the present study, although the primary dataset is based on GCMs from CMIP6, the bias-corrected outputs serve the purpose of RCM-level detail because:

- The resolution has been refined to 0.25° (~25 km),
- Biases in daily precipitation and temperatures have been effectively reduced,
- And the dataset covers critical climate scenarios and periods for South Asia.

This makes the dataset functionally like RCM outputs, but without the need for computationally intensive dynamic downscaling.

## 4.3 RESULT

Thus, for this study, high-resolution, bias-corrected climate dataset specifically developed for South Asia and the Indian sub-continental river basins, including the Narmada River Basin. The dataset was created by Mishra et al. (2020) using outputs from 13 General Circulation Models (GCMs) that participated in CMIP6. It provides daily time series of precipitation, maximum temperature, and minimum temperature at a spatial resolution of 0.25° (~25 km), which is suitable for regional- and basin-scale impact studies.

The raw outputs from these GCMs are available at varying spatial resolutions, typically ranging from ~0.7° to 2.5° grids, which are too coarse for local or basin-scale analysis. Additionally, due to differences in model physics and parameterizations, the outputs often show systematic biases when compared to observed climate records, especially for precipitation patterns and temperature extremes. Thus, to make these projections suitable for hydrological and climate impact studies such as for the Narmada River Basin bias correction and downscaling are required. These steps ensure that the data reflect realistic local conditions and can be confidently used for long-term planning, policy formulation, and vulnerability assessment.

Table 1 CMIP6 GCMs Used in the Study

| S.No | GCM Model Name | Modeling Institution |
|---|---|---|
| 1 | BCC-CSM2-MR | Beijing Climate Center, China Meteorological Administration |
| 2 | CanESM5 | Canadian Centre for Climate Modelling and Analysis |
| 3 | CMCC-ESM2 | Centro Euro-Mediterraneo sui Cambiamenti Climatici |
| 4 | CNRM-CM6-1 | Centre National de Recherches Météorologiques |
| 5 | EC-Earth3 | EC-Earth Consortium |
| 6 | GFDL-ESM4 | NOAA Geophysical Fluid Dynamics Laboratory |
| 7 | INM-CM5 | Institute of Numerical Mathematics, Russia |
| 8 | IPSL-CM6A-LR | Institut Pierre Simon Laplace |
| 9 | MIROC6 | Japan Agency for Marine-Earth Science and Technology |
| 10 | MPI-ESM1-2-HR | Max Planck Institute for Meteorology |

| | | |
|---|---|---|
| 11 | MRI-ESM2-0 | Meteorological Research Institute, Japan |
| 12 | NESM3 | Nanjing University of Information Science and Technology |
| 13 | NorESM2-LM | Norwegian Climate Centre |

Thus, the integration of GCM and RCM outputs enables a more accurate and scalable assessment of future climatic conditions at the basin level. This hybrid approach ensures that both global climate drivers and localized effects are effectively captured, offering a reliable foundation for climate impact studies. Following the extraction of daily data for the historical period (1951–2014) and future scenarios—SSP126, SSP245, SSP370, and SSP585 (2015–2100)—the datasets were systematically aggregated to derive monthly, seasonal, and annual values for key climatic parameters, including maximum, minimum, and mean temperatures, as well as precipitation. Furthermore, these derived datasets were utilized to generate spatiotemporal maps at monthly, seasonal, and annual scales for each scenario. This mapping effort allows for a comprehensive visualization and comparison of climatic trends and extremes across different time horizons. Such detailed climatological mapping supports robust hydrological modeling, vulnerability assessments, and informed decision-making in the context of climate change adaptation and sustainable water resource management.

Figure 71: Spatial distribution of monthly values of maximum temperature for the Historical, SSP126, SSP245, SSP370, and SSP585 scenarios.

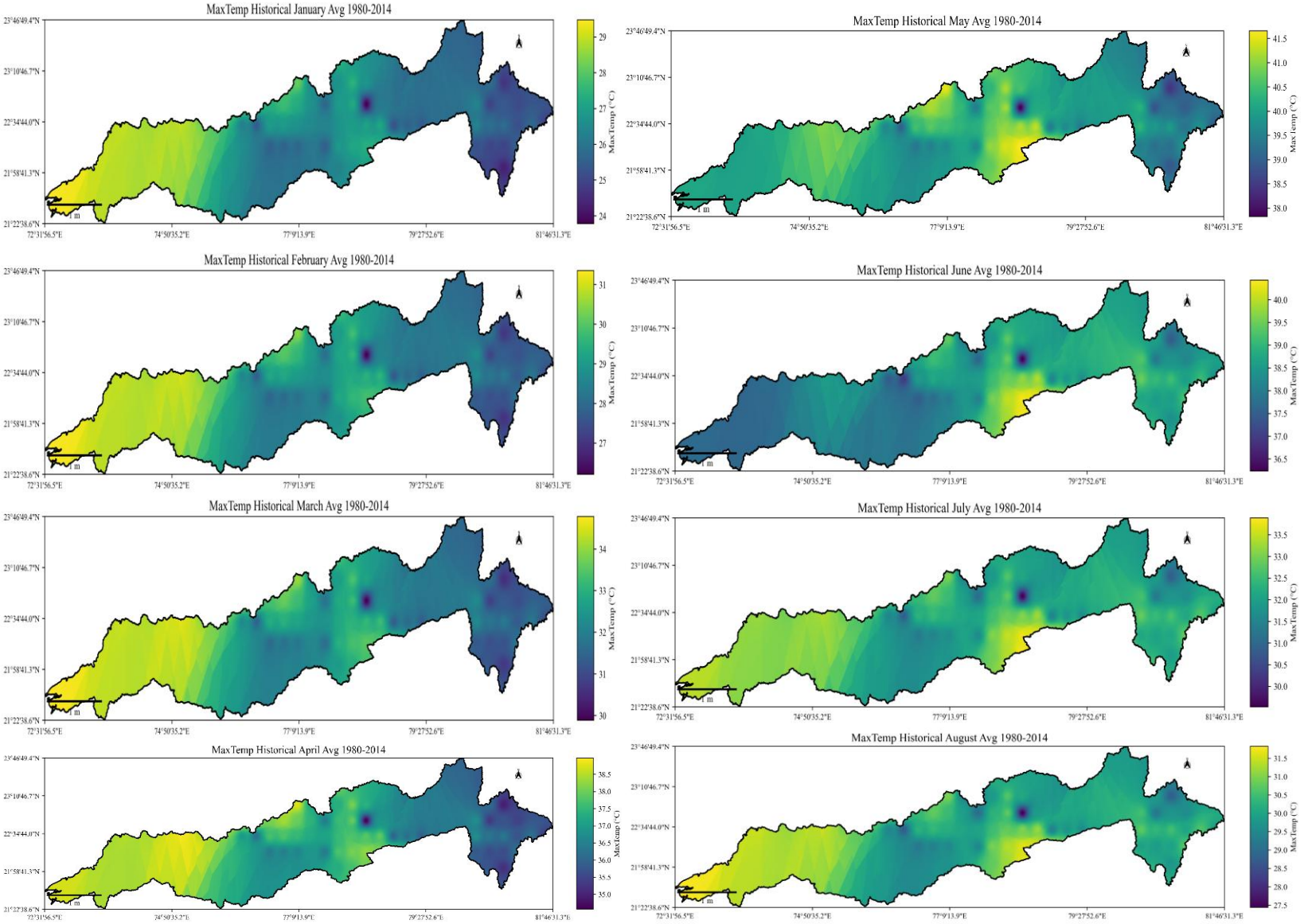

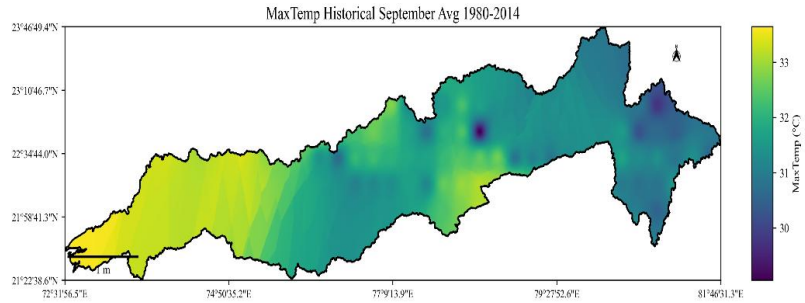
MaxTemp Historical September Avg 1980-2014
MaxTemp (°C)

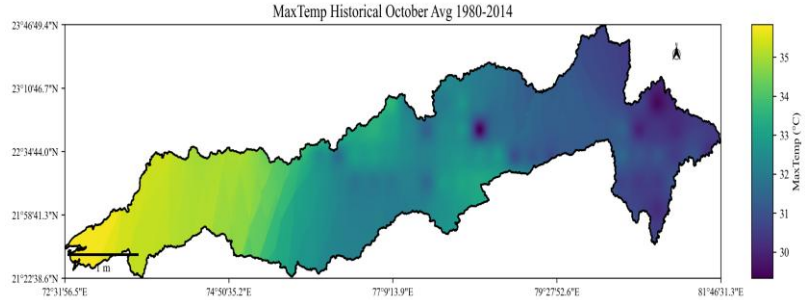
MaxTemp Historical October Avg 1980-2014
MaxTemp (°C)

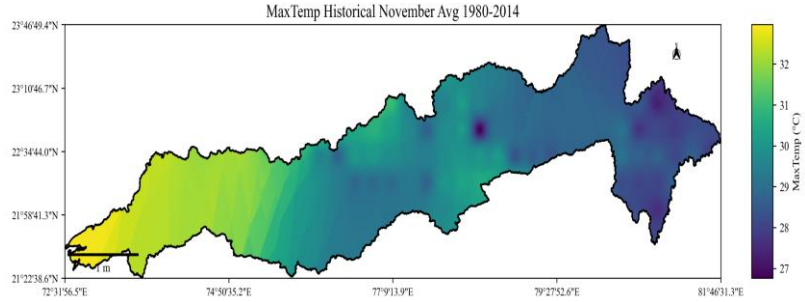
MaxTemp Historical November Avg 1980-2014
MaxTemp (°C)

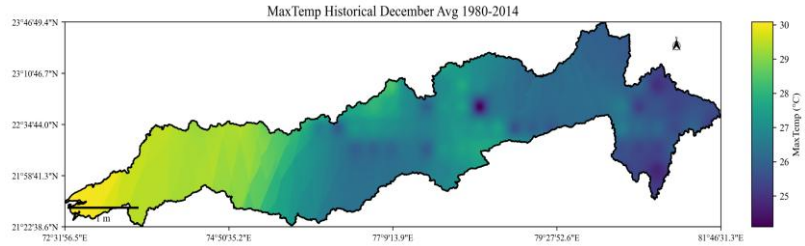
MaxTemp Historical December Avg 1980-2014
MaxTemp (°C)

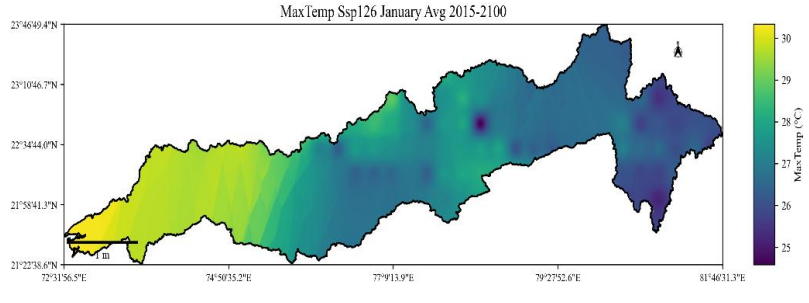
MaxTemp Ssp126 January Avg 2015-2100
MaxTemp (°C)

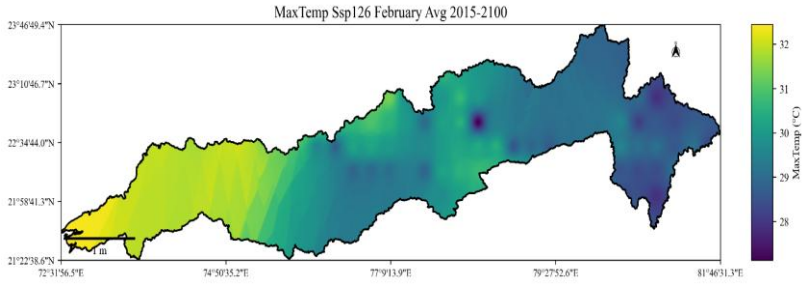
MaxTemp Ssp126 February Avg 2015-2100
MaxTemp (°C)

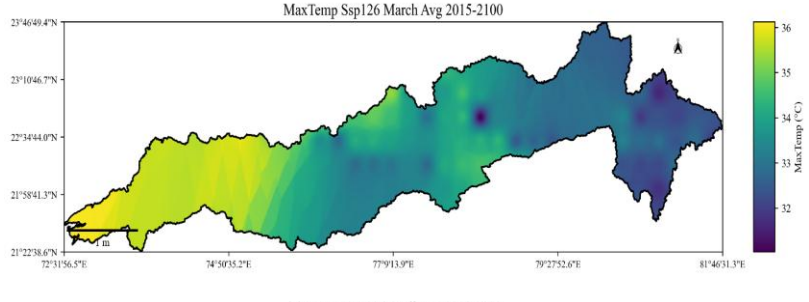
MaxTemp Ssp126 March Avg 2015-2100
MaxTemp (°C)

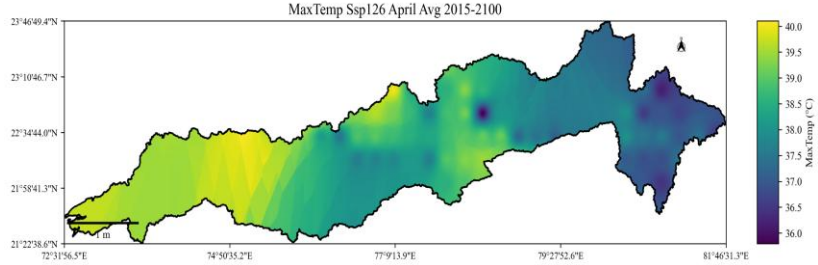
MaxTemp Ssp126 April Avg 2015-2100
MaxTemp (°C)

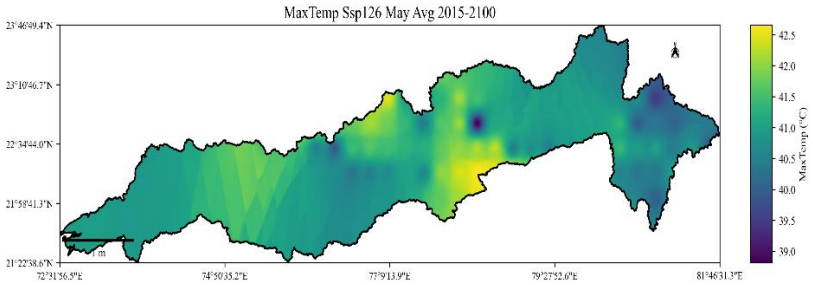
MaxTemp Ssp126 May Avg 2015-2100
MaxTemp (°C)

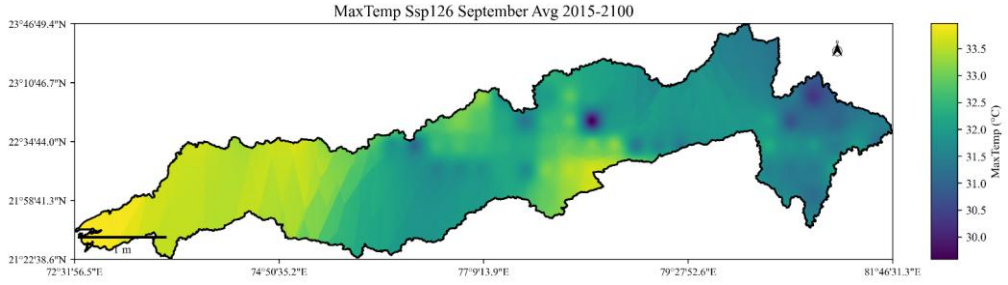
MaxTemp Ssp126 September Avg 2015-2100
MaxTemp (°C)

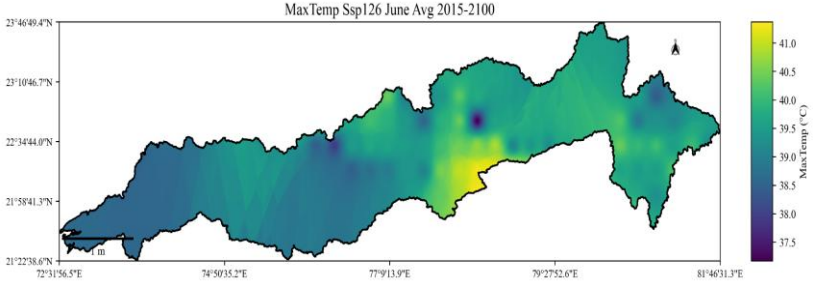
MaxTemp Ssp126 June Avg 2015-2100
MaxTemp (°C)

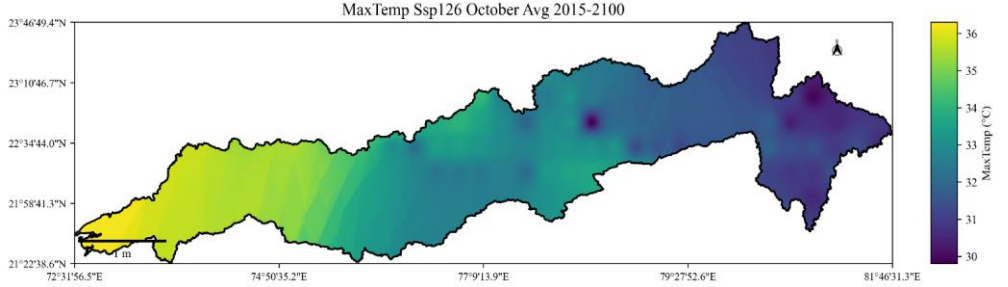
MaxTemp Ssp126 October Avg 2015-2100
MaxTemp (°C)

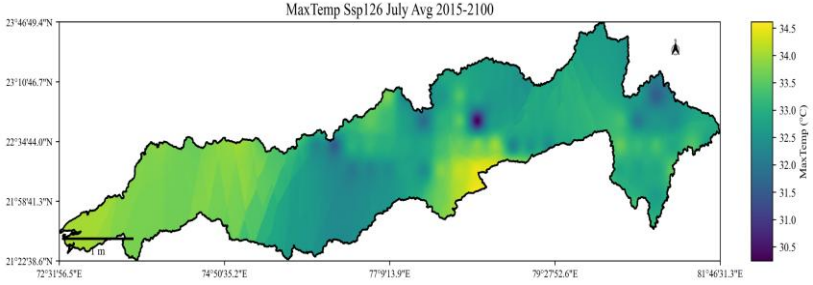
MaxTemp Ssp126 July Avg 2015-2100
MaxTemp (°C)

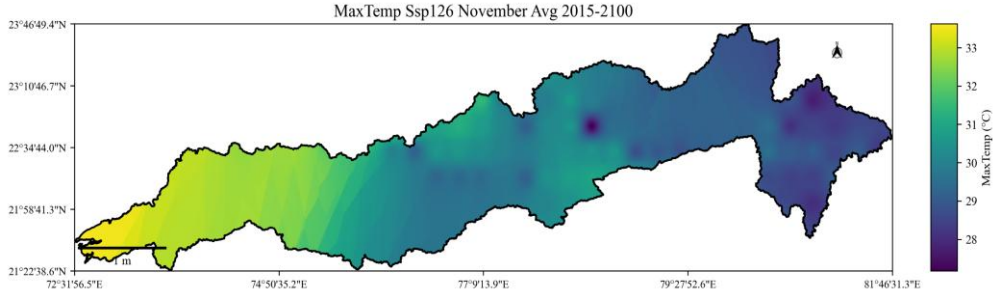
MaxTemp Ssp126 November Avg 2015-2100
MaxTemp (°C)

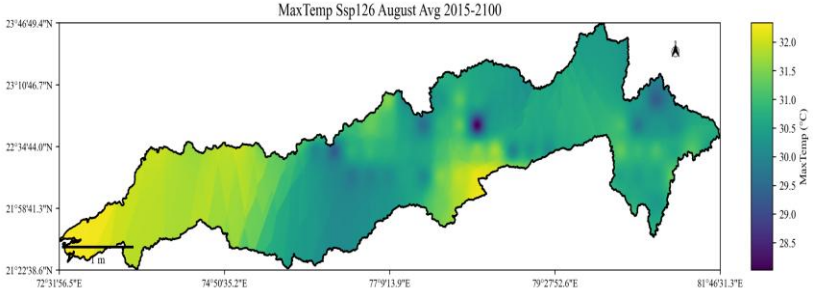
MaxTemp Ssp126 August Avg 2015-2100
MaxTemp (°C)

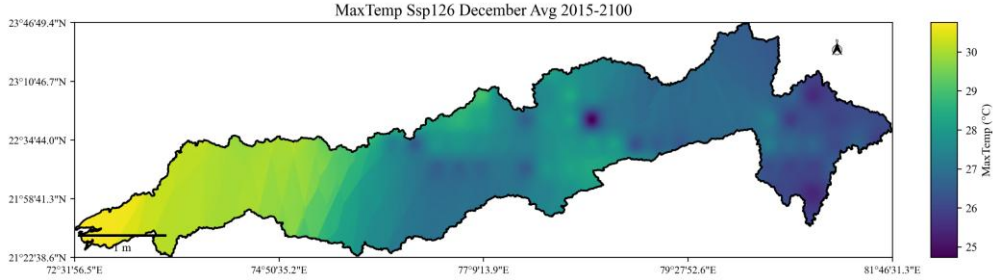
MaxTemp Ssp126 December Avg 2015-2100
MaxTemp (°C)

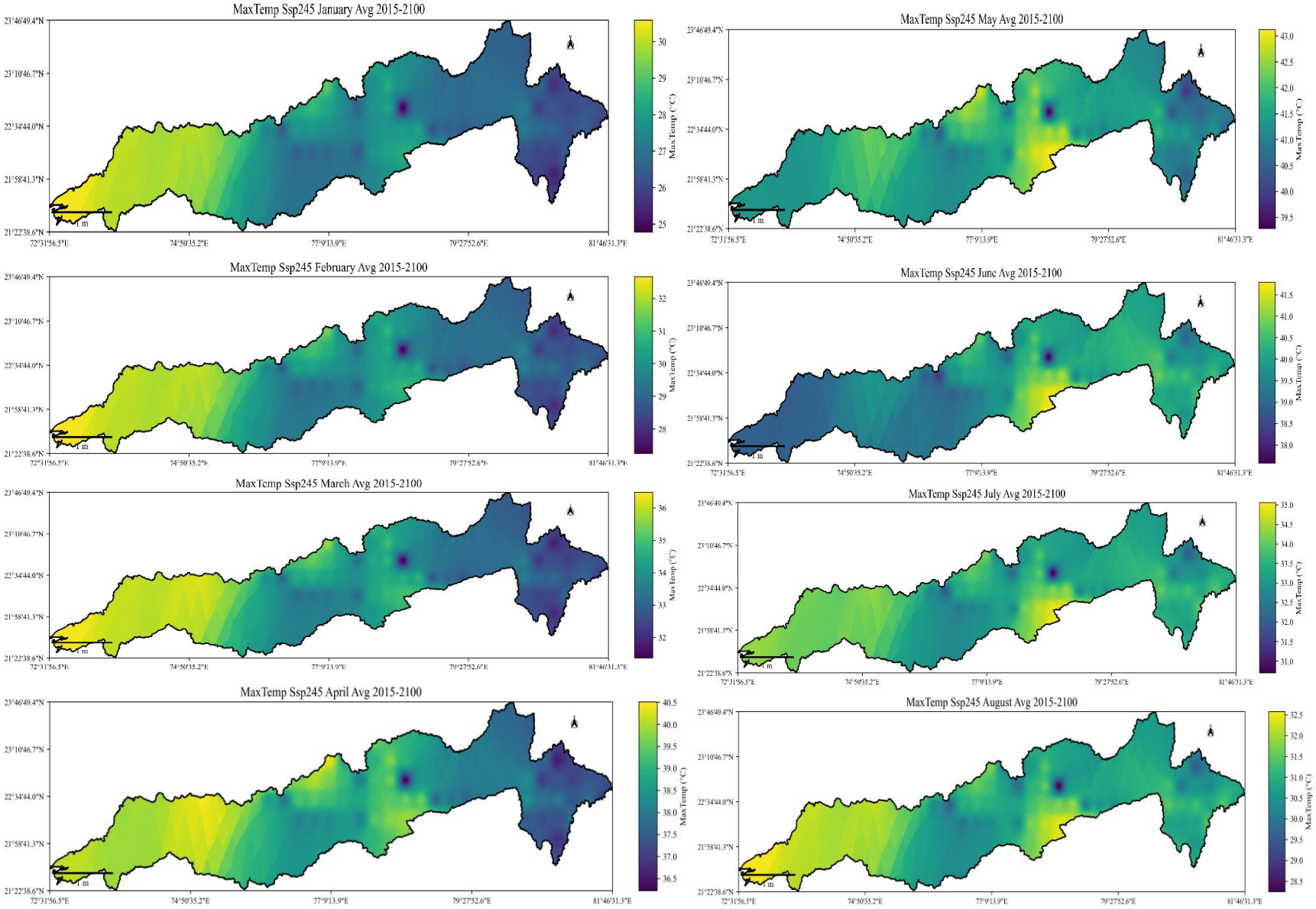
MaxTemp Ssp245 January Avg 2015-2100
MaxTemp Ssp245 May Avg 2015-2100
MaxTemp Ssp245 February Avg 2015-2100
MaxTemp Ssp245 June Avg 2015-2100
MaxTemp Ssp245 March Avg 2015-2100
MaxTemp Ssp245 July Avg 2015-2100
MaxTemp Ssp245 April Avg 2015-2100
MaxTemp Ssp245 August Avg 2015-2100
MaxTemp (°C)
23°46'49.4"N
23°10'46.7"N
22°34'44.0"N
21°58'41.3"N
21°22'38.6"N
72°31'56.5"E
74°50'35.2"E
77°9'13.9"E
79°27'52.6"E
81°46'31.3"E

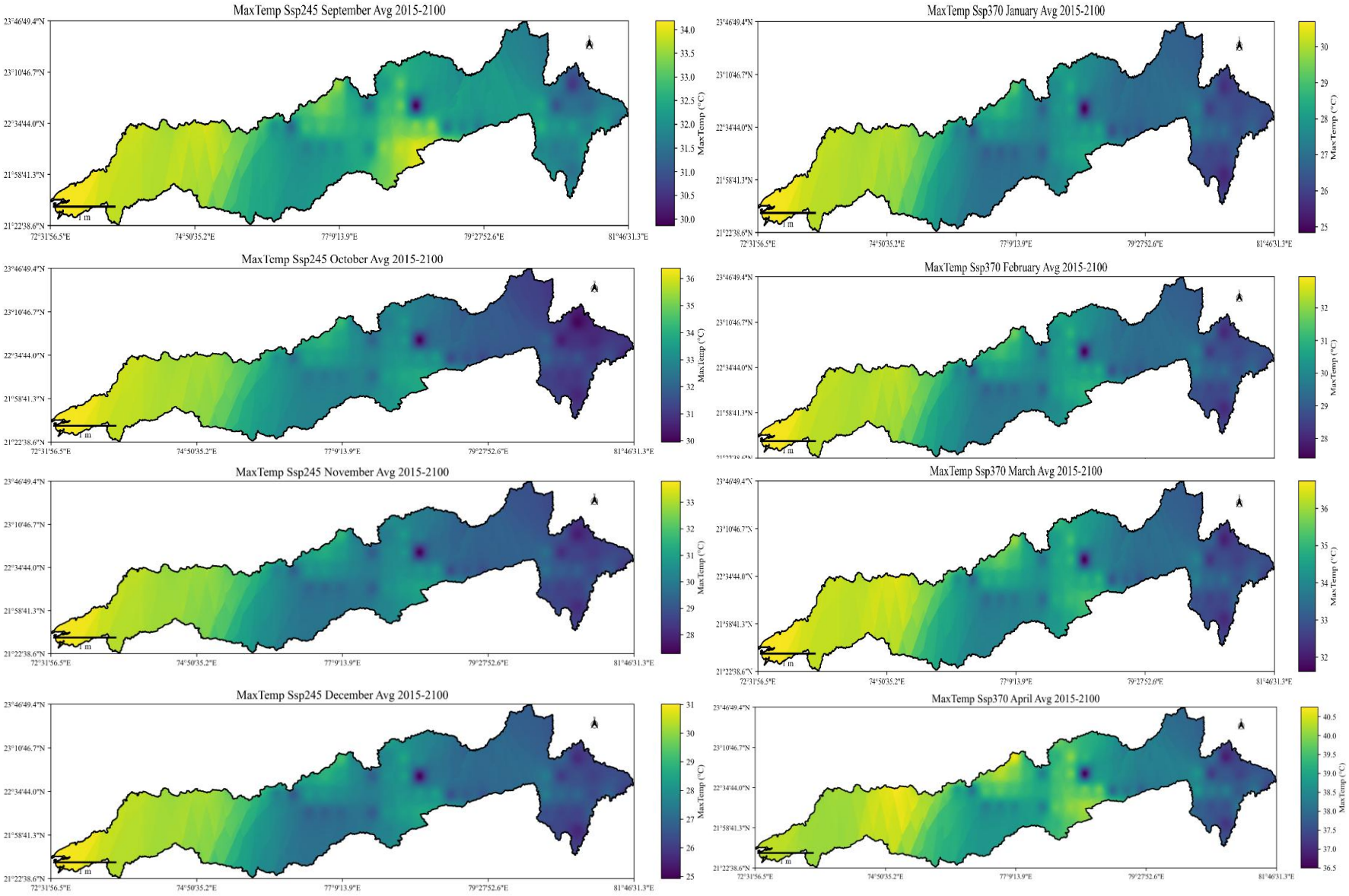
MaxTemp Ssp245 September Avg 2015-2100
MaxTemp Ssp370 January Avg 2015-2100
MaxTemp Ssp245 October Avg 2015-2100
MaxTemp Ssp370 February Avg 2015-2100
MaxTemp Ssp245 November Avg 2015-2100
MaxTemp Ssp370 March Avg 2015-2100
MaxTemp Ssp245 December Avg 2015-2100
MaxTemp Ssp370 April Avg 2015-2100
MaxTemp (°C)
23°46'49.4"N
23°10'46.7"N
22°34'44.0"N
21°58'41.3"N
21°22'38.6"N
72°31'56.5"E
74°50'35.2"E
77°9'13.9"E
79°27'52.6"E
81°46'31.3"E

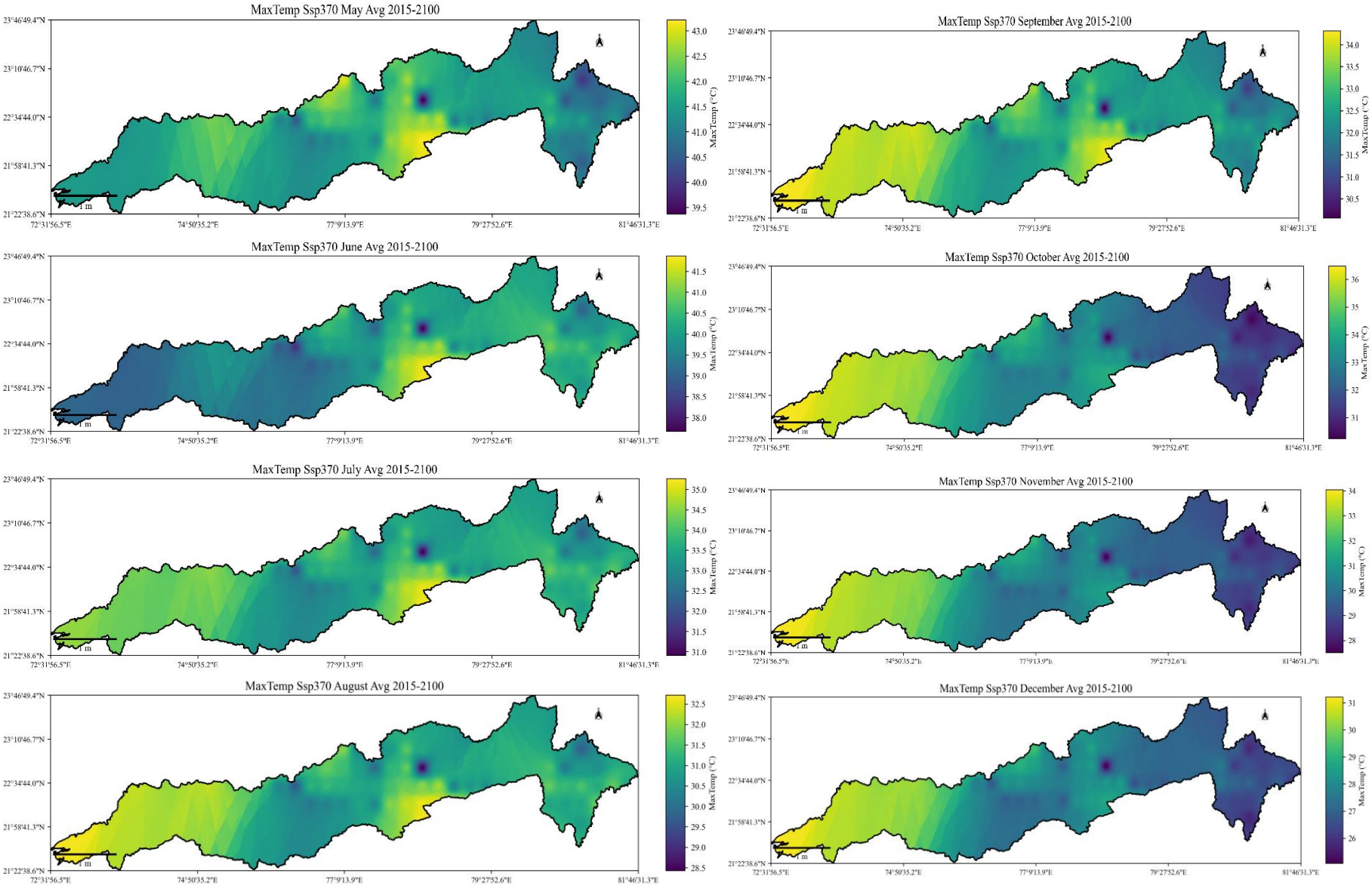
MaxTemp Ssp370 May Avg 2015-2100
MaxTemp Ssp370 September Avg 2015-2100
MaxTemp Ssp370 June Avg 2015-2100
MaxTemp Ssp370 October Avg 2015-2100
MaxTemp Ssp370 July Avg 2015-2100
MaxTemp Ssp370 November Avg 2015-2100
MaxTemp Ssp370 August Avg 2015-2100
MaxTemp Ssp370 December Avg 2015-2100
MaxTemp (°C)
23°46'49.4"N
23°10'46.7"N
22°34'44.0"N
21°58'41.3"N
21°22'38.6"N
72°31'56.5"E
74°50'35.2"E
77°9'13.9"E
79°27'52.6"E
81°46'31.3"E

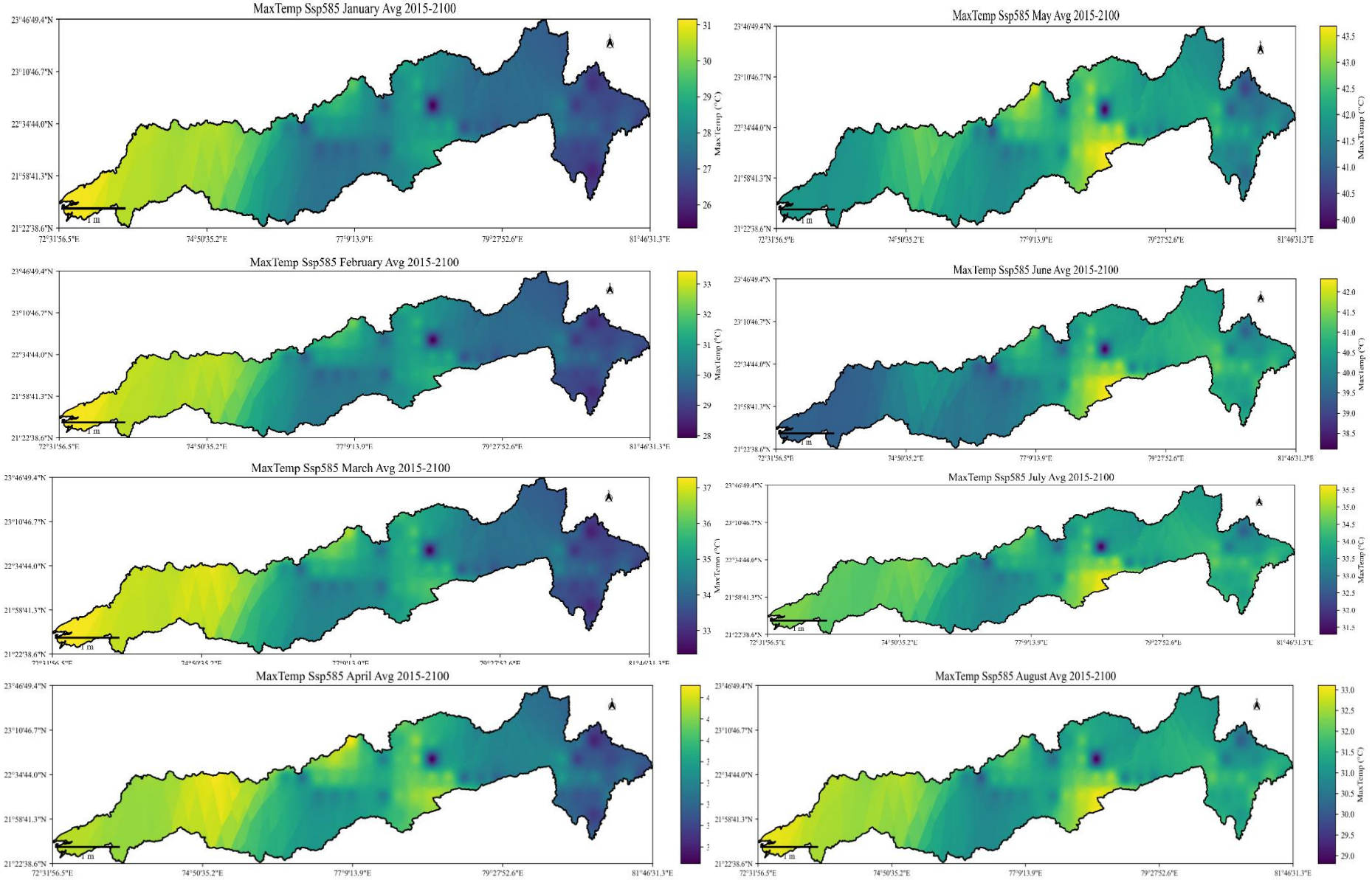
MaxTemp Ssp585 January Avg 2015-2100
MaxTemp Ssp585 May Avg 2015-2100
MaxTemp Ssp585 February Avg 2015-2100
MaxTemp Ssp585 June Avg 2015-2100
MaxTemp Ssp585 March Avg 2015-2100
MaxTemp Ssp585 July Avg 2015-2100
MaxTemp Ssp585 April Avg 2015-2100
MaxTemp Ssp585 August Avg 2015-2100
MaxTemp (°C)
23°46'49.4"N
23°10'46.7"N
22°34'44.0"N
21°58'41.3"N
21°22'38.6"N
72°31'56.5"E
74°50'35.2"E
77°9'13.9"E
79°27'52.6"E
81°46'31.3"E

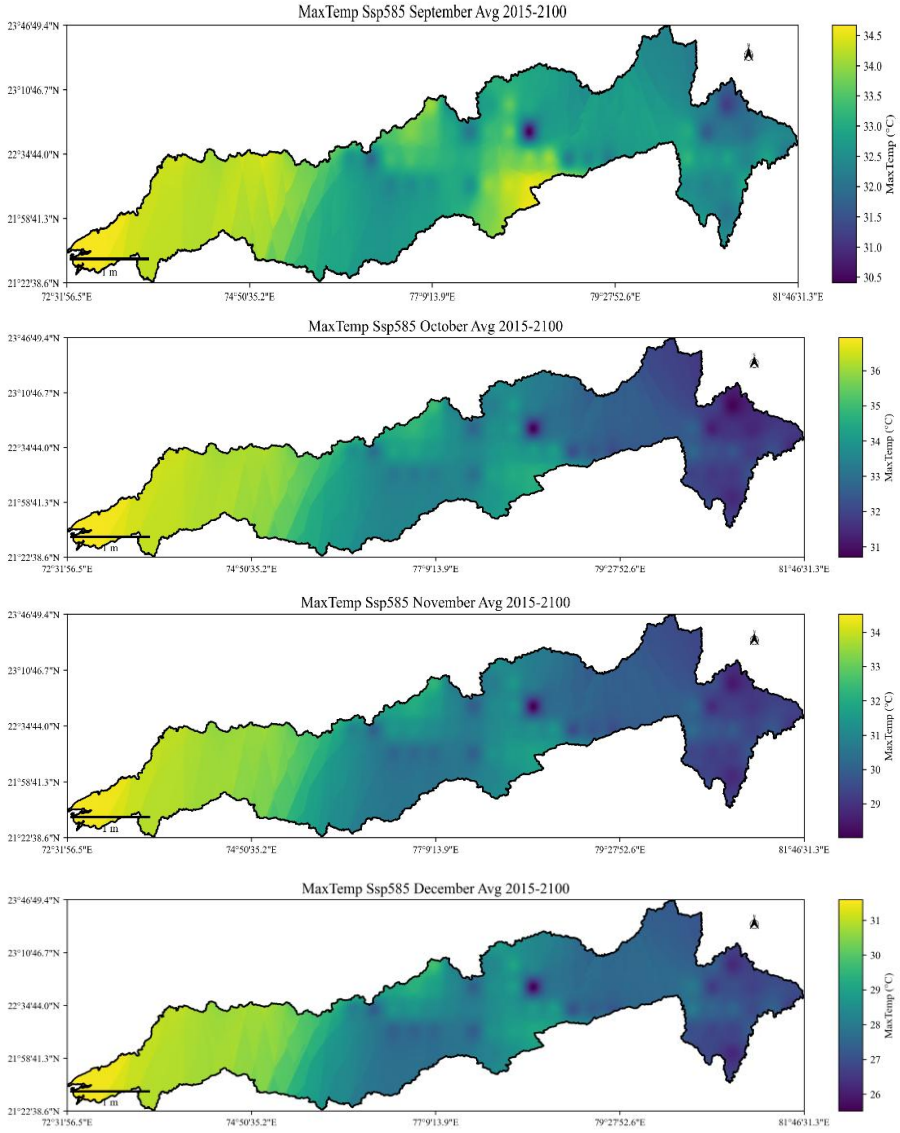
MaxTemp Ssp585 September Avg 2015-2100
MaxTemp Ssp585 October Avg 2015-2100
MaxTemp Ssp585 November Avg 2015-2100
MaxTemp Ssp585 December Avg 2015-2100
MaxTemp (°C)
23°46'49.4"N
23°10'46.7"N
22°34'44.0"N
21°58'41.3"N
21°22'38.6"N
72°31'56.5"E
74°50'35.2"E
77°9'13.9"E
79°27'52.6"E
81°46'31.3"E

Figure 72: Spatial distribution of monthly values of minimum temperatures for the Historical, SSP126, SSP245, SSP370, and SSP585 scenarios.

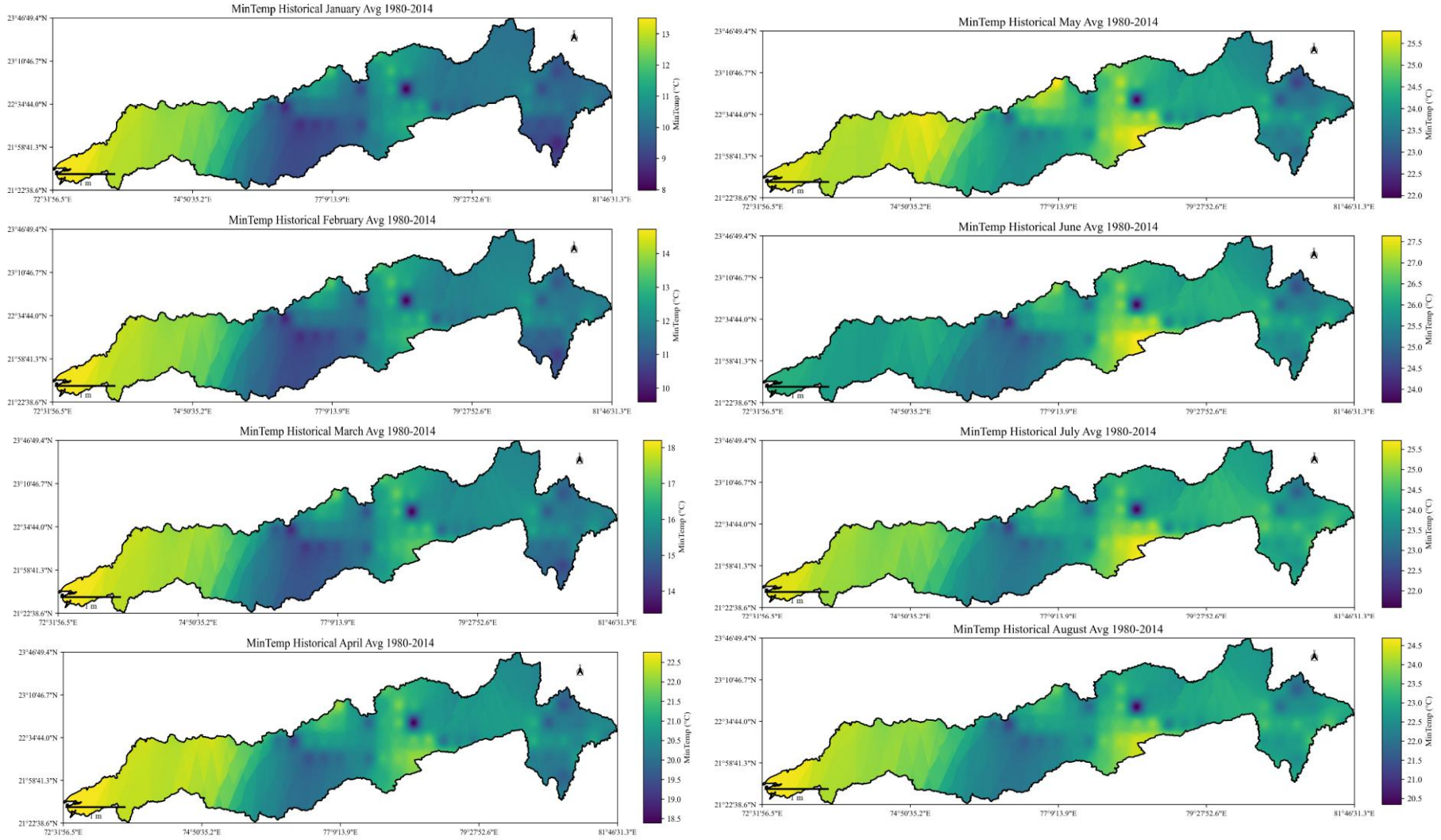

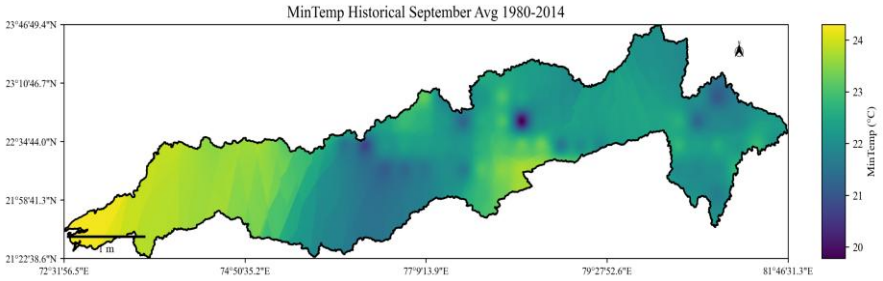
MinTemp Historical September Avg 1980-2014
23°46'49.4"N
23°10'46.7"N
22°34'44.0"N
21°58'41.3"N
21°22'38.6"N
72°31'56.5"E
74°50'35.2"E
77°9'13.9"E
79°27'52.6"E
81°46'31.3"E
MinTemp (°C)
24
23
22
21
20

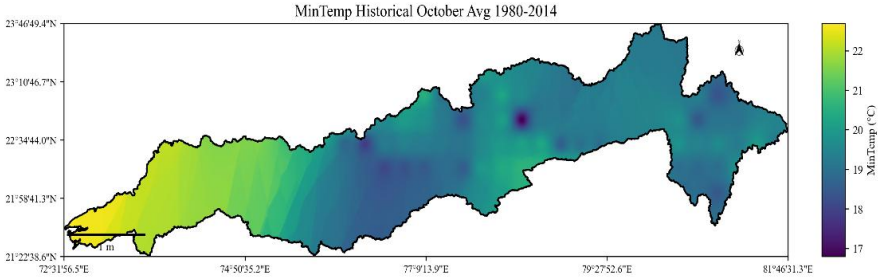
MinTemp Historical October Avg 1980-2014
23°46'49.4"N
23°10'46.7"N
22°34'44.0"N
21°58'41.3"N
21°22'38.6"N
72°31'56.5"E
74°50'35.2"E
77°9'13.9"E
79°27'52.6"E
81°46'31.3"E
MinTemp (°C)
22
21
20
19
18
17

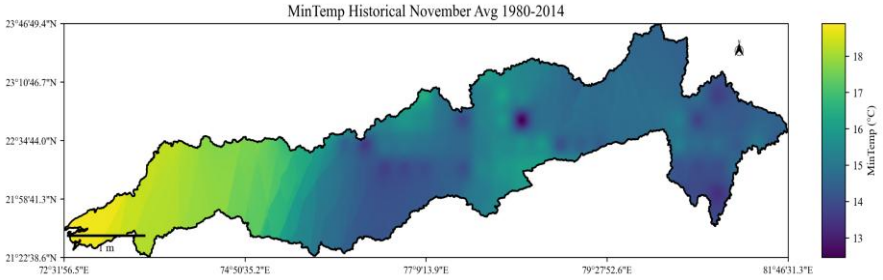
MinTemp Historical November Avg 1980-2014
23°46'49.4"N
23°10'46.7"N
22°34'44.0"N
21°58'41.3"N
21°22'38.6"N
72°31'56.5"E
74°50'35.2"E
77°9'13.9"E
79°27'52.6"E
81°46'31.3"E
MinTemp (°C)
18
17
16
15
14
13

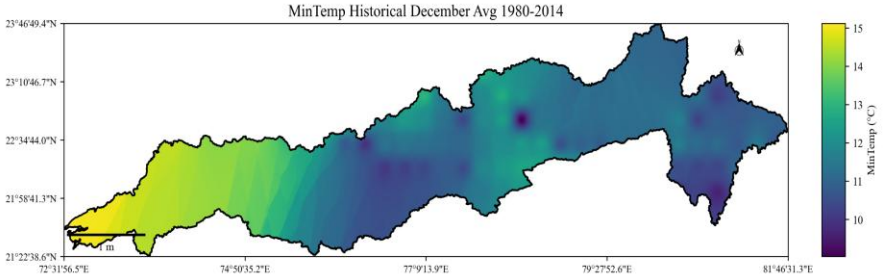
MinTemp Historical December Avg 1980-2014
23°46'49.4"N
23°10'46.7"N
22°34'44.0"N
21°58'41.3"N
21°22'38.6"N
72°31'56.5"E
74°50'35.2"E
77°9'13.9"E
79°27'52.6"E
81°46'31.3"E
MinTemp (°C)
15
14
13
12
11
10

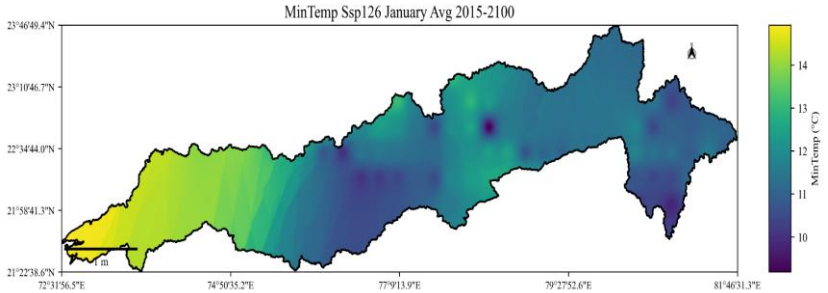
MinTemp Ssp126 January Avg 2015-2100
23°46'49.4"N
23°10'46.7"N
22°34'44.0"N
21°58'41.3"N
21°22'38.6"N
72°31'56.5"E
74°50'35.2"E
77°9'13.9"E
79°27'52.6"E
81°46'31.3"E
MinTemp (°C)
14
13
12
11
10

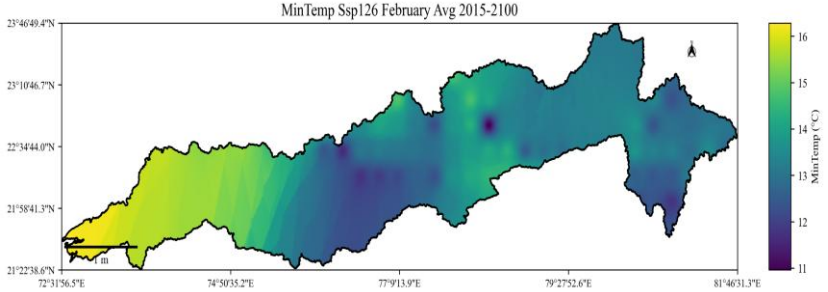
MinTemp Ssp126 February Avg 2015-2100
23°46'49.4"N
23°10'46.7"N
22°34'44.0"N
21°58'41.3"N
21°22'38.6"N
72°31'56.5"E
74°50'35.2"E
77°9'13.9"E
79°27'52.6"E
81°46'31.3"E
MinTemp (°C)
16
15
14
13
12
11

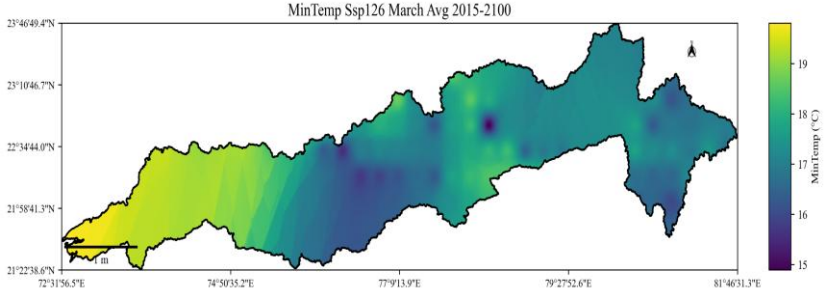
MinTemp Ssp126 March Avg 2015-2100
23°46'49.4"N
23°10'46.7"N
22°34'44.0"N
21°58'41.3"N
21°22'38.6"N
72°31'56.5"E
74°50'35.2"E
77°9'13.9"E
79°27'52.6"E
81°46'31.3"E
MinTemp (°C)
19
18
17
16
15

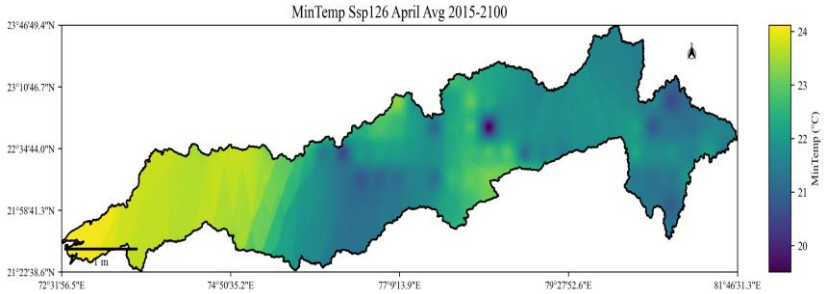
MinTemp Ssp126 April Avg 2015-2100
23°46'49.4"N
23°10'46.7"N
22°34'44.0"N
21°58'41.3"N
21°22'38.6"N
72°31'56.5"E
74°50'35.2"E
77°9'13.9"E
79°27'52.6"E
81°46'31.3"E
MinTemp (°C)
24
23
22
21
20

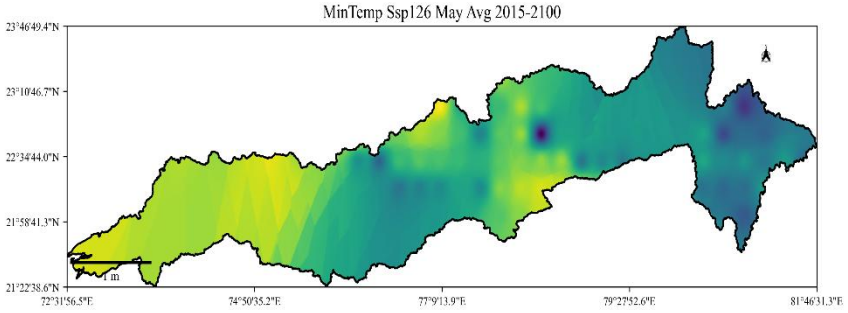
MinTemp Ssp126 May Avg 2015-2100
23°46'49.4"N
23°10'46.7"N
22°34'44.0"N
21°58'41.3"N
21°22'38.6"N
72°31'56.5"E
74°50'35.2"E
77°9'13.9"E
79°27'52.6"E
81°46'31.3"E

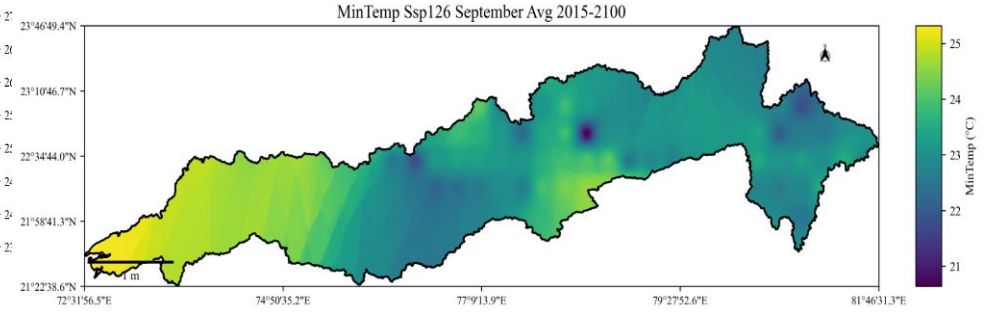
MinTemp Ssp126 September Avg 2015-2100
MinTemp (°C)

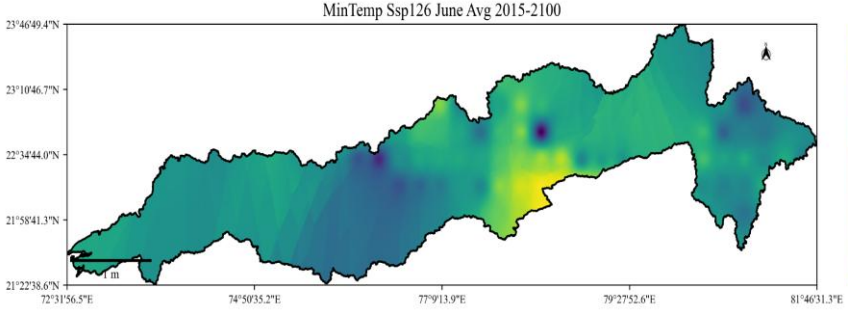
MinTemp Ssp126 June Avg 2015-2100

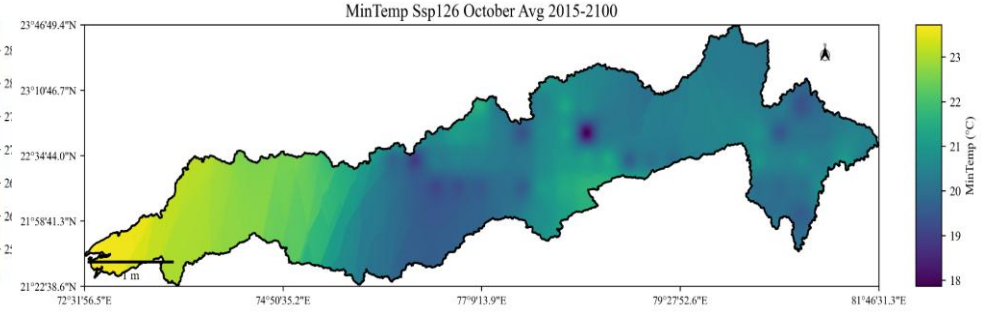
MinTemp Ssp126 October Avg 2015-2100
MinTemp (°C)

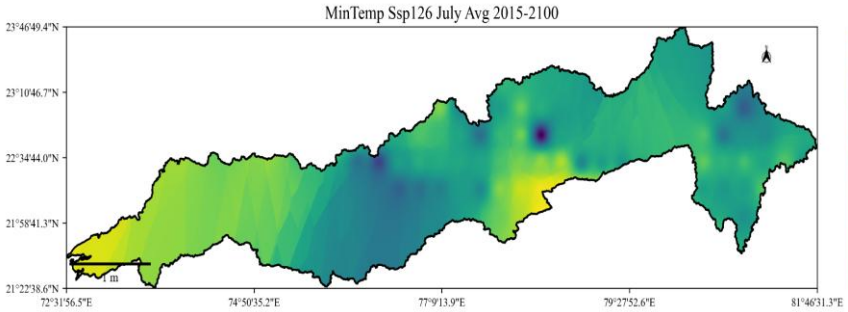
MinTemp Ssp126 July Avg 2015-2100

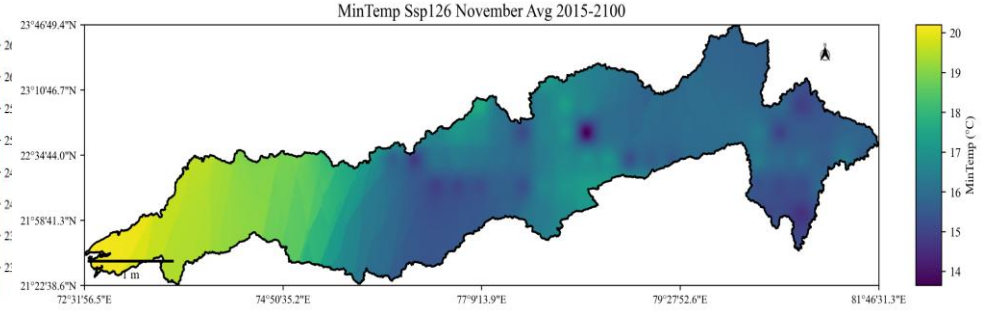
MinTemp Ssp126 November Avg 2015-2100
MinTemp (°C)

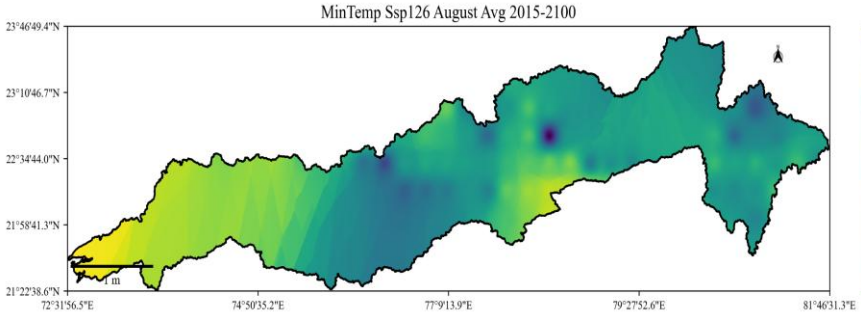
MinTemp Ssp126 August Avg 2015-2100

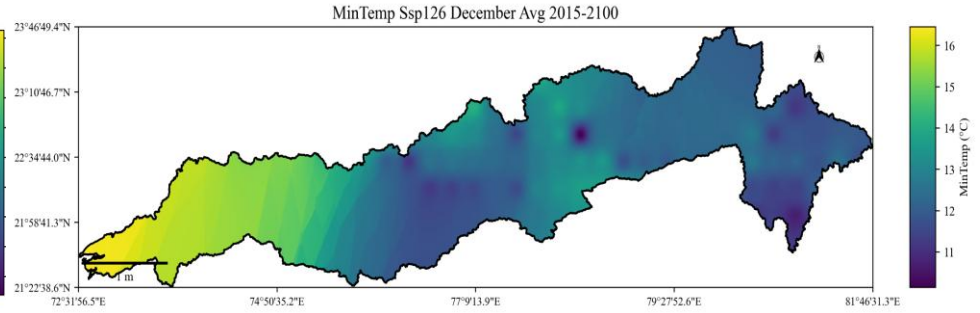
MinTemp Ssp126 December Avg 2015-2100
MinTemp (°C)

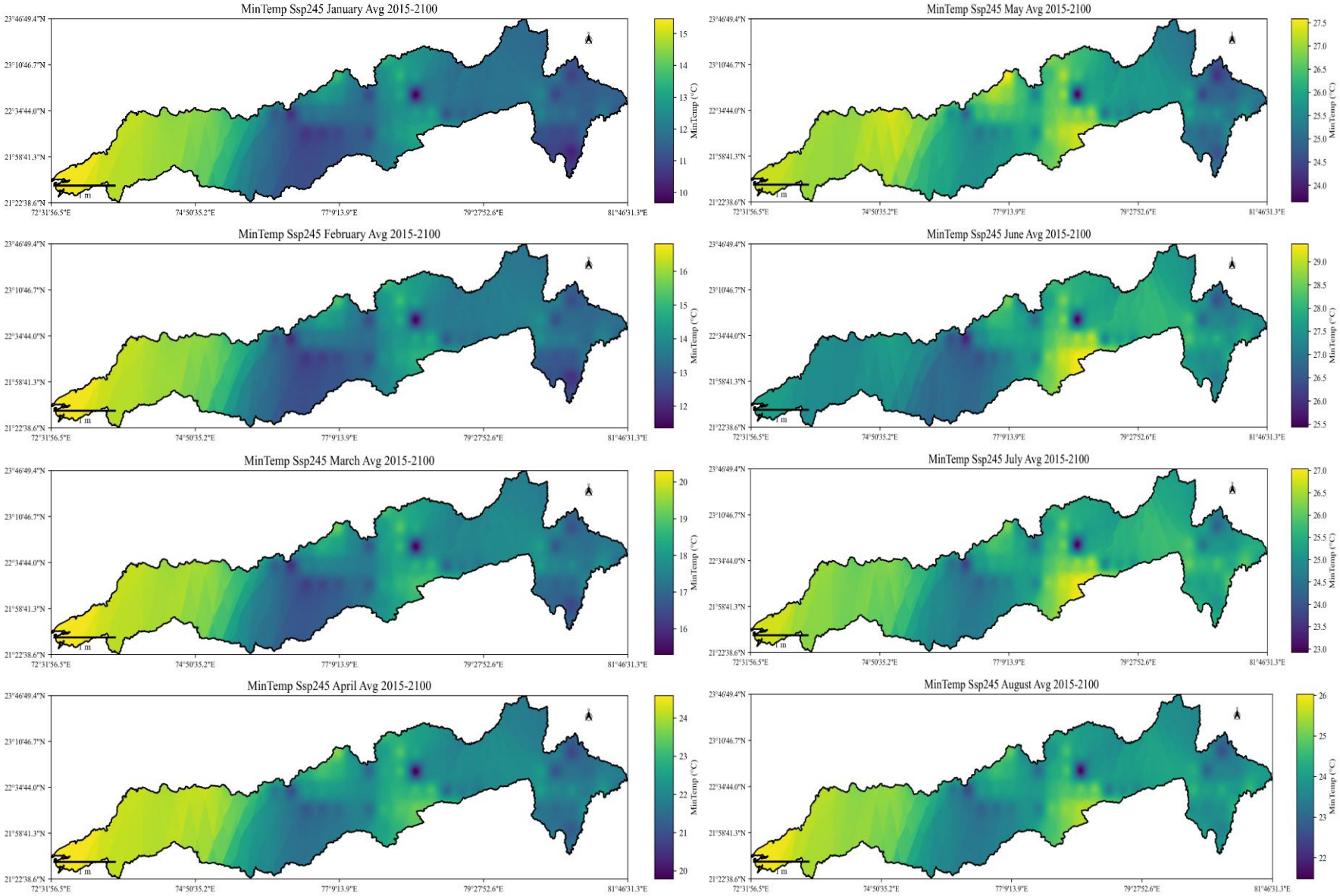
MinTemp Ssp245 January Avg 2015-2100
MinTemp Ssp245 May Avg 2015-2100
MinTemp Ssp245 February Avg 2015-2100
MinTemp Ssp245 June Avg 2015-2100
MinTemp Ssp245 March Avg 2015-2100
MinTemp Ssp245 July Avg 2015-2100
MinTemp Ssp245 April Avg 2015-2100
MinTemp Ssp245 August Avg 2015-2100
MinTemp (°C)
23°46'49.4"N
23°10'46.7"N
22°34'44.0"N
21°58'41.3"N
21°22'38.6"N
72°31'56.5"E
74°50'35.2"E
77°9'13.9"E
79°27'52.6"E
81°46'31.3"E

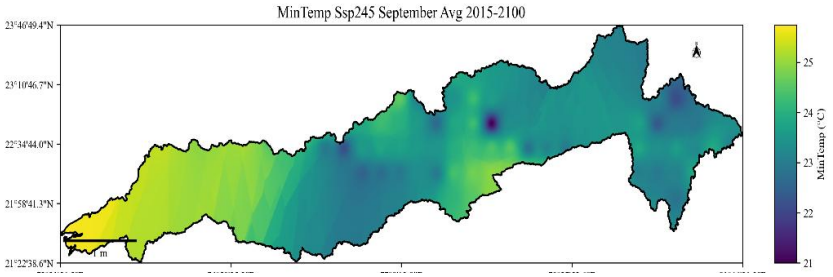
MinTemp Ssp245 September Avg 2015-2100
MinTemp (°C)

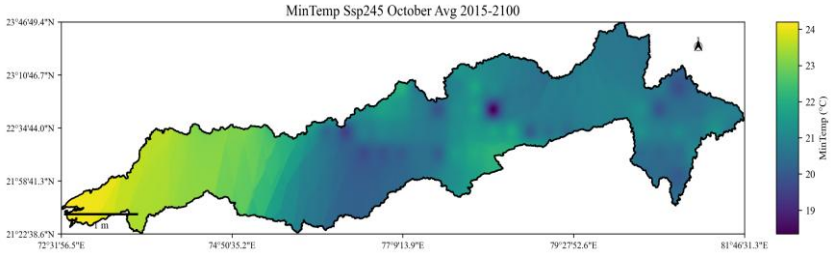
MinTemp Ssp245 October Avg 2015-2100
MinTemp (°C)

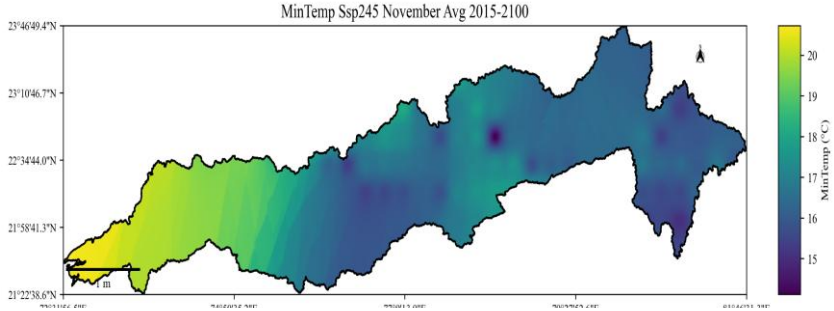
MinTemp Ssp245 November Avg 2015-2100
MinTemp (°C)

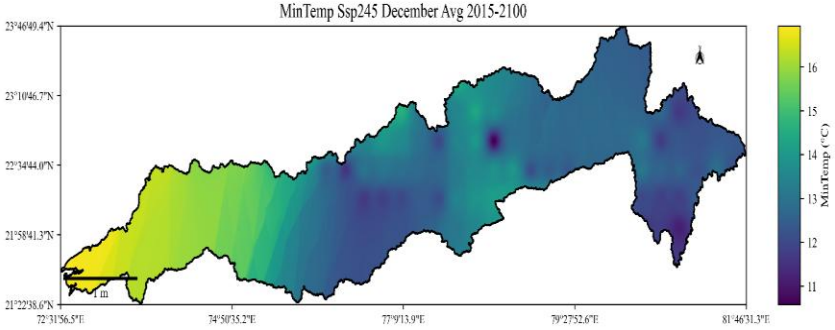
MinTemp Ssp245 December Avg 2015-2100
MinTemp (°C)

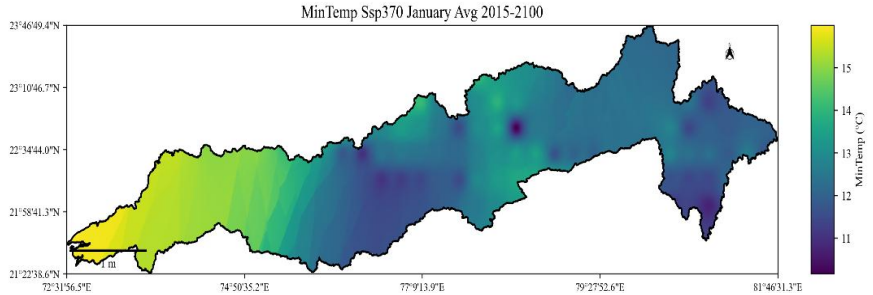
MinTemp Ssp370 January Avg 2015-2100
MinTemp (°C)

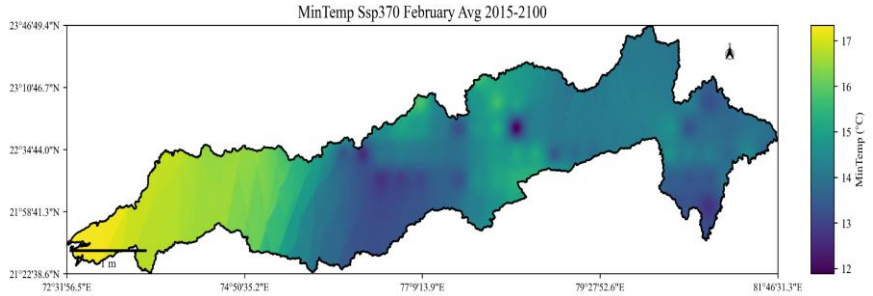
MinTemp Ssp370 February Avg 2015-2100
MinTemp (°C)

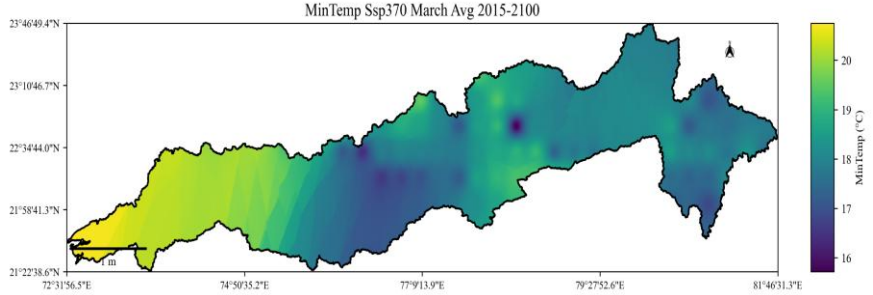
MinTemp Ssp370 March Avg 2015-2100
MinTemp (°C)

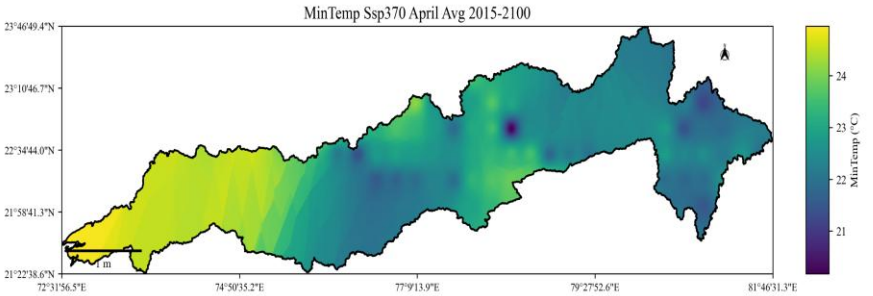
MinTemp Ssp370 April Avg 2015-2100
MinTemp (°C)

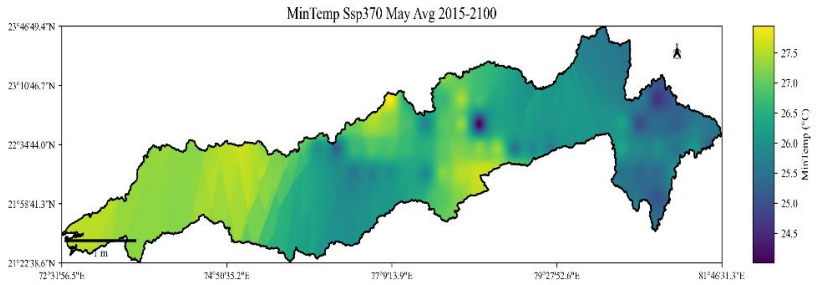
MinTemp Ssp370 May Avg 2015-2100
23°46'49.4"N
23°10'46.7"N
22°34'44.0"N
21°58'41.3"N
21°22'38.6"N
72°31'56.5"E
74°50'35.2"E
77°9'13.9"E
79°27'52.6"E
81°46'31.3"E
MinTemp (°C)
27.5
27.0
26.5
26.0
25.5
25.0
24.5

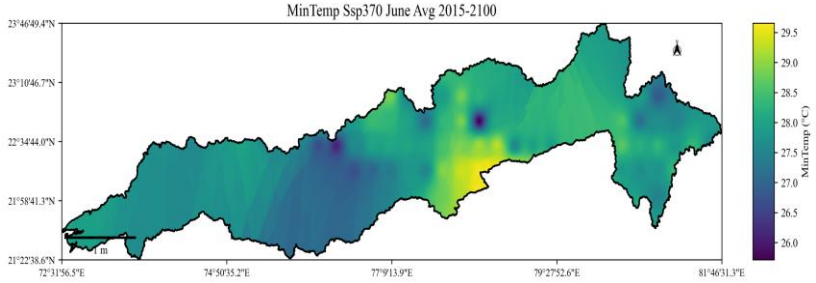
MinTemp Ssp370 June Avg 2015-2100
23°46'49.4"N
23°10'46.7"N
22°34'44.0"N
21°58'41.3"N
21°22'38.6"N
72°31'56.5"E
74°50'35.2"E
77°9'13.9"E
79°27'52.6"E
81°46'31.3"E
MinTemp (°C)
29.5
29.0
28.5
28.0
27.5
27.0
26.5
26.0

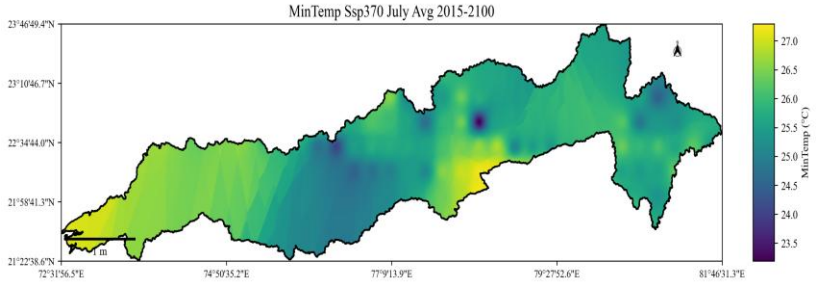
MinTemp Ssp370 July Avg 2015-2100
23°46'49.4"N
23°10'46.7"N
22°34'44.0"N
21°58'41.3"N
21°22'38.6"N
72°31'56.5"E
74°50'35.2"E
77°9'13.9"E
79°27'52.6"E
81°46'31.3"E
MinTemp (°C)
27.0
26.5
26.0
25.5
25.0
24.5
24.0
23.5

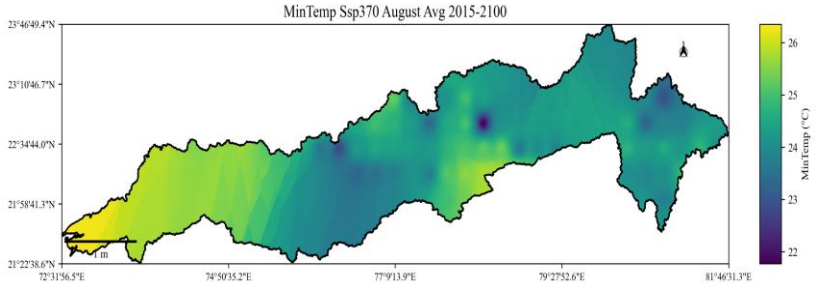
MinTemp Ssp370 August Avg 2015-2100
23°46'49.4"N
23°10'46.7"N
22°34'44.0"N
21°58'41.3"N
21°22'38.6"N
72°31'56.5"E
74°50'35.2"E
77°9'13.9"E
79°27'52.6"E
81°46'31.3"E
MinTemp (°C)
26
25
24
23
22

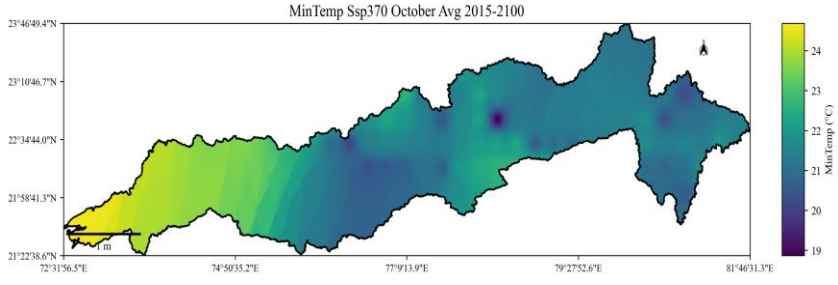
MinTemp Ssp370 October Avg 2015-2100
23°46'49.4"N
23°10'46.7"N
22°34'44.0"N
21°58'41.3"N
21°22'38.6"N
72°31'56.5"E
74°50'35.2"E
77°9'13.9"E
79°27'52.6"E
81°46'31.3"E
MinTemp (°C)
24
23
22
21
20
19

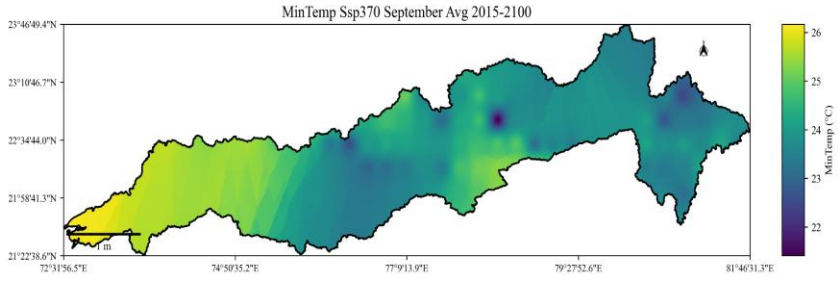
MinTemp Ssp370 September Avg 2015-2100
23°46'49.4"N
23°10'46.7"N
22°34'44.0"N
21°58'41.3"N
21°22'38.6"N
72°31'56.5"E
74°50'35.2"E
77°9'13.9"E
79°27'52.6"E
81°46'31.3"E
MinTemp (°C)
26
25
24
23
22

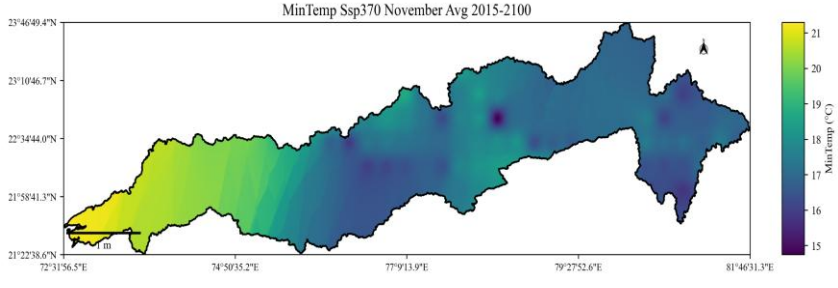
MinTemp Ssp370 November Avg 2015-2100
23°46'49.4"N
23°10'46.7"N
22°34'44.0"N
21°58'41.3"N
21°22'38.6"N
72°31'56.5"E
74°50'35.2"E
77°9'13.9"E
79°27'52.6"E
81°46'31.3"E
MinTemp (°C)
21
20
19
18
17
16
15

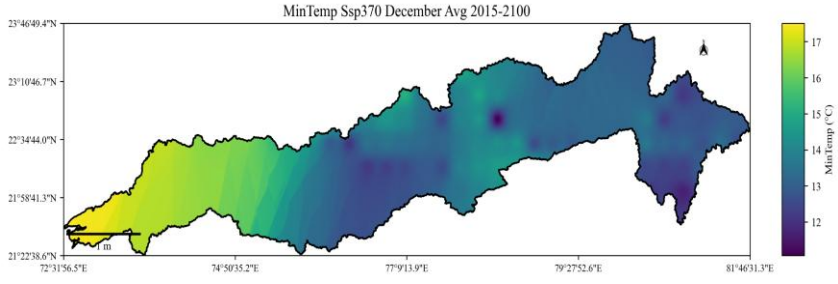
MinTemp Ssp370 December Avg 2015-2100
23°46'49.4"N
23°10'46.7"N
22°34'44.0"N
21°58'41.3"N
21°22'38.6"N
72°31'56.5"E
74°50'35.2"E
77°9'13.9"E
79°27'52.6"E
81°46'31.3"E
MinTemp (°C)
17
16
15
14
13
12

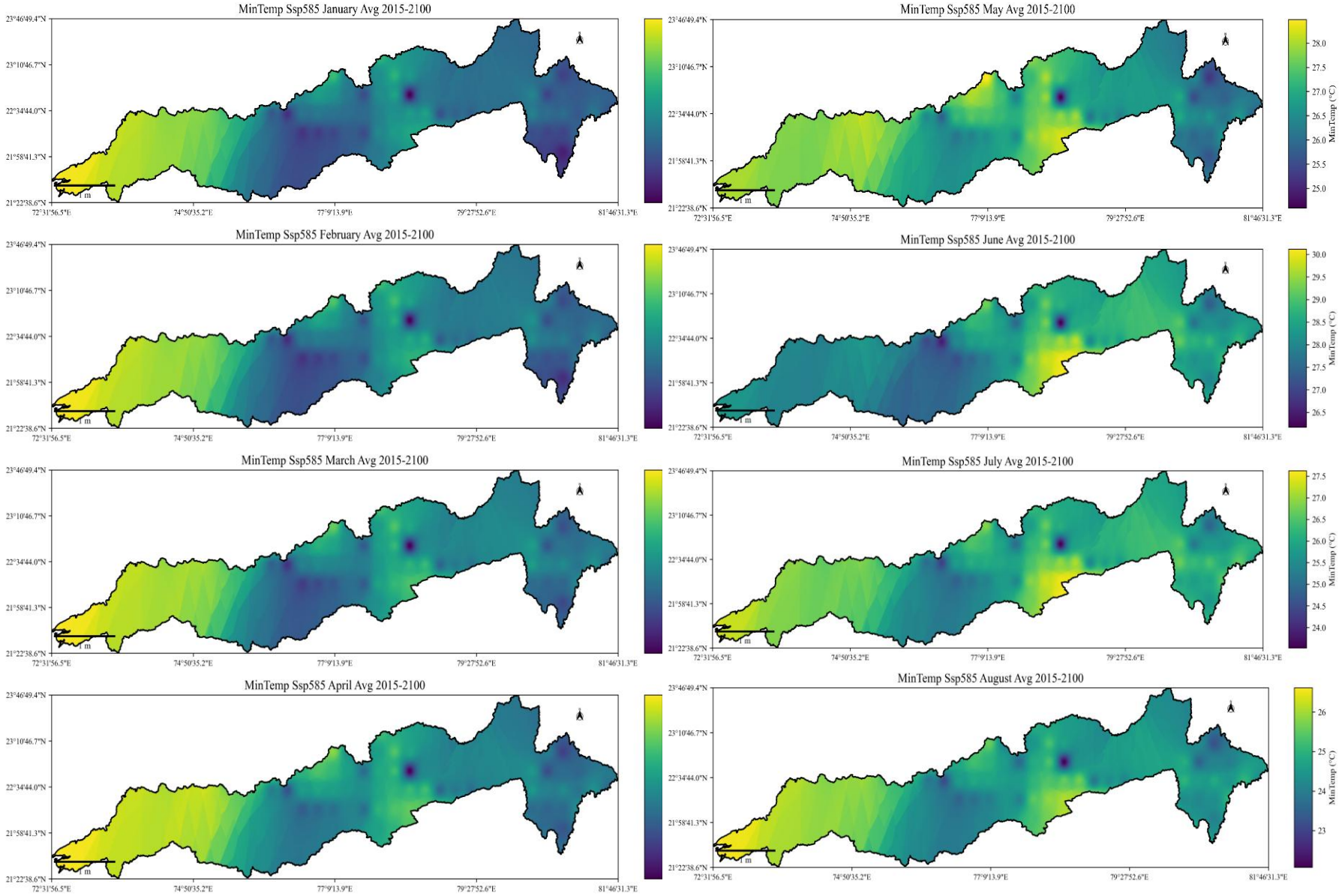
MinTemp Ssp585 January Avg 2015-2100
MinTemp Ssp585 February Avg 2015-2100
MinTemp Ssp585 March Avg 2015-2100
MinTemp Ssp585 April Avg 2015-2100
MinTemp Ssp585 May Avg 2015-2100
MinTemp Ssp585 June Avg 2015-2100
MinTemp Ssp585 July Avg 2015-2100
MinTemp Ssp585 August Avg 2015-2100
23°46'49.4"N
23°10'46.7"N
22°34'44.0"N
21°58'41.3"N
21°22'38.6"N
72°31'56.5"E
74°50'35.2"E
77°9'13.9"E
79°27'52.6"E
81°46'31.3"E
MinTemp (°C)

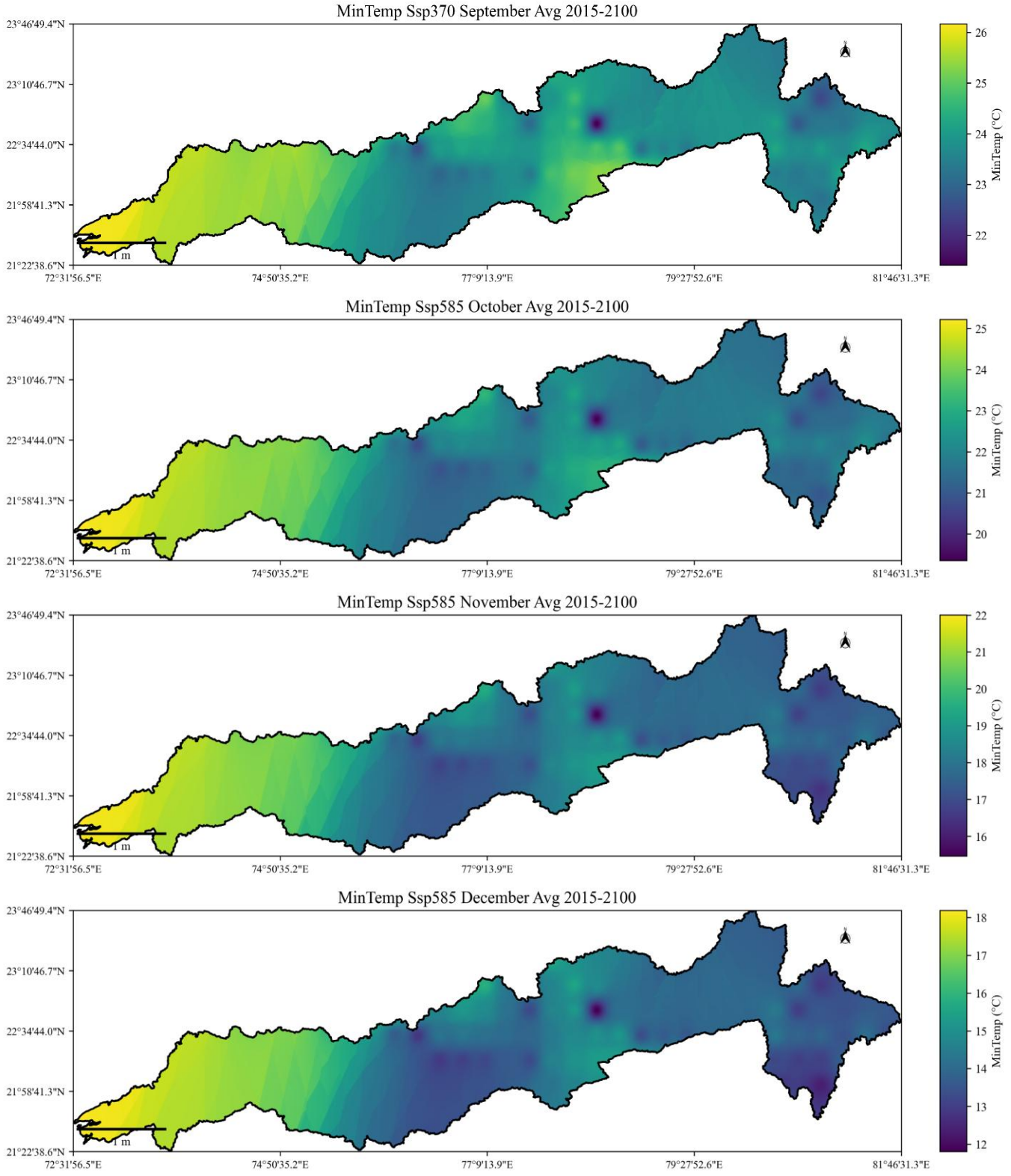
MinTemp Ssp370 September Avg 2015-2100
MinTemp Ssp585 October Avg 2015-2100
MinTemp Ssp585 November Avg 2015-2100
MinTemp Ssp585 December Avg 2015-2100
23°46'49.4"N
23°10'46.7"N
22°34'44.0"N
21°58'41.3"N
21°22'38.6"N
72°31'56.5"E
74°50'35.2"E
77°9'13.9"E
79°27'52.6"E
81°46'31.3"E
1 m
MinTemp (°C)

Figure 73Spatial distribution of monthly values of Mean temperatures for the Historical, SSP126, SSP245, SSP370, and SSP585 scenarios

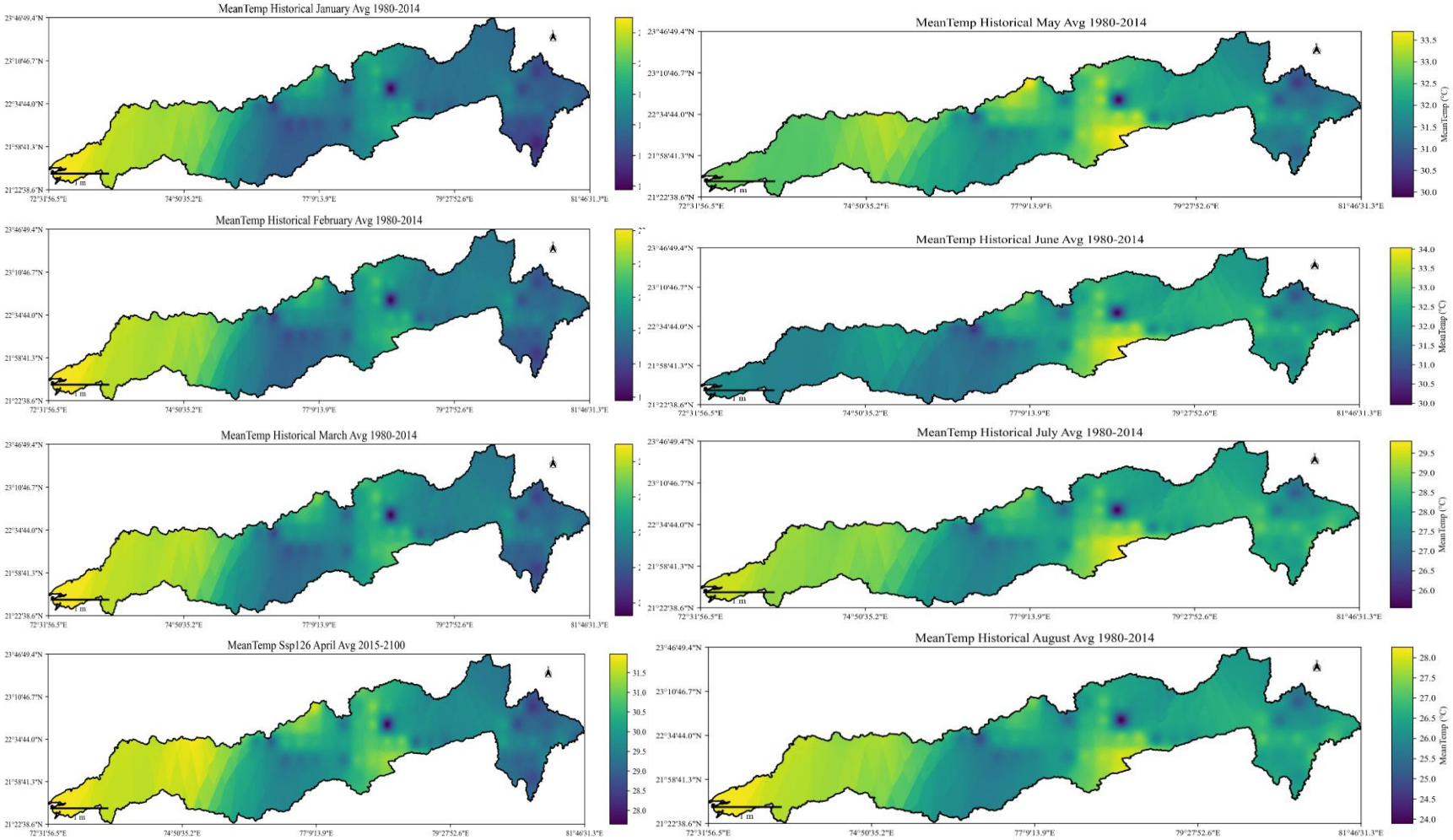

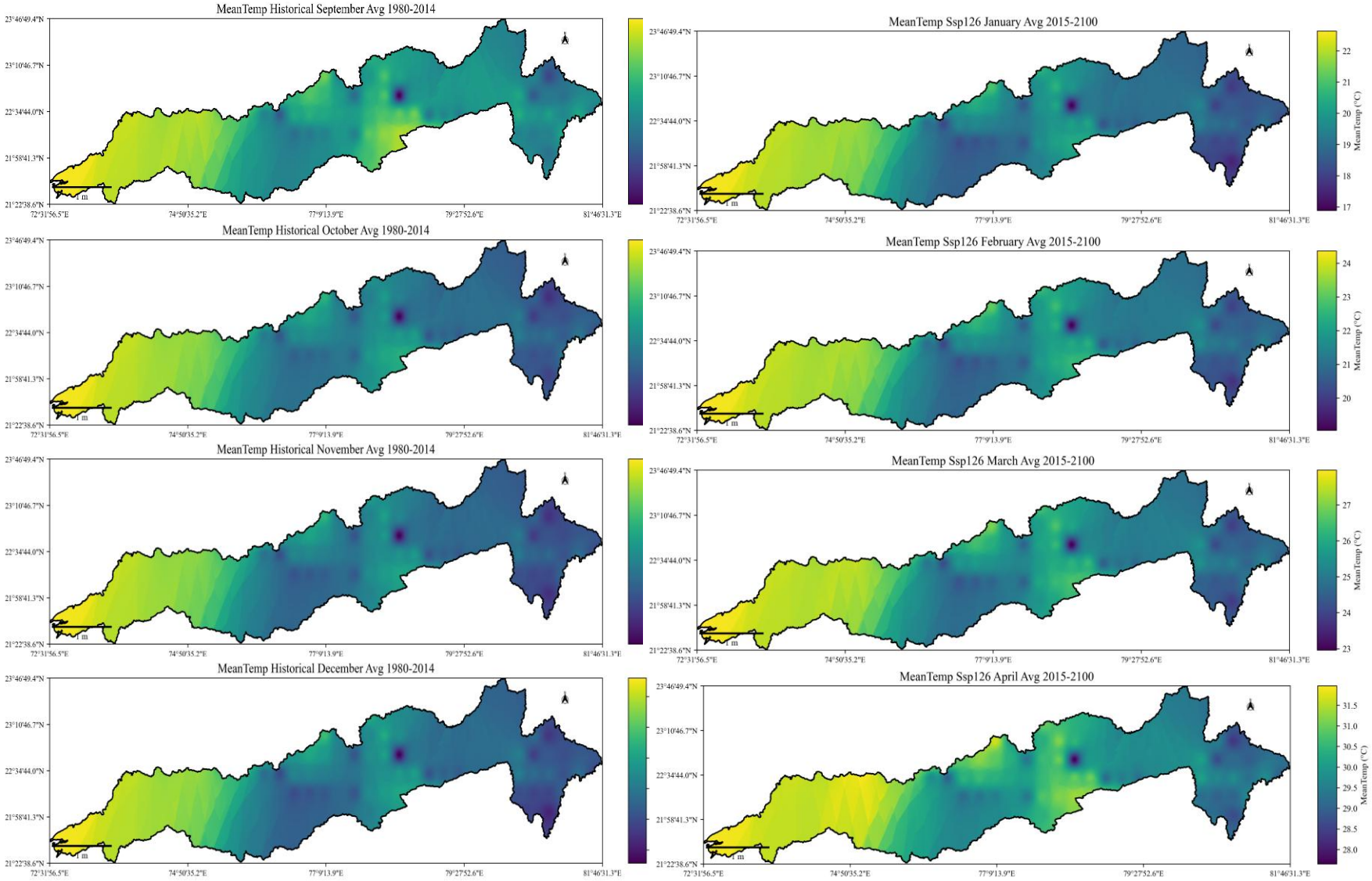
MeanTemp Historical September Avg 1980-2014
MeanTemp Ssp126 January Avg 2015-2100
MeanTemp Historical October Avg 1980-2014
MeanTemp Ssp126 February Avg 2015-2100
MeanTemp Historical November Avg 1980-2014
MeanTemp Ssp126 March Avg 2015-2100
MeanTemp Historical December Avg 1980-2014
MeanTemp Ssp126 April Avg 2015-2100
MeanTemp (°C)
23°46'49.4"N
23°10'46.7"N
22°34'44.0"N
21°58'41.3"N
21°22'38.6"N
72°31'56.5"E
74°50'35.2"E
77°9'13.9"E
79°27'52.6"E
81°46'31.3"E

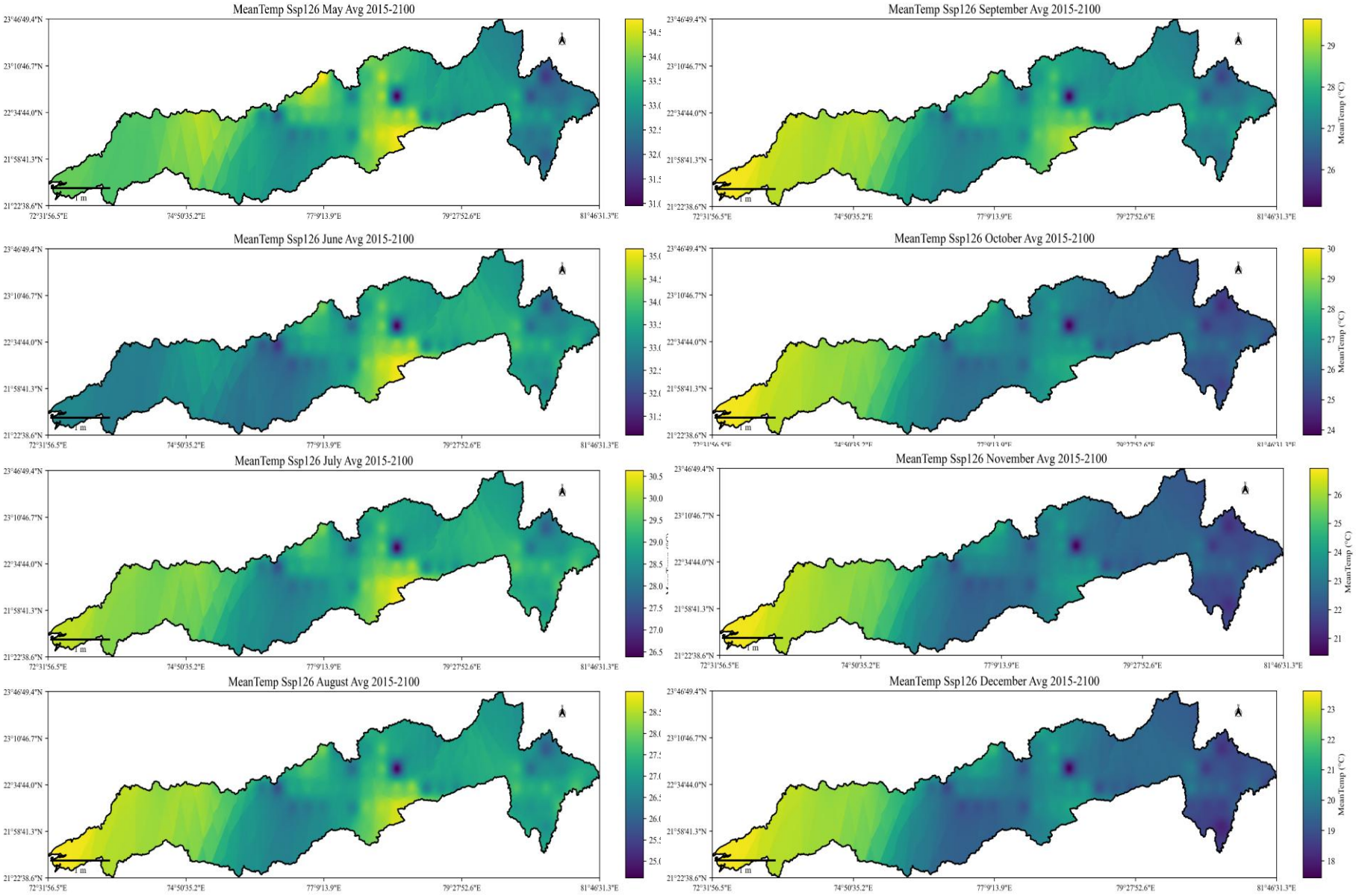
MeanTemp Ssp126 May Avg 2015-2100
MeanTemp Ssp126 September Avg 2015-2100
MeanTemp Ssp126 June Avg 2015-2100
MeanTemp Ssp126 October Avg 2015-2100
MeanTemp Ssp126 July Avg 2015-2100
MeanTemp Ssp126 November Avg 2015-2100
MeanTemp Ssp126 August Avg 2015-2100
MeanTemp Ssp126 December Avg 2015-2100
MeanTemp (°C)

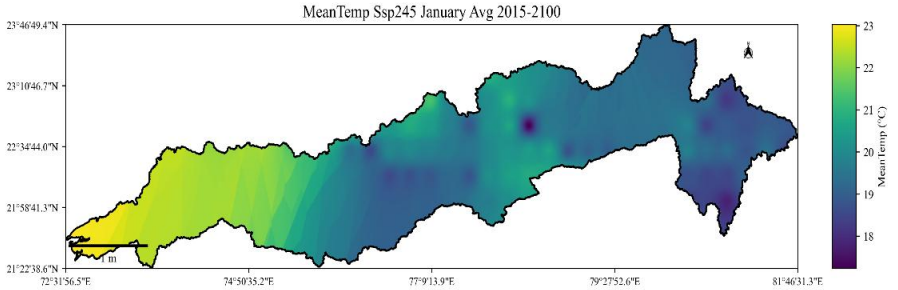
MeanTemp Ssp245 January Avg 2015-2100
23°46'49.4"N
23°10'46.7"N
22°34'44.0"N
21°58'41.3"N
21°22'38.6"N
72°31'56.5"E
74°50'35.2"E
77°9'13.9"E
79°27'52.6"E
81°46'31.3"E
MeanTemp (°C)
23
22
21
20
19
18

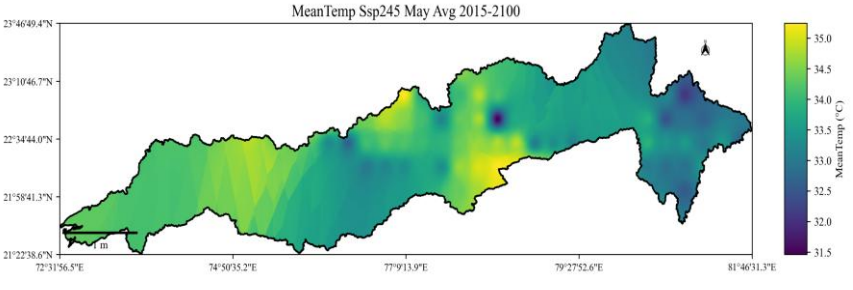
MeanTemp Ssp245 May Avg 2015-2100
23°46'49.4"N
23°10'46.7"N
22°34'44.0"N
21°58'41.3"N
21°22'38.6"N
72°31'56.5"E
74°50'35.2"E
77°9'13.9"E
79°27'52.6"E
81°46'31.3"E
MeanTemp (°C)
35.0
34.5
34.0
33.5
33.0
32.5
32.0
31.5

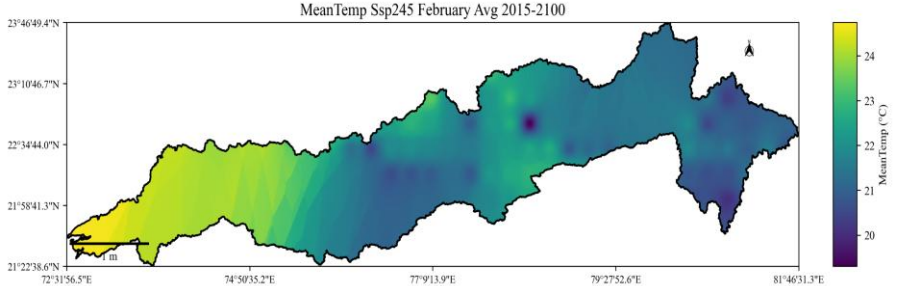
MeanTemp Ssp245 February Avg 2015-2100
23°46'49.4"N
23°10'46.7"N
22°34'44.0"N
21°58'41.3"N
21°22'38.6"N
72°31'56.5"E
74°50'35.2"E
77°9'13.9"E
79°27'52.6"E
81°46'31.3"E
MeanTemp (°C)
24
23
22
21
20

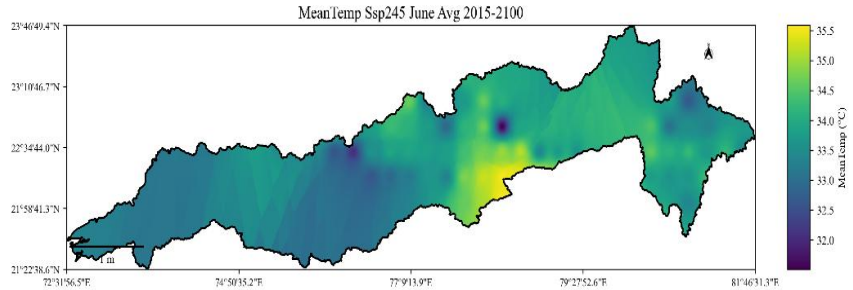
MeanTemp Ssp245 June Avg 2015-2100
23°46'49.4"N
23°10'46.7"N
22°34'44.0"N
21°58'41.3"N
21°22'38.6"N
72°31'56.5"E
74°50'35.2"E
77°9'13.9"E
79°27'52.6"E
81°46'31.3"E
MeanTemp (°C)
35.5
35.0
34.5
34.0
33.5
33.0
32.5
32.0

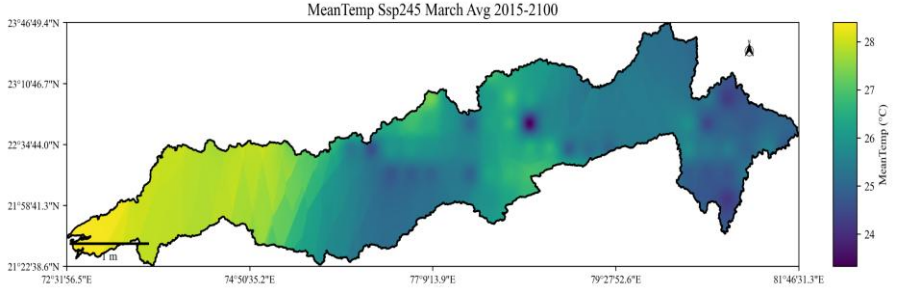
MeanTemp Ssp245 March Avg 2015-2100
23°46'49.4"N
23°10'46.7"N
22°34'44.0"N
21°58'41.3"N
21°22'38.6"N
72°31'56.5"E
74°50'35.2"E
77°9'13.9"E
79°27'52.6"E
81°46'31.3"E
MeanTemp (°C)
28
27
26
25
24

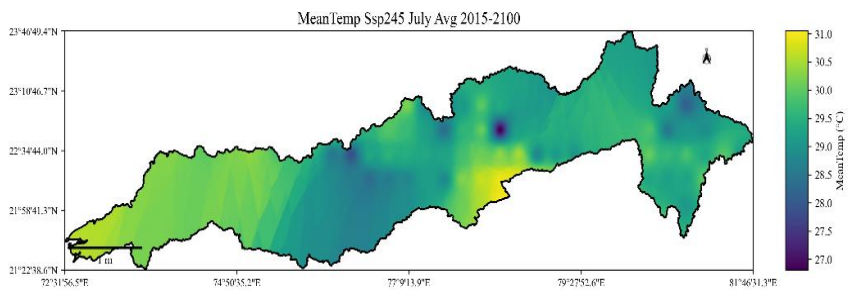
MeanTemp Ssp245 July Avg 2015-2100
23°46'49.4"N
23°10'46.7"N
22°34'44.0"N
21°58'41.3"N
21°22'38.6"N
72°31'56.5"E
74°50'35.2"E
77°9'13.9"E
79°27'52.6"E
81°46'31.3"E
MeanTemp (°C)
31.0
30.5
30.0
29.5
29.0
28.5
28.0
27.5
27.0

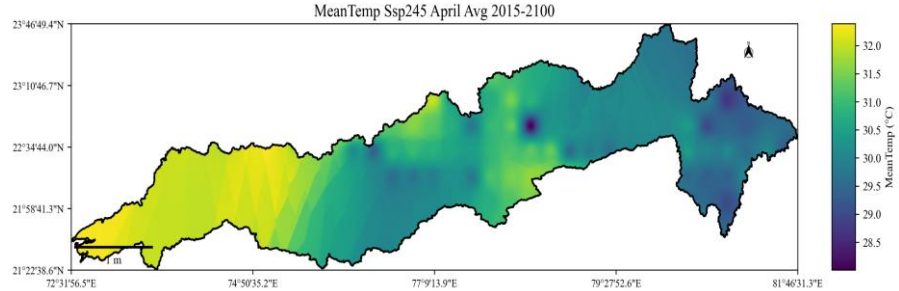
MeanTemp Ssp245 April Avg 2015-2100
23°46'49.4"N
23°10'46.7"N
22°34'44.0"N
21°58'41.3"N
21°22'38.6"N
72°31'56.5"E
74°50'35.2"E
77°9'13.9"E
79°27'52.6"E
81°46'31.3"E
MeanTemp (°C)
32.0
31.5
31.0
30.5
30.0
29.5
29.0
28.5

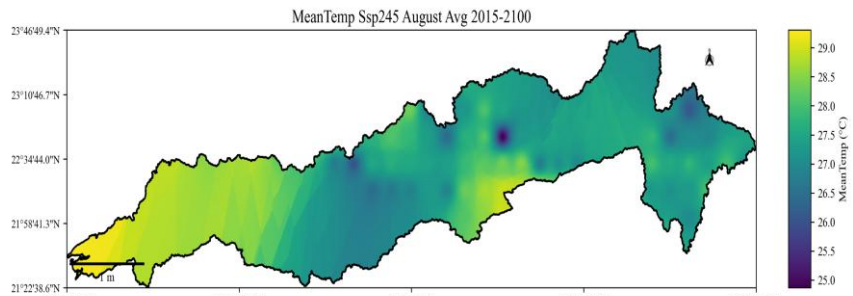
MeanTemp Ssp245 August Avg 2015-2100
23°46'49.4"N
23°10'46.7"N
22°34'44.0"N
21°58'41.3"N
21°22'38.6"N
72°31'56.5"E
74°50'35.2"E
77°9'13.9"E
79°27'52.6"E
81°46'31.3"E
MeanTemp (°C)
29.0
28.5
28.0
27.5
27.0
26.5
26.0
25.5
25.0

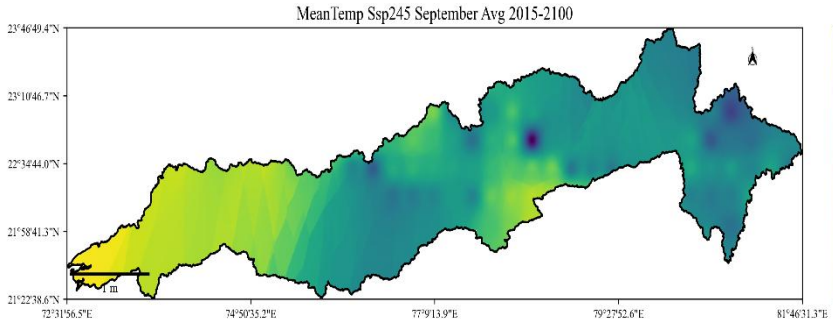
MeanTemp Ssp245 September Avg 2015-2100
23°46'49.4"N
23°10'46.7"N
22°34'44.0"N
21°58'41.3"N
21°22'38.6"N
72°31'56.5"E
74°50'35.2"E
77°9'13.9"E
79°27'52.6"E
81°46'31.3"E
29
28
27
26

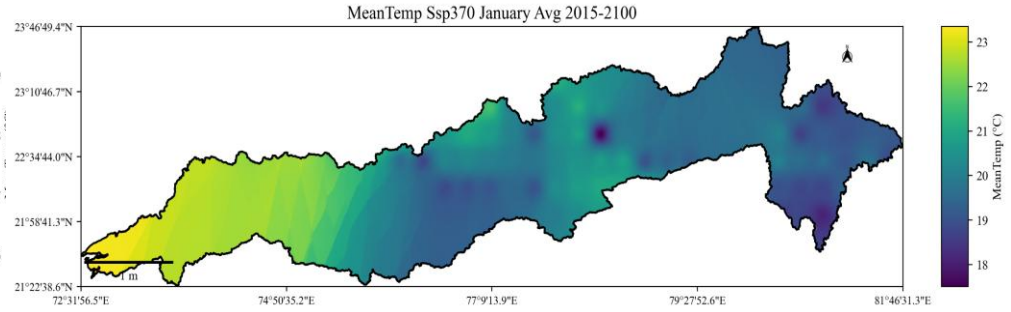
MeanTemp Ssp370 January Avg 2015-2100
23°46'49.4"N
23°10'46.7"N
22°34'44.0"N
21°58'41.3"N
21°22'38.6"N
72°31'56.5"E
74°50'35.2"E
77°9'13.9"E
79°27'52.6"E
81°46'31.3"E
MeanTemp (°C)
23
22
21
20
19
18

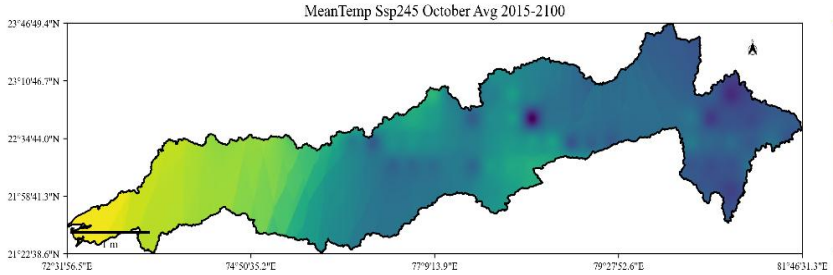
MeanTemp Ssp245 October Avg 2015-2100
23°46'49.4"N
23°10'46.7"N
22°34'44.0"N
21°58'41.3"N
21°22'38.6"N
72°31'56.5"E
74°50'35.2"E
77°9'13.9"E
79°27'52.6"E
81°46'31.3"E
30
29
28
27
26
25

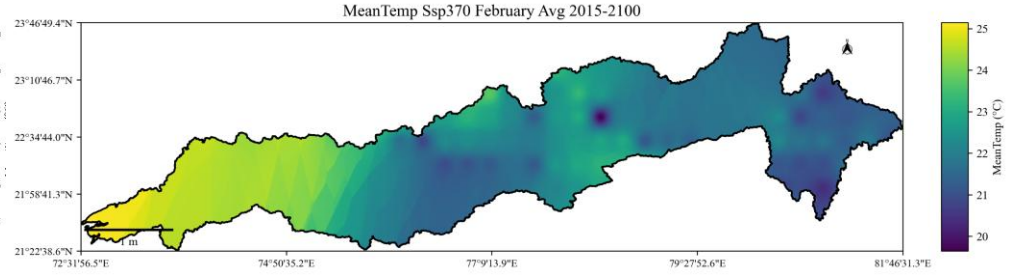
MeanTemp Ssp370 February Avg 2015-2100
23°46'49.4"N
23°10'46.7"N
22°34'44.0"N
21°58'41.3"N
21°22'38.6"N
72°31'56.5"E
74°50'35.2"E
77°9'13.9"E
79°27'52.6"E
81°46'31.3"E
MeanTemp (°C)
25
24
23
22
21
20

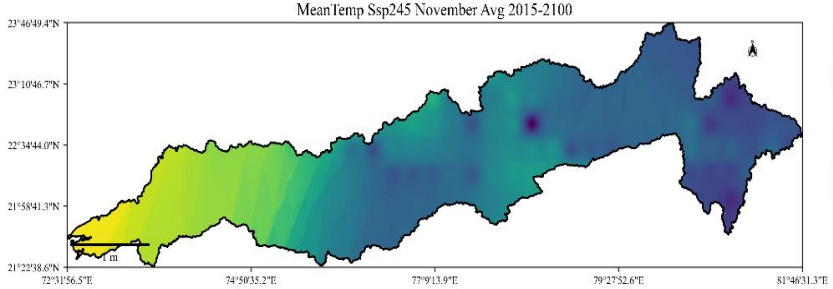
MeanTemp Ssp245 November Avg 2015-2100
23°46'49.4"N
23°10'46.7"N
22°34'44.0"N
21°58'41.3"N
21°22'38.6"N
72°31'56.5"E
74°50'35.2"E
77°9'13.9"E
79°27'52.6"E
81°46'31.3"E
27
26
25
24
23
22
21

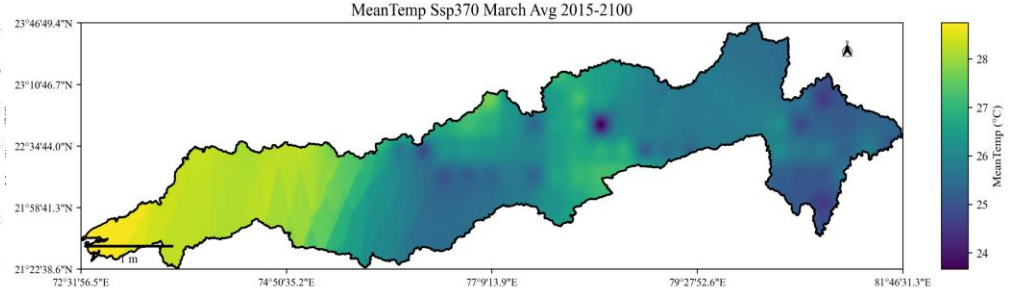
MeanTemp Ssp370 March Avg 2015-2100
23°46'49.4"N
23°10'46.7"N
22°34'44.0"N
21°58'41.3"N
21°22'38.6"N
72°31'56.5"E
74°50'35.2"E
77°9'13.9"E
79°27'52.6"E
81°46'31.3"E
MeanTemp (°C)
28
27
26
25
24

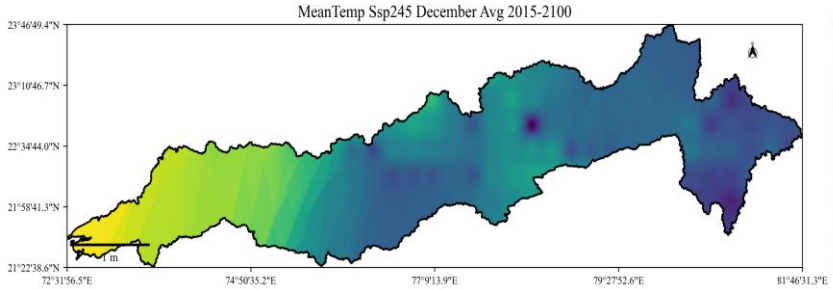
MeanTemp Ssp245 December Avg 2015-2100
23°46'49.4"N
23°10'46.7"N
22°34'44.0"N
21°58'41.3"N
21°22'38.6"N
72°31'56.5"E
74°50'35.2"E
77°9'13.9"E
79°27'52.6"E
81°46'31.3"E
23
22
21
20
19
18

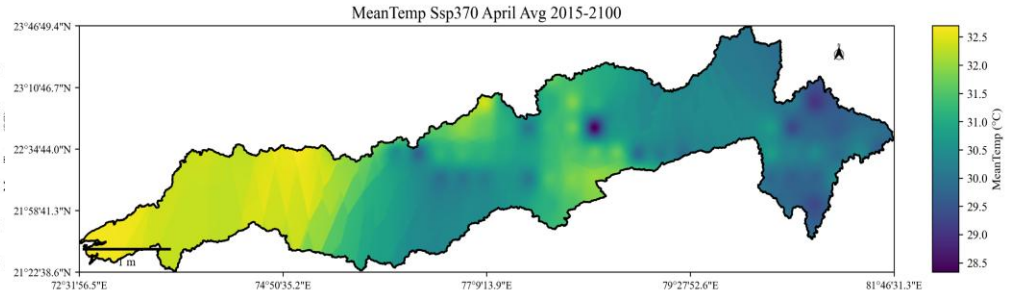
MeanTemp Ssp370 April Avg 2015-2100
23°46'49.4"N
23°10'46.7"N
22°34'44.0"N
21°58'41.3"N
21°22'38.6"N
72°31'56.5"E
74°50'35.2"E
77°9'13.9"E
79°27'52.6"E
81°46'31.3"E
MeanTemp (°C)
32.5
32.0
31.5
31.0
30.5
30.0
29.5
29.0
28.5

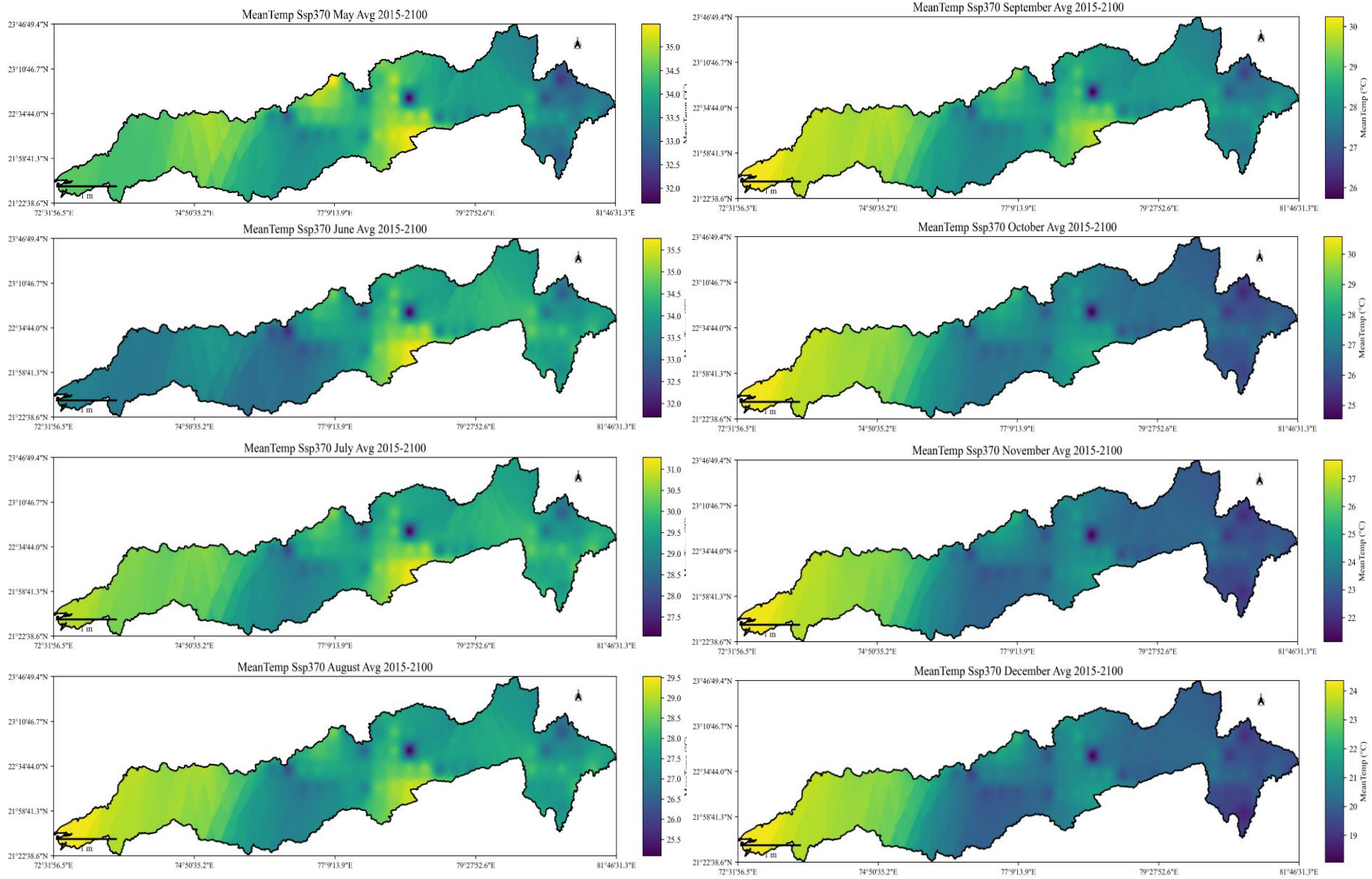
MeanTemp Ssp370 May Avg 2015-2100
MeanTemp Ssp370 September Avg 2015-2100
MeanTemp Ssp370 June Avg 2015-2100
MeanTemp Ssp370 October Avg 2015-2100
MeanTemp Ssp370 July Avg 2015-2100
MeanTemp Ssp370 November Avg 2015-2100
MeanTemp Ssp370 August Avg 2015-2100
MeanTemp Ssp370 December Avg 2015-2100
MeanTemp (°C)
23°46'49.4"N
23°10'46.7"N
22°34'44.0"N
21°58'41.3"N
21°22'38.6"N
72°31'56.5"E
74°50'35.2"E
77°9'13.9"E
79°27'52.6"E
81°46'31.3"E

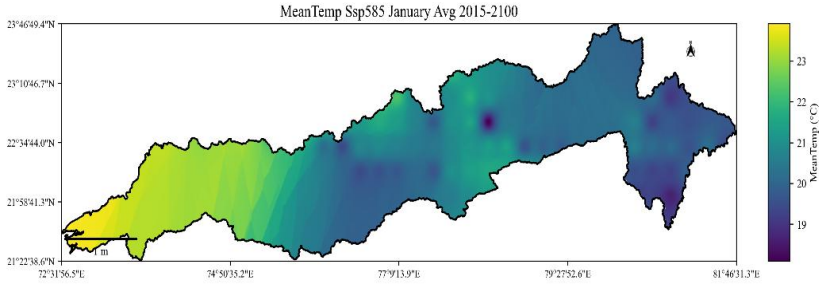
MeanTemp Ssp585 January Avg 2015-2100
23°46'49.4"N
23°10'46.7"N
22°34'44.0"N
21°58'41.3"N
21°22'38.6"N
72°31'56.5"E
74°50'35.2"E
77°9'13.9"E
79°27'52.6"E
81°46'31.3"E
MeanTemp (°C)

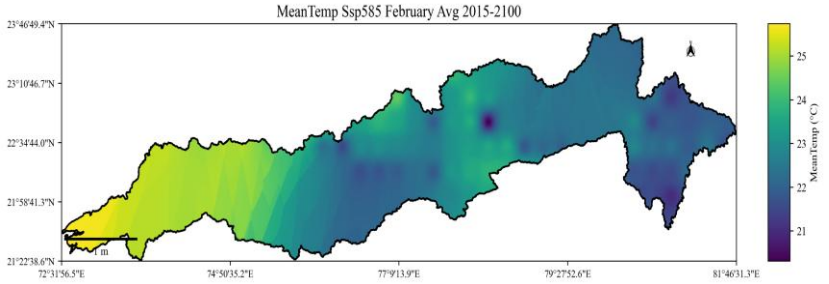
MeanTemp Ssp585 February Avg 2015-2100
23°46'49.4"N
23°10'46.7"N
22°34'44.0"N
21°58'41.3"N
21°22'38.6"N
72°31'56.5"E
74°50'35.2"E
77°9'13.9"E
79°27'52.6"E
81°46'31.3"E
MeanTemp (°C)

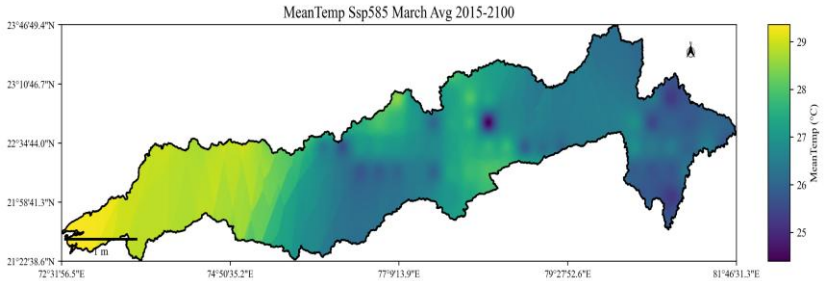
MeanTemp Ssp585 March Avg 2015-2100
23°46'49.4"N
23°10'46.7"N
22°34'44.0"N
21°58'41.3"N
21°22'38.6"N
72°31'56.5"E
74°50'35.2"E
77°9'13.9"E
79°27'52.6"E
81°46'31.3"E
MeanTemp (°C)

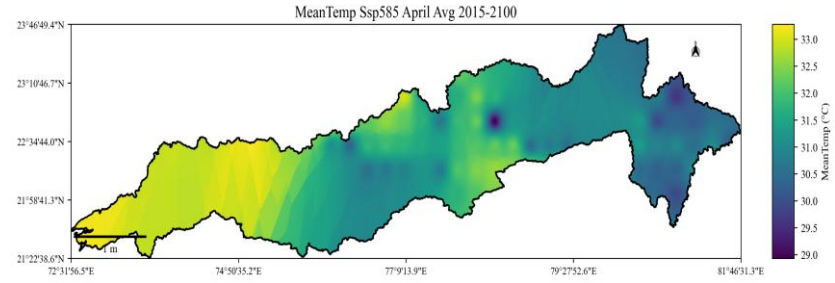
MeanTemp Ssp585 April Avg 2015-2100
23°46'49.4"N
23°10'46.7"N
22°34'44.0"N
21°58'41.3"N
21°22'38.6"N
72°31'56.5"E
74°50'35.2"E
77°9'13.9"E
79°27'52.6"E
81°46'31.3"E
MeanTemp (°C)

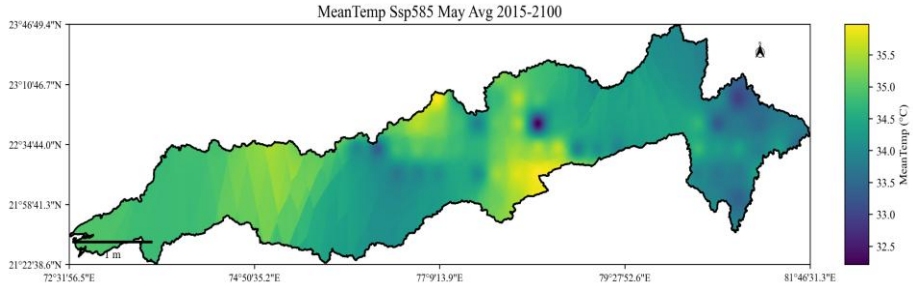
MeanTemp Ssp585 May Avg 2015-2100
23°46'49.4"N
23°10'46.7"N
22°34'44.0"N
21°58'41.3"N
21°22'38.6"N
72°31'56.5"E
74°50'35.2"E
77°9'13.9"E
79°27'52.6"E
81°46'31.3"E
MeanTemp (°C)

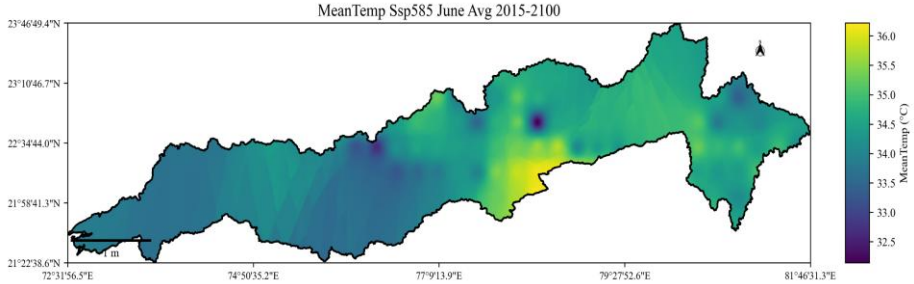
MeanTemp Ssp585 June Avg 2015-2100
23°46'49.4"N
23°10'46.7"N
22°34'44.0"N
21°58'41.3"N
21°22'38.6"N
72°31'56.5"E
74°50'35.2"E
77°9'13.9"E
79°27'52.6"E
81°46'31.3"E
MeanTemp (°C)

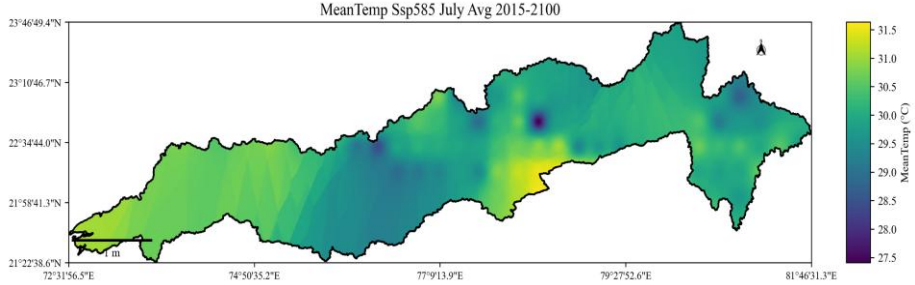
MeanTemp Ssp585 July Avg 2015-2100
23°46'49.4"N
23°10'46.7"N
22°34'44.0"N
21°58'41.3"N
21°22'38.6"N
72°31'56.5"E
74°50'35.2"E
77°9'13.9"E
79°27'52.6"E
81°46'31.3"E
MeanTemp (°C)

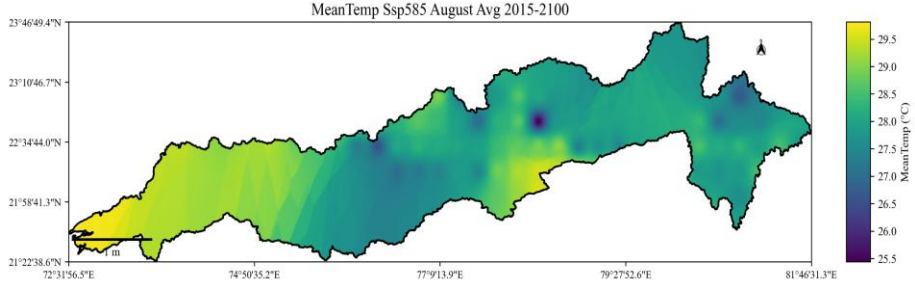
MeanTemp Ssp585 August Avg 2015-2100
23°46'49.4"N
23°10'46.7"N
22°34'44.0"N
21°58'41.3"N
21°22'38.6"N
72°31'56.5"E
74°50'35.2"E
77°9'13.9"E
79°27'52.6"E
81°46'31.3"E
MeanTemp (°C)

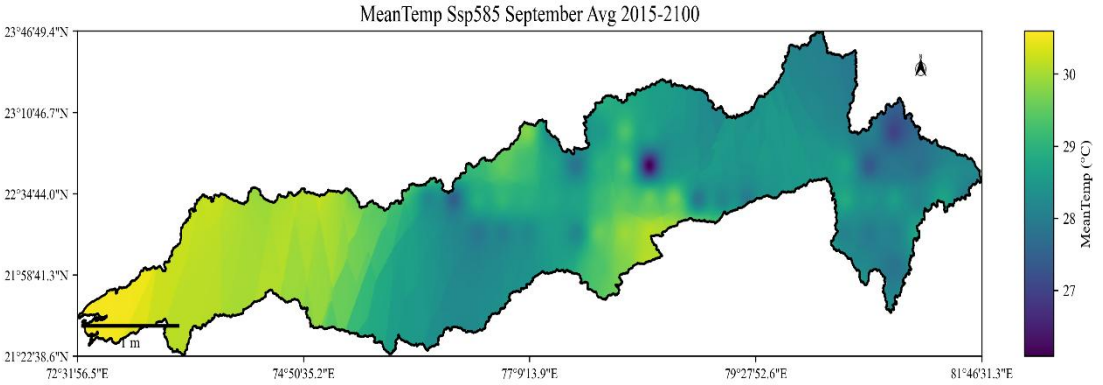
MeanTemp Ssp585 September Avg 2015-2100
23°46'49.4"N
23°10'46.7"N
22°34'44.0"N
21°58'41.3"N
21°22'38.6"N
72°31'56.5"E
74°50'35.2"E
77°9'13.9"E
79°27'52.6"E
81°46'31.3"E
1 m
MeanTemp (°C)
30
29
28
27

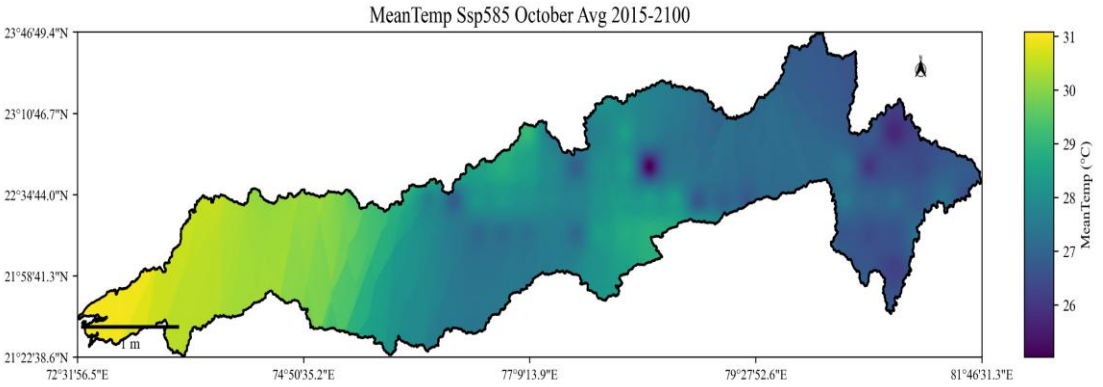
MeanTemp Ssp585 October Avg 2015-2100
23°46'49.4"N
23°10'46.7"N
22°34'44.0"N
21°58'41.3"N
21°22'38.6"N
72°31'56.5"E
74°50'35.2"E
77°9'13.9"E
79°27'52.6"E
81°46'31.3"E
1 m
MeanTemp (°C)
31
30
29
28
27
26

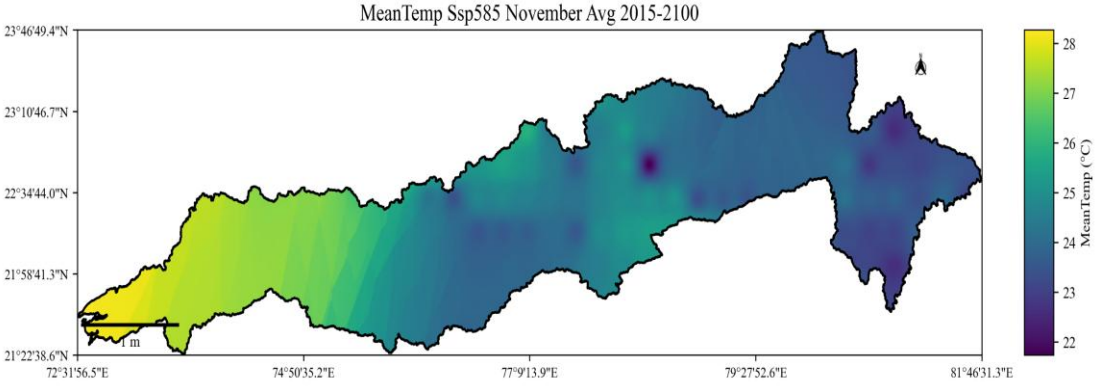
MeanTemp Ssp585 November Avg 2015-2100
23°46'49.4"N
23°10'46.7"N
22°34'44.0"N
21°58'41.3"N
21°22'38.6"N
72°31'56.5"E
74°50'35.2"E
77°9'13.9"E
79°27'52.6"E
81°46'31.3"E
1 m
MeanTemp (°C)
28
27
26
25
24
23
22

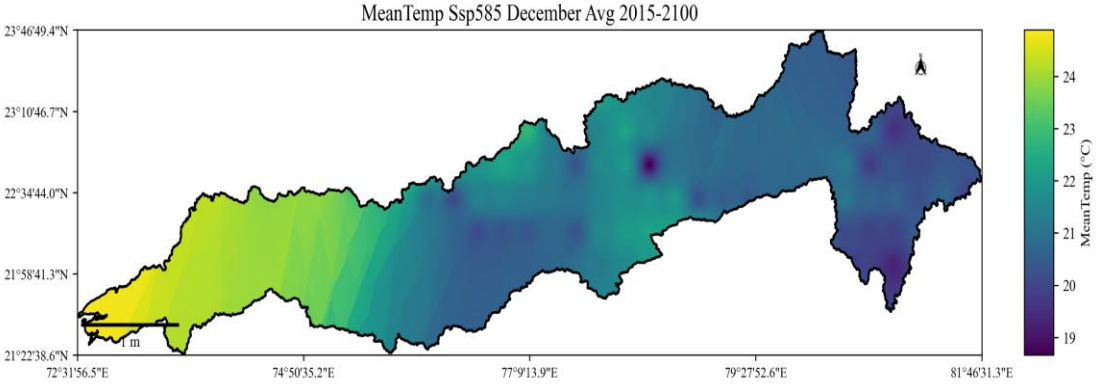
MeanTemp Ssp585 December Avg 2015-2100
23°46'49.4"N
23°10'46.7"N
22°34'44.0"N
21°58'41.3"N
21°22'38.6"N
72°31'56.5"E
74°50'35.2"E
77°9'13.9"E
79°27'52.6"E
81°46'31.3"E
1 m
MeanTemp (°C)
24
23
22
21
20
19

Figure 74:Spatial distribution of monthly values of Precipitation for the Historical, SSP126, SSP245, SSP370, and SSP585 scenarios

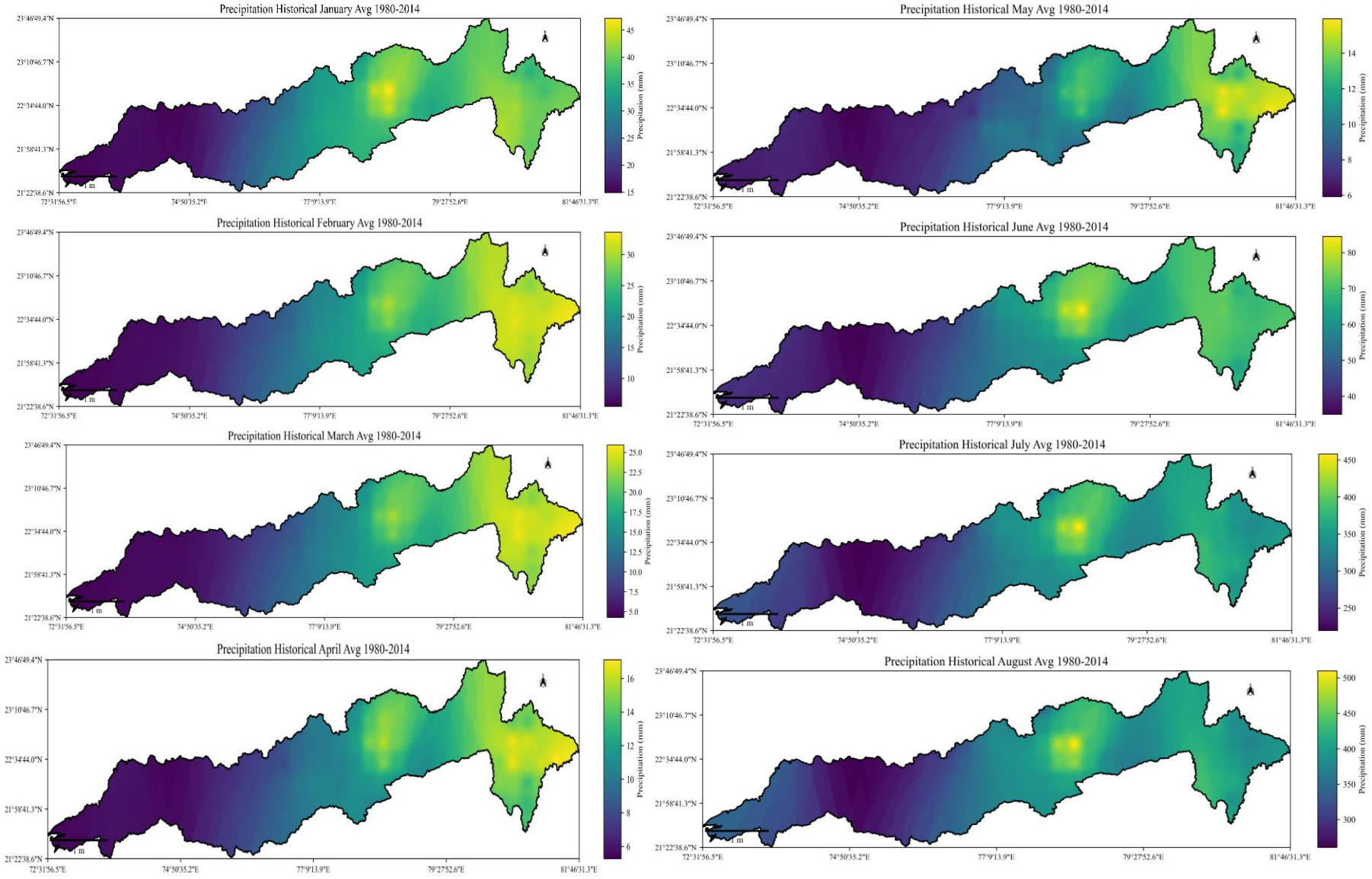

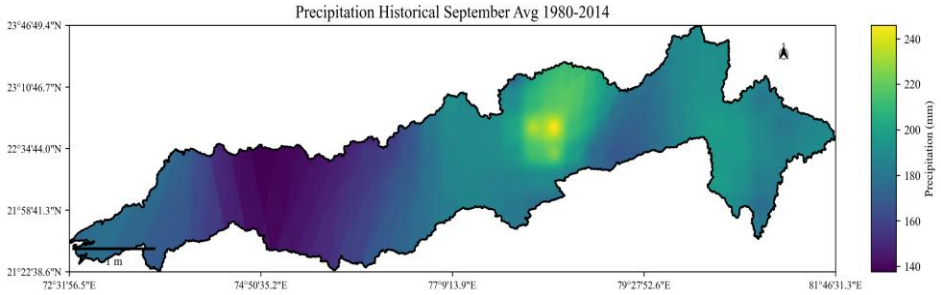
Precipitation Historical September Avg 1980-2014
23°46'49.4"N
23°10'46.7"N
22°34'44.0"N
21°58'41.3"N
21°22'38.6"N
72°31'56.5"E
74°50'35.2"E
77°9'13.9"E
79°27'52.6"E
81°46'31.3"E
Precipitation (mm)
240
220
200
180
160
140

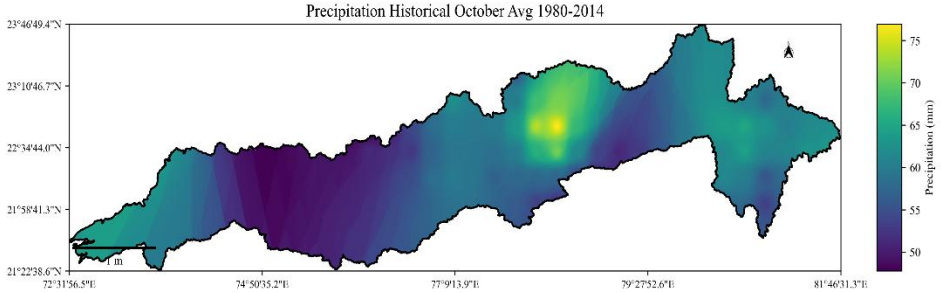
Precipitation Historical October Avg 1980-2014
23°46'49.4"N
23°10'46.7"N
22°34'44.0"N
21°58'41.3"N
21°22'38.6"N
72°31'56.5"E
74°50'35.2"E
77°9'13.9"E
79°27'52.6"E
81°46'31.3"E
Precipitation (mm)
75
70
65
60
55
50

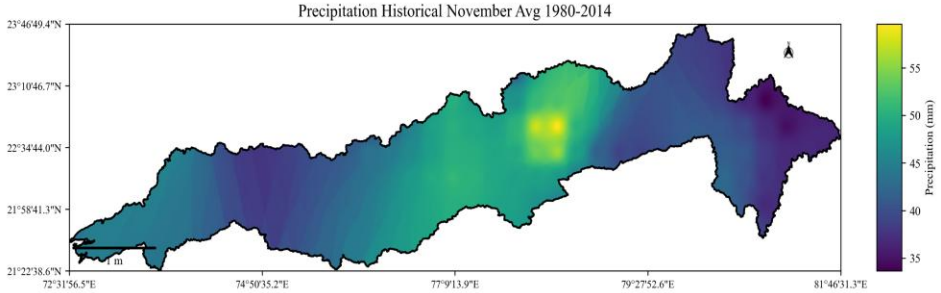
Precipitation Historical November Avg 1980-2014
23°46'49.4"N
23°10'46.7"N
22°34'44.0"N
21°58'41.3"N
21°22'38.6"N
72°31'56.5"E
74°50'35.2"E
77°9'13.9"E
79°27'52.6"E
81°46'31.3"E
Precipitation (mm)
55
50
45
40
35

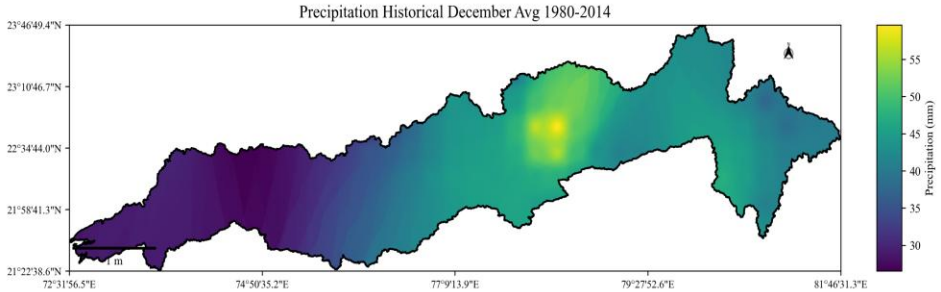
Precipitation Historical December Avg 1980-2014
23°46'49.4"N
23°10'46.7"N
22°34'44.0"N
21°58'41.3"N
21°22'38.6"N
72°31'56.5"E
74°50'35.2"E
77°9'13.9"E
79°27'52.6"E
81°46'31.3"E
Precipitation (mm)
55
50
45
40
35
30

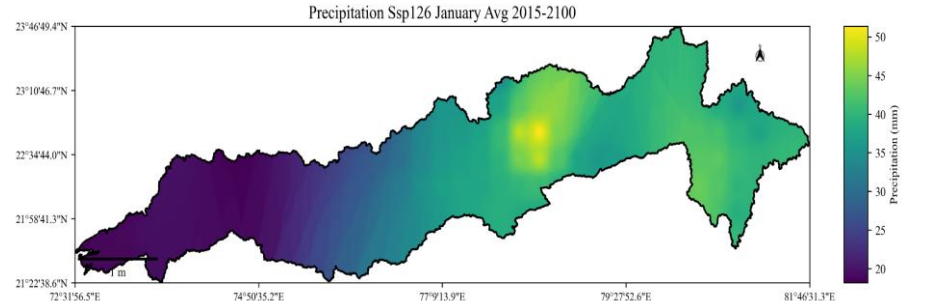
Precipitation Ssp126 January Avg 2015-2100
23°46'49.4"N
23°10'46.7"N
22°34'44.0"N
21°58'41.3"N
21°22'38.6"N
72°31'56.5"E
74°50'35.2"E
77°9'13.9"E
79°27'52.6"E
81°46'31.3"E
Precipitation (mm)
50
45
40
35
30
25
20

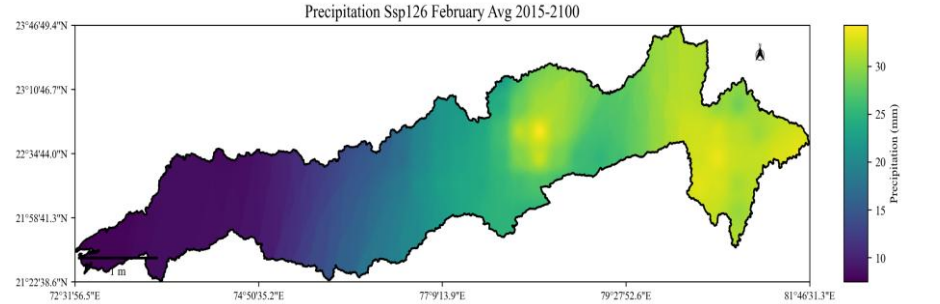
Precipitation Ssp126 February Avg 2015-2100
23°46'49.4"N
23°10'46.7"N
22°34'44.0"N
21°58'41.3"N
21°22'38.6"N
72°31'56.5"E
74°50'35.2"E
77°9'13.9"E
79°27'52.6"E
81°46'31.3"E
Precipitation (mm)
30
25
20
15
10

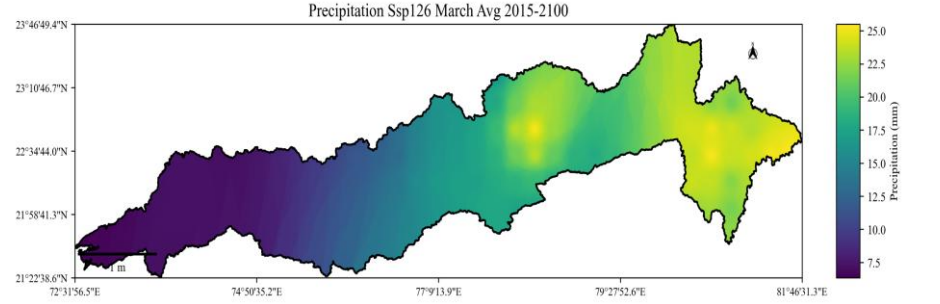
Precipitation Ssp126 March Avg 2015-2100
23°46'49.4"N
23°10'46.7"N
22°34'44.0"N
21°58'41.3"N
21°22'38.6"N
72°31'56.5"E
74°50'35.2"E
77°9'13.9"E
79°27'52.6"E
81°46'31.3"E
Precipitation (mm)
25.0
22.5
20.0
17.5
15.0
12.5
10.0
7.5

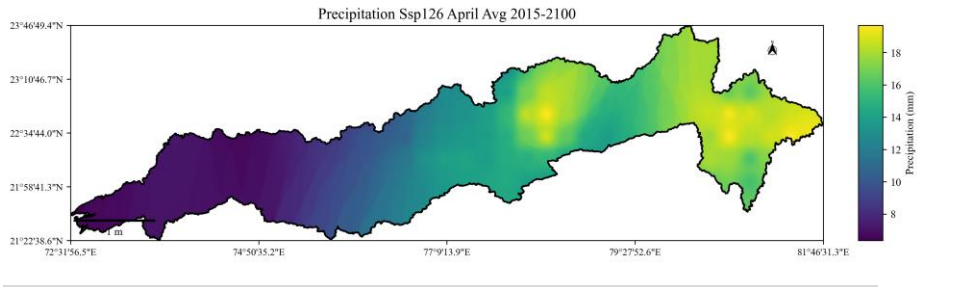
Precipitation Ssp126 April Avg 2015-2100
23°46'49.4"N
23°10'46.7"N
22°34'44.0"N
21°58'41.3"N
21°22'38.6"N
72°31'56.5"E
74°50'35.2"E
77°9'13.9"E
79°27'52.6"E
81°46'31.3"E
Precipitation (mm)
18
16
14
12
10
8

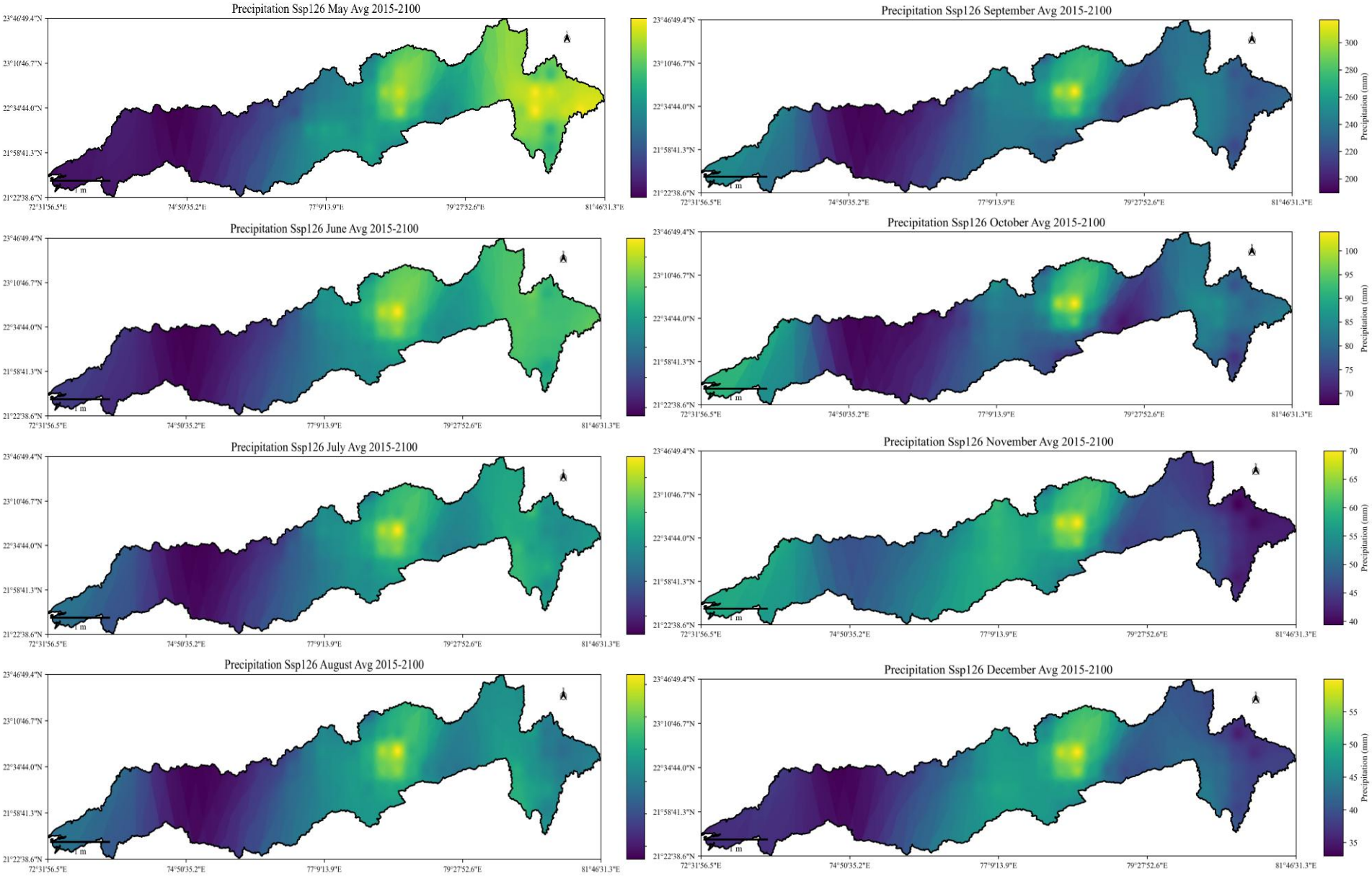
Precipitation Ssp126 May Avg 2015-2100
Precipitation Ssp126 September Avg 2015-2100
Precipitation Ssp126 June Avg 2015-2100
Precipitation Ssp126 October Avg 2015-2100
Precipitation Ssp126 July Avg 2015-2100
Precipitation Ssp126 November Avg 2015-2100
Precipitation Ssp126 August Avg 2015-2100
Precipitation Ssp126 December Avg 2015-2100
Precipitation (mm)
23°46'49.4"N
23°10'46.7"N
22°34'44.0"N
21°58'41.3"N
21°22'38.6"N
72°31'56.5"E
74°50'35.2"E
77°9'13.9"E
79°27'52.6"E
81°46'31.3"E

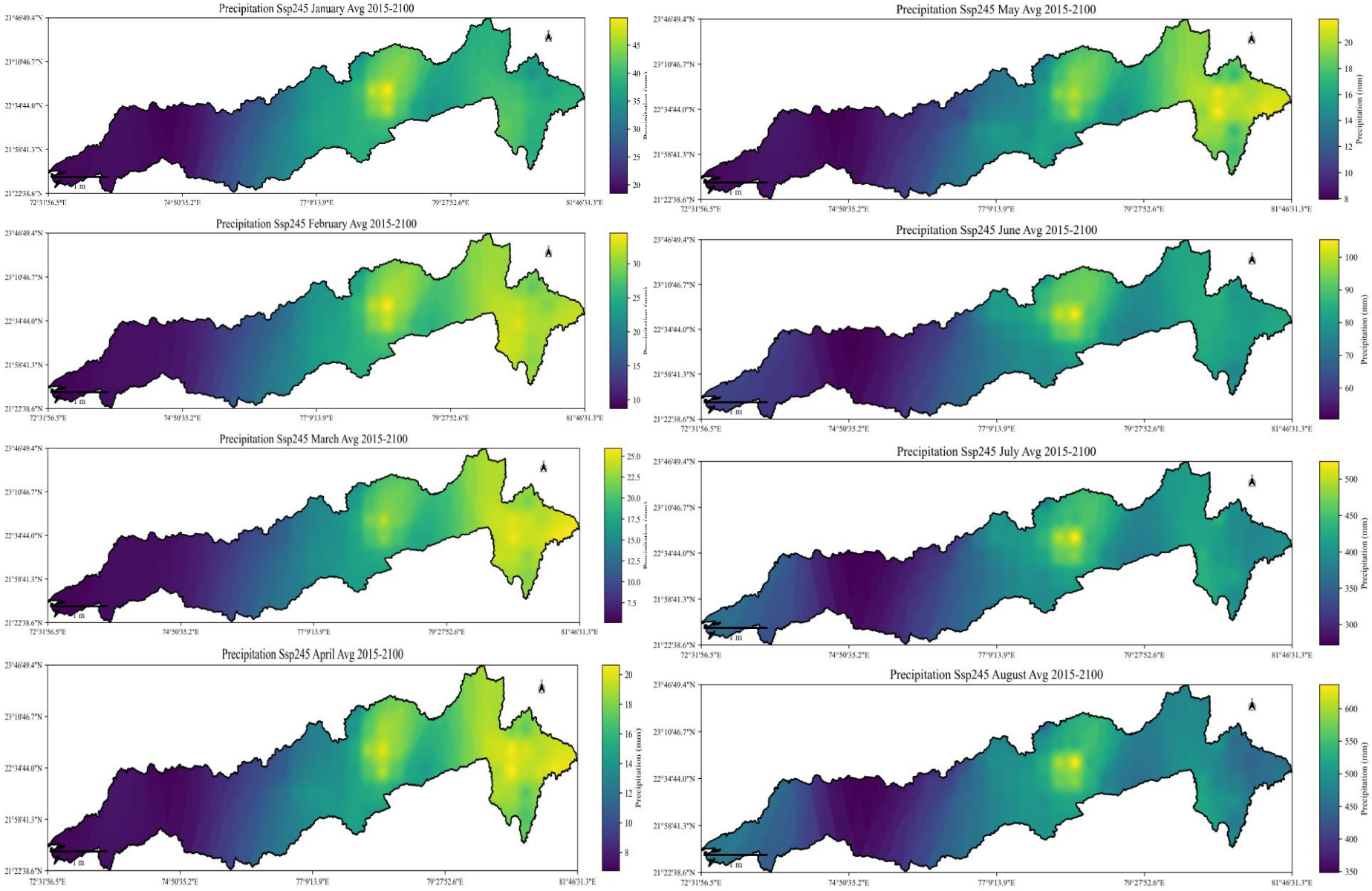
Precipitation Ssp245 January Avg 2015-2100
Precipitation Ssp245 February Avg 2015-2100
Precipitation Ssp245 March Avg 2015-2100
Precipitation Ssp245 April Avg 2015-2100
Precipitation Ssp245 May Avg 2015-2100
Precipitation Ssp245 June Avg 2015-2100
Precipitation Ssp245 July Avg 2015-2100
Precipitation Ssp245 August Avg 2015-2100
Precipitation (mm)
72°31'56.5"E
74°50'35.2"E
77°9'13.9"E
79°27'52.6"E
81°46'31.3"E

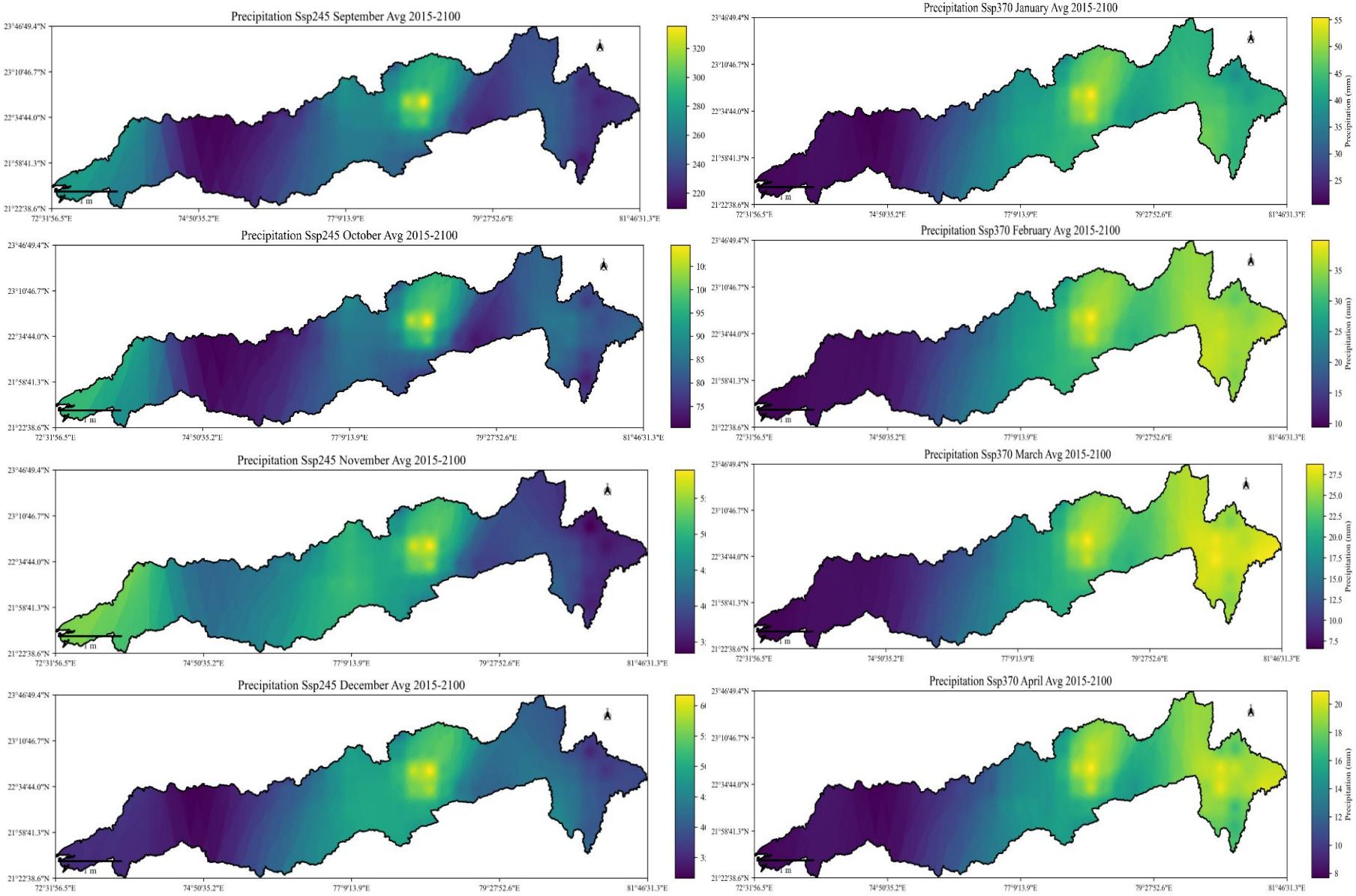
Precipitation Ssp245 September Avg 2015-2100
Precipitation Ssp370 January Avg 2015-2100
Precipitation Ssp245 October Avg 2015-2100
Precipitation Ssp370 February Avg 2015-2100
Precipitation Ssp245 November Avg 2015-2100
Precipitation Ssp370 March Avg 2015-2100
Precipitation Ssp245 December Avg 2015-2100
Precipitation Ssp370 April Avg 2015-2100
Precipitation (mm)
23°46'49.4"N
23°10'46.7"N
22°34'44.0"N
21°58'41.3"N
21°22'38.6"N
72°31'56.5"E
74°50'35.2"E
77°9'13.9"E
79°27'52.6"E
81°46'31.3"E

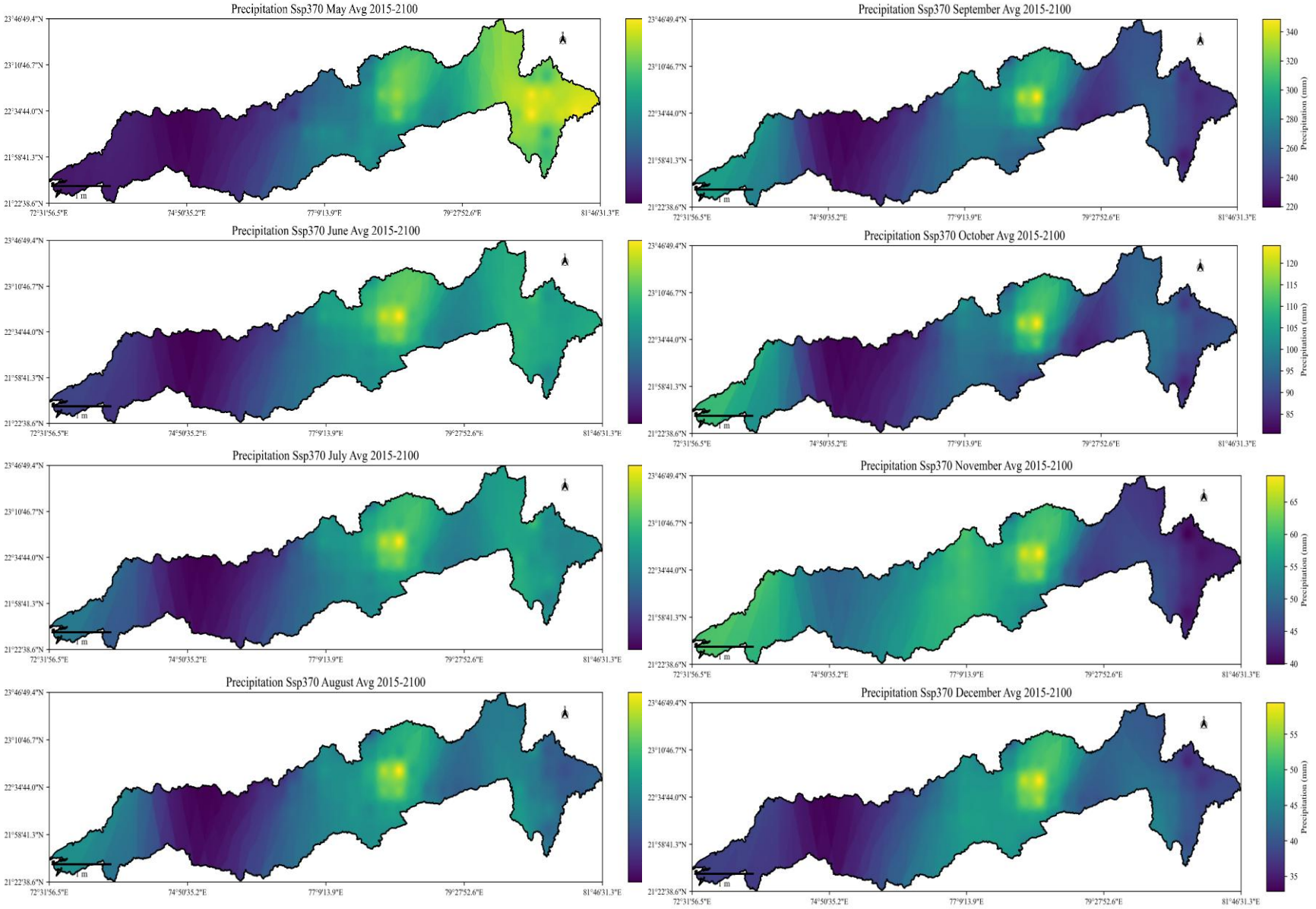
Precipitation Ssp370 May Avg 2015-2100
Precipitation Ssp370 September Avg 2015-2100
Precipitation Ssp370 June Avg 2015-2100
Precipitation Ssp370 October Avg 2015-2100
Precipitation Ssp370 July Avg 2015-2100
Precipitation Ssp370 November Avg 2015-2100
Precipitation Ssp370 August Avg 2015-2100
Precipitation Ssp370 December Avg 2015-2100
Precipitation (mm)
23°46'49.4"N
23°10'46.7"N
22°34'44.0"N
21°58'41.3"N
21°22'38.6"N
72°31'56.5"E
74°50'35.2"E
77°9'13.9"E
79°27'52.6"E
81°46'31.3"E

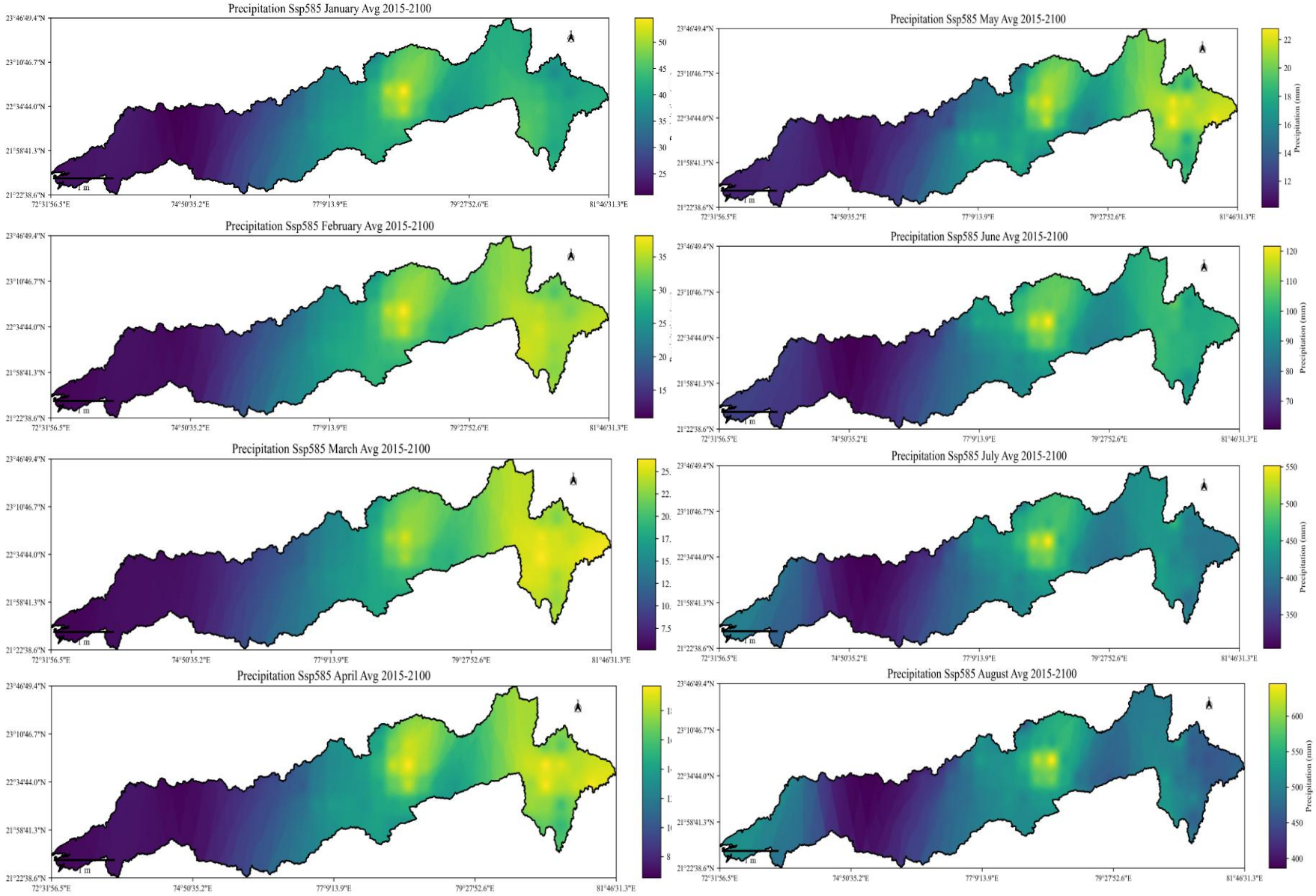
Precipitation Ssp585 January Avg 2015-2100
Precipitation Ssp585 May Avg 2015-2100
Precipitation Ssp585 February Avg 2015-2100
Precipitation Ssp585 June Avg 2015-2100
Precipitation Ssp585 March Avg 2015-2100
Precipitation Ssp585 July Avg 2015-2100
Precipitation Ssp585 April Avg 2015-2100
Precipitation Ssp585 August Avg 2015-2100
Precipitation (mm)
23°46'49.4"N
23°10'46.7"N
22°34'44.0"N
21°58'41.3"N
21°22'38.6"N
72°31'56.5"E
74°50'35.2"E
77°9'13.9"E
79°27'52.6"E
81°46'31.3"E

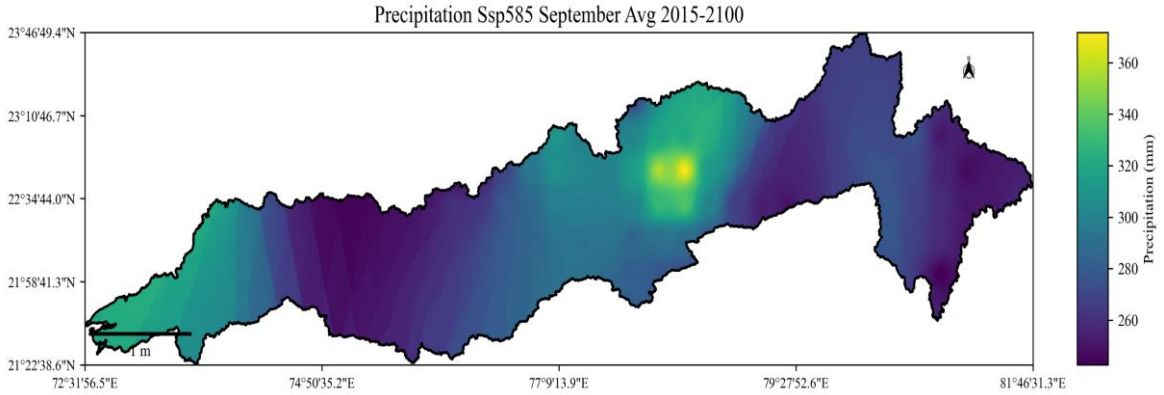
Precipitation Ssp585 September Avg 2015-2100
23°46'49.4"N
23°10'46.7"N
22°34'44.0"N
21°58'41.3"N
21°22'38.6"N
72°31'56.5"E
74°50'35.2"E
77°9'13.9"E
79°27'52.6"E
81°46'31.3"E
1 m
360
340
320
300
280
260
Precipitation (mm)

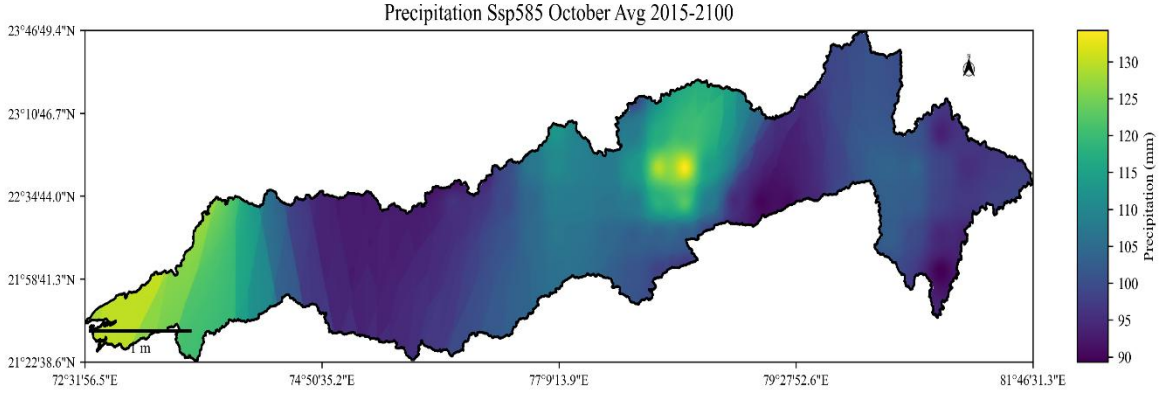
Precipitation Ssp585 October Avg 2015-2100
23°46'49.4"N
23°10'46.7"N
22°34'44.0"N
21°58'41.3"N
21°22'38.6"N
72°31'56.5"E
74°50'35.2"E
77°9'13.9"E
79°27'52.6"E
81°46'31.3"E
1 m
130
125
120
115
110
105
100
95
90
Precipitation (mm)

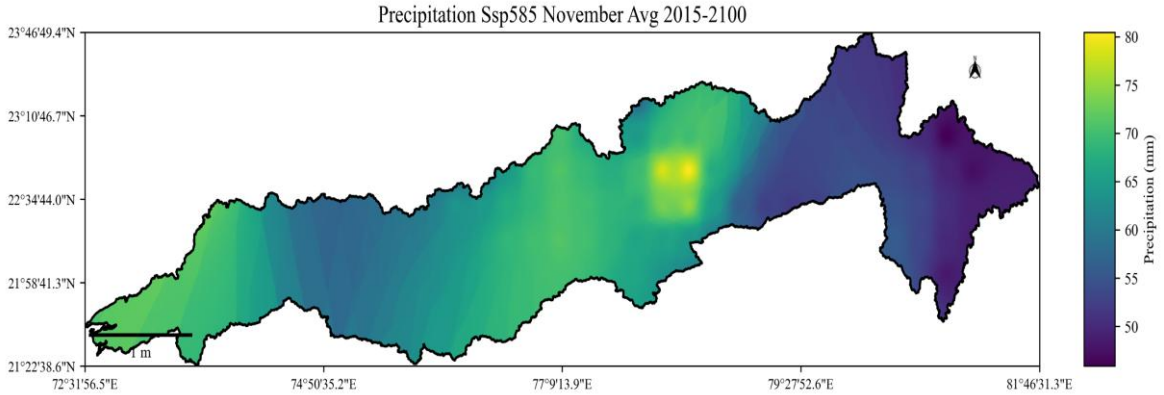
Precipitation Ssp585 November Avg 2015-2100
23°46'49.4"N
23°10'46.7"N
22°34'44.0"N
21°58'41.3"N
21°22'38.6"N
72°31'56.5"E
74°50'35.2"E
77°9'13.9"E
79°27'52.6"E
81°46'31.3"E
1 m
80
75
70
65
60
55
50
Precipitation (mm)

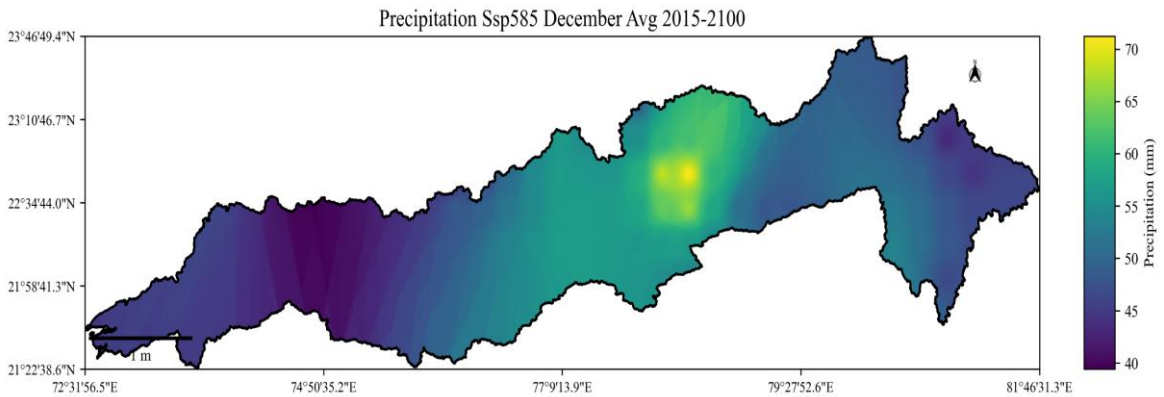
Precipitation Ssp585 December Avg 2015-2100
23°46'49.4"N
23°10'46.7"N
22°34'44.0"N
21°58'41.3"N
21°22'38.6"N
72°31'56.5"E
74°50'35.2"E
77°9'13.9"E
79°27'52.6"E
81°46'31.3"E
1 m
70
65
60
55
50
45
40
Precipitation (mm)

Table 2: Tabulation of statistics of monthly Maximum temperature under the scenarios of Historical, Ssp126, and Ssp245

| Months | Historical (1980-2014) | | | | Ssp126 (2015-2100) | | | | Ssp245 (2015-2100) | | | |
|---|---|---|---|---|---|---|---|---|---|---|---|---|
| | Maximum Temperature | | | | | | | | | | | |
| | Mean | Min | Max | StdDev | Mean | Min | Max | StdDev | Mean | Min | Max | StdDev |
| January | 26.812 | 23.784 | 29.477 | 1.284 | 27.619 | 24.586 | 30.332 | 1.307 | 27.824 | 24.79 | 30.584 | 1.319 |
| February | 29.107 | 26.213 | 31.352 | 1.121 | 30.058 | 27.13 | 32.442 | 1.189 | 30.194 | 27.253 | 32.664 | 1.213 |
| March | 32.709 | 29.887 | 34.78 | 1.084 | 33.909 | 31.032 | 36.122 | 1.184 | 34.238 | 31.367 | 36.481 | 1.208 |
| April | 37.238 | 34.567 | 38.979 | 0.987 | 38.431 | 35.797 | 40.101 | 0.94 | 38.847 | 36.226 | 40.508 | 0.941 |
| May | 40.099 | 37.825 | 41.656 | 0.52 | 41.074 | 38.817 | 42.655 | 0.49 | 41.512 | 39.282 | 43.121 | 0.49 |
| June | 38.415 | 36.236 | 40.427 | 0.574 | 39.359 | 37.174 | 41.368 | 0.569 | 39.749 | 37.584 | 41.784 | 0.603 |
| July | 32.379 | 29.529 | 33.89 | 0.583 | 33.065 | 30.245 | 34.61 | 0.557 | 33.487 | 30.702 | 35.056 | 0.533 |
| August | 30.344 | 27.443 | 31.823 | 0.68 | 31.128 | 28.253 | 32.576 | 0.668 | 31.128 | 28.253 | 32.576 | 0.668 |
| September | 31.928 | 29.054 | 33.644 | 31.928 | 32.401 | 29.588 | 33.965 | 0.808 | 32.656 | 29.865 | 34.18 | 0.784 |
| October | 32.617 | 29.328 | 35.835 | 32.617 | 33.081 | 29.807 | 36.301 | 1.64 | 33.212 | 29.961 | 36.378 | 1.617 |
| November | 29.923 | 26.763 | 32.963 | 29.923 | 30.391 | 27.178 | 33.62 | 1.497 | 30.516 | 27.295 | 33.796 | 1.516 |
| December | 27.196 | 24.102 | 30.082 | 27.196 | 27.824 | 24.734 | 30.756 | 1.366 | 28.033 | 24.933 | 31.009 | 1.38 |

The monthly statistics of maximum temperature under historical (1980–2014) and future climate scenarios (SSP126, SSP245, SSP370, SSP585 for 2015–2100) reveal a consistent warming trend across all months, with a gradual intensification under higher

emission pathways. Under the historical scenario, maximum temperatures range from **~26.8°C in January** to **~40.1°C in May**, indicating a clear seasonal cycle with summer months (April–June) experiencing the highest temperatures. The standard deviation is generally low during peak summer (e.g., ~0.52°C in May), reflecting stable temperature behaviour during this period. In the low-emission scenario (SSP126), the temperature increase is moderate, with January's rising to 27.62°C, and May peaking at 41.07°C, marking an increase of about 1°C compared to the historical baseline. As the emission intensity increases, warming becomes more pronounced. Under SSP245, March and April exhibit more notable increases (e.g., March rises to 34.24°C, from 32.71°C historically), while May and June reach mean temperatures of 41.51°C and 39.75°C respectively.

Table 3: Tabulation of statistics of monthly Maximum temperature under the scenarios of Ssp370 and Ssp585

| **Months** | **Ssp370 (2015-2100)** | | | | **Ssp585 (2015-2100)** | | | |
|---|---|---|---|---|---|---|---|---|
| | **Maximum Temperature** | | | | | | | |
| | **Mean** | **Min** | **Max** | **StdDev** | **Mean** | **Min** | **Max** | **StdDev** |
| **January** | 27.892 | 24.845 | 30.699 | 1.333 | 28.386 | 25.361 | 31.153 | 1.314 |
| **February** | 30.375 | 27.406 | 32.948 | 1.269 | 30.88 | 27.934 | 33.43 | 1.266 |
| **March** | 34.494 | 31.62 | 36.738 | 1.213 | 35.174 | 32.343 | 37.291 | 1.178 |
| **April** | 39.12 | 36.499 | 40.75 | 0.918 | 39.717 | 37.113 | 41.285 | 0.87 |
| **May** | 41.629 | 39.373 | 43.215 | 0.495 | 42.095 | 39.832 | 43.684 | 0.468 |
| **June** | 39.848 | 37.674 | 41.865 | 0.603 | 40.286 | 38.114 | 42.318 | 0.601 |
| **July** | 33.688 | 30.911 | 35.264 | 0.531 | 34.029 | 31.296 | 35.636 | 0.508 |

| | | | | | | | | |
|---|---|---|---|---|---|---|---|---|
| **August** | 31.298 | 28.433 | 32.715 | 0.65 | 31.646 | 28.813 | 33.103 | 0.636 |
| **September** | 32.85 | 30.065 | 34.311 | 0.741 | 33.204 | 30.409 | 34.668 | 0.748 |
| **October** | 33.435 | 30.243 | 36.474 | 1.545 | 33.901 | 30.709 | 36.931 | 1.557 |
| **November** | 30.734 | 27.52 | 34.036 | 1.525 | 31.223 | 28.013 | 34.528 | 1.539 |
| **December** | 28.177 | 25.076 | 31.205 | 1.392 | 19.564 | 16.569 | 22.601 | 1.35 |

The high-emission scenarios—SSP370 and SSP585—project significantly higher maximum temperatures across all months. Under SSP370, the highest monthly mean is 41.63°C in May, while SSP585 projects an even higher value of 42.10°C, indicating a ~2°C increase over the historical period. Similarly, in cooler months like January and February, the temperature increase is nearly 1.5°C to 2°C, suggesting a reduction in seasonal contrast. Interestingly, a consistent pattern emerges where July and August, typically monsoon months, show smaller increases in temperature (~1–1.5°C), potentially due to cloud cover and precipitation moderating temperature rise. However, even during these months, SSP585 projects substantial warming (e.g., July mean: 34.03°C, historically ~32.38°C). Notably, October and November, marking the post-monsoon season, show rising variability (standard deviations >1.5°C), which may reflect increasing uncertainty and spatial variability in warming patterns during transition months. A significant anomaly is observed in December under SSP585, with a mean of 19.56°C, which seems inconsistent with the trend and may be a data entry error requiring verification. Thus, overall, the results clearly demonstrate a scenario-dependent intensification of warming, with higher emission pathways leading to sharper increases in monthly maximum temperatures. This rising trend could have severe implications for agriculture, water demand, human health, and ecosystem stability, particularly during the already hot pre-monsoon season.

The monthly mean temperature trends across the historical (1980–2014) and future periods (2015–2100) under the CMIP6 scenarios SSP126, SSP245, SSP370, and SSP585 exhibit a progressive warming pattern, with temperature increases closely following the intensity of greenhouse gas emissions associated with each scenario. Under the historical baseline, monthly mean temperatures vary from ~18.8°C in January to ~32.3°C in May, with the highest temperatures occurring during the pre-monsoon summer months (April–June). The lowest temperatures are observed in the winter months (December–January), reflecting the typical seasonal climatic cycle of the region. In the low-emission pathway (SSP126), an increase of approximately 1°C is observed across most months when compared to the historical average. For instance, January warms from 18.78°C to 19.80°C, and May rises from 32.31°C to 33.36°C. The standard deviation values remain like historical levels, suggesting that while the mean temperatures rise, inter-annual variability does not significantly increase under this scenario.

Table 4: Tabulation of statistics of monthly Mean temperature under the scenarios of Historical, Ssp126, and Ssp245

| **Months** | **Historical (1980-2014)** | | | | **Ssp126 (2015-2100)** | | | | **Ssp245 (2015-2100)** | | | |
|---|---|---|---|---|---|---|---|---|---|---|---|---|
| | **Mean Temperature** | | | | | | | | | | | |
| | **Mean** | **Min** | **Max** | **StdDev** | **Mean** | **Min** | **Max** | **StdDev** | **Mean** | **Min** | **Max** | **StdDev** |
| **January** | 18.775 | 15.886 | 21.494 | 1.228 | 19.801 | 16.886 | 22.632 | 1.276 | 20.159 | 17.234 | 23.028 | 1.293 |
| **February** | 20.694 | 17.9 | 23.04 | 1.07 | 21.878 | 19.047 | 24.364 | 1.137 | 22.16 | 19.307 | 24.74 | 1.174 |
| **March** | 24.377 | 21.639 | 26.49 | 1.004 | 25.749 | 22.962 | 27.965 | 1.063 | 26.133 | 23.333 | 28.398 | 1.091 |
| **April** | 29.149 | 26.478 | 30.754 | 0.884 | 30.35 | 27.654 | 31.969 | 0.89 | 30.724 | 28.008 | 32.387 | 0.921 |
| **May** | 32.311 | 29.889 | 33.698 | 0.572 | 33.363 | 30.954 | 34.762 | 0.574 | 33.84 | 31.462 | 35.243 | 0.569 |

| | | | | | | | | | | | | |
|---|---|---|---|---|---|---|---|---|---|---|---|---|
| **June** | 32.147 | 29.962 | 34.034 | 0.504 | 33.245 | 31.088 | 35.156 | 0.516 | 33.646 | 31.512 | 35.585 | 0.545 |
| **July** | 28.305 | 25.559 | 29.804 | 0.601 | 29.11 | 26.387 | 30.629 | 0.581 | 29.518 | 26.815 | 31.046 | 0.563 |
| **August** | 26.708 | 23.895 | 28.258 | 0.689 | 27.419 | 24.609 | 28.984 | 0.69 | 27.694 | 24.869 | 29.304 | 0.705 |
| **September** | 27.234 | 24.418 | 28.973 | 0.807 | 27.924 | 25.114 | 29.643 | 0.799 | 27.924 | 25.114 | 29.643 | 0.799 |
| **October** | 26.237 | 23.063 | 29.264 | 1.341 | 26.989 | 23.836 | 30.012 | 1.335 | 26.989 | 23.836 | 30.012 | 1.335 |
| **November** | 22.721 | 19.612 | 25.931 | 1.404 | 23.57 | 20.414 | 26.913 | 1.448 | 23.57 | 20.414 | 26.913 | 1.448 |
| **December** | 19.564 | 16.569 | 22.601 | 1.350 | 20.455 | 17.439 | 23.606 | 1.394 | 20.788 | 17.76 | 23.973 | 1.406 |

The medium-emission scenario (SSP245) shows a stronger warming signal, with March mean temperatures increasing from 24.38°C (historical) to 26.13°C, and June rising from 32.15°C to 33.65°C. The monsoon months, such as July and August, also show warming (~1.2°C increase), although the temperatures remain lower due to seasonal rainfall and cloud cover.

Table 5: Tabulation of statistics of monthly Mean temperature under the scenarios of Ssp370, and Ssp585

| **Months** | **Ssp370 (2015-2100)** | | | | **Ssp585 (2015-2100)** | | | |
|---|---|---|---|---|---|---|---|---|
| | **Mean Temperature** | | | | | | | |
| | **Mean** | **Min** | **Max** | **StdDev** | **Mean** | **Min** | **Max** | **StdDev** |
| **January** | 20.44 | 17.506 | 23.349 | 1.306 | 21.022 | 18.098 | 23.914 | 1.299 |
| **February** | 22.518 | 19.647 | 25.144 | 1.198 | 23.147 | 20.31 | 25.735 | 1.19 |

| | | | | | | | | |
|---|---|---|---|---|---|---|---|---|
| **March** | 26.469 | 23.668 | 28.745 | 1.091 | 27.169 | 24.397 | 29.357 | 1.066 |
| **April** | 31.05 | 28.339 | 32.697 | 0.914 | 31.643 | 28.932 | 33.275 | 0.904 |
| **May** | 34.071 | 31.69 | 35.483 | 0.564 | 34.579 | 32.217 | 35.977 | 0.524 |
| **June** | 33.846 | 31.694 | 35.762 | 0.547 | 34.277 | 32.143 | 36.218 | 0.565 |
| **July** | 29.754 | 27.051 | 31.28 | 0.561 | 30.084 | 27.412 | 31.632 | 0.541 |
| **August** | 27.928 | 25.101 | 29.53 | 0.7 | 28.246 | 25.442 | 29.811 | 0.687 |
| **September** | 28.546 | 25.739 | 30.24 | 0.783 | 28.905 | 26.088 | 30.597 | 0.79 |
| **October** | 27.674 | 24.556 | 30.581 | 1.3 | 28.162 | 25.032 | 31.08 | 1.327 |
| **November** | 24.292 | 21.133 | 27.669 | 1.457 | 24.89 | 21.739 | 28.269 | 1.465 |
| **December** | 21.114 | 18.073 | 24.359 | 1.423 | 21.689 | 18.664 | 24.889 | 1.406 |

Under the higher emission pathways—SSP370 and SSP585—the temperature rise becomes more pronounced. In SSP370, May reaches a monthly average of 34.07°C, while in SSP585, it increases to 34.58°C, which is over 2°C higher than the historical value. Warming is even more substantial during the cooler months: for example, December rises from 19.56°C in the historical period to 21.69°C in SSP585, indicating a significant reduction in seasonal contrast and milder winters under a warming climate. The standard deviation values remain relatively stable across all scenarios, indicating that while the average temperatures increase, the spread of the temperature distribution does not change significantly. However, some months—such as November and December—continue to exhibit higher standard deviations (~1.4–1.5°C), which may reflect ongoing seasonal transitions or influence of extreme temperature events

during those periods. Notably, SSP585, the most aggressive emission scenario, consistently exhibits the highest monthly mean temperatures throughout the year. For example:

- January: increases from 18.78°C (historical) to 21.02°C
- March: from 24.38°C to 27.17°C
- July: from 28.31°C to 30.08°C

These shifts in mean temperatures have serious implications for regional hydrology, agriculture, and human health. The warming during already hot months could lead to increased evapotranspiration, heat stress, and irrigation demands, while warming in cooler months could disrupt traditional cropping patterns and biodiversity.

Table 6: Tabulation of statistics of monthly Minimum temperature under the scenarios of Historical, Ssp126, and Ssp245

| Months | Historical (1980-2014) | | | | Ssp126 (2015-2100) | | | | Ssp245 (2015-2100) | | | |
|---|---|---|---|---|---|---|---|---|---|---|---|---|
| | Minimum Temperature | | | | | | | | | | | |
| | Mean | Min | Max | StdDev | Mean | Min | Max | StdDev | Mean | Min | Max | StdDev |
| **January** | 10.737 | 7.989 | 13.512 | 1.211 | 11.983 | 9.186 | 14.932 | 1.277 | 12.494 | 9.678 | 15.473 | 1.298 |
| **February** | 12.282 | 9.587 | 14.728 | 1.079 | 13.699 | 10.963 | 16.285 | 1.137 | 14.125 | 11.361 | 16.816 | 1.178 |
| **March** | 16.044 | 13.39 | 18.2 | 0.987 | 17.589 | 14.891 | 19.808 | 1.01 | 18.028 | 15.298 | 20.315 | 1.038 |
| **April** | 21.059 | 18.388 | 22.763 | 0.841 | 22.269 | 19.512 | 24.123 | 0.892 | 22.6 | 19.789 | 24.589 | 0.952 |
| **May** | 24.522 | 21.953 | 25.788 | 0.682 | 25.653 | 23.092 | 27.048 | 0.736 | 26.168 | 23.641 | 27.587 | 0.73 |

| | | | | | | | | | | | | |
|---|---|---|---|---|---|---|---|---|---|---|---|---|
| **June** | 25.88 | 23.688 | 27.642 | 0.500 | 27.131 | 25.002 | 28.944 | 0.513 | 27.543 | 25.44 | 29.386 | 0.529 |
| **July** | 24.231 | 21.589 | 25.719 | 0.631 | 25.156 | 22.529 | 26.647 | 0.614 | 25.548 | 22.927 | 27.037 | 0.602 |
| **August** | 23.073 | 20.346 | 24.693 | 0.705 | 23.935 | 21.191 | 25.635 | 0.721 | 24.26 | 21.485 | 26.032 | 0.745 |
| **September** | 22.539 | 19.782 | 24.303 | 0.772 | 23.447 | 20.641 | 25.321 | 0.809 | 23.821 | 20.999 | 25.745 | 0.829 |
| **October** | 19.856 | 16.797 | 22.693 | 1.157 | 20.898 | 17.864 | 23.723 | 1.128 | 21.389 | 18.344 | 24.207 | 1.135 |
| **November** | 15.519 | 12.461 | 18.899 | 1.415 | 16.749 | 13.65 | 20.205 | 1.431 | 17.223 | 14.122 | 20.729 | 1.453 |
| **December** | 11.931 | 9.036 | 15.12 | 1.369 | 13.086 | 10.144 | 16.455 | 1.441 | 13.542 | 10.588 | 16.938 | 1.453 |

The monthly minimum temperature trends for the historical period (1980–2014) and future projections (2015–2100) under CMIP6 scenarios—SSP126, SSP245, SSP370, and SSP585—clearly indicate a systematic increase in minimum temperatures across all months and emission pathways. This warming of nighttime or early morning temperatures is particularly significant for sectors like agriculture and health, as it affects crop phenology, pest dynamics, and thermal comfort. During the historical period, minimum temperatures range from ~10.7°C in January (winter) to ~25.9°C in June (monsoon onset), with the coldest months being December and January, and the warmest nights in May and June. The standard deviation remains relatively low for summer months (~0.5–0.7°C), indicating more stable night-time temperatures during peak heat periods. Under the low-emission scenario (SSP126), there is a notable increase of ~1°C to 1.5°C across most months. For example, January rises from 10.74°C to 11.98°C, while May increases from 24.52°C to 25.65°C. Similarly, December experiences a rise from 11.93°C to 13.09°C, indicating less intense winter cooling under even the most optimistic emissions scenario. The moderate-emission scenario (SSP245) amplifies this warming trend further. Minimum temperatures in March

rise to 18.03°C, and June to 27.54°C, compared to 16.04°C and 25.88°C historically, respectively. Winter warming becomes more apparent as December increases to 13.54°C, reducing cold extremes that are crucial for certain crops and ecological cycles.

Table 7: Tabulation of statistics of monthly Minimum temperature under the scenarios of Ssp370 and Ssp585

| Months | Ssp370 (2015-2100) | | | | Ssp585 (2015-2100) | | | |
|---|---|---|---|---|---|---|---|---|
| | Minimum Temperature | | | | | | | |
| | Mean | Min | Max | StdDev | Mean | Min | Max | StdDev |
| **January** | 12.988 | 10.167 | 16 | 1.306 | 13.657 | 10.835 | 16.676 | 1.313 |
| **February** | 14.66 | 11.888 | 17.34 | 1.178 | 15.414 | 12.687 | 18.04 | 1.16 |
| **March** | 18.444 | 15.716 | 20.752 | 1.039 | 19.164 | 16.451 | 21.423 | 1.019 |
| **April** | 22.98 | 20.178 | 24.957 | 0.955 | 23.568 | 20.75 | 25.578 | 0.976 |
| **May** | 26.512 | 24.007 | 27.948 | 0.701 | 27.063 | 24.601 | 28.492 | 0.655 |
| **June** | 27.845 | 25.715 | 29.658 | 0.529 | 28.267 | 26.172 | 30.119 | 0.56 |
| **July** | 25.819 | 23.191 | 27.295 | 0.6 | 26.138 | 23.528 | 27.627 | 0.583 |
| **August** | 24.847 | 22.071 | 26.618 | 0.742 | 24.847 | 22.071 | 26.618 | 0.742 |
| **September** | 24.242 | 21.412 | 26.17 | 0.834 | 24.607 | 21.767 | 26.525 | 0.841 |
| **October** | 21.913 | 18.868 | 24.688 | 1.126 | 22.422 | 19.355 | 25.228 | 1.153 |
| **November** | 17.849 | 14.746 | 21.303 | 1.423 | 18.557 | 15.465 | 22.009 | 1.422 |

| | | | | | | | | |
|---|---|---|---|---|---|---|---|---|
| **December** | 14.051 | 11.069 | 17.512 | 1.474 | 14.771 | 11.808 | 18.189 | 1.455 |

In high-emission pathways (SSP370 and SSP585), the minimum temperatures rise even more dramatically. Under SSP370, January averages 12.99°C, while under SSP585, it reaches 13.66°C—an increase of nearly 3°C compared to the historical period. Similarly, June, which already had the highest minimums historically, climbs to 28.27°C under SSP585. This implies very warm nights even during monsoon, which can influence evaporation, nighttime energy demand (e.g., for cooling), and crop stress.

The warming is particularly stark during the cooler months:

- December rises from 11.93°C (historical) to 14.77°C under SSP585,
- February increases from 12.28°C to 15.41°C, indicating a 2–3°C rise in winter night-time temperatures.

Standard deviation values remain largely consistent across all scenarios, suggesting that while mean temperatures rise, the interannual variability does not increase significantly. However, some variability persists during transitional months (October–November), potentially due to uneven warming trends during shifting seasons. These results indicate a pronounced warming of minimum temperatures, particularly in winter and post-monsoon months, with greater magnitude under higher emissions scenarios. This reduction in the diurnal temperature range (difference between max and min temperatures) could have widespread implications:

- Agriculture: Shorter chilling periods, reduced crop yields for temperature-sensitive crops.
- Health: Increased heat stress due to warmer nights.
- Hydrology: Reduced snow accumulation in upstream basins, higher evapotranspiration rates.

Table 8: Tabulation of statistics of monthly Precipitation under the scenarios of Historical, Ssp126 and Ssp245

| Months | Historical (1980-2014) | | | | Ssp126 (2015-2100) | | | | Ssp245 (2015-2100) (2015-2100) | | | | |
|---|---|---|---|---|---|---|---|---|---|---|---|---|---|
| | Precipitation | | | | | | | | | | | | |
| | Mean | Min | Max | StdDev | Mean | Min | Max | StdDev | Mean | Min | Max | StdDev | StdDev |
| January | 30.535 | 14.911 | 47.207 | 9.63 | 33.019 | 18.184 | 51.391 | 9.009 | 32.55 | 18.521 | 49.936 | 8.4 | 1.284 |
| February | 19.113 | 5.472 | 33.647 | 9.01 | 21.309 | 7.486 | 34.312 | 8.777 | 21.815 | 8.718 | 34.532 | 8.107 | 1.121 |
| March | 14.327 | 4.279 | 25.942 | 7.01 | 16.039 | 6.338 | 25.515 | 6.119 | 15.092 | 5.135 | 25.967 | 6.596 | 1.084 |
| April | 10.448 | 5.271 | 17.121 | 3.61 | 12.922 | 6.369 | 19.69 | 4.215 | 13.347 | 6.773 | 20.648 | 4.437 | 0.987 |
| May | 9.841 | 5.919 | 15.952 | 2.87 | 14.839 | 8.632 | 22.221 | 4.103 | 14.19 | 7.956 | 21.799 | 4.24 | 0.52 |
| June | 56.254 | 34.97 | 84.557 | 13.31 | 72.063 | 47.256 | 106.234 | 15.49 | 72.156 | 50.534 | 105.311 | 12.859 | 0.574 |
| July | 313.771 | 219.69 | 458.07 | 53.95 | 375.746 | 273.294 | 530.459 | 55.353 | 370.52 | 272.079 | 524.425 | 53.356 | 0.583 |
| August | 360.71 | 260.81 | 509.97 | 53.54 | 440.989 | 330.169 | 615.585 | 56.371 | 457.133 | 348.581 | 636.941 | 55.338 | 0.68 |
| September | 176.978 | 137.64 | 245.95 | 20.49 | 231.404 | 189.672 | 316.842 | 21.946 | 247.04 | 209.366 | 335.404 | 22.699 | 31.928 |
| October | 57.713 | 47.77 | 76.96 | 5.59 | 79.311 | 67.6 | 104.008 | 6.928 | 82.442 | 70.473 | 109.529 | 7.439 | 32.617 |
| November | 43.768 | 33.66 | 59.61 | 4.88 | 52.257 | 39.374 | 70.007 | 5.922 | 45.207 | 33.437 | 58.934 | 5.377 | 29.923 |
| December | 39.607 | 26.54 | 59.62 | 7.59 | 42.023 | 32.968 | 59.996 | 5.498 | 42.271 | 31.611 | 61.778 | 6.403 | 27.196 |

In January, precipitation increases from 30.54 mm in the historical period to around 33–36 mm across all future scenarios. The consistent rise, especially under SSP370 and SSP585, suggests a trend toward wetter winter months, possibly influenced by intensified Western Disturbances. This may affect winter cropping patterns, water availability, and could even increase the likelihood of winter flooding in localized low-lying areas.

Table 9: Tabulation of statistics of monthly Precipitation under the scenarios of Ssp370 and Ssp585

| Months | Ssp370 (2015-2100) | | | | Ssp585 (2015-2100) | | | |
|---|---|---|---|---|---|---|---|---|
| | Precipitation | | | | | | | |
| | Mean | Min | Max | StdDev | Mean | Min | Max | StdDev |
| January | 36.168 | 20.553 | 55.415 | 9.364 | 35.511 | 21.037 | 54.605 | 8.767 |
| February | 24.776 | 9.401 | 39.939 | 9.614 | 24.588 | 10.824 | 38.196 | 8.588 |
| March | 17.902 | 6.587 | 28.765 | 7.288 | 15.643 | 5.093 | 26.417 | 7.007 |
| April | 13.893 | 7.688 | 20.951 | 4.144 | 12.863 | 6.548 | 19.706 | 12.863 |
| May | 14.418 | 8.345 | 22.542 | 4.313 | 15.97 | 10.164 | 22.786 | 3.68 |
| June | 81.508 | 57.555 | 116.824 | 13.84 | 85.627 | 60.798 | 121.584 | 14.768 |
| July | 366.114 | 275.389 | 508.859 | 48.395 | 398.043 | 304.479 | 551.915 | 49.282 |
| August | 460.746 | 366.067 | 625.249 | 47.13 | 480.381 | 386.172 | 645.707 | 47.041 |
| September | 258.777 | 219.631 | 348.582 | 23.305 | 279.447 | 242.7 | 371.72 | 24.686 |

| | | | | | | | | |
|---|---|---|---|---|---|---|---|---|
| **October** | 93.987 | 80.53 | 124.081 | 8.248 | 103.965 | 89.326 | 134.25 | 9.967 |
| **November** | 53.135 | 39.891 | 69.088 | 6.178 | 62.048 | 45.905 | 80.466 | 7.537 |
| **December** | 41.897 | 32.881 | 59.45 | 5.168 | 50.315 | 39.413 | 71.254 | 6.18 |

February also shows a steady increase in rainfall from 19.11 mm historically to 24.78 mm (SSP370) and 24.59 mm (SSP585). These increases, particularly under high-emission scenarios, may result in greater early-season soil moisture, which can benefit certain crops, but may also increase the risk of cold-season pest outbreaks or early weed growth. In March, precipitation increases from 14.33 mm to 15–18 mm depending on the scenario. Although modest, this shift may lead to more frequent pre-monsoon showers, potentially disrupting harvesting of Rabi crops or causing unexpected rainfall events that could affect agricultural scheduling. April shows precipitation rising from 10.45 mm (historical) to as high as 13.89 mm (SSP370). This trend could lead to higher humidity and early convection activity, creating conditions conducive to localized thunderstorms or unseasonal rain affecting flowering stages in crops. In May, the increase from 9.84 mm to up to 15.97 mm (SSP585) indicates significant pre-monsoon intensification. This could result in early monsoon-like rainfall, influencing sowing decisions, particularly for crops dependent on the precise arrival of monsoon rains. It may also lead to heat and humidity stress, both agriculturally and in urban areas.

June sees a notable jump from 56.25 mm to 85.63 mm under SSP585. This early monsoon month becoming wetter suggests a stronger monsoon onset, which can be beneficial for early crop growth. However, it also raises concerns about soil erosion, flash floods, and the need for early deployment of irrigation and drainage infrastructure. July, a peak month, increases from 313.77 mm historically to 398.04 mm under SSP585. Such high rainfall volumes can enhance groundwater recharge and reservoir levels, but may also increase the risk of flooding, urban waterlogging, and crop inundation, especially in poorly drained areas. August, historically the wettest month (360.71 mm), is projected to become even wetter with precipitation reaching 480.38 mm under SSP585. This increase of over 100 mm

may amplify runoff volumes, stressing existing water management systems. Agricultural fields could face waterlogging, and critical infrastructure such as roads, railways, and power grids might be more vulnerable to extreme weather events. In September, rainfall increases from 176.98 mm to 279.45 mm in SSP585, pointing toward a prolonged monsoon season. This could delay the harvest of Kharif crops and the sowing of Rabi crops. Extended wetness may also increase the risk of post-monsoon pests and fungal diseases in crops and affect soil drying rates needed for field preparation. October rises from 57.71 mm historically to 103.97 mm under SSP585, almost a twofold increase. Such enhancement in post-monsoon rainfall could delay agricultural operations, damage harvested crops, and increase surface runoff, especially in hilly areas. November also shows an increase from 43.77 mm to 62.05 mm, particularly under SSP585. Higher rainfall this month may disrupt Rabi sowing schedules, particularly for wheat and mustard, and could increase moisture stress in germination phases if the rainfall is intense and erratic. Finally, December precipitation increases from 39.61 mm historically to 50.32 mm under SSP585. These wetter conditions may affect winter crop performance and contribute to higher humidity levels, potentially exacerbating the spread of leaf and stem fungal diseases in crops like wheat and gram.

Following the plotting and extraction of monthly statistics for precipitation, maximum, minimum, and mean temperatures under all historical and future scenarios (SSP126, SSP245, SSP370, and SSP585), the data were further aggregated to produce seasonal datasets. These seasonal datasets were derived by calculating the average temperatures and total precipitation corresponding to four climatological seasons: Winter (December–February), Pre-Monsoon (March–May), Monsoon (June–September), and Post-Monsoon (October–November). After the seasonal aggregation, spatial plots were generated to visualize the distribution of seasonal climate variables across the basin. These plots allow for a clearer understanding of regional climatic shifts and enable direct comparison of baseline (historical) and projected (future) conditions. They also help identify critical climate-sensitive zones, such as areas experiencing significant warming during pre-monsoon or increased rainfall during monsoon and post-monsoon periods.These visualizations are crucial for interpreting seasonal trends and for communicating results effectively to stakeholders involved in water resource planning, agricultural scheduling, and climate adaptation policymaking.

Figure 75: Spatial distribution of seasonal values of Maximum temperature for the Historical, SSP126, SSP245, SSP370, and SSP585 scenarios

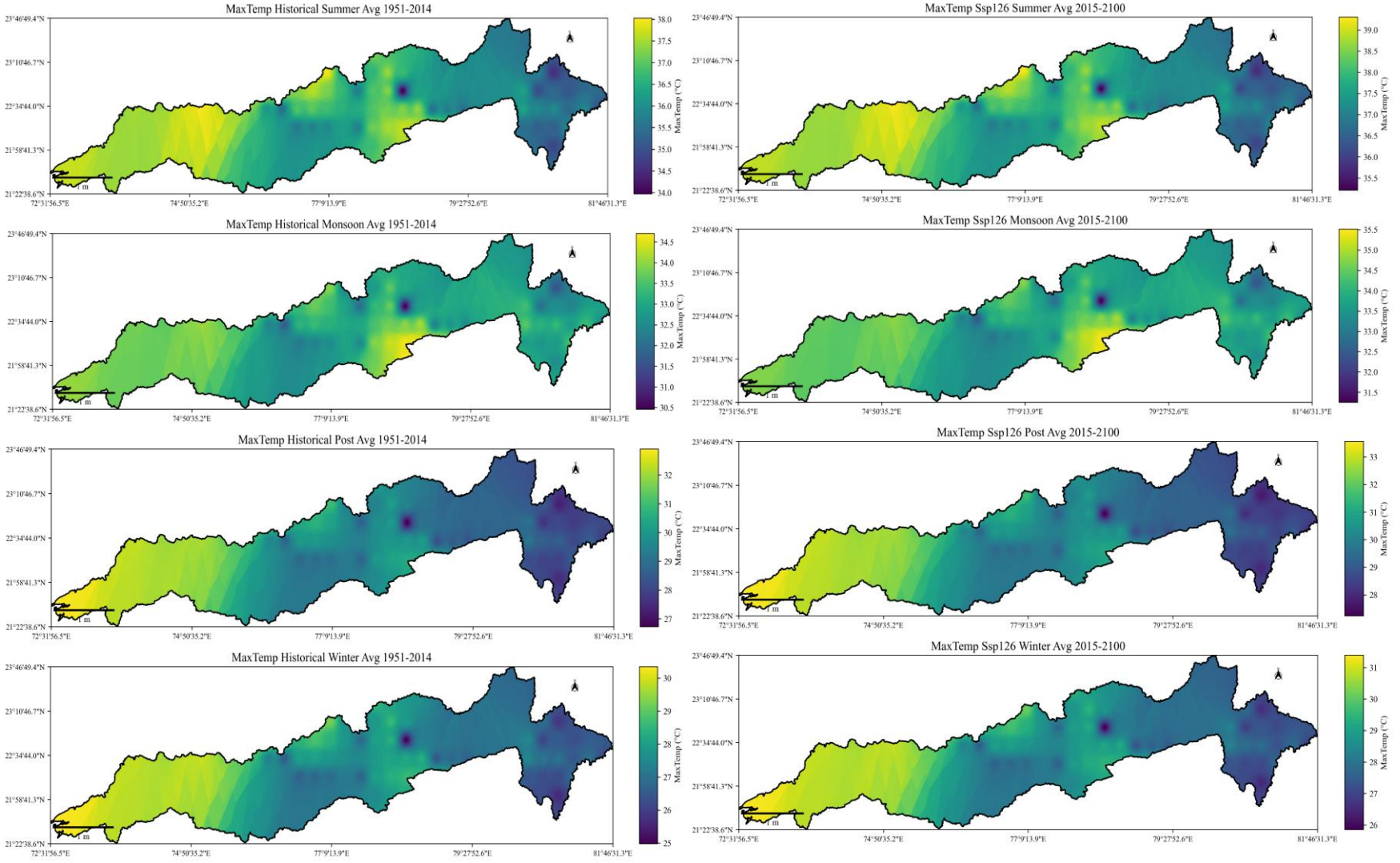

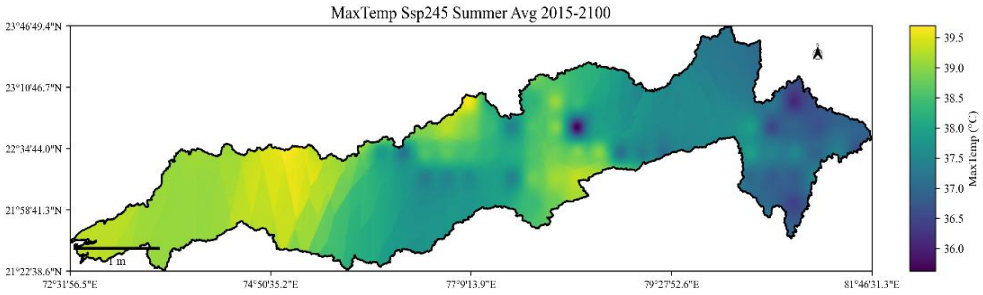
MaxTemp Ssp245 Summer Avg 2015-2100
23°46'49.4"N
23°10'46.7"N
22°34'44.0"N
21°58'41.3"N
21°22'38.6"N
72°31'56.5"E
74°50'35.2"E
77°9'13.9"E
79°27'52.6"E
81°46'31.3"E
MaxTemp (°C)
39.5
39.0
38.5
38.0
37.5
37.0
36.5
36.0

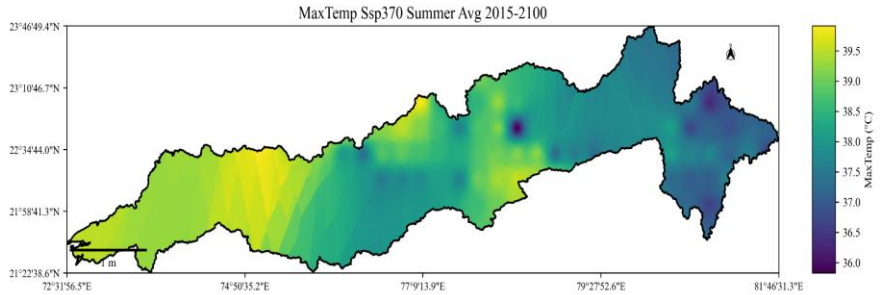
MaxTemp Ssp370 Summer Avg 2015-2100
23°46'49.4"N
23°10'46.7"N
22°34'44.0"N
21°58'41.3"N
21°22'38.6"N
72°31'56.5"E
74°50'35.2"E
77°9'13.9"E
79°27'52.6"E
81°46'31.3"E
MaxTemp (°C)
39.5
39.0
38.5
38.0
37.5
37.0
36.5
36.0

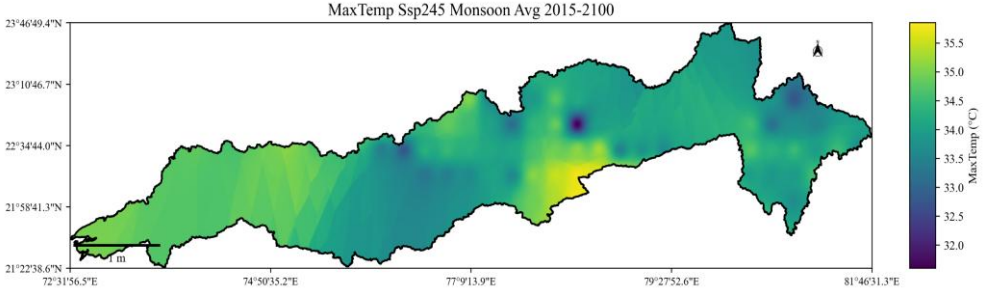
MaxTemp Ssp245 Monsoon Avg 2015-2100
23°46'49.4"N
23°10'46.7"N
22°34'44.0"N
21°58'41.3"N
21°22'38.6"N
72°31'56.5"E
74°50'35.2"E
77°9'13.9"E
79°27'52.6"E
81°46'31.3"E
MaxTemp (°C)
35.5
35.0
34.5
34.0
33.5
33.0
32.5
32.0

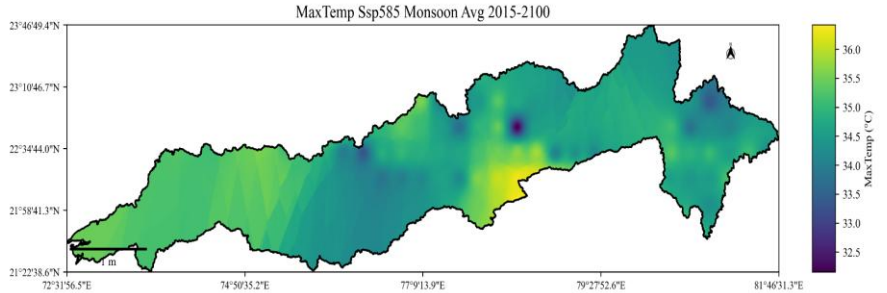
MaxTemp Ssp585 Monsoon Avg 2015-2100
23°46'49.4"N
23°10'46.7"N
22°34'44.0"N
21°58'41.3"N
21°22'38.6"N
72°31'56.5"E
74°50'35.2"E
77°9'13.9"E
79°27'52.6"E
81°46'31.3"E
MaxTemp (°C)
36.0
35.5
35.0
34.5
34.0
33.5
33.0
32.5

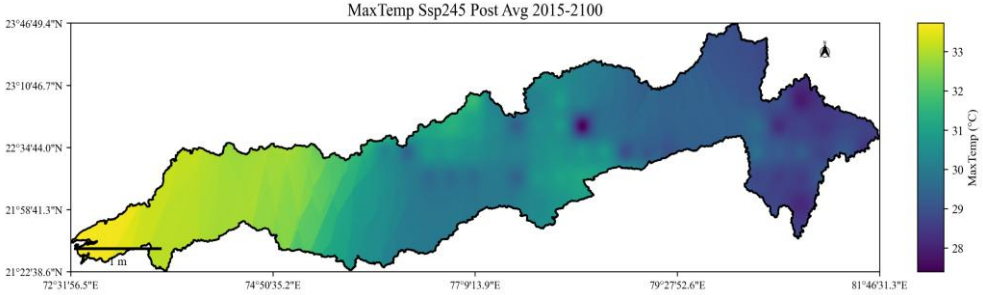
MaxTemp Ssp245 Post Avg 2015-2100
23°46'49.4"N
23°10'46.7"N
22°34'44.0"N
21°58'41.3"N
21°22'38.6"N
72°31'56.5"E
74°50'35.2"E
77°9'13.9"E
79°27'52.6"E
81°46'31.3"E
MaxTemp (°C)
33
32
31
30
29
28

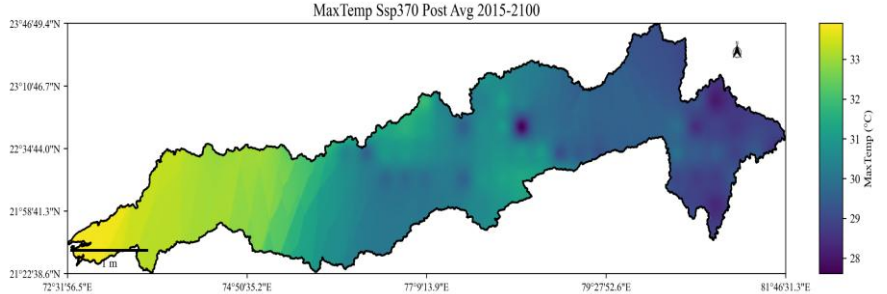
MaxTemp Ssp370 Post Avg 2015-2100
23°46'49.4"N
23°10'46.7"N
22°34'44.0"N
21°58'41.3"N
21°22'38.6"N
72°31'56.5"E
74°50'35.2"E
77°9'13.9"E
79°27'52.6"E
81°46'31.3"E
MaxTemp (°C)
33
32
31
30
29
28

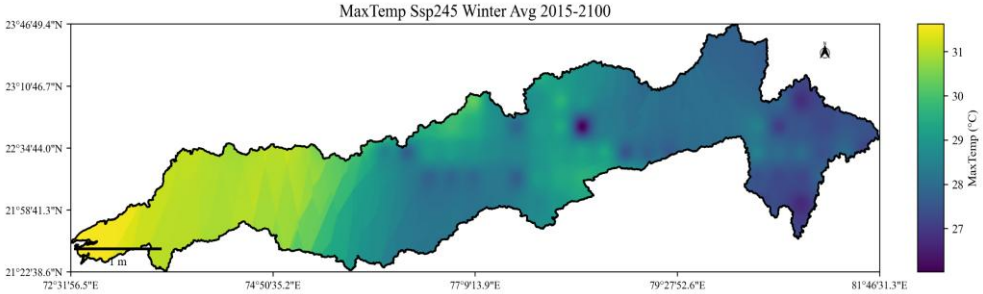
MaxTemp Ssp245 Winter Avg 2015-2100
23°46'49.4"N
23°10'46.7"N
22°34'44.0"N
21°58'41.3"N
21°22'38.6"N
72°31'56.5"E
74°50'35.2"E
77°9'13.9"E
79°27'52.6"E
81°46'31.3"E
MaxTemp (°C)
31
30
29
28
27

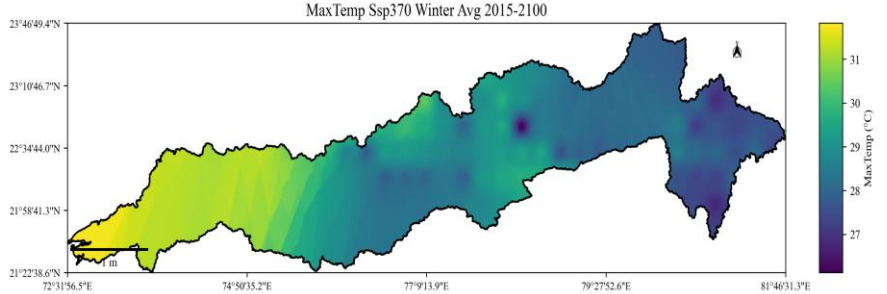
MaxTemp Ssp370 Winter Avg 2015-2100
23°46'49.4"N
23°10'46.7"N
22°34'44.0"N
21°58'41.3"N
21°22'38.6"N
72°31'56.5"E
74°50'35.2"E
77°9'13.9"E
79°27'52.6"E
81°46'31.3"E
MaxTemp (°C)
31
30
29
28
27

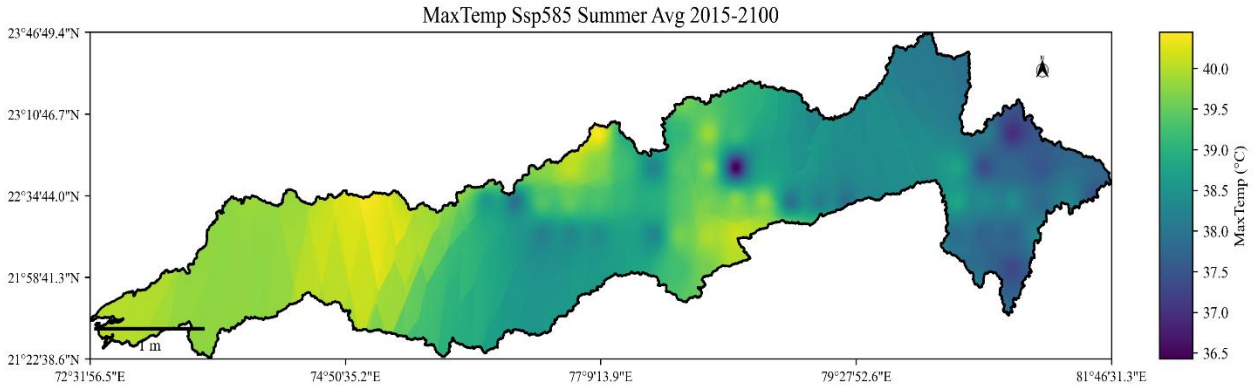
MaxTemp Ssp585 Summer Avg 2015-2100
23°46'49.4"N
23°10'46.7"N
22°34'44.0"N
21°58'41.3"N
21°22'38.6"N
72°31'56.5"E
74°50'35.2"E
77°9'13.9"E
79°27'52.6"E
81°46'31.3"E
1 m
40.0
39.5
39.0
38.5
38.0
37.5
37.0
36.5
MaxTemp (°C)

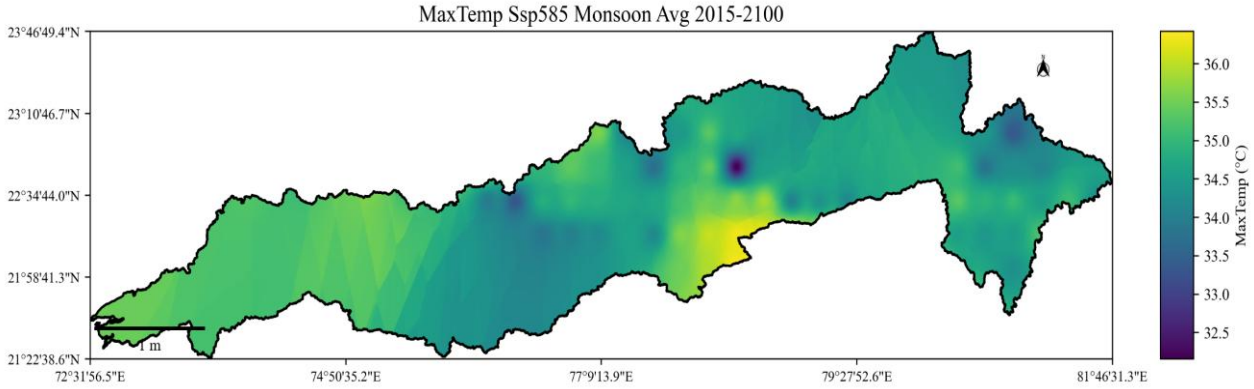
MaxTemp Ssp585 Monsoon Avg 2015-2100
23°46'49.4"N
23°10'46.7"N
22°34'44.0"N
21°58'41.3"N
21°22'38.6"N
72°31'56.5"E
74°50'35.2"E
77°9'13.9"E
79°27'52.6"E
81°46'31.3"E
1 m
36.0
35.5
35.0
34.5
34.0
33.5
33.0
32.5
MaxTemp (°C)

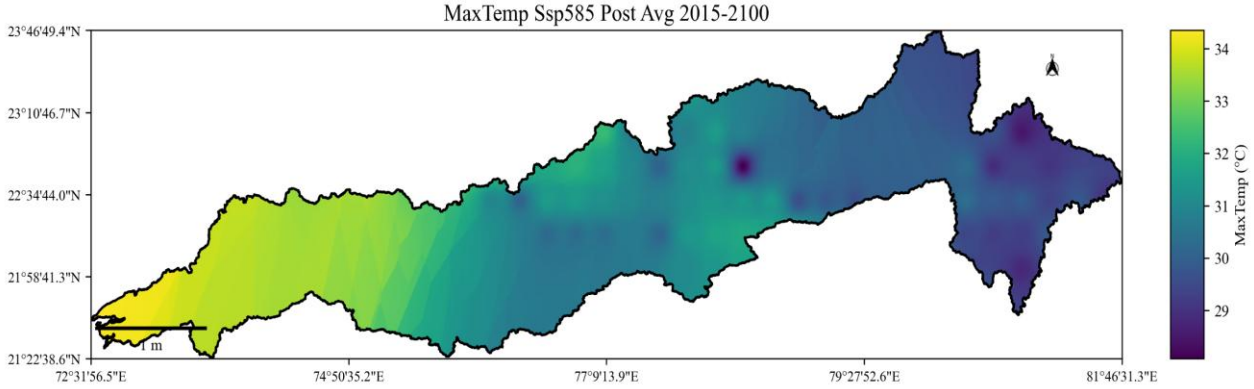
MaxTemp Ssp585 Post Avg 2015-2100
23°46'49.4"N
23°10'46.7"N
22°34'44.0"N
21°58'41.3"N
21°22'38.6"N
72°31'56.5"E
74°50'35.2"E
77°9'13.9"E
79°27'52.6"E
81°46'31.3"E
1 m
34
33
32
31
30
29
MaxTemp (°C)

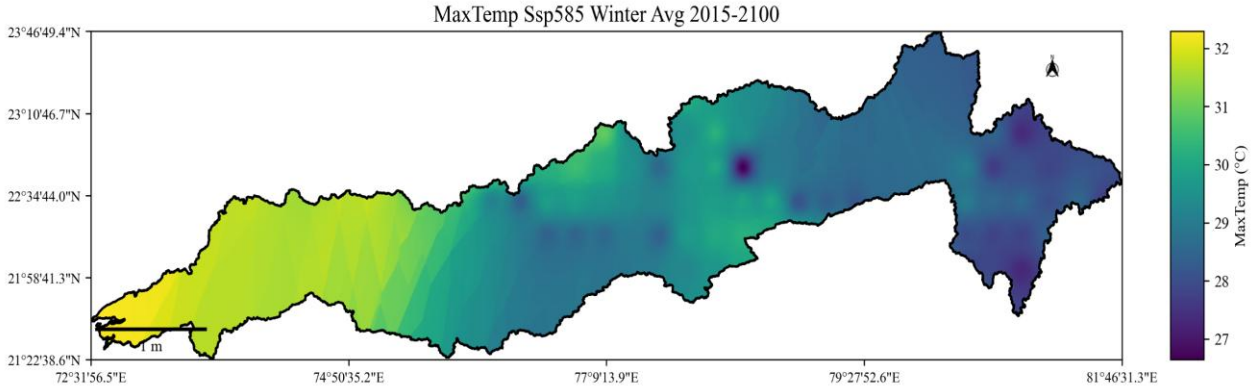
MaxTemp Ssp585 Winter Avg 2015-2100
23°46'49.4"N
23°10'46.7"N
22°34'44.0"N
21°58'41.3"N
21°22'38.6"N
72°31'56.5"E
74°50'35.2"E
77°9'13.9"E
79°27'52.6"E
81°46'31.3"E
1 m
32
31
30
29
28
27
MaxTemp (°C)

Figure 76: Spatial distribution of seasonal values of Mean temperature for the Historical, SSP126, SSP245, SSP370, and SSP585 scenarios

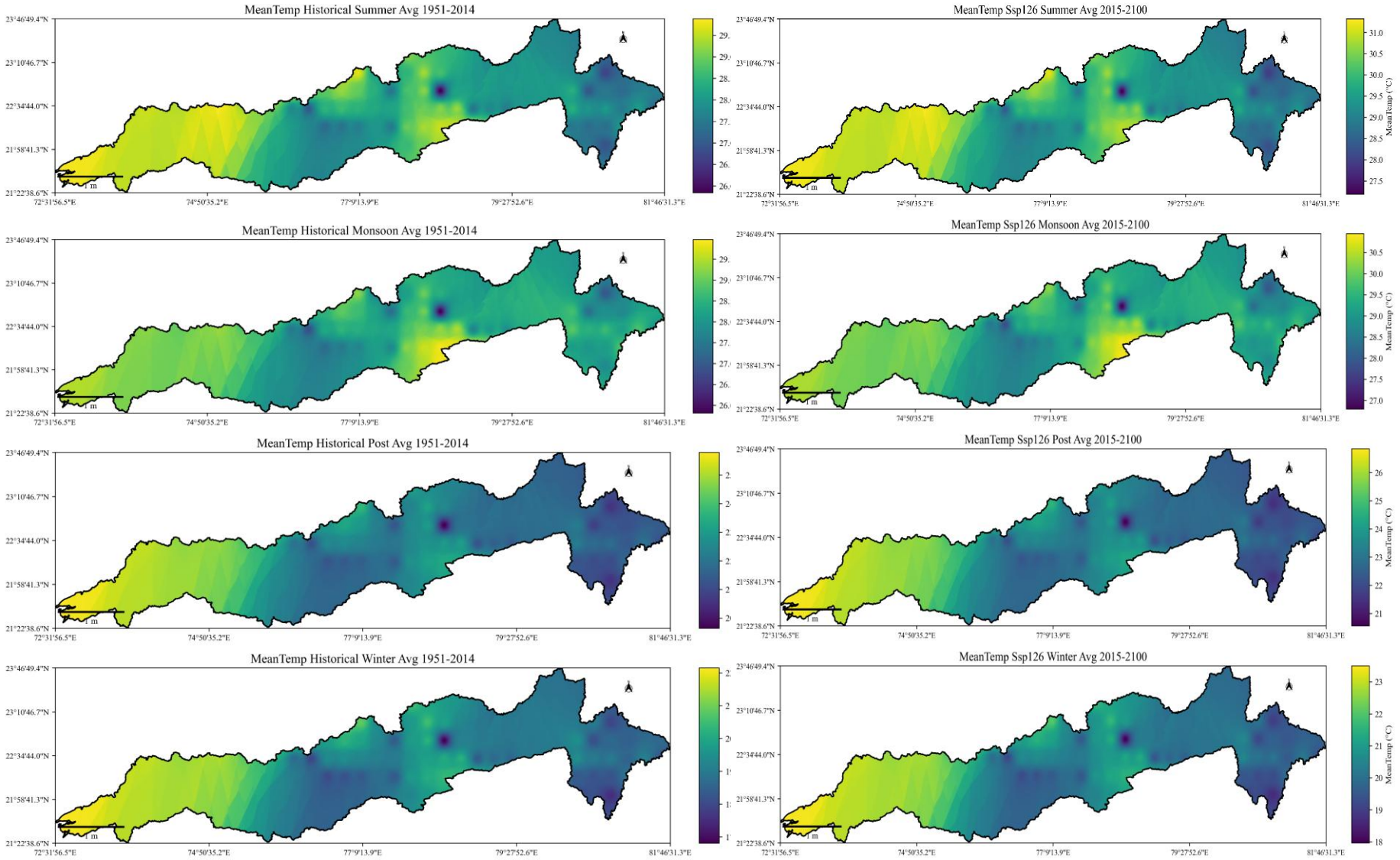

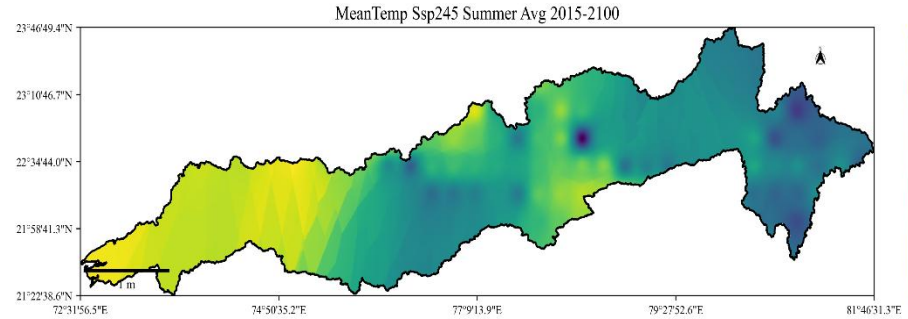
MeanTemp Ssp245 Summer Avg 2015-2100
23°46'49.4"N
23°10'46.7"N
22°34'44.0"N
21°58'41.3"N
21°22'38.6"N
72°31'56.5"E
74°50'35.2"E
77°9'13.9"E
79°27'52.6"E
81°46'31.3"E
MeanTemp (°C)

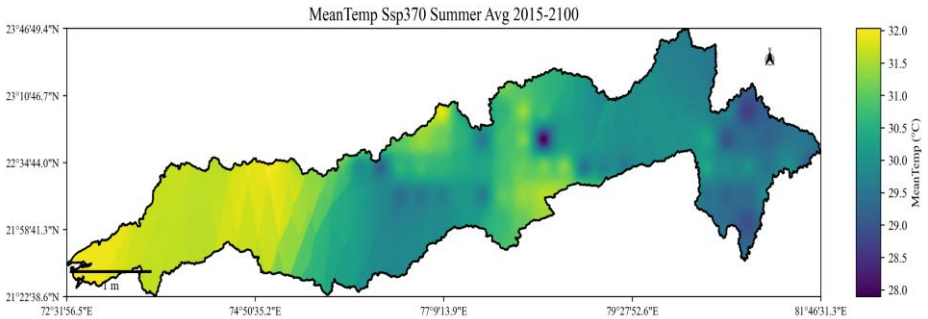
MeanTemp Ssp370 Summer Avg 2015-2100
23°46'49.4"N
23°10'46.7"N
22°34'44.0"N
21°58'41.3"N
21°22'38.6"N
72°31'56.5"E
74°50'35.2"E
77°9'13.9"E
79°27'52.6"E
81°46'31.3"E
MeanTemp (°C)

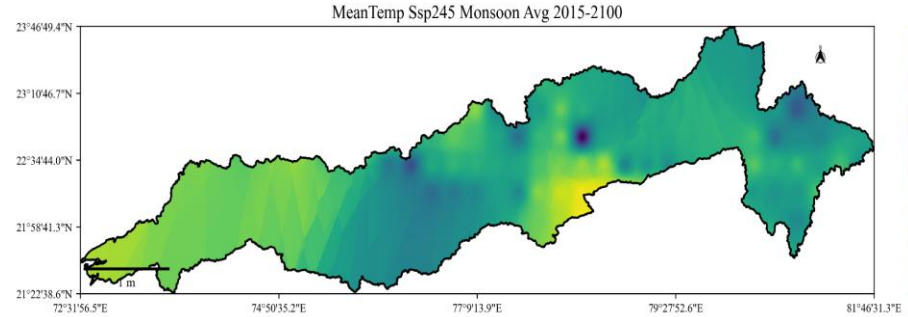
MeanTemp Ssp245 Monsoon Avg 2015-2100
23°46'49.4"N
23°10'46.7"N
22°34'44.0"N
21°58'41.3"N
21°22'38.6"N
72°31'56.5"E
74°50'35.2"E
77°9'13.9"E
79°27'52.6"E
81°46'31.3"E
MeanTemp (°C)

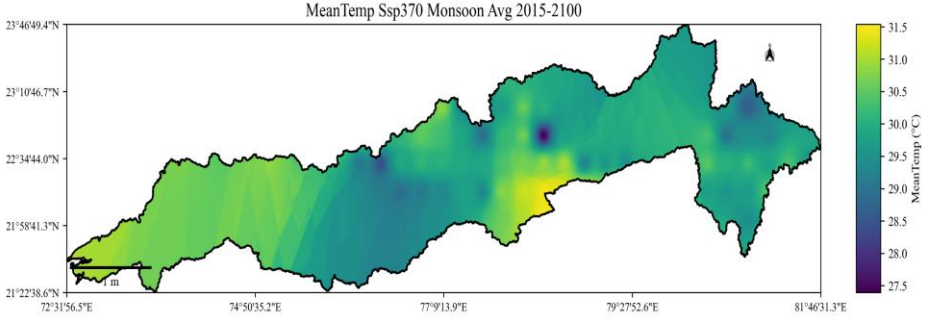
MeanTemp Ssp370 Monsoon Avg 2015-2100
23°46'49.4"N
23°10'46.7"N
22°34'44.0"N
21°58'41.3"N
21°22'38.6"N
72°31'56.5"E
74°50'35.2"E
77°9'13.9"E
79°27'52.6"E
81°46'31.3"E
MeanTemp (°C)

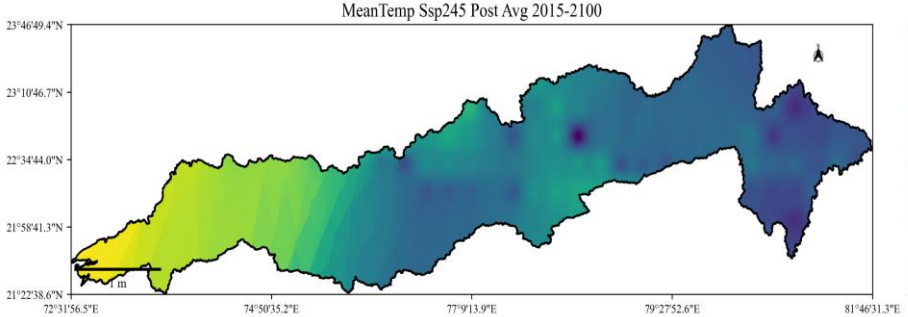
MeanTemp Ssp245 Post Avg 2015-2100
23°46'49.4"N
23°10'46.7"N
22°34'44.0"N
21°58'41.3"N
21°22'38.6"N
72°31'56.5"E
74°50'35.2"E
77°9'13.9"E
79°27'52.6"E
81°46'31.3"E
MeanTemp (°C)

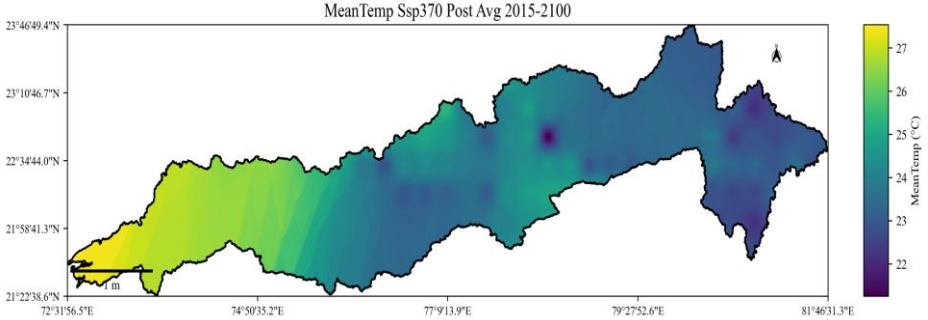
MeanTemp Ssp370 Post Avg 2015-2100
23°46'49.4"N
23°10'46.7"N
22°34'44.0"N
21°58'41.3"N
21°22'38.6"N
72°31'56.5"E
74°50'35.2"E
77°9'13.9"E
79°27'52.6"E
81°46'31.3"E
MeanTemp (°C)

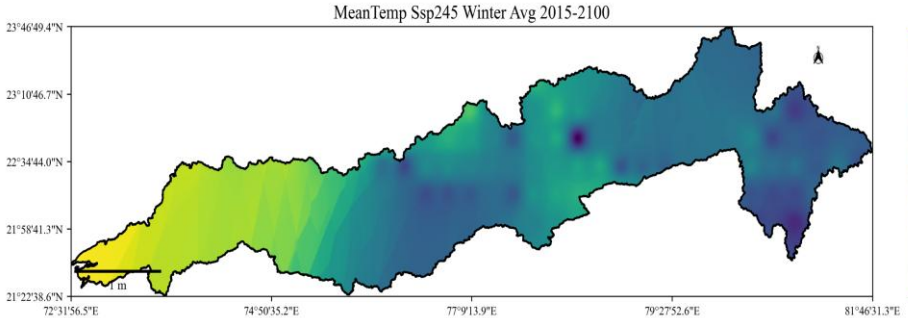
MeanTemp Ssp245 Winter Avg 2015-2100
23°46'49.4"N
23°10'46.7"N
22°34'44.0"N
21°58'41.3"N
21°22'38.6"N
72°31'56.5"E
74°50'35.2"E
77°9'13.9"E
79°27'52.6"E
81°46'31.3"E
MeanTemp (°C)

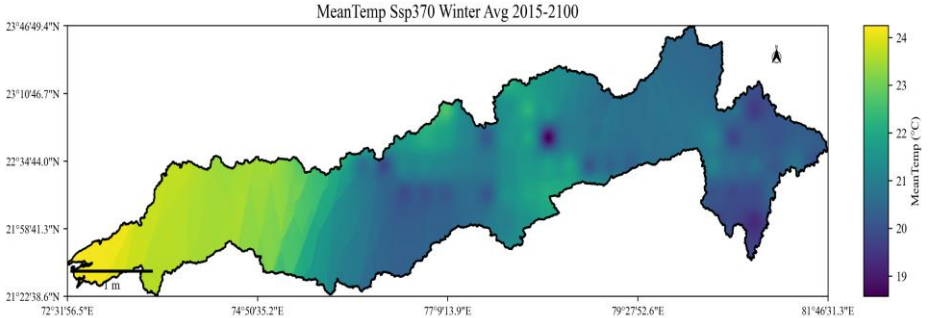
MeanTemp Ssp370 Winter Avg 2015-2100
23°46'49.4"N
23°10'46.7"N
22°34'44.0"N
21°58'41.3"N
21°22'38.6"N
72°31'56.5"E
74°50'35.2"E
77°9'13.9"E
79°27'52.6"E
81°46'31.3"E
MeanTemp (°C)

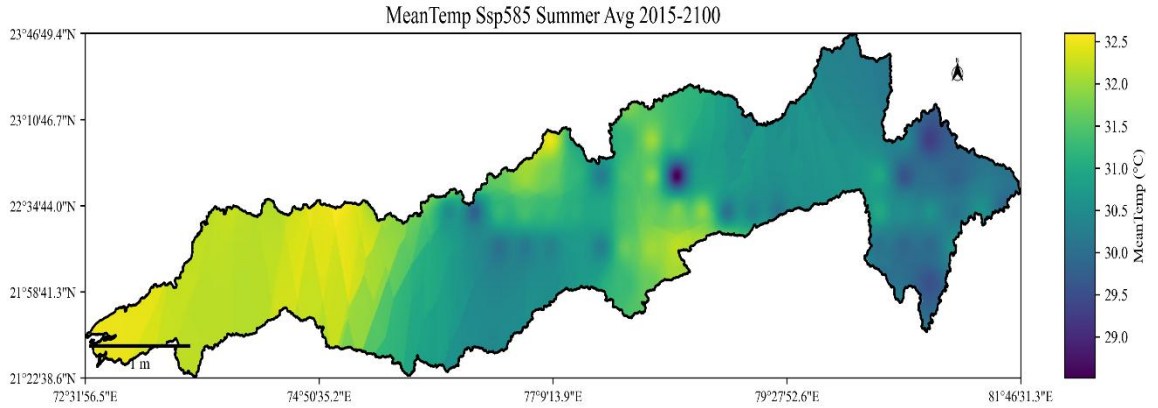
MeanTemp Ssp585 Summer Avg 2015-2100
23°46'49.4"N
23°10'46.7"N
22°34'44.0"N
21°58'41.3"N
21°22'38.6"N
72°31'56.5"E
74°50'35.2"E
77°9'13.9"E
79°27'52.6"E
81°46'31.3"E
0 m
MeanTemp (°C)
32.5
32.0
31.5
31.0
30.5
30.0
29.5
29.0

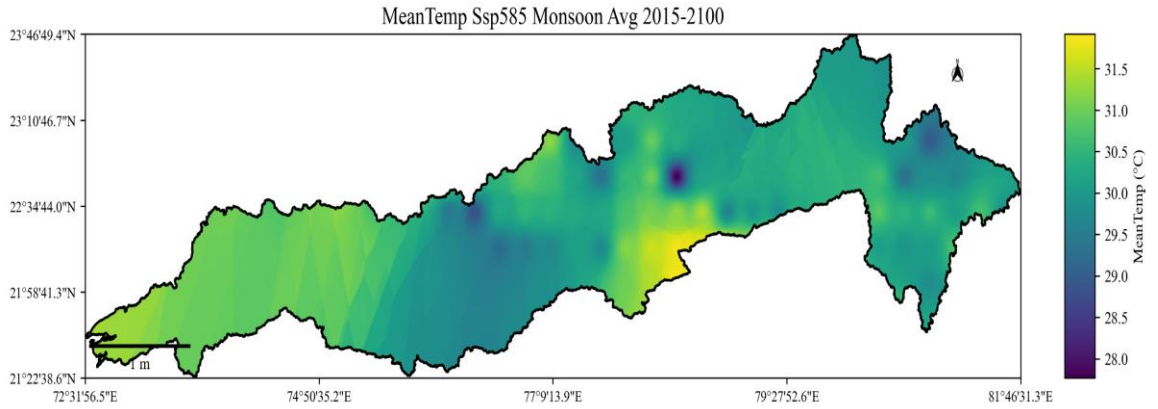
MeanTemp Ssp585 Monsoon Avg 2015-2100
23°46'49.4"N
23°10'46.7"N
22°34'44.0"N
21°58'41.3"N
21°22'38.6"N
72°31'56.5"E
74°50'35.2"E
77°9'13.9"E
79°27'52.6"E
81°46'31.3"E
0 m
MeanTemp (°C)
31.5
31.0
30.5
30.0
29.5
29.0
28.5
28.0

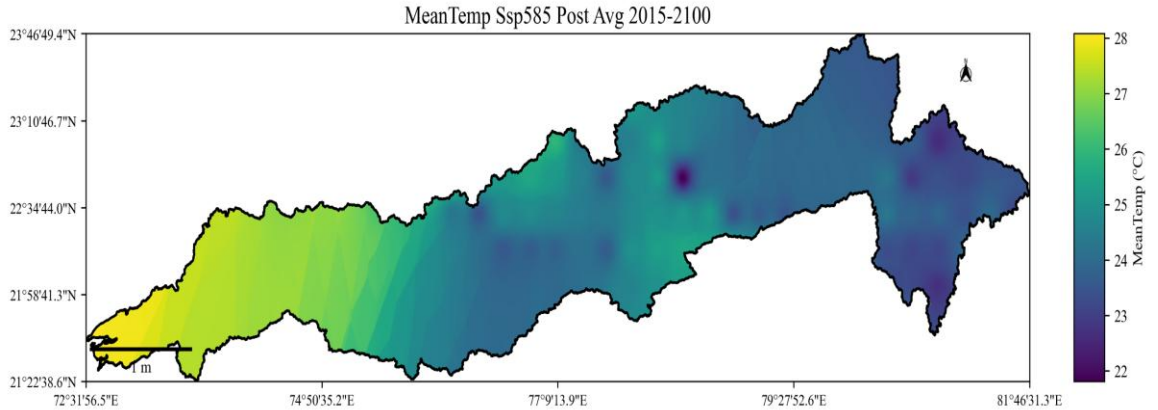
MeanTemp Ssp585 Post Avg 2015-2100
23°46'49.4"N
23°10'46.7"N
22°34'44.0"N
21°58'41.3"N
21°22'38.6"N
72°31'56.5"E
74°50'35.2"E
77°9'13.9"E
79°27'52.6"E
81°46'31.3"E
0 m
MeanTemp (°C)
28
27
26
25
24
23
22

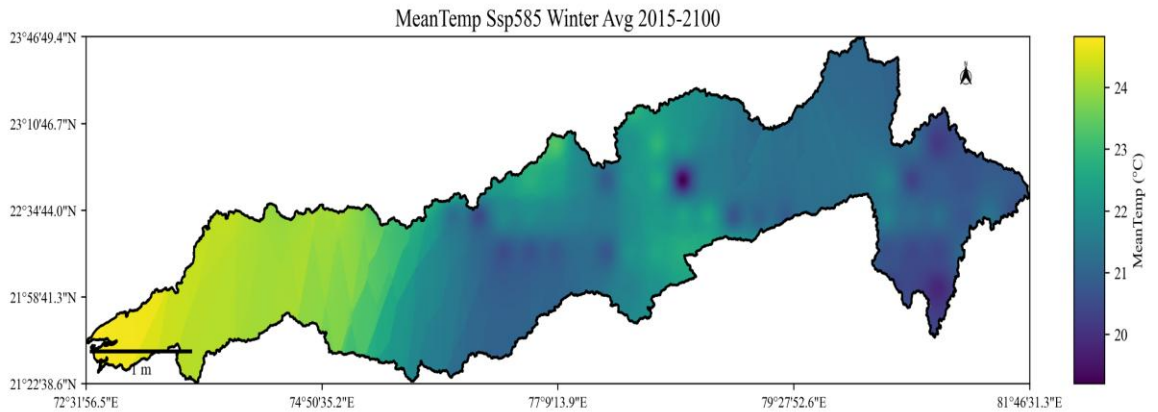
MeanTemp Ssp585 Winter Avg 2015-2100
23°46'49.4"N
23°10'46.7"N
22°34'44.0"N
21°58'41.3"N
21°22'38.6"N
72°31'56.5"E
74°50'35.2"E
77°9'13.9"E
79°27'52.6"E
81°46'31.3"E
0 m
MeanTemp (°C)
24
23
22
21
20

Figure 77: Spatial distribution of seasonal values of Minimum temperature for the Historical, SSP126, SSP245, SSP370, and SSP585 scenarios

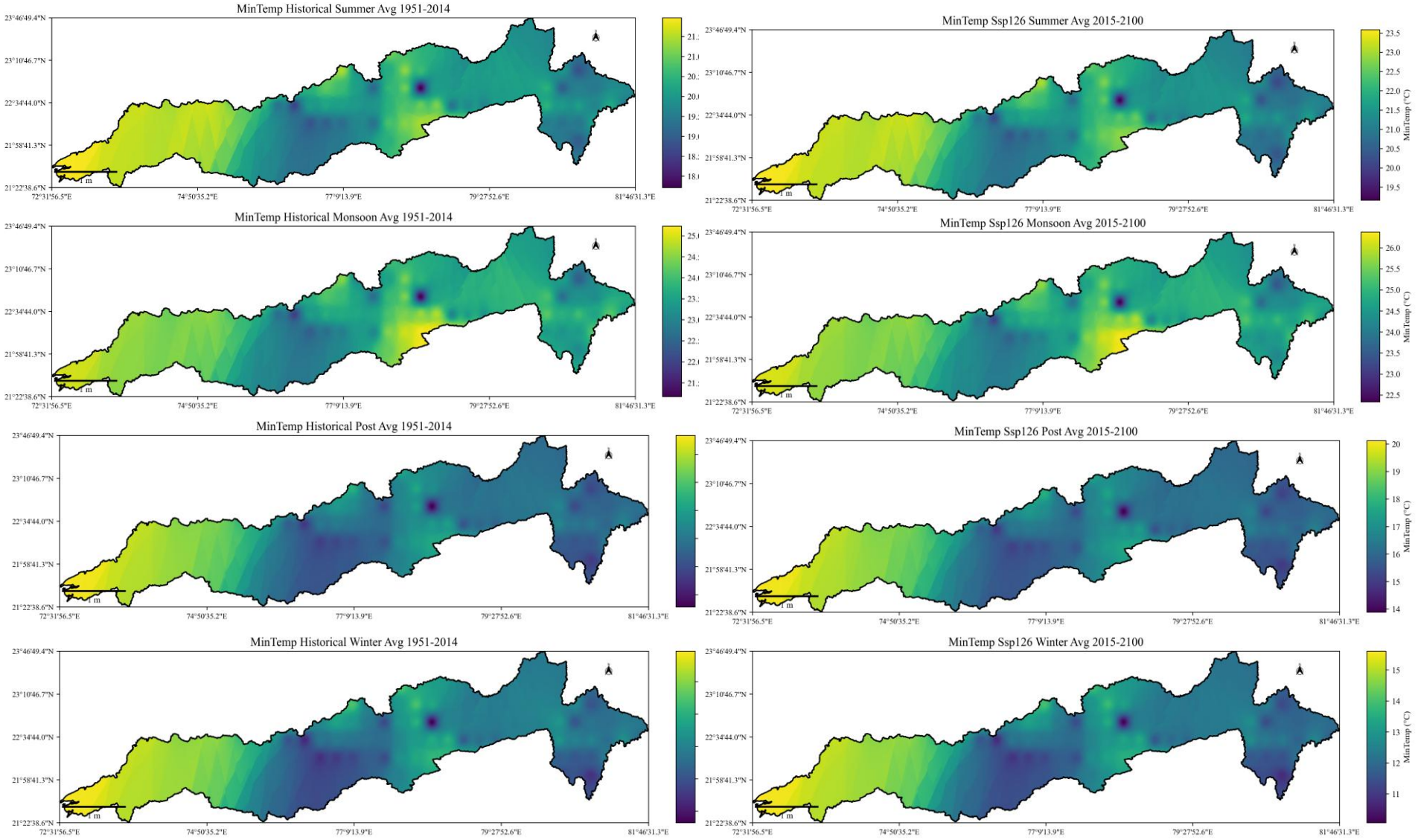

MinTemp Ssp245 Summer Avg 2015-2100

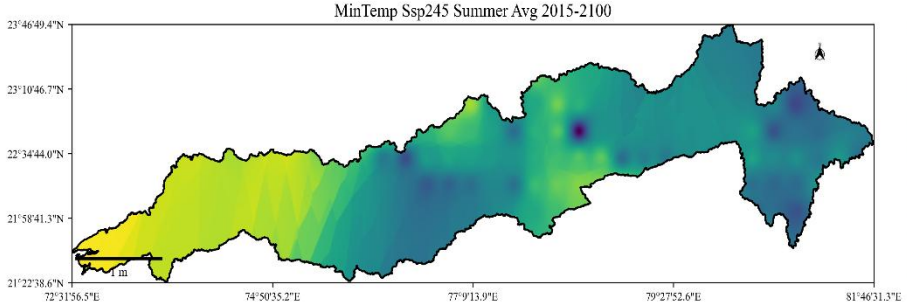


MinTemp Ssp245 Summer Avg 2015-2100

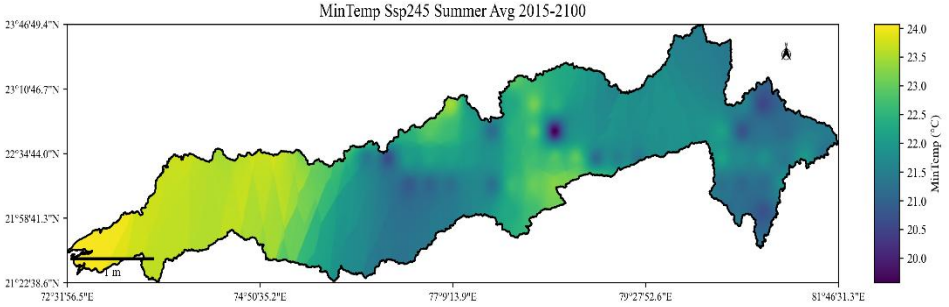


MinTemp Ssp245 Monsoon Avg 2015-2100

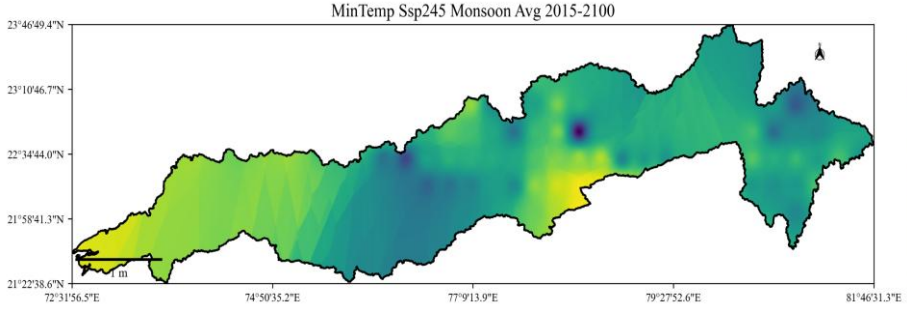


MinTemp Ssp245 Monsoon Avg 2015-2100

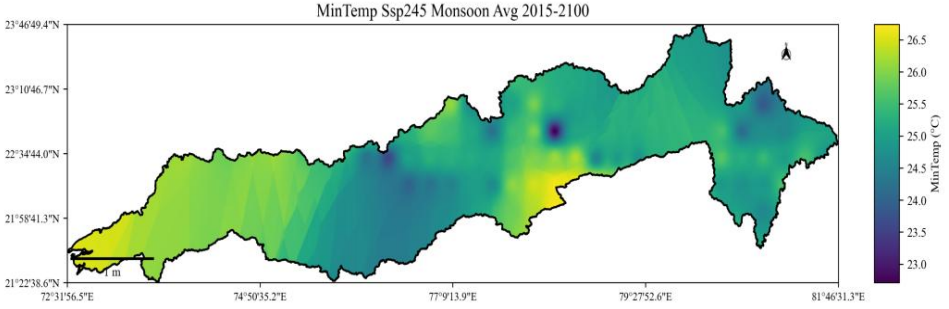


MinTemp Ssp245 Post Avg 2015-2100

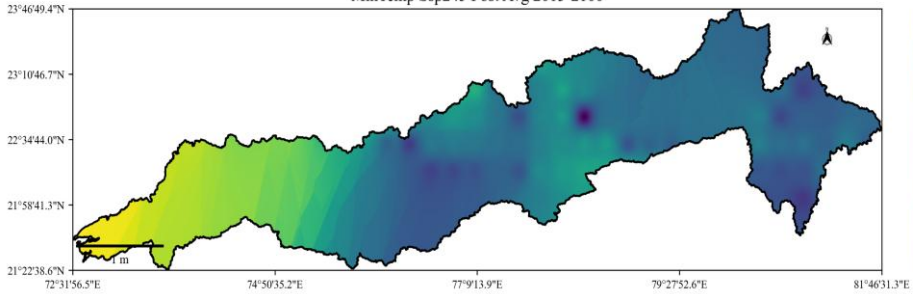


MinTemp Ssp245 Post Avg 2015-2100

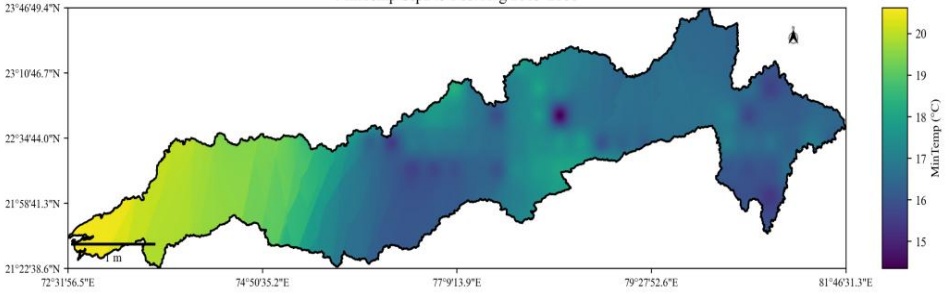


MinTemp Ssp126 Winter Avg 2015-2100

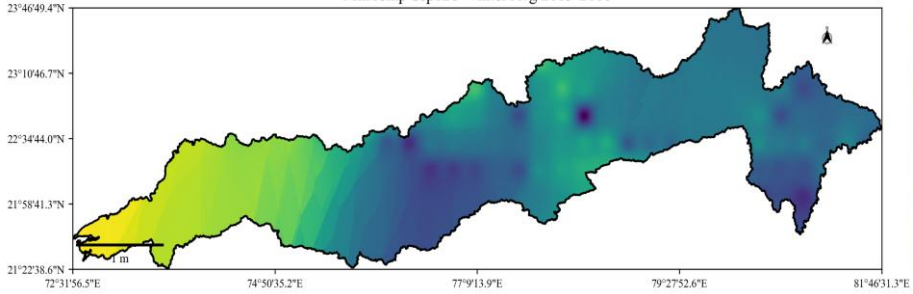


MinTemp Ssp245 Winter Avg 2015-2100

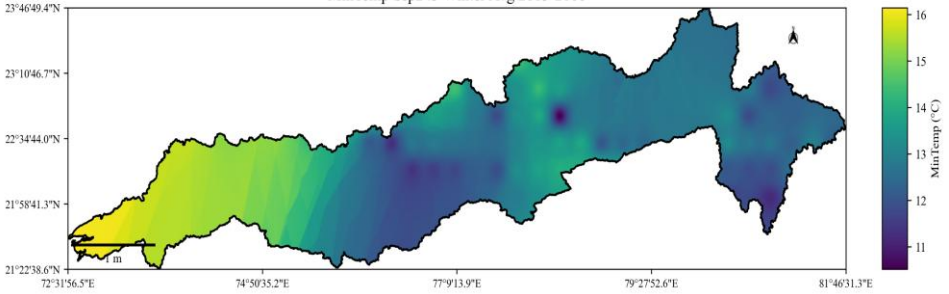

Figure 78:Spatial distribution of seasonal values of Precipitation for the Historical, SSP126, SSP245, SSP370, and SSP585 scenarios

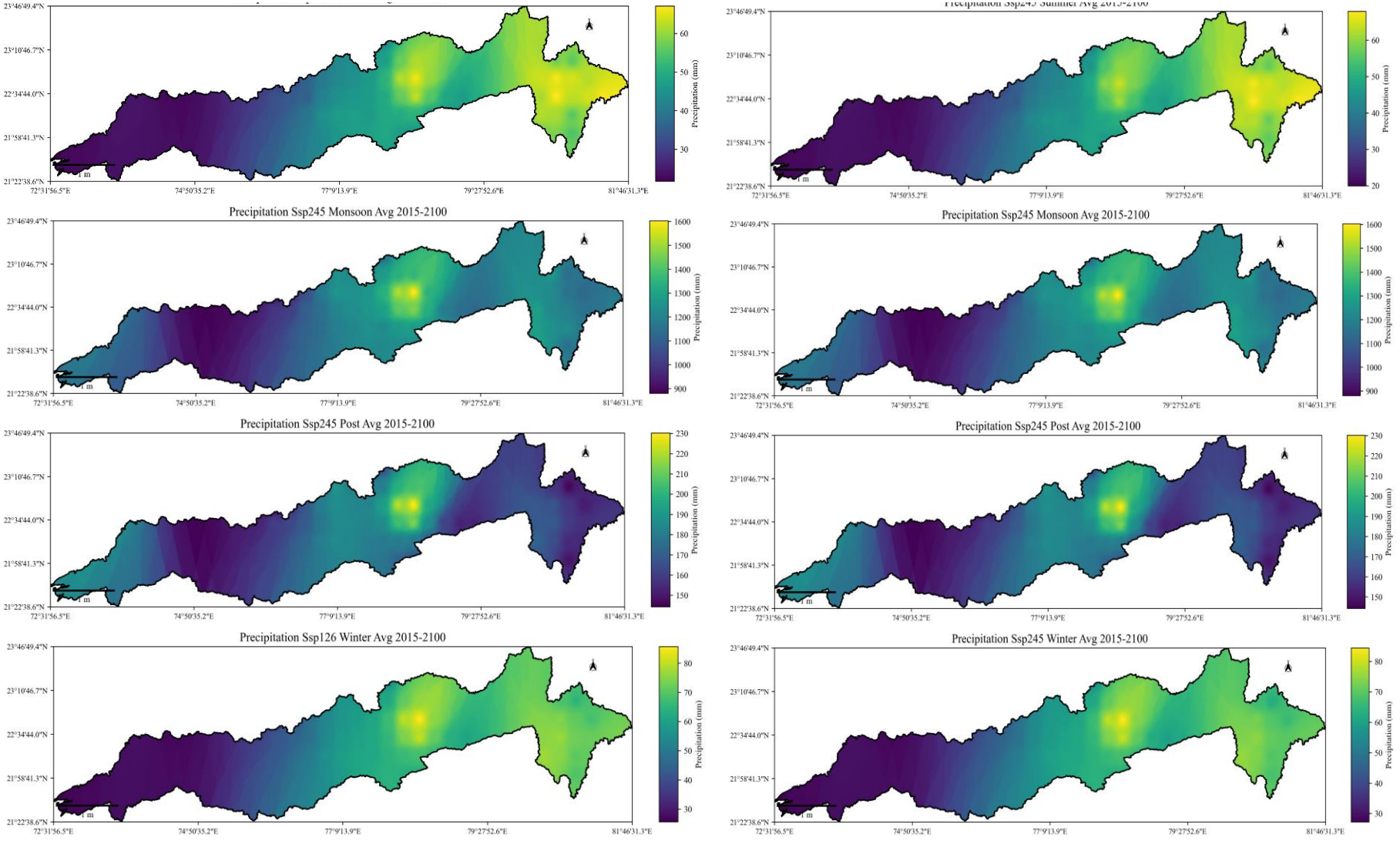

Precipitation Ssp370 Summer Avg 2015-2100

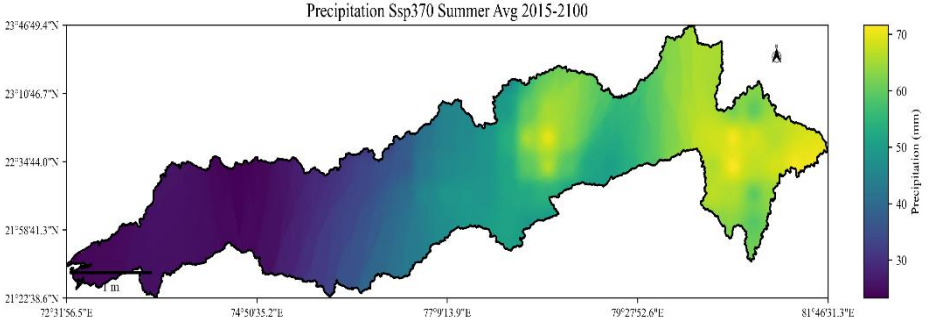


Precipitation Ssp585 Summer Avg 2015-2100

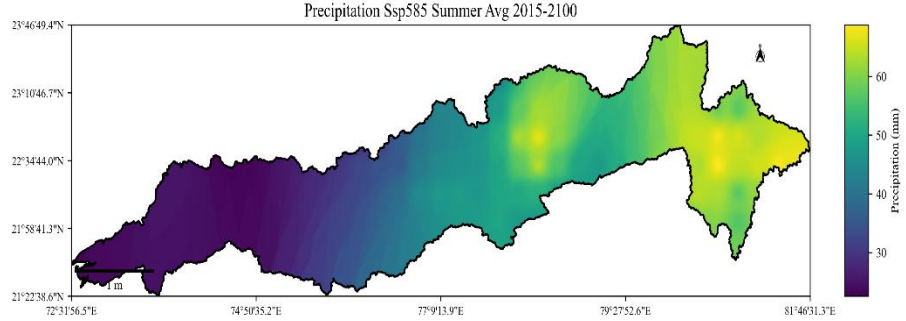


Precipitation Ssp370 Monsoon Avg 2015-2100

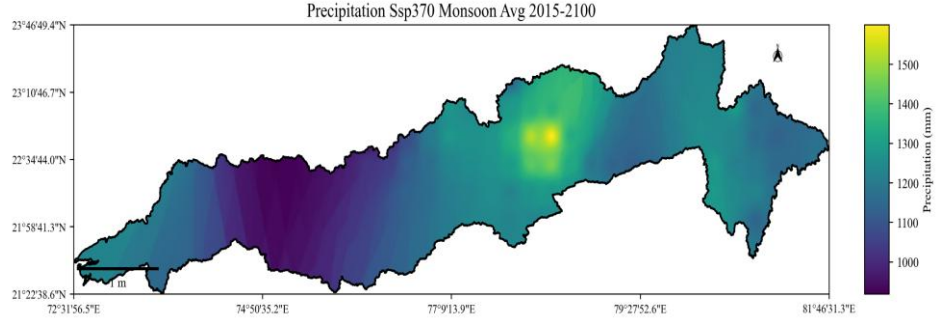


Precipitation Ssp585 Monsoon Avg 2015-2100

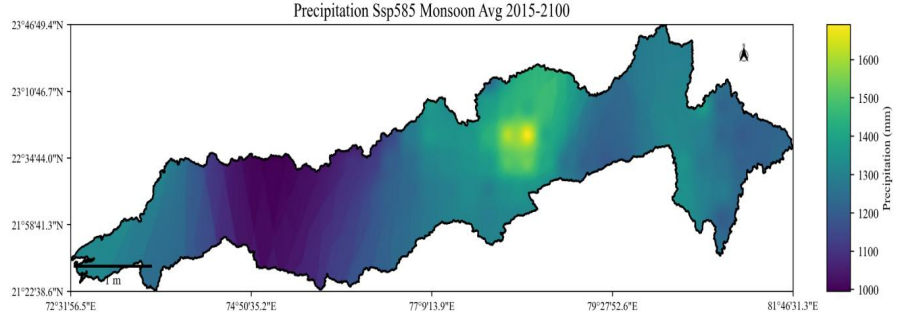


Precipitation Ssp370 Post Avg 2015-2100

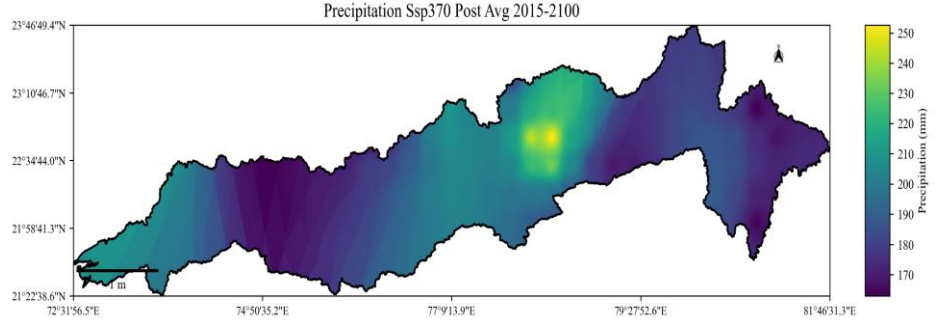


Precipitation Ssp585 Post Avg 2015-2100

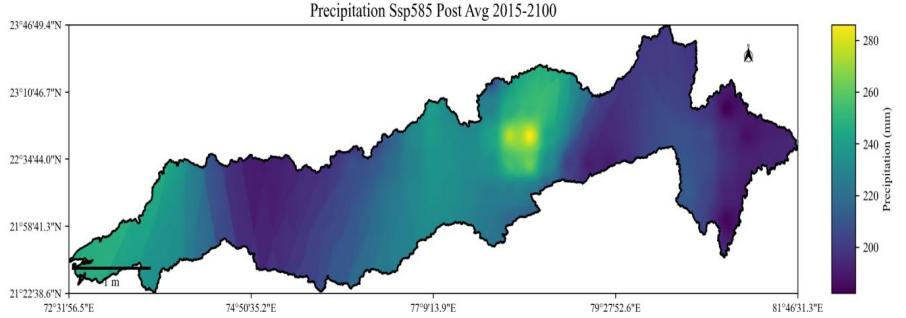


Precipitation Ssp370 Winter Avg 2015-2100

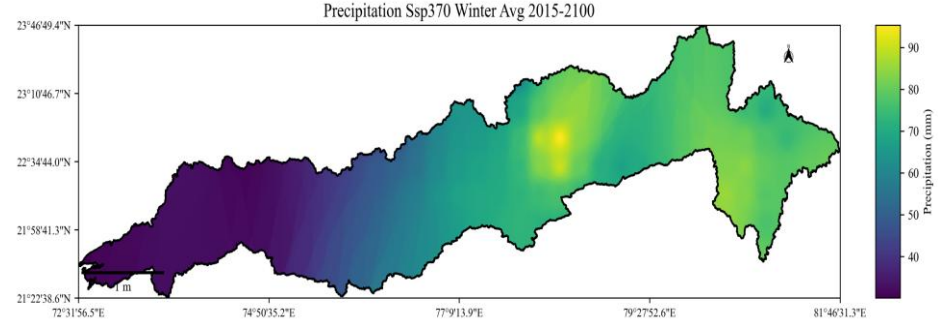


Precipitation Ssp370 Winter Avg 2015-2100

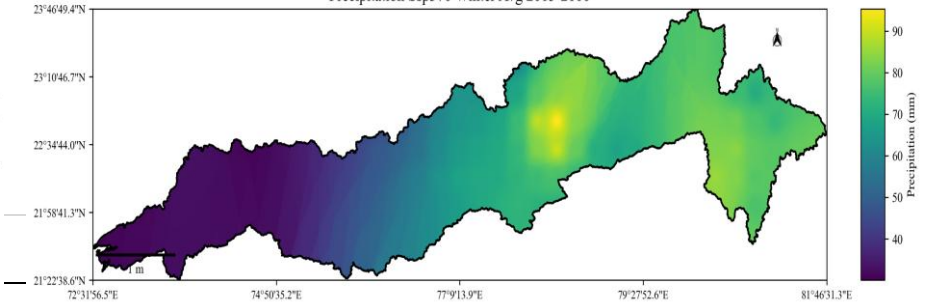

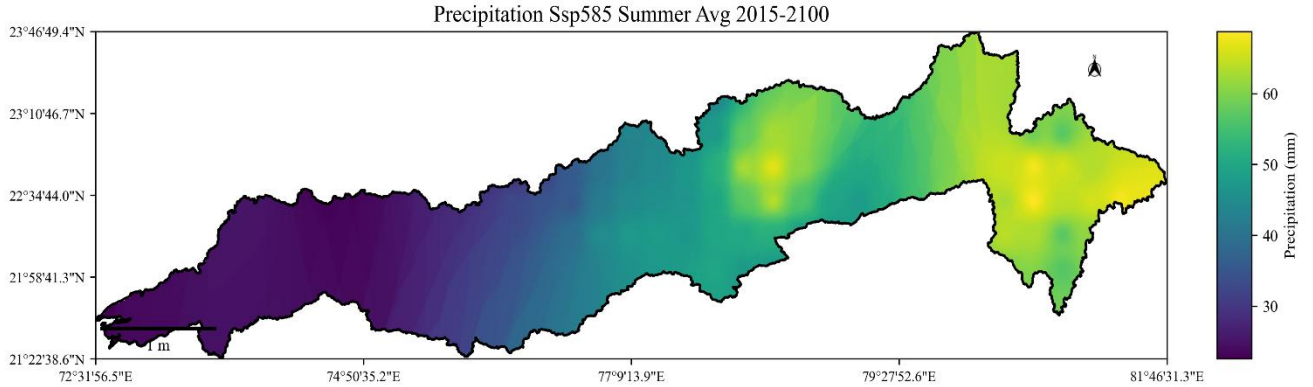
Precipitation Ssp585 Summer Avg 2015-2100
23°46'49.4"N
23°10'46.7"N
22°34'44.0"N
21°58'41.3"N
21°22'38.6"N
72°31'56.5"E
74°50'35.2"E
77°9'13.9"E
79°27'52.6"E
81°46'31.3"E
1 m
Precipitation (mm)
60
50
40
30

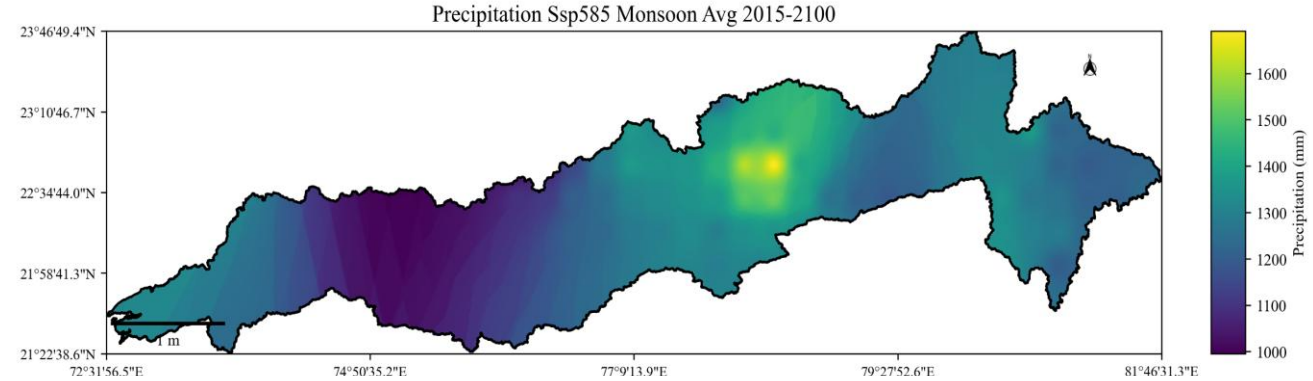
Precipitation Ssp585 Monsoon Avg 2015-2100
23°46'49.4"N
23°10'46.7"N
22°34'44.0"N
21°58'41.3"N
21°22'38.6"N
72°31'56.5"E
74°50'35.2"E
77°9'13.9"E
79°27'52.6"E
81°46'31.3"E
1 m
Precipitation (mm)
1600
1500
1400
1300
1200
1100
1000

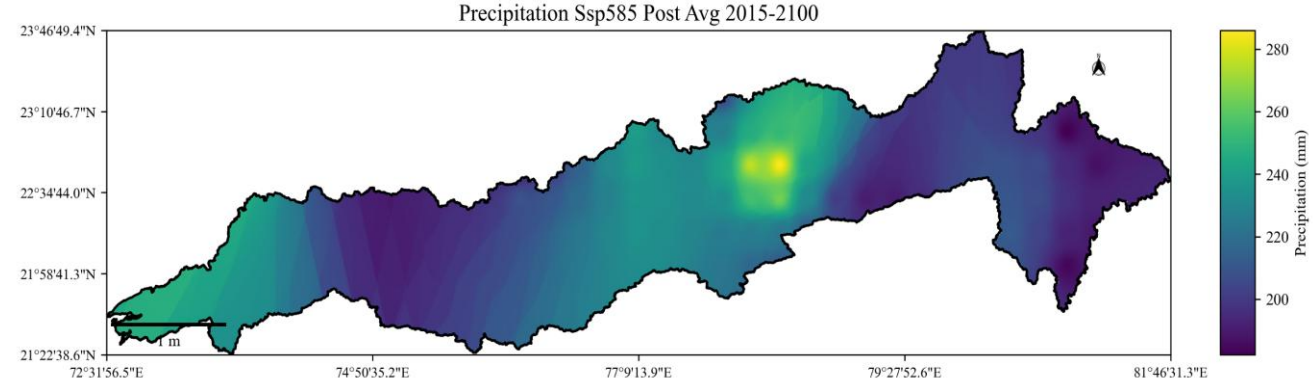
Precipitation Ssp585 Post Avg 2015-2100
23°46'49.4"N
23°10'46.7"N
22°34'44.0"N
21°58'41.3"N
21°22'38.6"N
72°31'56.5"E
74°50'35.2"E
77°9'13.9"E
79°27'52.6"E
81°46'31.3"E
1 m
Precipitation (mm)
280
260
240
220
200

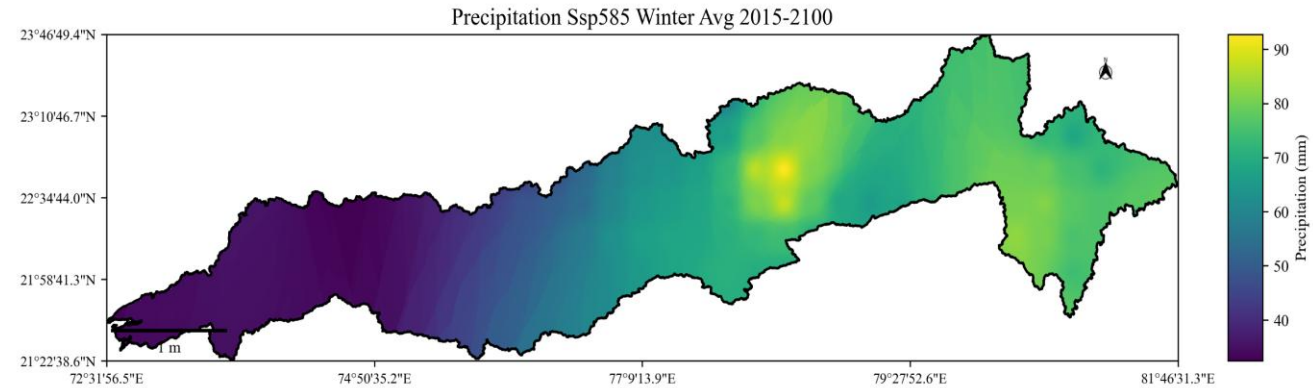
Precipitation Ssp585 Winter Avg 2015-2100
23°46'49.4"N
23°10'46.7"N
22°34'44.0"N
21°58'41.3"N
21°22'38.6"N
72°31'56.5"E
74°50'35.2"E
77°9'13.9"E
79°27'52.6"E
81°46'31.3"E
1 m
Precipitation (mm)
90
80
70
60
50
40

Table 10: Tabulation of statistics of seasonal Maximum temperature under the scenarios of Historical, Ssp126, Ssp245, Ssp370 and Ssp585

| Months | Historical (1980-2014) | | | | Ssp126 (2015-2100) | | | | Ssp245 (2015-2100) (2015-2100) | | | |
|---|---|---|---|---|---|---|---|---|---|---|---|---|
| | Maximum Temperature (° C) | | | | | | | | | | | |
| | Mean | Min | Max | StdDev | Mean | Min | Max | StdDev | Mean | Min | Max | StdDev |
| Summer | 36.558 | 33.973 | 38.025 | 0.794 | 37.805 | 35.215 | 39.306 | 0.813 | 38.199 | 35.625 | 39.696 | 0.816 |
| Monsoon | 33.168 | 30.464 | 34.702 | 0.537 | 33.932 | 31.258 | 35.511 | 0.517 | 34.255 | 31.601 | 35.851 | 0.503 |
| Post-Monsoon | 29.893 | 26.729 | 32.898 | 1.435 | 30.432 | 27.24 | 33.559 | 1.496 | 30.587 | 27.396 | 33.727 | 1.499 |
| Winter | 27.926 | 24.983 | 30.345 | 1.183 | 28.838 | 25.858 | 31.387 | 1.248 | 29.009 | 26.021 | 31.624 | 1.266 |

| Months | Ssp370 (2015-2100) | | | | Ssp585 (2015-2100) (2015-2100) | | | |
|---|---|---|---|---|---|---|---|---|
| | Maximum Temperature (° C) | | | | | | | |
| | Mean | Min | Max | StdDev | Mean | Min | Max | StdDev |
| Summer | 38.414 | 35.831 | 39.912 | 0.817 | 38.995 | 36.429 | 40.443 | 0.774 |
| Monsoon | 34.421 | 31.771 | 36.024 | 0.495 | 34.791 | 32.158 | 36.42 | 0.487 |
| Post-Monsoon | 30.782 | 27.613 | 33.905 | 1.483 | 31.244 | 28.08 | 34.349 | 1.486 |
| Winter | 29.133 | 26.125 | 31.823 | 1.301 | 29.633 | 26.647 | 32.291 | 1.29 |

The seasonal analysis of maximum temperature under historical and CMIP6 future scenarios reveals a consistent warming trend across all seasons, with the magnitude of warming increasing with emission intensity. In the Summer season (March–May), historical maximum temperature averages 36.56°C, with values rising progressively across scenarios—37.81°C (SSP126), 38.20°C (SSP245), 38.41°C (SSP370), and reaching 38.99°C under SSP585. This shows an approximate increase of 2.4°C in extreme scenarios, indicating greater thermal stress during the pre-monsoon heatwave-prone months, which could significantly affect human health, agriculture, and energy demands. During the Monsoon season (June–September), historical maximum temperatures average 33.17°C, with modest increases observed in all future pathways: up to 34.79°C in SSP585. Although the rise is smaller compared to summer, the increase under wetter atmospheric conditions suggests potential discomfort due to combined heat and humidity (high heat index) and increased evapotranspiration, potentially stressing water resources and crops. For the post-monsoon season (October–November), temperatures rise from 29.89°C historically to 31.24°C in SSP585—an increase of ~1.35°C. This extension of higher temperatures into the post-monsoon period may lead to shorter recovery periods for ecosystems and soil moisture and delay the onset of cooler conditions necessary for Rabi crop sowing.

In Winter (December–February), a warming trend is also evident, with the average maximum temperature increasing from 27.93°C to 29.63°C under SSP585. This ~1.7°C rise may result in milder winters, affecting the chilling requirements for winter crops (such as wheat and mustard), pest survival rates, and possibly leading to shifts in phenological patterns. Across all seasons, the standard deviation values remain relatively low and stable, suggesting that while mean temperatures are increasing, the interannual variability is not significantly affected. However, even minor temperature increases during critical growing periods can result in non-linear impacts on crop yields, water demand, and public health outcomes due to increased frequency and intensity of heatwaves.

Table 11: Tabulation of statistics of seasonal Mean temperature under the scenarios of Historical, Ssp126, Ssp245, Ssp370 and Ssp585

| Months | Historical (1980-2014) | | | | Ssp126 (2015-2100) | | | | Ssp245 (2015-2100) (2015-2100) | | | |
|---|---|---|---|---|---|---|---|---|---|---|---|---|
| | Mean Temperature (° C) | | | | | | | | | | | |
| | Mean | Min | Max | StdDev | Mean | Min | Max | StdDev | Mean | Min | Max | StdDev |
| Summer | 28.453 | 25.845 | 29.883 | 0.778 | 29.821 | 27.19 | 31.317 | 0.819 | 30.232 | 27.601 | 31.746 | 0.834 |
| Monsoon | 28.46 | 25.819 | 29.965 | 0.568 | 29.425 | 26.8 | 30.944 | 0.558 | 30.019 | 27.396 | 31.536 | 0.544 |
| Post-Monsoon | 22.726 | 19.647 | 25.786 | 1.345 | 23.671 | 20.563 | 26.843 | 1.39 | 23.986 | 20.874 | 27.176 | 1.402 |
| Winter | 19.64 | 16.814 | 22.146 | 1.136 | 20.84 | 17.966 | 23.498 | 1.206 | 21.159 | 18.27 | 23.884 | 1.233 |

| Months | Ssp370 (2015-2100) | | | | Ssp585 (2015-2100) (2015-2100) | | | |
|---|---|---|---|---|---|---|---|---|
| | Mean Temperature (° C) | | | | | | | |
| | Mean | Min | Max | StdDev | Mean | Min | Max | StdDev |
| Summer | 30.53 | 27.899 | 32.032 | 0.829 | 31.13 | 28.515 | 32.596 | 0.803 |
| Monsoon | 30.378 | 27.771 | 31.915 | 0.53 | 30.378 | 27.771 | 31.915 | 0.53 |
| Post-Monsoon | 24.36 | 21.254 | 27.536 | 1.391 | 24.914 | 21.812 | 28.079 | 1.397 |
| Winter | 21.479 | 18.576 | 24.247 | 1.252 | 22.084 | 19.204 | 24.825 | 1.245 |

The seasonal mean temperature analysis reveals a consistent warming trend across all four seasons under future climate scenarios, with the intensity of warming correlating with the severity of greenhouse gas emissions. In the Summer season, the mean temperature during the historical period is 28.45°C. This increases to 29.82°C under SSP126, 30.23°C under SSP245, and reaches up to 31.13°C in SSP585. The total rise from the historical baseline to SSP585 is approximately 2.7°C, which is substantial. Such elevated summer temperatures may lead to increased heat stress, higher evapotranspiration, increased irrigation demands, and greater electricity consumption for cooling in urban areas. Crops and livestock may also face heightened vulnerability, especially in regions already prone to heatwaves. During the Monsoon season (June–September), the historical average of 28.46°C gradually rises across all scenarios, peaking at 30.38°C under SSP370 and SSP585. Though the rise is relatively smaller (~1.9°C), its combination with higher humidity during the monsoon may lead to extremely high discomfort indices (heat index) and could reduce labor productivity, especially for outdoor workers. Elevated temperatures may also intensify the monsoon rainfall-runoff relationship, impacting flood patterns and increasing the risk of soil erosion. The post-monsoon season (October–November) shows a warming trend from 22.73°C historically to 24.91°C under SSP585, marking an increase of over 2.1°C. This warming during the crop transition season may disrupt traditional sowing cycles, affect crop germination, and reduce the available recovery time between monsoon harvesting and Rabi sowing. Warmer conditions may also lead to increased weed growth and pest survival, requiring greater agricultural input adjustments.

In Winter, mean temperatures rise from 19.64°C in the historical period to 22.08°C in SSP585, a difference of ~2.4°C. This warming trend could significantly affect chilling requirements for certain crops (like apples, wheat, mustard), shorten the duration of cold spells, and increase the survival rate of winter pests and diseases. It also has implications for ecosystems and public health, particularly for elderly populations who rely on colder winter conditions for comfort. Despite these shifts in average temperatures, the standard deviation values remain relatively stable across seasons and scenarios, indicating that interannual variability does not change significantly even as mean temperatures rise. However, the absolute increase in temperatures alone is enough to push several climatic thresholds, especially in temperature-sensitive sectors such as agriculture, water resources, and public health infrastructure.

Table 12: Tabulation of statistics of seasonal Minimum temperature under the Historical scenarios, Ssp126, Ssp245, Ssp370 and Ssp585

| Months | Historical (1980-2014) | | | | Ssp126 (2015-2100) | | | | Ssp245 (2015-2100) (2015-2100) | | | |
|---|---|---|---|---|---|---|---|---|---|---|---|---|
| | Minimum Temperature (° C) | | | | | | | | | | | |
| | Mean | Min | Max | StdDev | Mean | Min | Max | StdDev | Mean | Min | Max | StdDev |
| Summer | 20.348 | 17.717 | 21.971 | 0.805 | 21.837 | 19.165 | 23.587 | 0.859 | 22.265 | 19.576 | 24.069 | 0.885 |
| Monsoon | 23.751 | 21.174 | 25.229 | 0.61 | 25.293 | 22.713 | 26.743 | 0.603 | 25.293 | 22.713 | 26.743 | 0.603 |
| Post-Monsoon | 15.559 | 12.564 | 18.674 | 1.302 | 16.911 | 13.886 | 20.128 | 1.329 | 17.385 | 14.351 | 20.625 | 1.344 |
| Winter | 11.354 | 8.645 | 13.948 | 1.137 | 12.841 | 10.075 | 15.608 | 1.206 | 13.31 | 10.52 | 16.145 | 1.237 |

| Months | Ssp370 (2015-2100) | | | | Ssp585 (2015-2100) (2015-2100) | | | |
|---|---|---|---|---|---|---|---|---|
| | Minimum Temperature (° C) | | | | | | | |
| | Mean | Min | Max | StdDev | Mean | Min | Max | StdDev |
| Summer | 22.646 | 19.967 | 24.43 | 0.875 | 23.265 | 20.601 | 25.011 | 0.861 |
| Monsoon | 25.616 | 23.022 | 27.048 | 0.601 | 25.965 | 23.385 | 27.409 | 0.584 |
| Post-Monsoon | 17.938 | 14.895 | 21.168 | 1.338 | 18.583 | 15.543 | 21.809 | 1.341 |
| Winter | 13.824 | 11.027 | 16.67 | 1.241 | 14.535 | 11.761 | 17.358 | 1.235 |

The seasonal analysis of minimum temperatures shows a strong and consistent warming trend across all scenarios, with the magnitude of increase becoming more pronounced under higher-emission pathways. Minimum temperatures are particularly crucial for understanding nighttime heat stress, crop germination, and cold season chilling requirements, making this parameter significant for climate impact assessments. During the Summer season, the historical minimum temperature averages 20.35°C, which increases to 21.84°C (SSP126), 22.27°C (SSP245), 22.65°C (SSP370), and peaks at 23.27°C in SSP585. The total rise of nearly 3°C under the highest-emission scenario indicates a significant warming of nights during the hottest part of the year. This can lead to reduced nighttime cooling, which exacerbates heatwave impacts, causes thermal discomfort in urban areas, and increases energy demands for cooling. It can also impair flowering and pollination in heat-sensitive crops, reducing agricultural productivity. For the Monsoon season, the increase in minimum temperatures is steady across scenarios. From 23.75°C historically, it rises to 25.29°C under SSP126 and SSP245, and further to 25.97°C under SSP585. Warmer nights during the monsoon can elevate soil and atmospheric humidity, increasing the risk of fungal diseases and pests in crops. Additionally, it may hinder rest and recovery during nighttime, particularly for laborers working in humid and heat-prone environments. In the post-monsoon season, a substantial increase is observed. The historical average of 15.56°C increases to 16.91°C (SSP126), 17.39°C (SSP245), 17.94°C (SSP370), and 18.58°C (SSP585). This seasonal warming may disrupt traditional sowing windows for Rabi crops, which often rely on a drop in temperatures to signal the start of the growing season. Additionally, warmer nights during this transitional season may lead to increased evapotranspiration and reduce soil moisture retention, affecting early crop establishment. The most pronounced changes are evident in the Winter season), where the historical minimum temperature of 11.35°C increases significantly to 12.84°C (SSP126), 13.31°C (SSP245), 13.82°C (SSP370), and up to 14.54°C under SSP585. This marks a warming of over 3°C in the coldest months. Such warming may drastically affect winter crop yields, especially those requiring a minimum number of chilling hours, such as wheat, mustard, and certain fruits (e.g., apples in colder regions). Additionally, pest populations that usually decline during cold spells may survive and reproduce earlier, increasing crop management burdens. From a health perspective, milder winters could impact respiratory disease patterns, alter seasonal energy consumption, and

affect human thermal comfort, particularly in vulnerable populations. Despite this warming trend, the standard deviation across all seasons remains similar to historical values, implying that while mean minimum temperatures rise, the variability does not increase significantly. However, this persistent upward shift in nighttime temperatures represents a significant climate signal with important ecological, agricultural, and socio-economic consequences.

Table 13: Tabulation of statistics of seasonal Precipitation under the Historical scenarios, Ssp126, Ssp245, Ssp370 and Ssp585

| Months | Historical (1980-2014) | | | | Ssp126 (2015-2100) | | | | Ssp245 (2015-2100) (2015-2100) | | | |
|---|---|---|---|---|---|---|---|---|---|---|---|---|
| | Precipitation (mm) | | | | | | | | | | | |
| | Mean | Min | Max | StdDev | Mean | Min | Max | StdDev | Mean | Min | Max | StdDev |
| Summer | 34.151 | 15.427 | 57.983 | 13.532 | 43.799 | 21.682 | 67.157 | 14.415 | 42.628 | 19.925 | 67.938 | 15.255 |
| Monsoon | 897.67 | 647.967 | 1283.022 | 138.206 | 1120.202 | 840.72 | 1569.12 | 145.398 | 1146.849 | 880.584 | 1602.082 | 137.461 |
| Post-Monsoon | 134.884 | 107.86 | 186.208 | 14.074 | 173.59 | 148.284 | 234.012 | 15.302 | 169.919 | 144.334 | 230.241 | 15.759 |
| Winter | 49.07 | 20.888 | 76.313 | 18.561 | 54.327 | 25.67 | 85.704 | 17.664 | 54.365 | 27.239 | 84.468 | 16.372 |

| Months | Ssp370 (2015-2100) | | | | Ssp585 (2015-2100) (2015-2100) | | | |
|---|---|---|---|---|---|---|---|---|
| | Precipitation (mm) | | | | | | | |
| | Mean | Min | Max | StdDev | Mean | Min | Max | StdDev |

| | | | | | | | | |
|---|---|---|---|---|---|---|---|---|
| **Summer** | 46.213 | 23.261 | 71.654 | 15.687 | 44.475 | 22.584 | 68.769 | 14.805 |
| **Monsoon** | 1167.144 | 918.701 | 1599.513 | 125.53 | 1243.498 | 995.297 | 1690.926 | 126.84 |
| **Post-Monsoon** | 189.019 | 162.943 | 252.62 | 16.524 | 216.328 | 182.277 | 285.97 | 19.714 |
| **Winter** | 60.944 | 30.063 | 95.354 | 18.854 | 60.099 | 32.445 | 92.802 | 17.242 |

The seasonal analysis of precipitation reveals a significant increase in rainfall across all seasons under future scenarios, with the most notable changes occurring during the monsoon and post-monsoon periods. The scale and distribution of precipitation changes have important implications for flood risk, water availability, agriculture, and infrastructure resilience. In the Summer season which traditionally receives limited rainfall, the historical average precipitation is 34.15 mm. Under future scenarios, this increases to 43.80 mm (SSP126), 42.63 mm (SSP245), 46.21 mm (SSP370), and 44.48 mm (SSP585). The increase of over 30% in high-emission scenarios suggests a potential shift in rainfall seasonality, with more frequent pre-monsoon showers or localized convective events. While this could benefit early soil moisture for sowing, it may also disrupt harvesting and increase the risk of flash floods, especially in urban areas or sloped terrain. The Monsoon season (June–September) experiences the most pronounced increases. Historically, the region receives ~898 mm, which increases to 1120.2 mm in SSP126, 1146.85 mm in SSP245, 1167.14 mm in SSP370, and up to 1243.50 mm in SSP585. The total rise of up to ~345 mm (~38%) under SSP585 indicates heavier and more intense rainfall events during the core monsoon season. This could overwhelm existing drainage infrastructure, increase soil erosion, and contribute to urban and riverine flooding. For agriculture, while enhanced rainfall may support rainfed farming and improve groundwater recharge, extreme downpours and variability may increase the risk of crop damage, delayed sowing, or harvest losses. In the post-monsoon season rainfall rises from 134.88 mm (historical) to 173.59 mm (SSP126), 169.92 mm (SSP245), 189.02 mm (SSP370), and reaches 216.33 mm under SSP585. The sharp increase of over 80 mm under high-emission scenarios suggests a delay in monsoon withdrawal and a potential extension of the rainy

season. This may interfere with Rabi crop sowing, increase pest infestations, and exacerbate waterlogging in low-lying fields. Additionally, wetter post-monsoon months could strain transportation and storage systems, especially for harvested monsoon crops.

The Winter season, which typically receives the least rainfall, shows a modest but consistent increase across scenarios—from 49.07 mm historically to 60.10 mm under SSP585. This ~23% rise may be attributed to more frequent or intense Western Disturbances. Increased winter precipitation could benefit Rabi crops, especially in water-scarce regions, but also heighten the risk of cold-season flooding, hailstorms, or unseasonal moisture stress in certain crops. Despite these changes in mean values, standard deviation values remain comparable to historical levels, indicating that year-to-year variability remains consistent, although the baseline level of rainfall has shifted upwards. This suggests that while the frequency of rainfall extremes may not drastically change, the intensity of regular events is likely to increase, necessitating a re-evaluation of hydrological modeling, flood control strategies, and cropping calendars.

Following the seasonal data extraction, the datasets were further aggregated to compute annual values for each climatic variable, including precipitation, maximum temperature, minimum temperature, and mean temperature. Subsequently, spatial plots of annual distributions were generated to visualize long-term trends across the study region under different climate scenarios. Additionally, annual statistical summaries—such as mean, minimum, maximum, and standard deviation were extracted to quantify interannual variability and long-term changes.

Figure 79: Spatial distribution of Annual values of Maximum temperature for the Historical, SSP126, SSP245, SSP370, and SSP585 scenarios

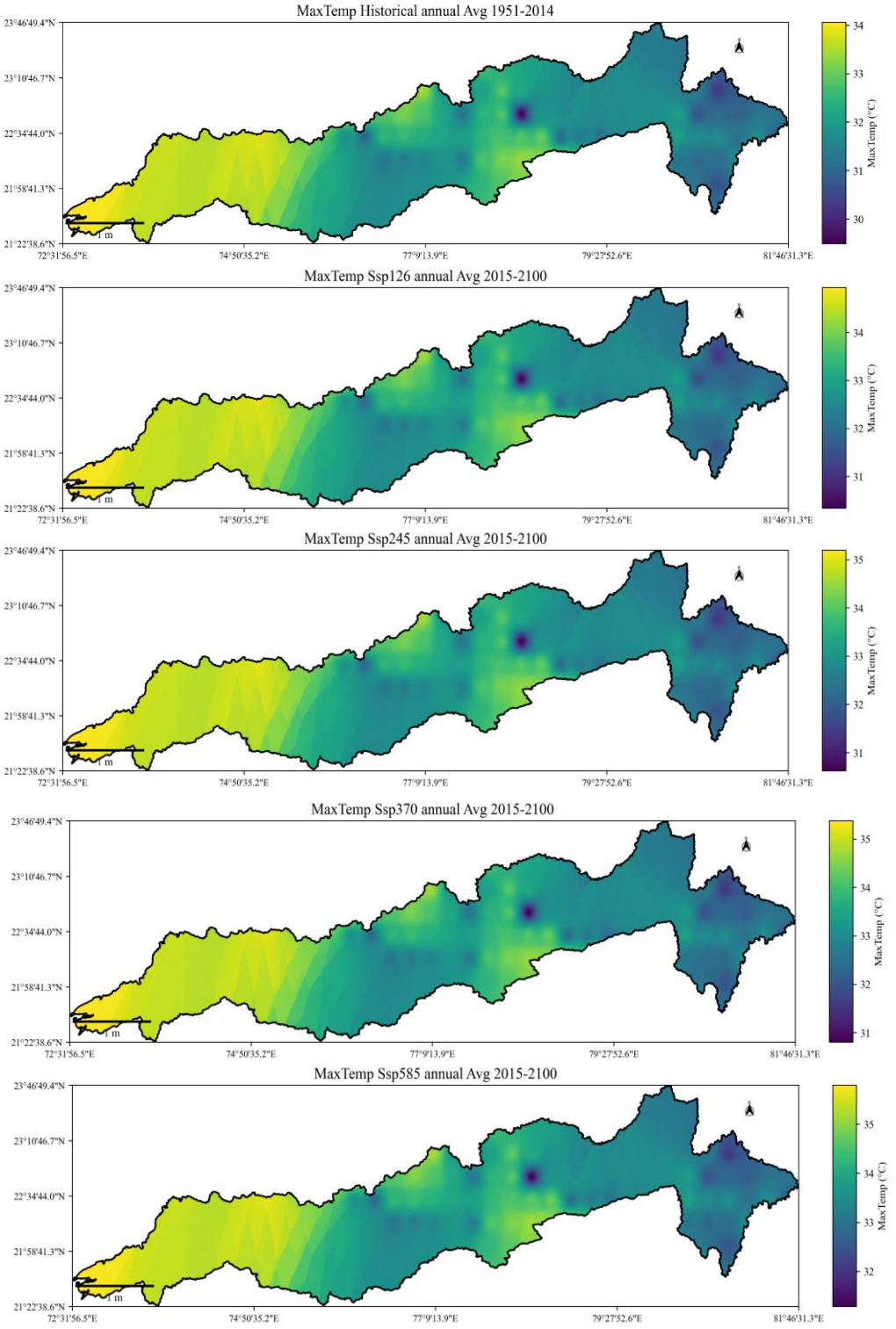

Figure 80: Spatial distribution of Annual values of Mean temperature for the Historical, SSP126, SSP245, SSP370, and SSP585 scenarios

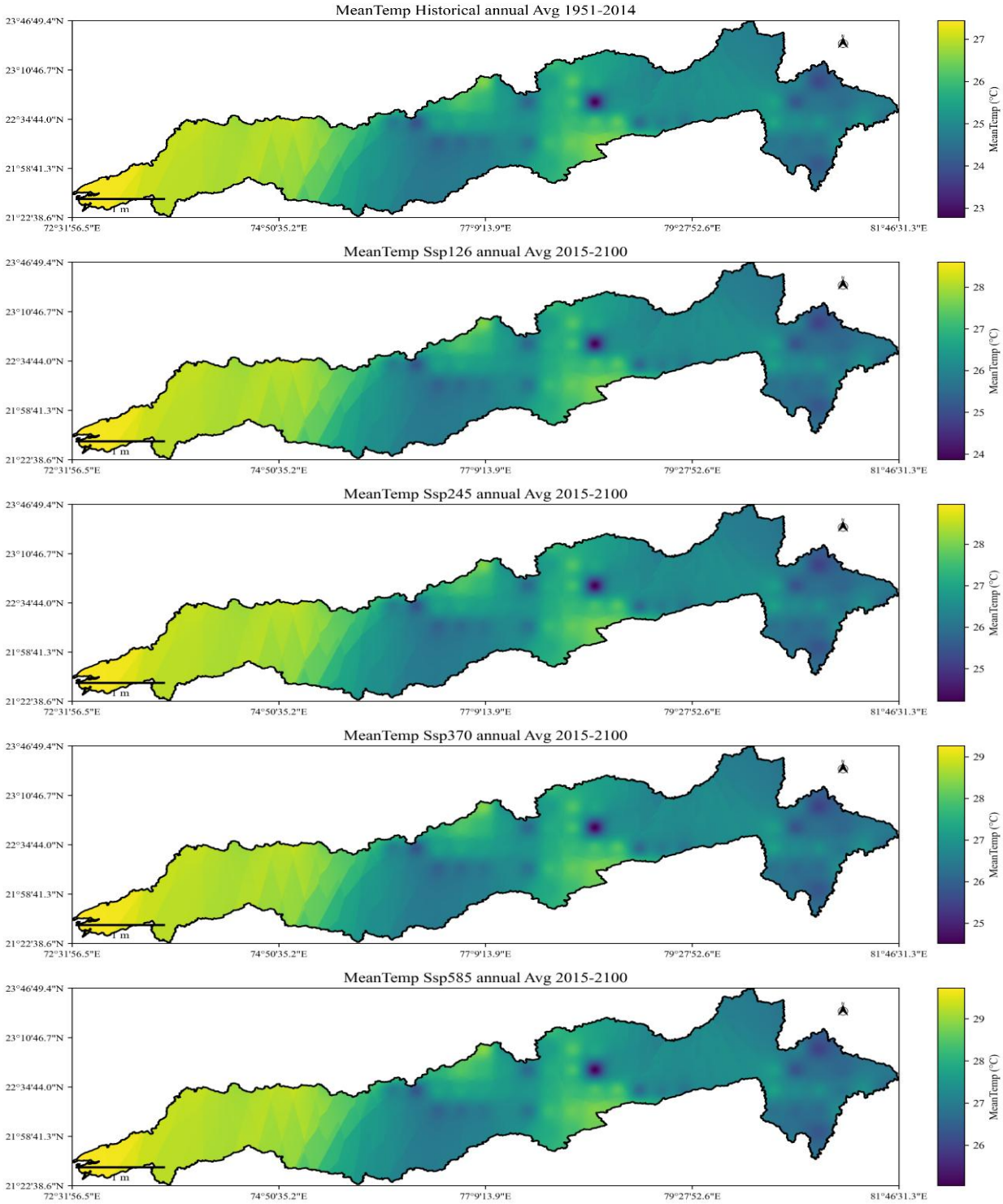

Figure 81: Spatial distribution of Annual values of Minimum temperature for the Historical, SSP126, SSP245, SSP370, and SSP585 scenarios

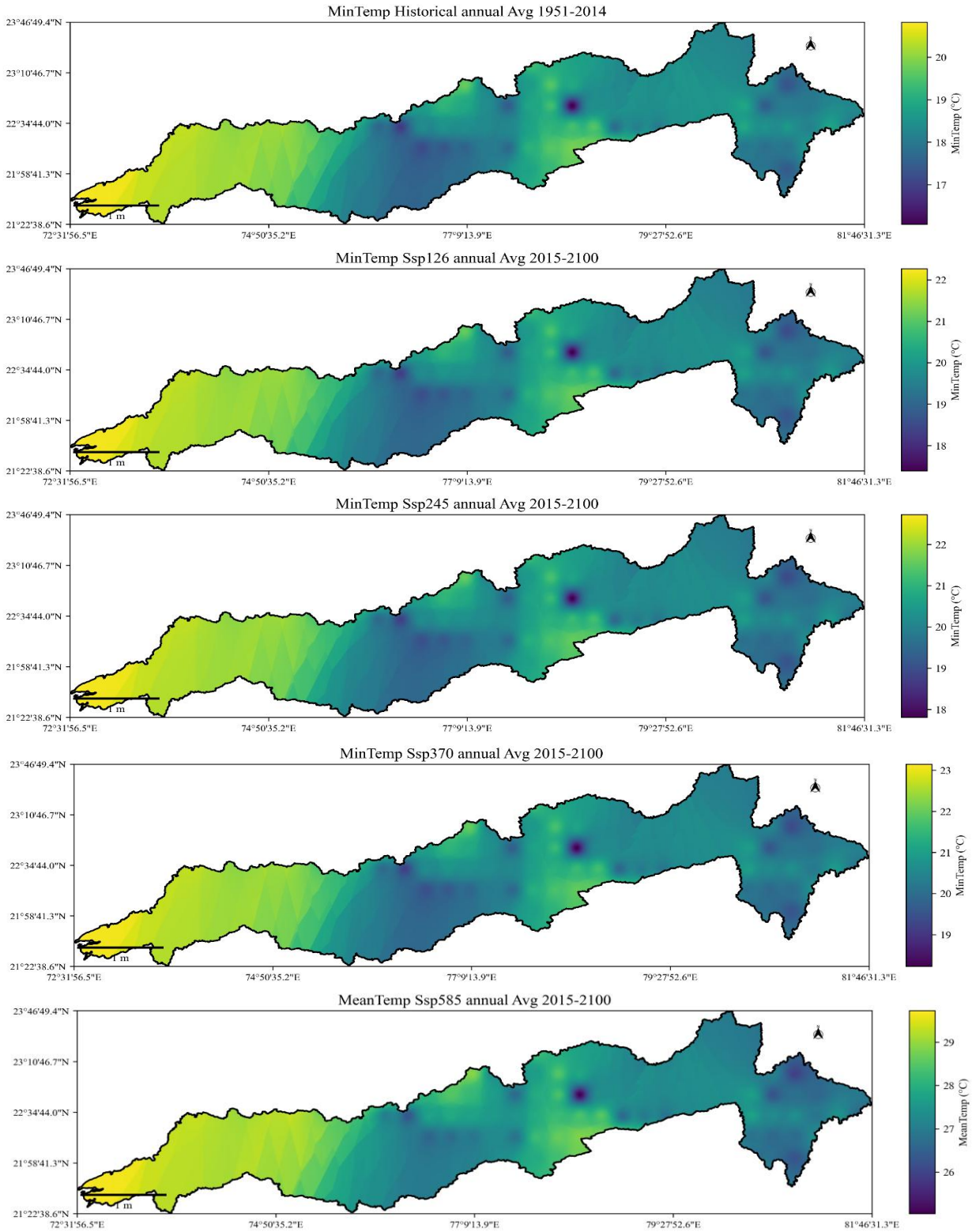

Figure 82: Spatial distribution of Annual values of Precipitation for the Historical, SSP126, SSP245, SSP370, and SSP585 scenarios

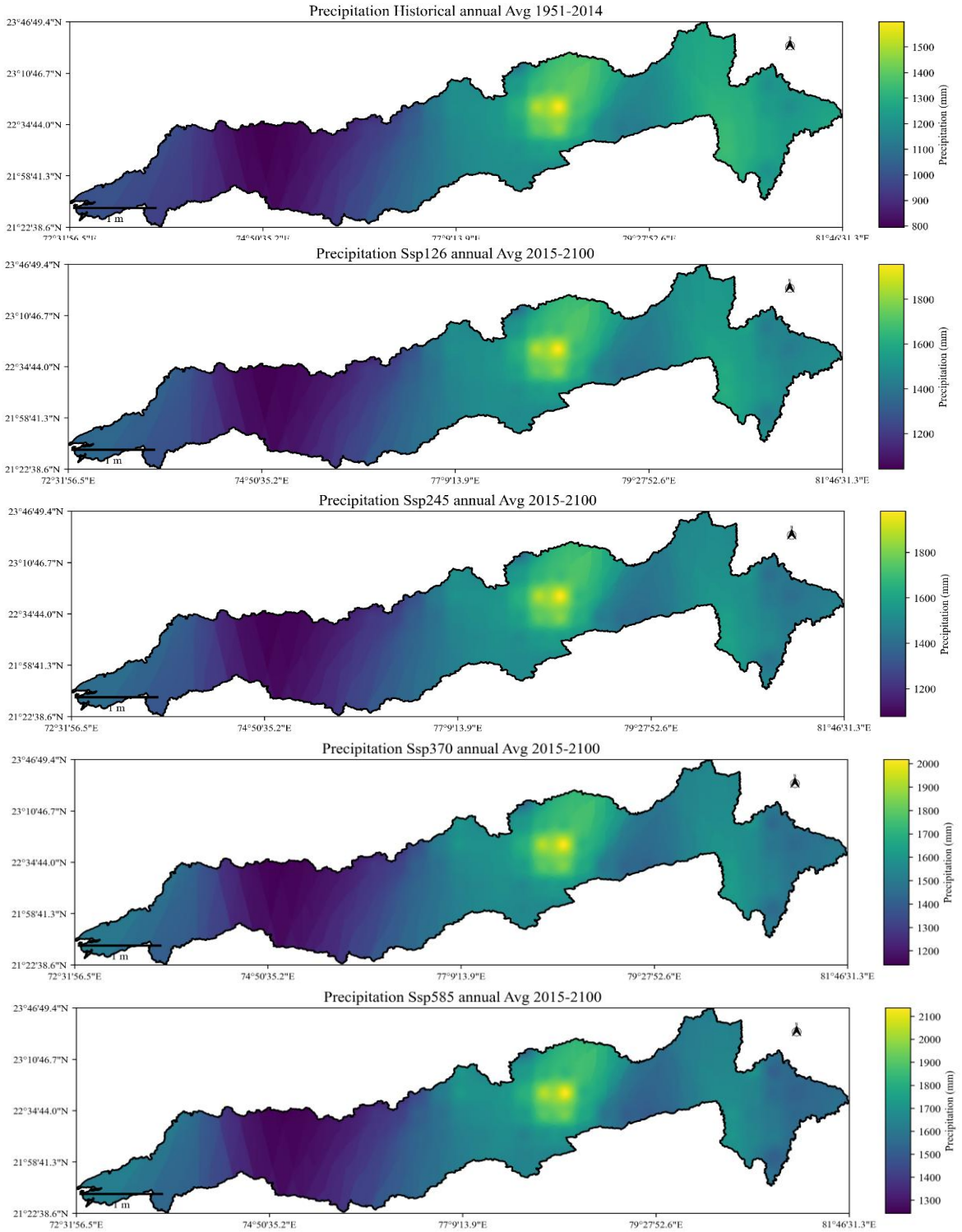

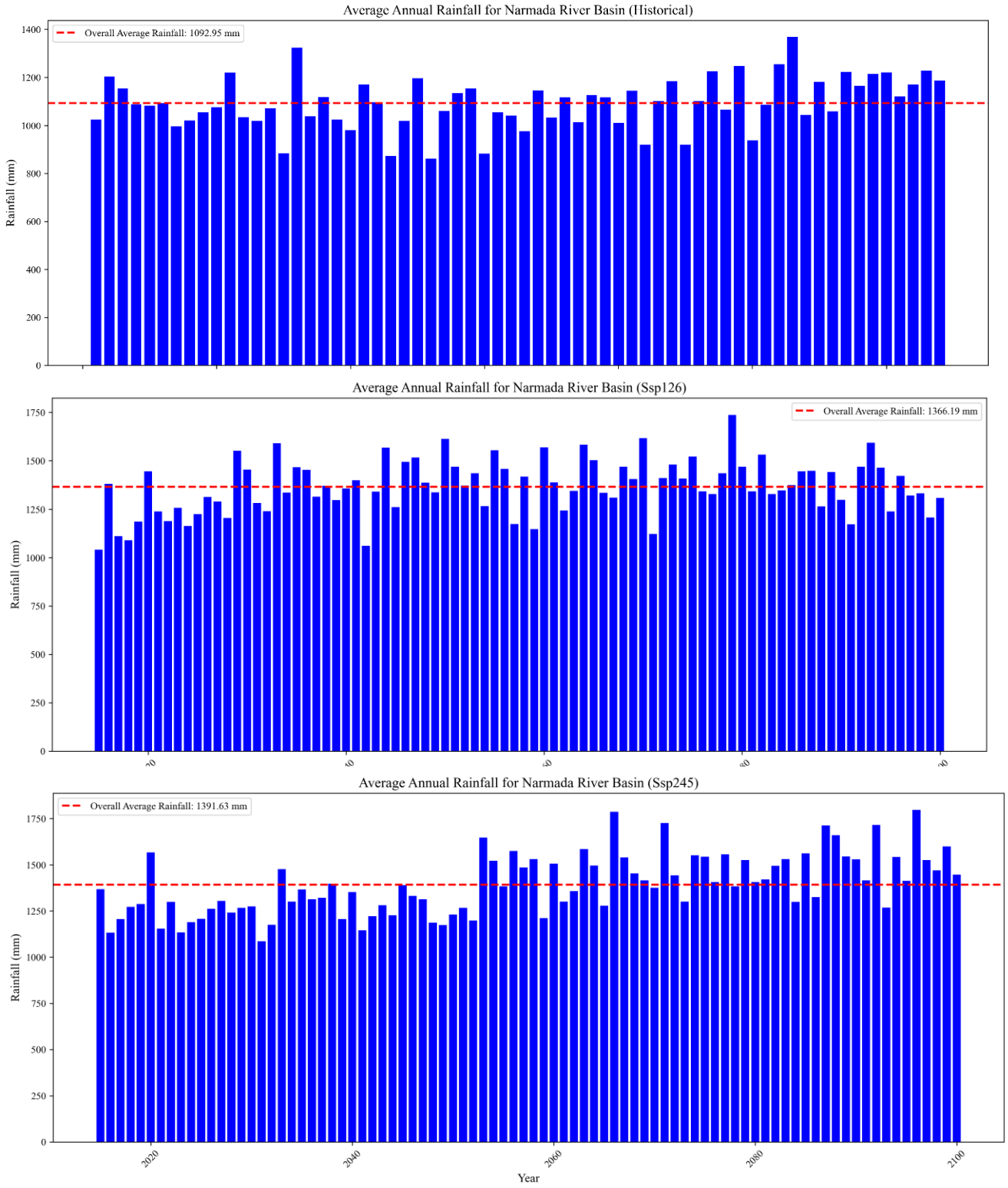


Figure 83: Temporal distribution of Annual values of Precipitation for the Historical, SSP126, and SSP245 scenario

The bar plots illustrate the interannual variability and average annual rainfall over the Narmada River Basin under three climate scenarios: Historical (1980–2014), SSP126, and SSP245. In the historical period, the average annual rainfall is approximately 1092.95 mm, with noticeable year-to-year fluctuations. Some years fall significantly below or rise above the mean, indicating moderate variability, but the majority of years remain within a relatively narrow band, suggesting a stable monsoon regime during the baseline period. Under the SSP126 scenario, which represents a low-emission, sustainability-focused pathway, the average annual rainfall increases to 1366.19 mm. The bars display greater spread and higher peak values compared to the historical period, reflecting both an increase in the mean precipitation and interannual variability. This suggests that even in a controlled-emission future, the basin is likely to receive higher rainfall, which could enhance groundwater recharge and water availability, but also raise concerns about increased risk of flash floods and soil erosion in some years. In the SSP245 scenario, a medium-emission pathway, the average annual rainfall rises further to 1391.63 mm. The graph indicates frequent high rainfall years, with several bars exceeding 1500 mm, pointing toward more intense wet years and greater interannual variability than the previous two scenarios. This trend implies that climate-driven intensification of monsoonal rainfall is likely under moderate emissions, necessitating robust water resource management, including reservoir operation adjustments, urban drainage upgrades, and agricultural planning to cope with both excess and deficit conditions. The bar plots for SSP370 and SSP585 reveal a continued and substantial increase in annual rainfall over the Narmada River Basin, indicating the potential impact of high-emission futures on the region’s hydrological regime.

Under the SSP370 scenario, the average annual rainfall rises to 1440.94 mm, compared to 1092.95 mm in the historical period. The bars in the plot show frequent occurrences of years exceeding 1500 mm, along with a visibly increasing trend toward the latter part of the century. Notably, rainfall variability also seems to increase, with both dry years (below 1000 mm) and very wet years (approaching or exceeding 1800 mm) appearing more frequently. This combination of rising average and greater extremes implies a more erratic and intense monsoon system, which may challenge current water management systems, exacerbate flash flood risks, and require adjustments in reservoir operation, agricultural scheduling, and disaster preparedness.

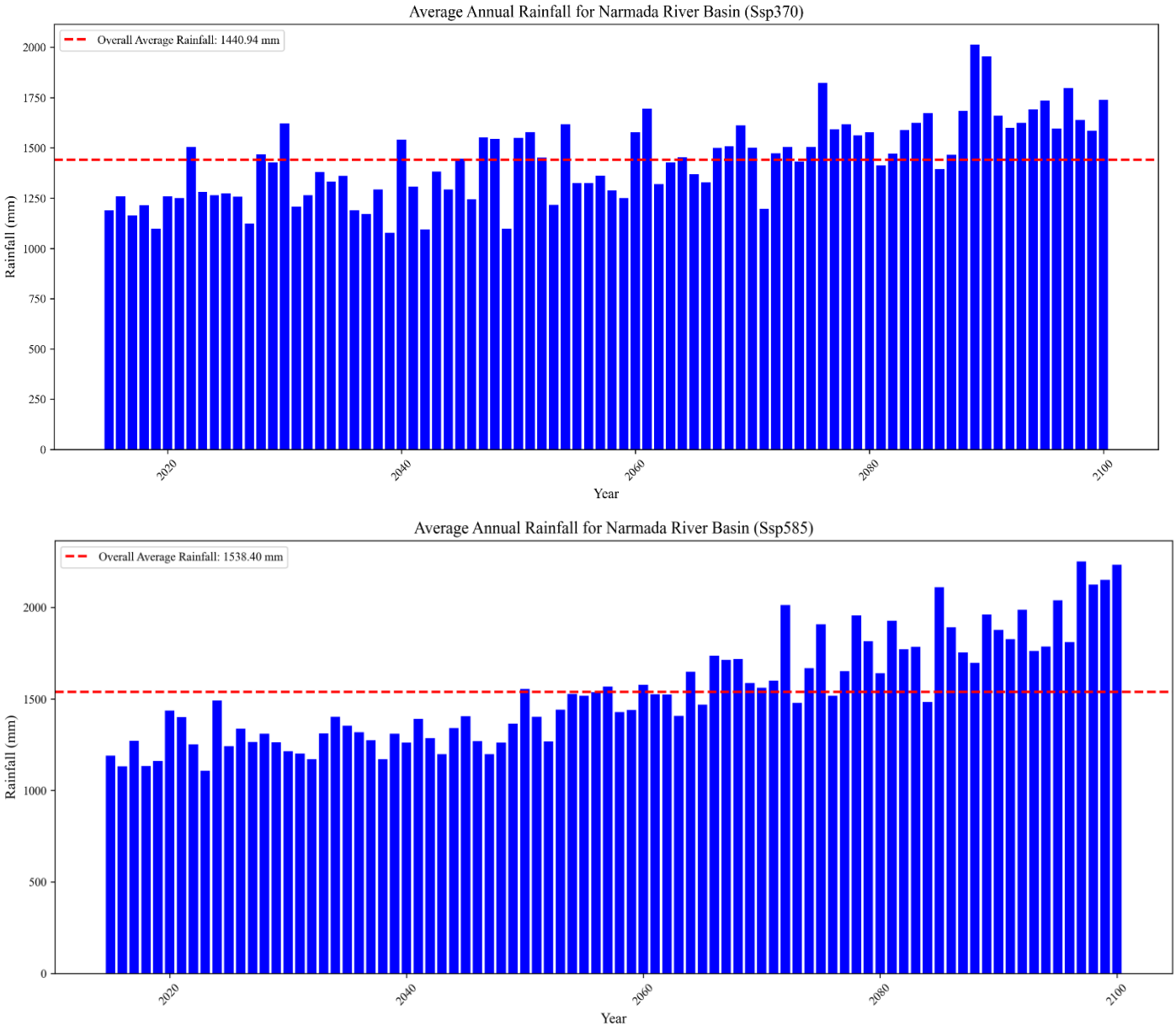


Figure 84: Temporal distribution of Annual values of Precipitation for the scenarios of Ssp370 and Ssp585

In the SSP585 scenario, which represents the highest-emission, fossil fuel-intensive pathway, the average annual rainfall reaches 1538.40 mm, the highest among all scenarios. The trend line suggests a clear upward trajectory, especially in the second half of the century, where several years exceed 1800–2000 mm. This dramatic rise in rainfall intensity and frequency of extreme events raises serious concerns for infrastructure resilience, sediment transport, landslide risk in upland areas, and urban flooding. The rising curve also points to a shift in baseline hydrological behaviour, necessitating major adaptations in irrigation planning, dam safety protocols, and basin-scale flood modelling. Overall, these high-emission scenarios not only mean increased rainfall, but also suggest a higher probability of extreme events and interannual variability, stressing the urgent need for climate-resilient planning frameworks, early warning systems, and region-specific adaptation strategies in the Narmada River Basin.

Figure 85: Monthly Average Temperature Distribution for the Narmada River Basin under Historical and Future Scenarios (SSP126 and SSP245).

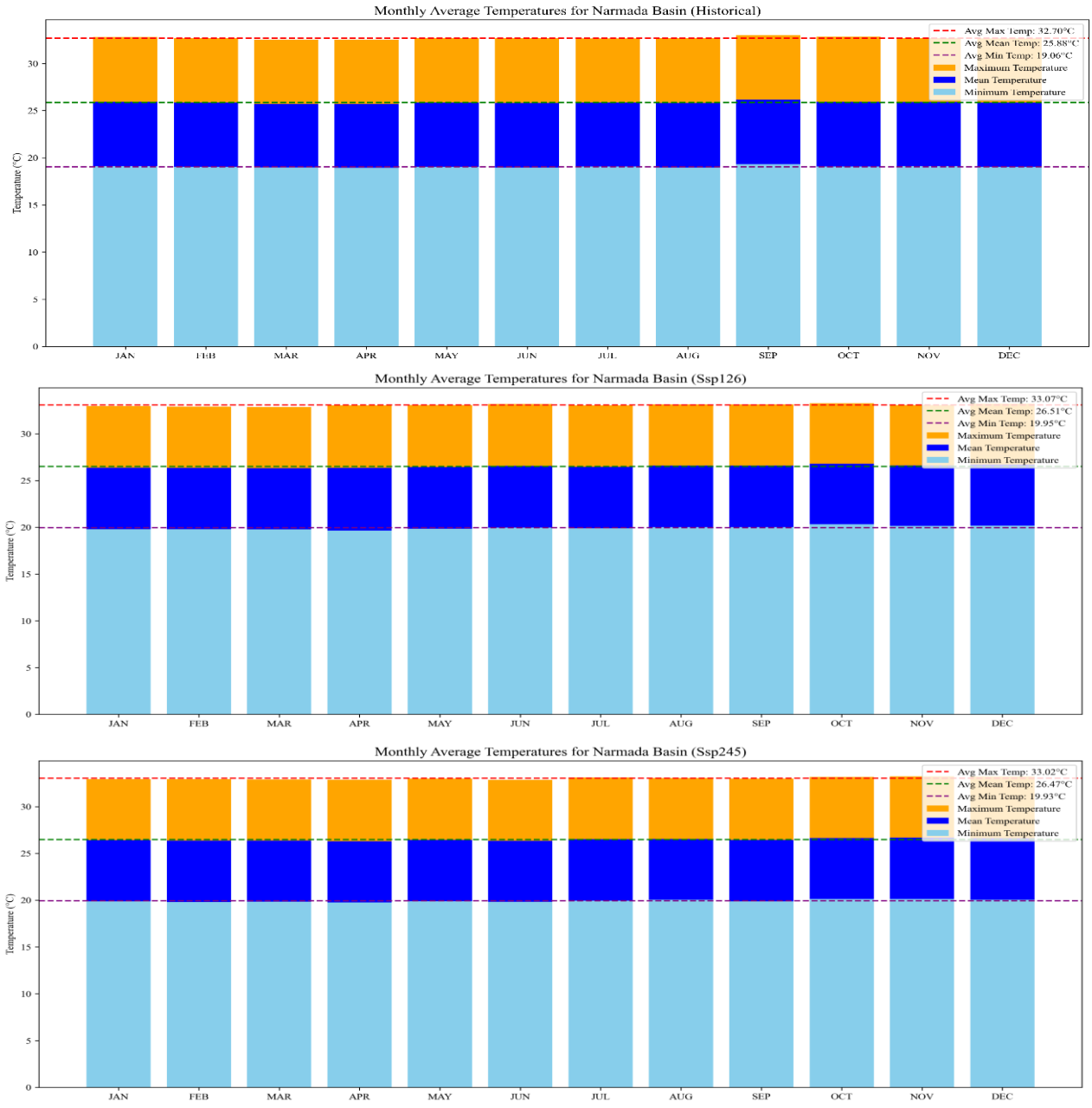

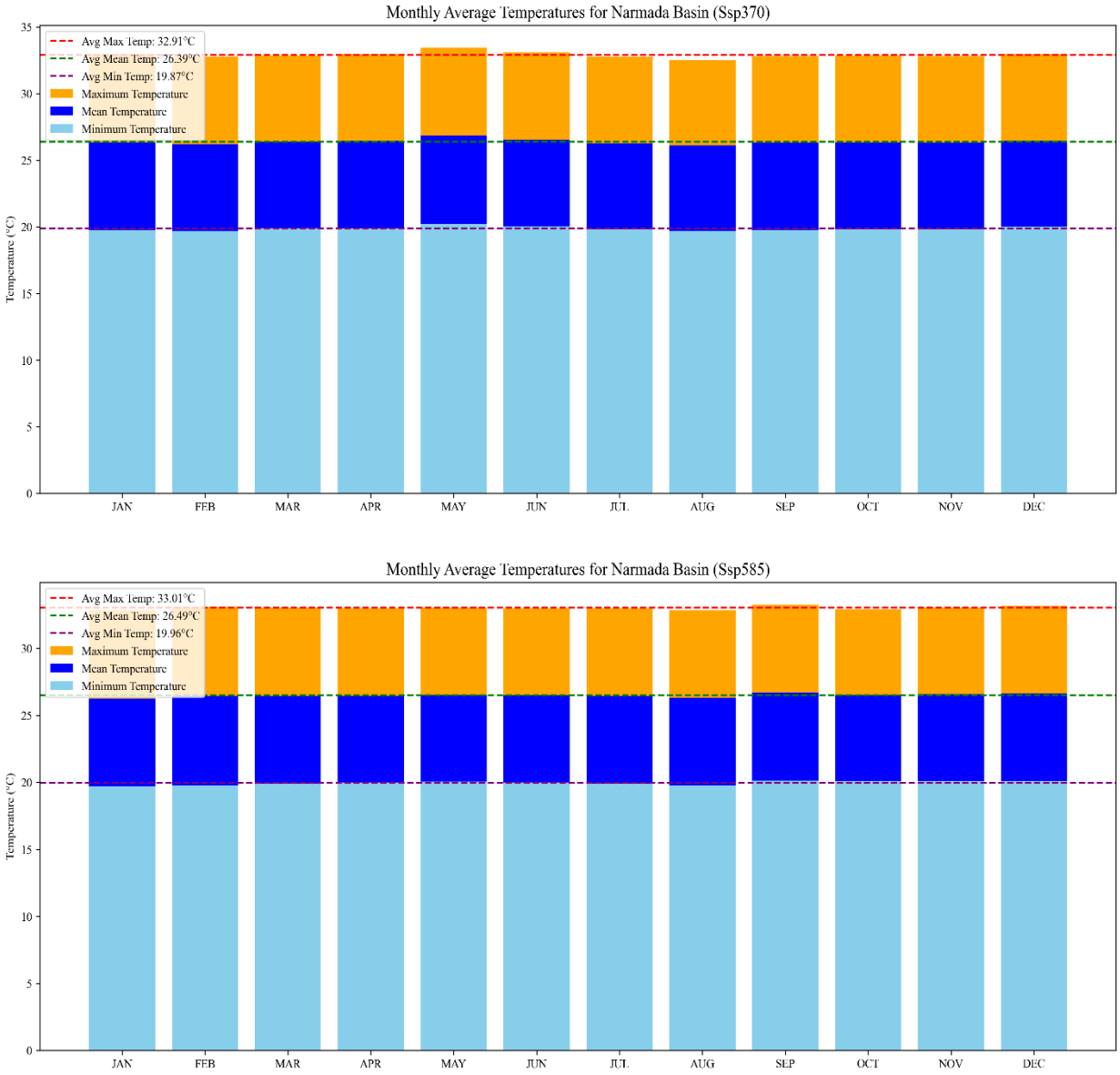


Figure 86: Monthly Average Temperature Distribution for the Narmada River Basin under Historical and Future Scenarios (SSP370 and SSP585)

The climate projections for the Narmada River Basin, derived from CMIP6 GCM ensembles, exhibit a consistent warming trend and increasing precipitation across all Shared Socioeconomic Pathways (SSPs). Both the statistical summaries and visual bar plots reinforce the shift in climate characteristics from the historical baseline (1980–2014) toward progressively warmer and wetter conditions under future scenarios, particularly under higher emission pathways.

Temperature Trends:

- The historical average maximum temperature is 32.32°C, which increases across all scenarios:
  - 33.18°C in SSP126,
  - 33.45°C in SSP245,
  - 33.63°C in SSP370,
  - and peaks at 34.10°C under SSP585.
- The mean temperature follows a similar rising pattern:
  - From 25.56°C historically to 26.66°C (SSP126), 27.01°C (SSP245), 27.31°C (SSP370), and 27.82°C (SSP585).
- The minimum temperature, indicative of nighttime warming, shows an even more dramatic increase—from 18.79°C to 21.54°C under SSP585. This consistent rise in nighttime temperatures suggests reduced diurnal temperature range, increased humidity retention, and greater heat stress during nights—a trend often linked to greenhouse gas-driven atmospheric warming.

The monthly average temperature plots reinforce these findings visually. They show uniformly elevated bars across all months in future scenarios, indicating that warming is year-round rather than seasonally constrained. Moreover, the plots demonstrate a flattening of seasonal thermal variation, with winter months warming significantly, which could disrupt agricultural cycles, chilling requirements, and ecosystem processes. Additionally, as emissions intensify from SSP126 to SSP585, the difference between maximum and minimum temperatures narrows, suggesting a more homogenized thermal profile. This may reduce recovery time during nights, worsen heat stress, and affect urban cooling cycles, especially in densely populated areas.

Precipitation Trends: The annual average precipitation also increases consistently across future scenarios:

- From 1115.78 mm in the historical period,
- to 1391.92 mm (SSP126),

- 1413.76 mm (SSP245),
- 1463.32 mm (SSP370),
- and up to 1564.40 mm (SSP585).

These increases represent a substantial ~40% rise in annual rainfall under the highest emission scenario compared to the historical average. The visual annual rainfall plots show not only a rising average but also a greater frequency of extreme wet years (with some exceeding 2000 mm under SSP585), pointing toward heightened flood risk, soil erosion, and the need for updated flood control infrastructure. While standard deviation values for precipitation remain relatively stable (ranging between ~163–184 mm), the shift in the mean itself indicates a baseline change in the region's hydrology. This can have cascading effects on reservoir operations, cropping patterns, sediment transport, and groundwater recharge.

| Months | Historical (1980-2014) | | | | Ssp126 (2015-2100) | | | | Ssp245 (2015-2100) (2015-2100) | | | |
|---|---|---|---|---|---|---|---|---|---|---|---|---|
| | Mean | Min | Max | StdDev | Mean | Min | Max | StdDev | Mean | Min | Max | StdDev |
| **Maximum Temperature (° C)** | 32.323 | 29.494 | 34.057 | 0.897 | 33.176 | 30.343 | 34.93 | 0.915 | 33.45 | 30.626 | 35.197 | 0.91 |
| **Mean Temperature (° C)** | 25.555 | 22.781 | 27.441 | 0.879 | 26.655 | 23.866 | 28.599 | 0.907 | 27.006 | 24.216 | 28.962 | 0.912 |
| **Minimum Temperature (° C)** | 18.786 | 16.069 | 20.825 | 0.896 | 20.133 | 17.389 | 22.269 | 0.927 | 20.562 | 17.806 | 22.726 | 0.94 |
| **Precipitation (mm)** | 1115.775 | 795.663 | 1597.666 | 179.763 | 1391.919 | 1041.737 | 1954.96 | 183.893 | 1413.762 | 1077.573 | 1980.93 | 174.751 |

Table 14: Tabulation of statistics of annual maximum, minimum and mean temperature and precipitation under the scenarios of Historical, Ssp126 and Ssp245

Table 15: Tabulation of statistics of annual maximum, minimum and mean temperature and precipitation under the scenarios of Ssp370 and Ssp585

| **Months** | **Ssp370 (2015-2100)** | | | | **Ssp585 (2015-2100) (2015-2100)** | | | |
|---|---|---|---|---|---|---|---|---|
| | | | | | | | | |
| | **Mean** | **Min** | **Max** | **StdDev** | **Mean** | **Min** | **Max** | **StdDev** |
| **Maximum Temperature (° C)** | 33.628 | 30.805 | 35.377 | 0.905 | 34.096 | 31.288 | 35.792 | 0.89 |
| **Mean Temperature (° C)** | 27.308 | 24.516 | 29.263 | 0.909 | 27.818 | 25.039 | 29.729 | 0.896 |
| **Minimum Temperature (° C)** | 20.989 | 18.227 | 23.149 | 0.936 | 21.54 | 18.791 | 23.666 | 0.924 |
| **Precipitation (mm)** | 1463.32 | 1139.695 | 2017.528 | 164.209 | 1564.401 | 1242.787 | 2136.639 | 163.017 |

# Chapter 5: Drought Characteristics

## 5.1 GENERAL

Droughts are among the most severe hydroclimatic extreme events, characterized by prolonged periods of water scarcity that significantly impact agriculture, water resources, and food security worldwide. In regions heavily reliant on monsoonal rainfall, such as India, droughts have historically led to devastating consequences, including major famines in the 19th and 20th centuries.

India's agricultural sector is predominantly rain-fed, making it highly dependent on the southwest monsoon, which occurs between June and September. This monsoon accounts for approximately 80% of the country’s total annual rainfall and plays a crucial role in replenishing surface water bodies, recharging groundwater, and sustaining crop production. However, any weakening or delay in monsoon activity can lead to severe drought conditions, causing water shortages, reduced agricultural yields, and economic distress, particularly for smallholder farmers.

Droughts in the Narmada Basin are primarily driven by variability in monsoon rainfall, which accounts for a significant portion of the annual precipitation. The basin experiences pronounced interannual and seasonal fluctuations in rainfall due to the influence of large-scale climate phenomena such as the El Niño-Southern Oscillation (ENSO), Indian Ocean Dipole (IOD), and changes in regional atmospheric circulation patterns. Studies have shown that the frequency and intensity of drought events in the Narmada Basin have increased in recent decades. The depletion of groundwater resources, land-use changes, and anthropogenic pressures have further exacerbated the region's susceptibility to drought. Additionally, the spatial heterogeneity of rainfall across the basin results in localized drought impacts, with certain sub-basins experiencing more severe water deficits than others.

## 5.2 DROUGHT ATLAS OF INDIA

Chuphal et al. (2024) developed a drought atlas of India using high-resolution (0.05°) precipitation and maximum and minimum temperature datasets. Existing observed precipitation and temperature datasets for India are available at a coarser spatial resolution

of 0.25° for the period 1901–2021. To enhance spatial resolution, high-resolution gridded precipitation and temperature data were generated by integrating shorter-period high-resolution products and applying Quantile-Quantile (QQ) mapping for bias correction. Bias-corrected precipitation from CHIRPS at 0.05° resolution was used as the reference dataset for correcting the gridded precipitation from IMD at the same resolution. Similarly, bias-corrected temperature data from the ERA5-Land reanalysis were employed to correct gridded temperature datasets. The performance of these high-resolution datasets was rigorously evaluated in terms of bias, seasonality, and spatial patterns against bias-corrected CHIRPS precipitation and ERA5-Land temperature data.

## 5.3 STANDARDIZED PRECIPITATION AND EVAPOTRANSPIRATION INDEX (SPEI)

Chuphal et al. (2024) estimated high-resolution and long-term (1901–2021) Standardized Precipitation Evapotranspiration Index (SPEI) to analyze drought characteristics across India. SPEI is a standardized drought index that integrates both precipitation and potential evapotranspiration (PET), thereby accounting for the influence of temperature on atmospheric water demand. While SPEI primarily reflects meteorological drought conditions, it does not directly incorporate hydrological or agricultural factors such as soil moisture or streamflow. However, when calculated at appropriate time scales, SPEI can exhibit strong correlations with soil moisture and streamflow-based drought indicators. High-resolution bias-corrected maximum and minimum temperature datasets were utilized to estimate PET, which was computed using the Hargreaves method due to the unavailability of comprehensive meteorological inputs required for the Penman-Monteith method. The resulting climatic water balance values were fitted to a log-logistic probability distribution, and SPEI values were computed using the SPEI package in R.

The estimated SPEI values were classified into distinct drought categories: abnormal drought (-0.8 to -0.5), moderate drought (-1.3 to -0.8), severe drought (-1.6 to -1.3), extreme drought (-2.0 to -1.6), and exceptional drought (less than -2.0), while values above -0.5 indicate normal or wet conditions. SPEI was computed at multiple temporal scales, including 1-month, 4-month, and 12-month periods. The 1-month SPEI is crucial for assessing short-term meteorological droughts and informing immediate decision-making. The 4-month SPEI is useful for evaluating seasonal drought conditions and is particularly relevant for agricultural drought assessments. The 12-month SPEI, on the other hand, provides insights

into long-term drought impacts on surface and groundwater resources. For monsoon season drought analysis, the 1-month SPEI was estimated individually for each summer monsoon month (June–September, JJAS). The 4-month SPEI was computed at the end of September and January to evaluate drought conditions for the summer monsoon (JJAS) and winter monsoon (ONDJ) seasons, respectively. Additionally, the 12-month SPEI was estimated at the end of December and May to assess drought conditions for the calendar year (January–December) and the water year (June–May), respectively. The gridded SPEI dataset was further utilized to compute mean SPEI values at multiple administrative levels, including country, states (including union territories), districts, and talukas (sub-districts), by aggregating the mean SPEI for grids corresponding to each geographical unit.

## 5.4 TEMPORAL AND SPATIAL VARIATION OF SPEI OVER NARMADA RIVER BASIN

The temporal and spatial variations of drought conditions over the Narmada River Basin were analysed using the Standardized Precipitation Evapotranspiration Index (SPEI) for the period 1901–2021.

Figure 87 displays the 12-month SPEI values computed at the end of December, which represent the cumulative climate water balance over the calendar year (January to December). This time scale is particularly effective in identifying long-term hydrological droughts, which influence surface water availability, reservoir storage, and groundwater recharge. The time series reveals alternating cycles of wet and dry periods, with several prominent drought events. Severe drought conditions are evident in 1918, corresponding to the infamous famine in India, with SPEI values well below -2.0 indicating exceptional drought. Similarly, the mid-1960s (1965 and 1966) mark a prolonged and severe drought phase that affected agriculture and water availability across much of central India. The year 2000 stands out as another significant dry period, coinciding with a weak monsoon. In more recent years, particularly between 2015 and 2019, the basin experienced recurring negative SPEI values, reflecting a series of back-to-back droughts or below-normal rainfall years, which would have stressed both agricultural production and water resources.

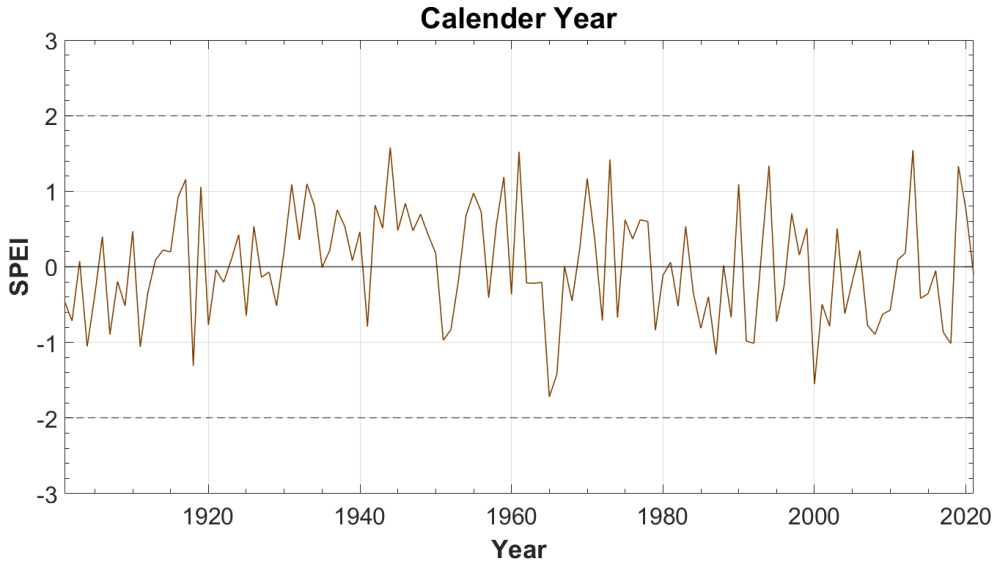


Figure 87 12-month SPEI at the end of December (Calendar year: January-December) for the period

Figure 88 presents the 12-month SPEI at the end of May, which corresponds to the water year (June to May). This analysis is critical for understanding droughts in relation to the monsoon-driven hydrological cycle. Since most of the annual rainfall in the basin occurs during the southwest monsoon (June–September), the May SPEI captures the impact of the entire preceding monsoon season and its aftermath. Low values in this time series are indicative of poor monsoon rainfall and its extended impact on water availability during the dry season. The timing of this index is particularly important for water resource managers, as it reflects the carryover effect of monsoon deficits on water availability leading into the next monsoon. Similar to the calendar year SPEI, drought signals for years such as 1918, 1965, 2000, and 2017–2019 are evident, underlining their hydrological significance.

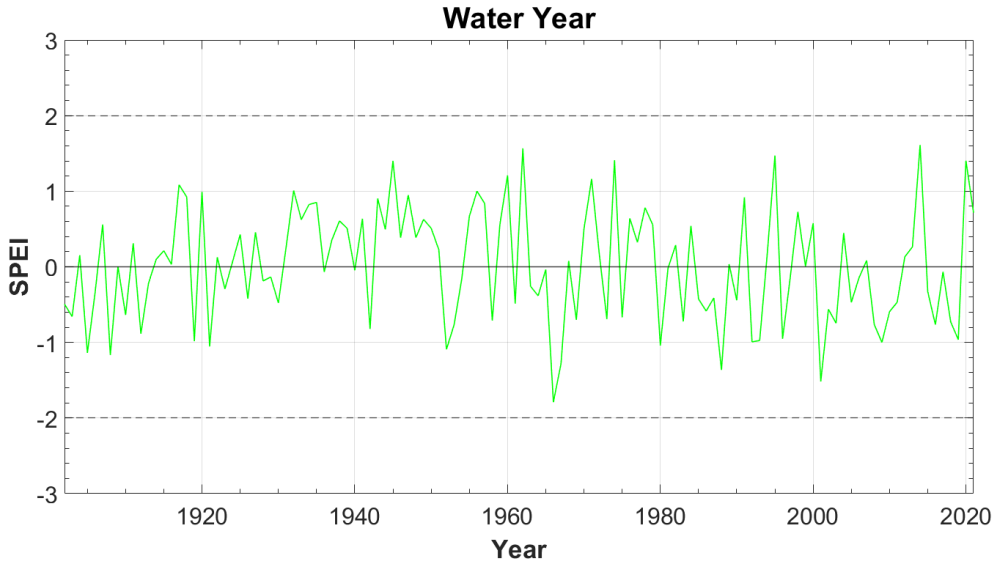


Figure 88: 12-month SPEI at the end of May (Water year: June-May) for the period 1901–2020

Moving to the 4-month SPEI, Figure 89 shows values calculated at the end of September, which represents the summer monsoon season (JJAS). This index is especially useful for assessing agricultural droughts, as it captures the primary crop-growing season in the region. Variability in this index reflects the onset, progression, and withdrawal anomalies of the monsoon, which are critical for sowing and crop productivity. Years like 1965, 2002, 2015, and 2018 display sharp declines in SPEI values during this season, suggesting late or failed monsoons that severely impacted rainfed agriculture. The consistency of low SPEI during consecutive monsoons also raises concerns regarding compound drought events, where multiple seasons of insufficient rainfall cause cumulative stress.

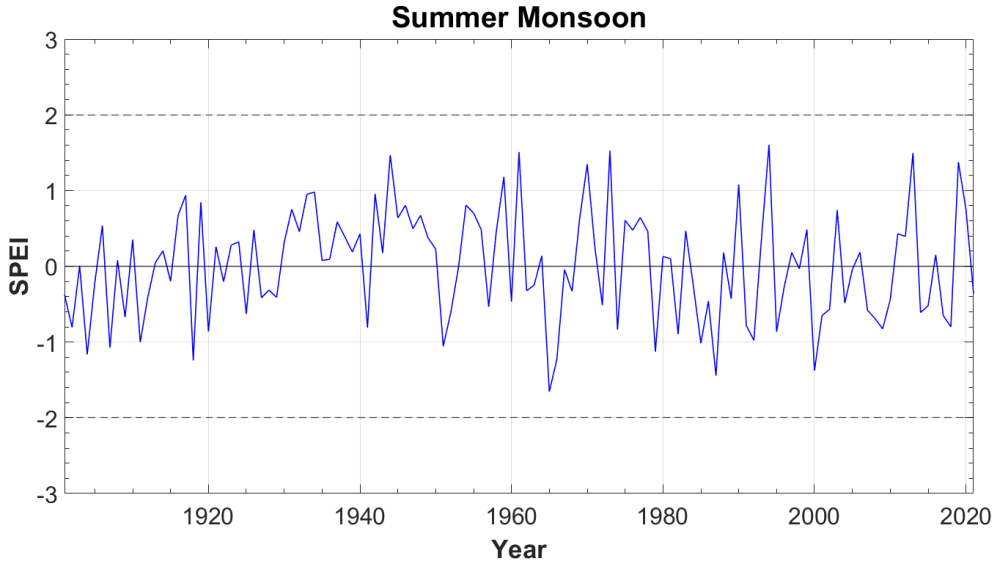


Figure 89 4-month SPEI at the end of September (Summer monsoon: JJAS) for the period 1901–2020

Figure 90, on the other hand, presents the 4-month SPEI at the end of January, encompassing the winter and post-monsoon period (ONDJ). This timeframe reflects the residual drought impact from the monsoon season and is crucial for understanding soil moisture deficits, groundwater recharge limitations, and planning for rabi (winter) cropping. It also indicates how the effects of a weak monsoon persist into the dry season. Notable dips in the January SPEI series highlight extended droughts and multi-seasonal water scarcity, emphasizing the delayed recovery of hydrological systems after poor monsoon years.

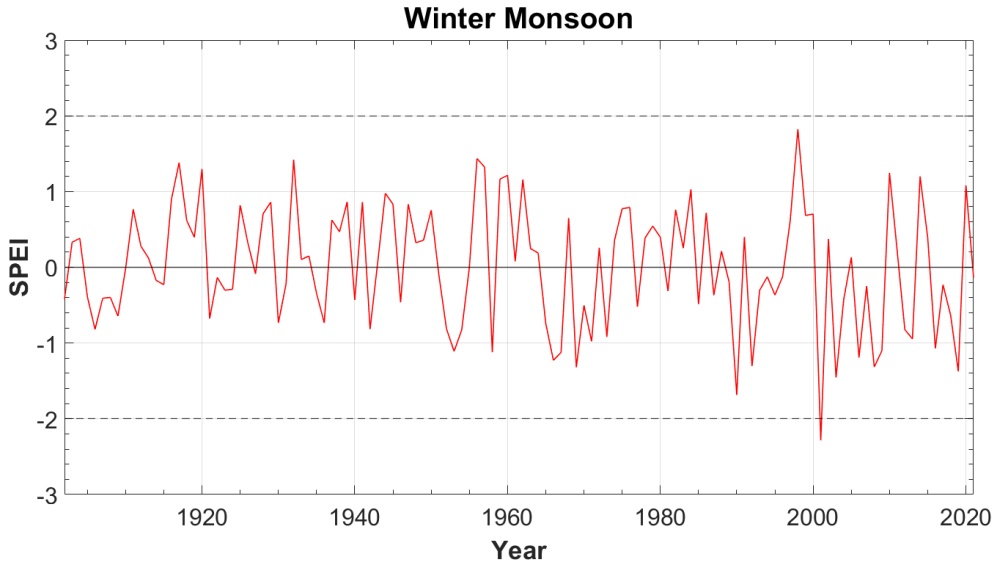


Figure 90: 4-month SPEI at the end of January (Winter monsoon: ONDJ) for the period 1901–2021

The spatial distribution of drought conditions across the Narmada River Basin has been assessed using SPEI maps for select drought years, capturing both historical and recent drought episodes. These maps provide insights into the geographic extent, severity, and variability of drought impacts across different sub-regions of the basin. The following figures illustrate the SPEI-based drought classification for major drought years:

The year 1918 represents one of the most severe droughts in India's recorded history. The SPEI spatial map for this year illustrates widespread drought stress across the entire Narmada River Basin. Most parts of the basin, especially the upper and central sub-basins, recorded SPEI values below -2.0, indicating exceptional drought. This reflects the large-scale rainfall deficiency and intense climatic stress that led to major agricultural and hydrological impacts, including famine conditions in many parts of India.

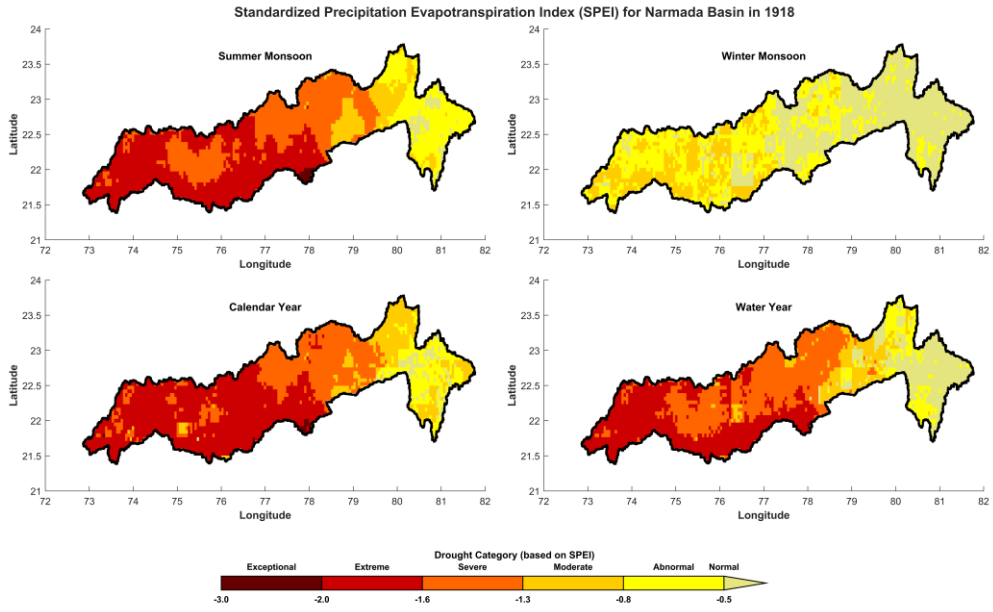


Figure 91: Standardized Precipitation Evapotranspiration Index (SPEI) for Narmada Basin (1918)

The years 1965 and 1966 together marked a period of back-to-back droughts, with far-reaching implications for water resources and food security. The 1965 SPEI map reveals severe drought conditions in the upper and eastern regions of the basin. In contrast, the 1966 map shows an expansion of drought severity into the middle and lower basin, suggesting that the drought persisted and spread geographically. The persistence of negative SPEI values in consecutive years highlights the compounded stress on groundwater recharge, reservoir storage, and crop production during this period.

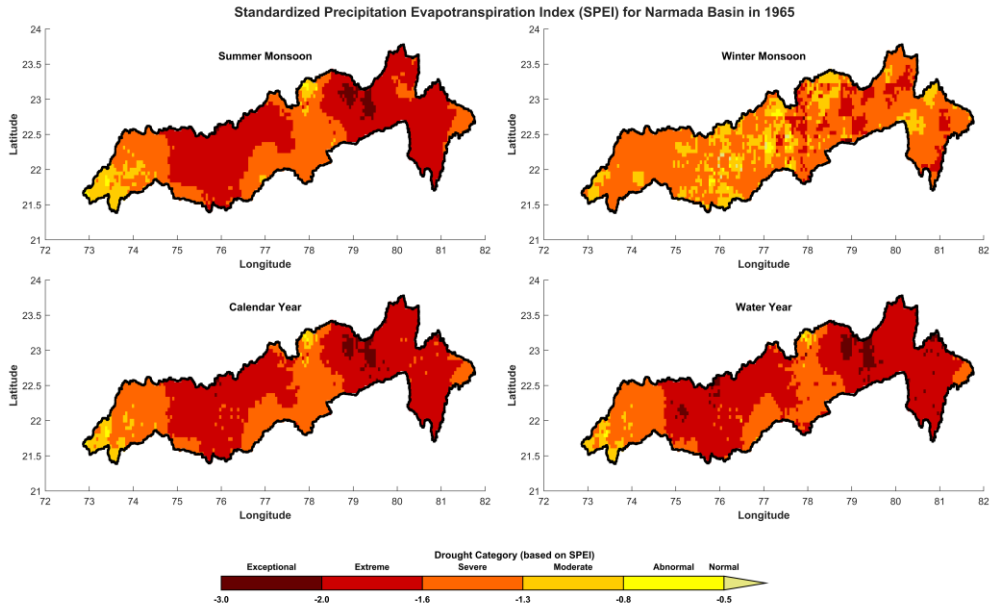


Figure 92 Standardized Precipitation Evapotranspiration Index (SPEI) for Narmada Basin (1965)

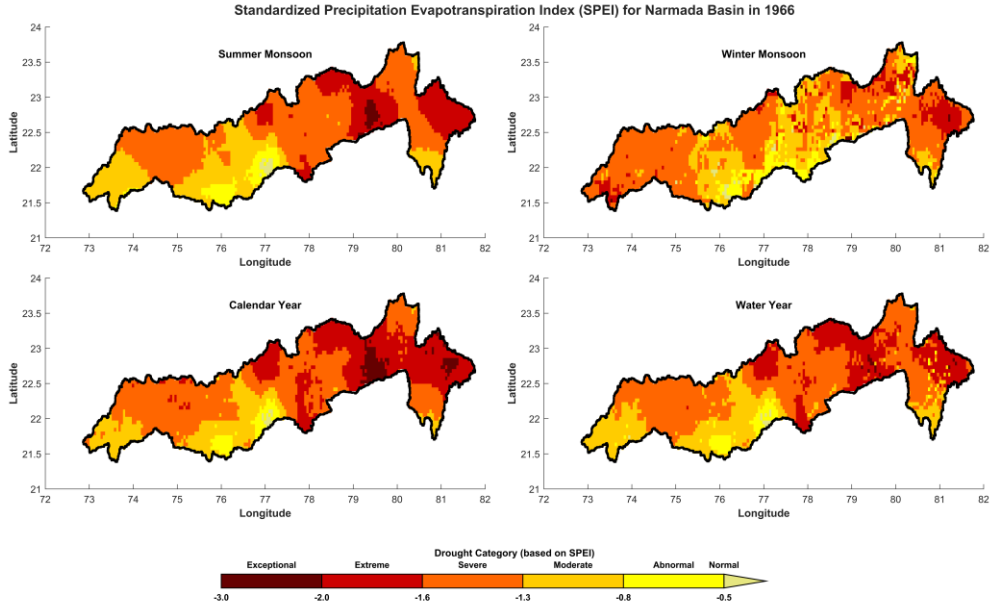


Figure 93 Standardized Precipitation Evapotranspiration Index (SPEI) for Narmada Basin (1966)

The spatial SPEI pattern for 2000 shows severe drought stress concentrated in the middle and lower sub-basins, including areas downstream of major reservoirs like Indira Sagar and Sardar Sarovar. These regions recorded SPEI values between -1.6 and -2.0, indicating severe to extreme drought. This spatial pattern aligns with field reports of agricultural losses, groundwater depletion, and stress on irrigation systems.

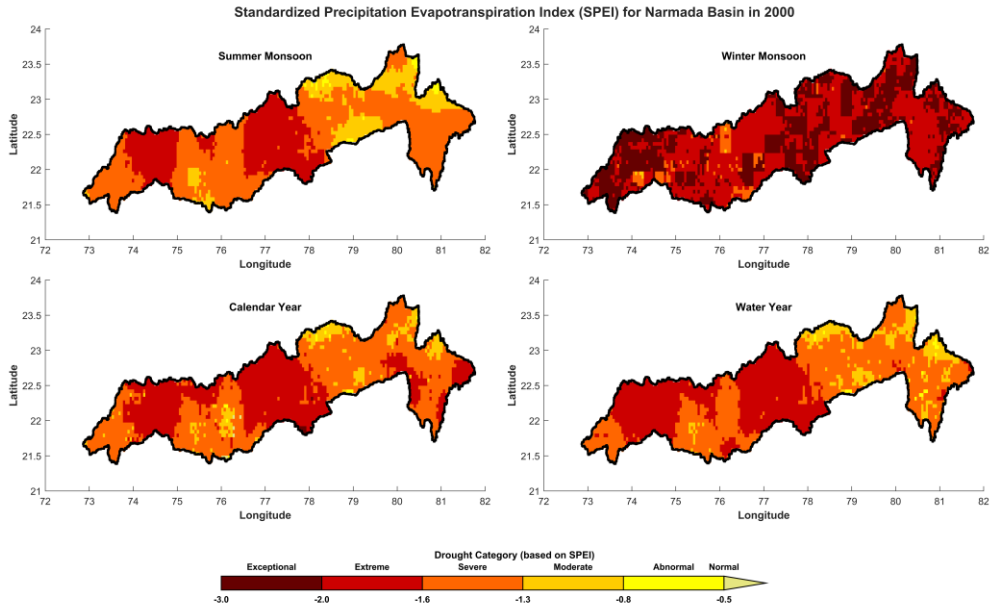


Figure 94 Standardized Precipitation Evapotranspiration Index (SPEI) for Narmada Basin (2000)

In recent years (2017 to 2020), the Narmada River Basin witnessed a sequence of drought-related fluctuations, reflecting the growing variability in monsoon performance and its impact on regional water availability. The year 2017 was marked by scattered moderate drought conditions, particularly in the central basin, due to uneven rainfall distribution during the monsoon season. This was followed by 2018, which saw a more widespread drought scenario—moderate to severe drought conditions prevailed across the upper and eastern parts of the basin, resulting in significant stress on agriculture and groundwater recharge. In 2019, drought conditions persisted but were highly variable across the basin; while western and coastal areas showed relatively stable conditions, the central and southern regions continued to face moderate to severe moisture deficits. A noticeable improvement occurred in 2020, with most regions of the basin transitioning into normal to wet conditions. This recovery was driven by a well-distributed and timely monsoon, which helped offset the cumulative impacts of the preceding dry years and restore water availability across the basin.

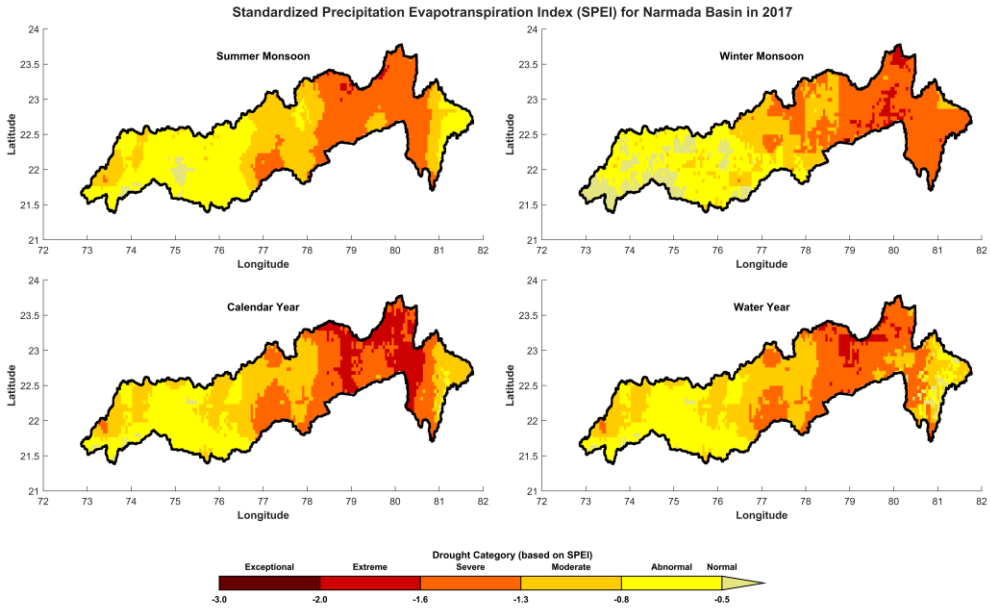


Figure 95: Standardized Precipitation Evapotranspiration Index (SPEI) for Narmada Basin (2017)

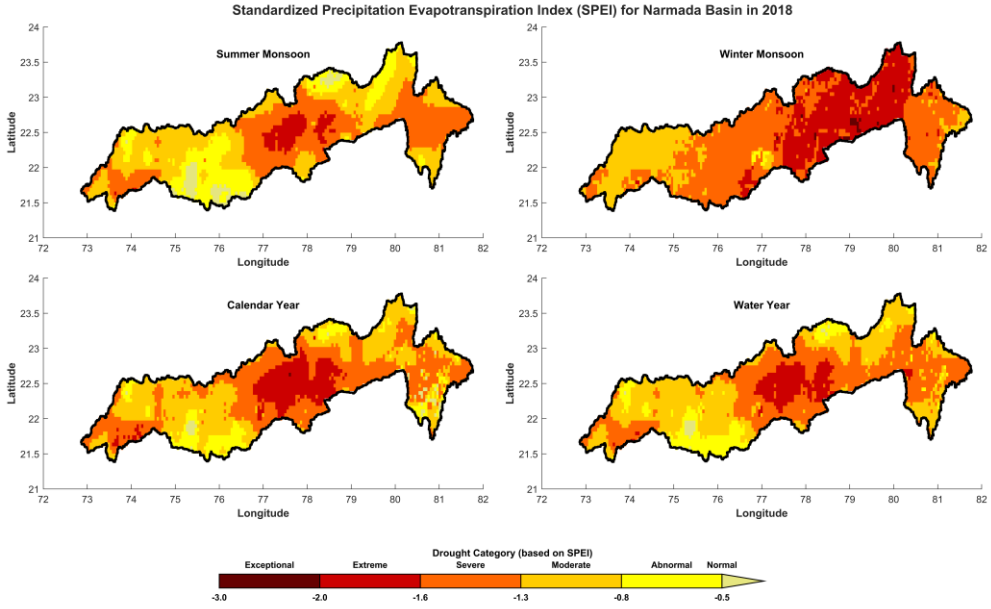


Figure 96 Standardized Precipitation Evapotranspiration Index (SPEI) for Narmada Basin (2018)

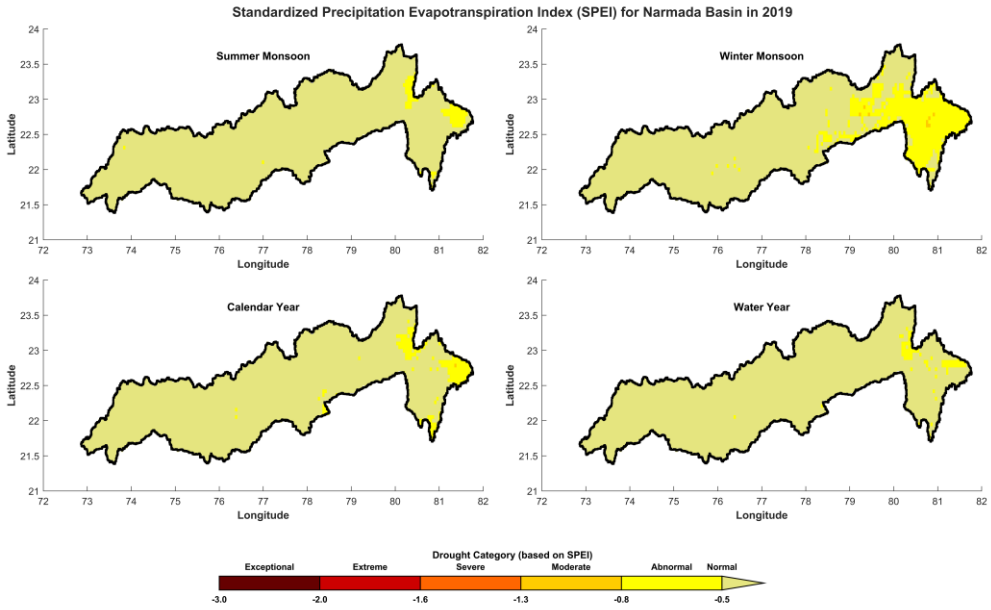


Figure 97 Standardized Precipitation Evapotranspiration Index (SPEI) for Narmada Basin (2019)

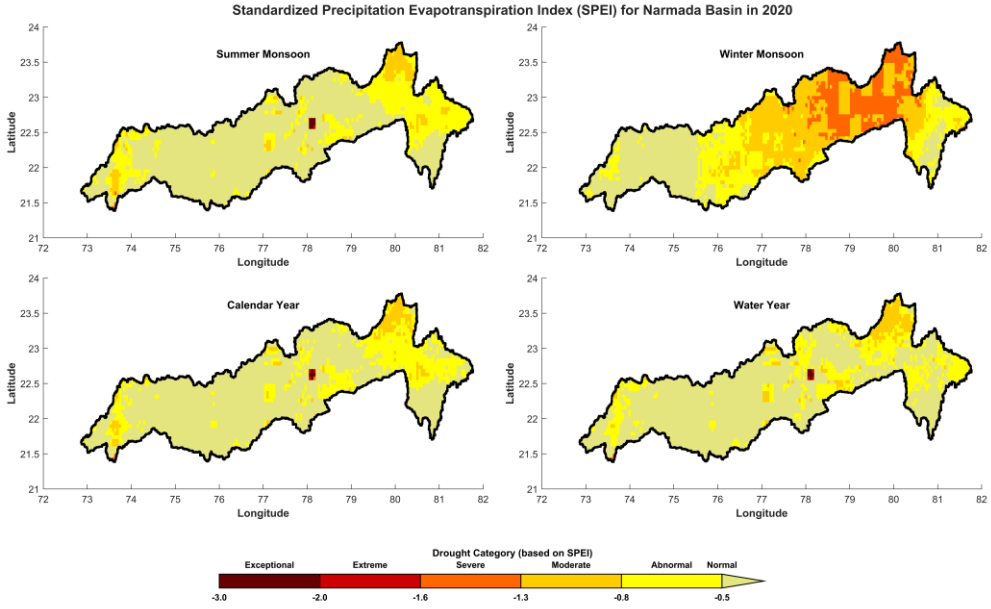


Figure 98 Standardized Precipitation Evapotranspiration Index (SPEI) for Narmada Basin (2020)

# Chapter 6: Conclusions and Utility

## 6.1 SUMMARY OF FINDINGS

This study provides a detailed assessment of the climatological and meteorological characteristics of the Narmada River Basin using multiple datasets, including observed station data, reanalysis products (ERA5), and climate model projections (CMIP6). The analysis highlights considerable spatial and temporal variability in key parameters such as rainfall, temperature, wind speed, relative humidity, solar radiation, and cloud cover. Rainfall patterns show strong inter-annual and decadal fluctuations, with varying spatial intensities across upper, middle, and lower parts of the basin. Temperature trends indicate consistent warming, especially during the pre-monsoon and monsoon months, with rising maximum and minimum temperatures. Wind speeds exhibit a slight declining trend, while relative humidity and cloud cover follow expected seasonal cycles. Solar radiation patterns reflect inverse behaviour with cloud cover, influencing evapotranspiration.

The Standardized Precipitation Evapotranspiration Index (SPEI) was used to analyze drought behaviour. Both temporal and spatial assessments reveal historical and recent drought episodes, including severe events in 1918, 1965–66 and 2000. Spatial analysis shows variability in drought severity across sub-basins, emphasizing the need for localized drought mitigation strategies. Climate model projections under different Shared Socioeconomic Pathways (SSPs) suggest continued warming and increased variability in precipitation. The outputs indicate potential intensification of extreme events, with greater warming and precipitation uncertainty under high-emission scenarios (e.g., SSP585).

## 6.2 CONCLUSIONS

The findings of this study underscore the complexity and evolving nature of the Narmada River Basin's climate. Key conclusions drawn from the analysis include:

- The basin is experiencing increased temperature trends and recurring drought episodes, consistent with regional climate change signals.
- Rainfall is highly variable across time and space, with the monsoon season playing a dominant role in shaping hydrological responses.

- Projected climate data from bias-corrected GCMs indicate a continued rise in temperatures and increased variability in rainfall patterns across future scenarios, with greater changes under higher emission pathways.
- SPEI-based drought analysis confirms that both historical and recent droughts have had spatially differentiated impacts, with upper and middle basin areas showing higher susceptibility.
- Climatic parameters such as wind speed, cloud cover, and solar radiation are also undergoing subtle changes that influence evapotranspiration and overall water balance in the basin.

These insights provide a scientific foundation for integrating climate data into basin-level planning and decision-making.

## 6.3 DATASET USAGE

The datasets used and developed in this study have high applicability for multi-sectoral planning and research in the Narmada River Basin. Their potential uses include:

- Hydrological and Climate Modeling: The gridded and station-based datasets are suitable for input into hydrological models (e.g., SWAT, HEC-HMS) and for simulating future water availability scenarios.
- Drought and Risk Assessment: The SPEI outputs can support early warning systems, vulnerability assessments, and policy planning related to agricultural droughts and water scarcity.
- Infrastructure Planning: The projected climate data are useful for designing resilient infrastructure, including dams, irrigation systems, and urban drainage networks.
- Water Resource Management: The findings can inform reservoir operation planning, irrigation scheduling, and groundwater recharge programs based on climate variability.

- Research and Policy Support: The processed datasets and visualizations serve as a knowledge base for government agencies, academic institutions, and NGOs working on climate adaptation and water sustainability in the region.

# Chapter 7: References

India-WRIS. India Water Resources Information System, Ministry of Jal Shakti, Government of India. Retrieved from https://indiawris.gov.in/wris

Mangukiya, N. K., et al. (2025). CAMELS-India: Catchment Attributes and Meteorology for Large-Sample Studies in India. [Data Source: CAMELS-India Dataset]

Central Water Commission (CWC). River discharge and water level data for monitoring stations across the Narmada River Basin. Government of India.

ERA5 Climate Data. European Centre for Medium-Range Weather Forecasts (ECMWF). Accessed via https://cds.climate.copernicus.eu

Chuphal, A., et al. (2024). Drought Atlas of India: High-resolution SPEI dataset for 1901–2021. Published in Scientific Data. https://www.nature.com/articles/s41597-023-02856-y

Mishra, V., et al. (2020). High-resolution bias-corrected CMIP6 climate projections for South Asia. Dataset used in the study includes outputs from 13 GCMs under the Coupled Model Intercomparison Project Phase 6 (CMIP6).

Giorgi, F., & Gutowski, W. J. (2015). Regional climate modeling: Status and perspectives. Journal of Regional Climate Studies, 7(1), 1–27.

Eyring, V., Bony, S., Meehl, G. A., et al. (2016). Overview of the Coupled Model Intercomparison Project Phase 6 (CMIP6) experimental design and organization. Geoscientific Model Development, 9, 1937–1958.

Jacob, D., et al. (2014). EURO-CORDEX: New high-resolution climate change projections for European impact research. Regional Environmental Change, 14(2), 563–578.

Sheffield, J., Goteti, G., & Wood, E. F. (2006). Development of a 50-year high-resolution global dataset of meteorological forcings for land surface modeling. Journal of Climate, 19(13), 3088–3111.